VIETNAM JOURNAL OF HYDRO - METEOROLOGY

ISSN 2525 - 2208

VIETNAM METEOROLOGICAL AND HYDROLOGICAL ADMINISTRATION

No 14
03-2023

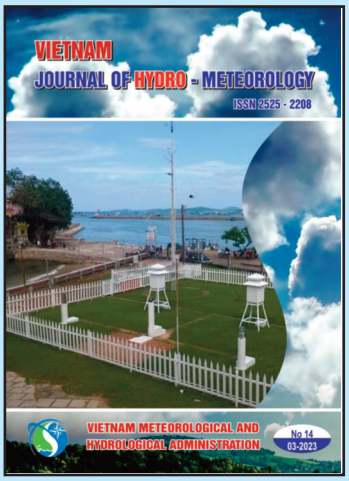

Publishing licence
No: 166/GP-BTTTT - Ministry of Information and Communication dated 17/04/2018

Editorial office
No 8 Phao Dai Lang, Dong Da, Ha Noi
Tel: 024.39364963
Email: tapchikttv@gmail.com

Engraving and printing
Vietnam Agriculture Investment Company Limited
Tel: 0243.5624399

VIETNAM JOURNAL OF HYDROMETEOROLOGY
Volume 14 - 03/2023

TABLE OF CONTENT

VIETNAM JOURNAL OF HYDROMETEOROLOGY

Research Article

Research on PAHs emission from small scale incinerators: A case study in Yen Lac District, Vinh Phuc Province

Nguyen Tien Dung[1*], Vu Duc Toan[2*], Nguyen Nu My Ha[3]

[1] Institute of Environmental Science and Technology, Vietnam Cooperative Alliance; nguyentiendunghb78@gmail.com
[2] ROOM strong research, Environmental and life science research laboratory, Thuyloi University; vuductoan@tlu.edu.vn; huongntl@tlu.edu.vn
[3] Ha Tinh University; ha.nguyennumy@htu.edu.vn

*Corresponding author: nguyentiendunghb78@gmail.com; vuductoan@tlu.edu.vn;

Tel.: +84–914953335

Received: 09 January 2023; Accepted: 06 February 2023; Published: 25 March 2023

Abstract: An evaluation of the PAHs emission from small scale incinerators (SSI) in Yen Lac district, Vinh Phuc province, Vietnam was assessed. Twenty-four representative dust samples from the SANKYO incinerators were taken. The concentration levels of PAHs in the samples were determined using gas chromatography coupled with mass spectrometry. The main applied research methods include field observation and sample analysis. The results of the analysis revealed the time trend variation of PAHs concentration in samples. In April, June, September, and November, Σ_{16}PAHs concentrations ranged from 97.83 to 113.0 µg/m^3, from 105.32 to 119.04 µg/m^3, from 107.25 to 118.73 µg/m^3 and from 101.56 to 139.48 µg/m^3, respectively. The mean percentages of L–PAHs, M–PAHs and H–PAHs in the analyzed dust samples are 55.7%, 33.8% and 10.5%, respectively. These values can be explained by the PAHs physical chemical properties as well as combustion technology of Sankyo incinerator. The emission factor of 16 PAHs is ranged from 0.0018 to 0.300mg/kg. The results of this study can be applied to estimate the amount of PAH generated when burning domestic waste in rural areas.

Keywords: PAHs; Emission factor; Small scale incinerators.

1. Introduction

In recent years, the problem of dust pollution in urban areas of Vietnam tends to increase [1–2]. Dust pollution in urban areas includes both internal and external sources, spreading from neighboring provinces. Dust exposure is statistically associated with a variety of dangerous diseases. The harm and danger of exposure to various types of dust depend on the characteristics of the emission source [1–2]. One of the sources of highly hazardous dust emissions is from small–scale domestic waste incinerators. Currently, to deal with pollution from domestic waste, many localities have chosen to invest in small scale domestic waste incinerators (SSI) as a solution. The above solution, although achieving short–term benefits, will have many consequences in the long run. Dust emitted from SSI contains many persistent toxic organic substances, which has caused significant pollution in the air, affecting the surrounding people. Therefore, assessing the harm, environmental risk level, toxic organic substances composition in dust from small scale incinerators is very necessary.

An aromatic compound with two or more fused arenes is called a polycyclic aromatic hydrocarbon (PAHs) [3]. They are primarily produced by the incomplete combustion of wood, grass, coal, fossil fuels, and municipal waste [4–5]. In most cases, PAHs are carcinogenic and hazardous to wildlife and humans [6]. PAHs have a low water solubility, hydrophobic nature and were often accumulated in various environmental systems including dust, soil, sediment and organisms [7–8].

In Vietnam, several studies have been conducted on the contamination of PAHs in air and street dust. Typically, the study about air PAHs samples at three surveyed locations in Hanoi in 2003 showed the PAHs concentration in the range of 144,93 to 295,63 ng/m^3 [9–10] determined the concentrations of PAHs in street dust samples range from 530 to 4700 µg kg^{-1} dry weight in Hanoi, Vietnam. However, to our knowledge, little data is available concerning PAHs emission from small scale domestic waste incinerators (SSI) in countryside's of Vietnam. International research often concentrated on 16 representative PAHs including: naphthalene (Nap), acenaphthylene (Acey), acenaphthene (Ace), fluorene (Flu), phenanthrene (Phe), anthracene (Ant), fluoranthene (Flt), pyrene (Pyr), chrysene (Chr), benzo[a]anthracene (BaA), benzo[b]fluoranthene (BbF), benzo[k]fluoranthene (BkF), benzo[a]pyrene (BaP), indeno [1,2,3–cd] pyrene (IcdP), dibenzo[a,h]anthracene (DahA), and benzo [g,h,i] pyrene (BghiP).

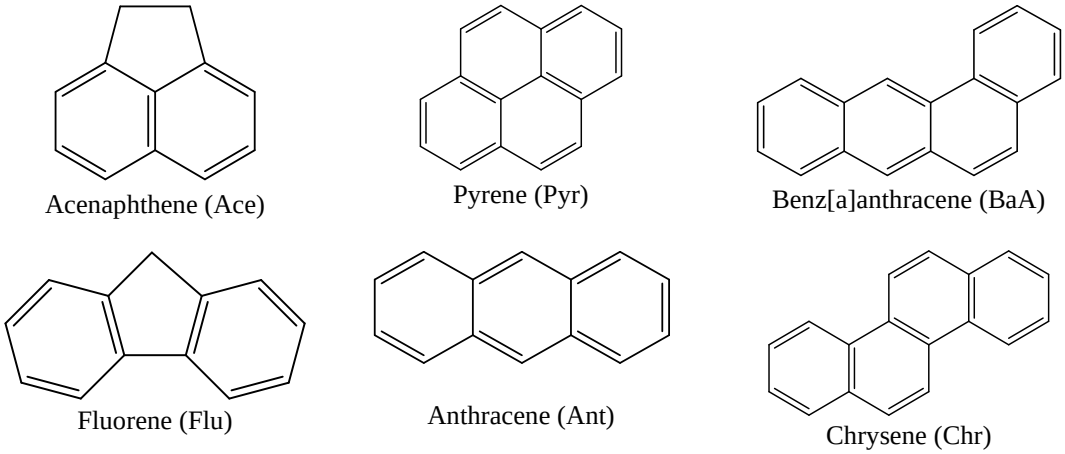

Figure 1. Some typical PAHs structures.

Rural areas in Vinh Phuc province emit about 600 tons of solid waste per day into the environment. The ability to collect and treat is about 70%, the rest is incinerated. In Vinh Phuc province, there are 33 SSI. The conventional incineration process consists of 3 main steps: classification, incineration, and treatment of dust and ash. When all three stages are combined synchronously, the basic pollution source will be solved. However, in Vinh Phuc province, only one stage has been completed, which is burning garbage, the remaining stages have not been thoroughly treated. The research area in Vinh Phuc was selected at the SSI in Yen Lac district. The SSI started operating in 2014, have a capacity of 500 kg/h and all use Sankyotechnology made in Thailand with a capacity of 500kg/h. However, in the process of using Sankyotechnology, the treatment of smoke and dust has not been thorough, and the lack of synchronous operation has also affected the environment. Therefore, the research of the PAHs emission in Yen Lac district, Vinh Phuc province is important. The research results can be applied to other rural areas with the same household waste composition and treatment technology as Vinh Phuc. The main objectives of the study include: i) Assessment of PAHs concentration in dust emitted from chimneys of SSI; ii) Assessment of ratio and composition of PAHs in dust samples; iii) Research on load and emission factor of PAHs from SSI.

2. Materials and methodology

2.1. Study area and sampling

2.1.1. Study area

The study area in Vinh Phuc was selected in Yen Lac district where has several SSI incinerators (Figure 2).

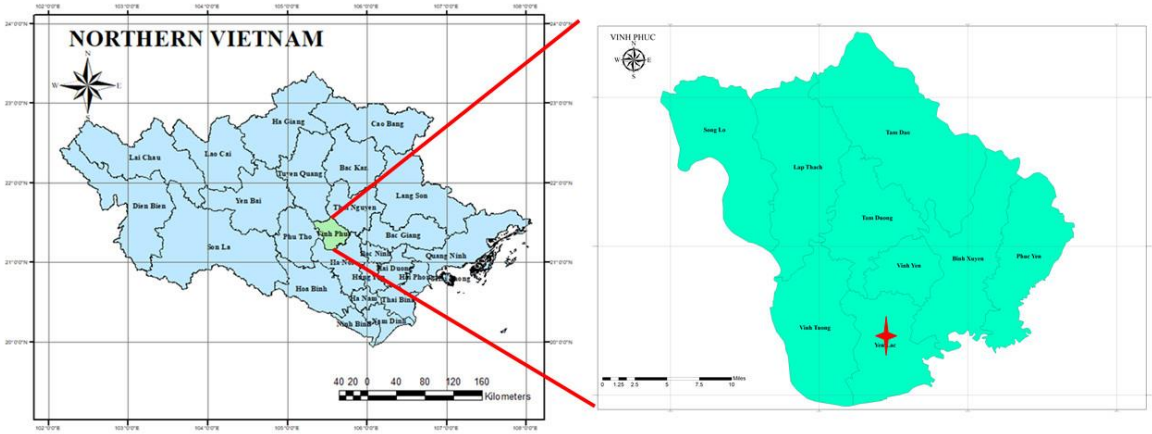

Figure 2. Location of the study area.

The composition of domestic solid waste in Yen Lac district has a combination of sources in purely agricultural areas and towns.

Table 1. Results of analysis of domestic solid wastecomposition in Yen Lac district.

No	Composition of domestic solid waste	Percentage (%)
1	Organic component	68.11
2	Waste paper, glass, metal	5.90
3	Plastic bags, plastic bottles	4.0
4	Toxic material (battery, paint…)	0.01
5	Porcelain, concrete, brick, coal slag, tires...	21.98

Sankyo incinerator uses natural gas fuel with the function of burning domestic solid waste for the entire population of Yen Lac district (Figure 2). The process consists of three steps: classification, burning, treatment of dust and ash.

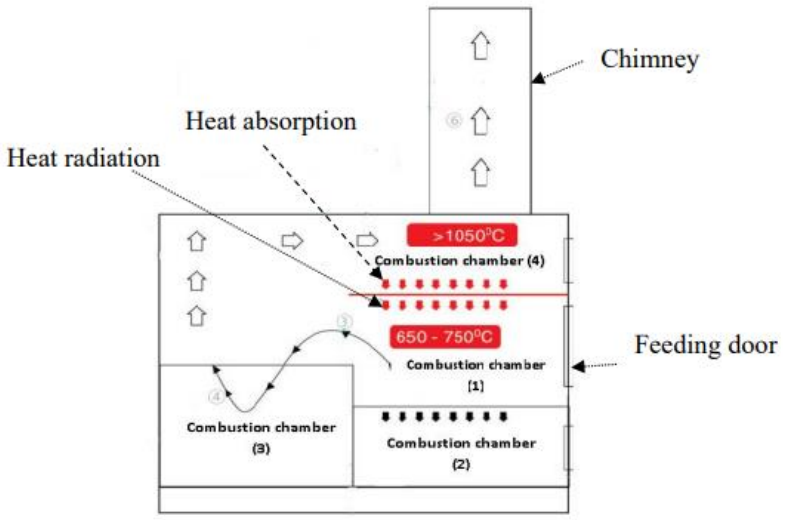

Figure 3. Simulation of Sankyo incinerator.

- Waste treatment process: The solid waste is collected and brought to the treatment area. Preliminary classification: bricks, glass, silt... non–combustible is removed for burial; nylon, plastic, metal... sold as scrap, the rest is burned. In the primary and secondary combustion chambers, the waste is burned at temperatures of 650^{o}C and 1050^{o}C, the retention time is about 2–3 seconds. Output waste includes smoke and ash (Figure 3).

- Exhaust gas treatment process: According to the design, the exhaust gas is cooled through the radiator ribs. Exhaust smoke is treated through dust traps staggered along the chimney to completely store dust before discharging.

- The composition of waste before being put into the incinerator: determined on average in 4 sampling periods.

2.1.2. Sampling

A total of 24 samples were collected from two SSI in Yen Lac district. Repeating sampling time is April, June, September, and December 2021 at each location of the waste incinerator. Samples were taken according to the instructions in Circular No. 40/2015/TT–BTNMT on technical process of emission monitoring. The samples were taken isokinetically using the train may be constructed by adaptation of an ARB Method 5 train. The train consists of a nozzle, probe, heated particulate filter, condenser, and sorbent module, followed by three impingers and a silica gel drying cartridge. An in–stack filter cannot be used because the filter material must be different than the Teflon required by the method at the in–stack temperatures. For sources emitting a large amount of particulate matter, a cyclone or similar device in the heated filter box may be used. Place 100 ml of the impinger solution in the first impinger and weigh. Record the total weight. Repeat the procedure for the second impinger. Leave the third impinger empty. Weigh the empty third impinger and record the weight. Just before assembling the sampling train, weigh 200 to 300 g of silica gel to the proximity 0.5 g directly into a tared impinger or silica gel cartridge. To adsorb gaseous PAH, a sorbent trap containing Amberlite resin (XAD–2) was used. Before use the resin (and the glass wool) was Soxhlet extracted by methylene chloride for 24 hours at approximately four cycles per hour and dried by pure nitrogen gas stream. The flue gas flow rate was measured by the integrated manometer in the train, and the isokinetic sampling gradient rate was maintained automatically by the device.

2.2. Study methods

Analysis of Polycyclic Aromatic Hydrocarbon in Airborne Particulate Matter Samples by Gas Chromatography in Combination with Mass Spectrometry (GC–MS). Quality assurance and quality control were conducted by performing laboratory blanks, sampling blanks, and recoveries of international sediment exchange for tests on organic contaminants samples.

Approximately l hour before HRGC/LRMS or HRGC/HRMS analysis, adjust the sample extract volume to approximately 500 µL. This is done by adding 50 µL of the recovery standard spike solution to the 450 µL final volume of the concentrated sample extract giving the sample extract concentration required. If the sample volume must be changed to achieve a desired detection limit, the recovery spike solution concentration must be adjusted accordingly to achieve the target concentrations. Inject a 2 µL aliquot of the sample extract onto the DB–5 column. Use the same volume when during calibration. Recommended GC/MS operating conditions. The presence of a given PAH has qualitatively confirmed the criteria are satisfied. The response for any quantitation or confirmation ion in the sample extract must not exceed the response of the highest concentration calibration standard. Collect, record, and store the data for the calculations required.

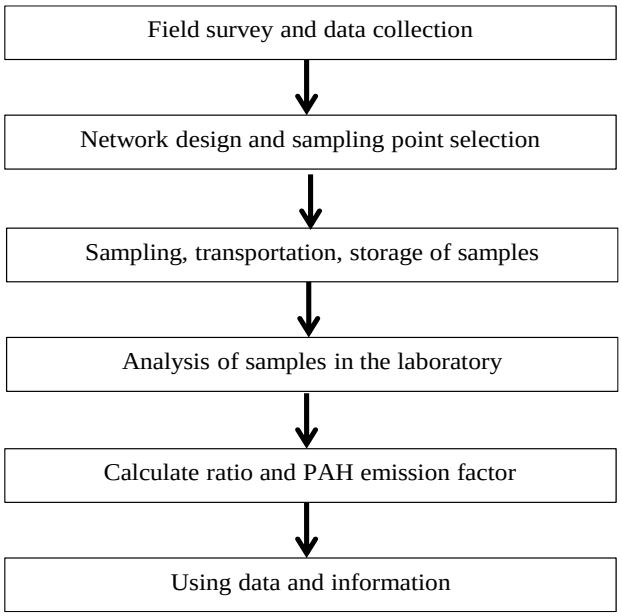

Figure 4. Research structure diagram.

Limit of detection (LOD) was calculated as 3 times signal–to–noise ratio obtained from lowest matrix–matched samples. Meanwhile, the method limit of quantification (LOQ) was calculated by 10 times signal to noise at the lowest concentration matrix–matched samples. The numbers of injection of blanks and QC samples in one analysis batch contained at least 20% of total numbers of injection. The method of determining the emission factor: Apply the direct observation method to calculate the emission factor of PAH from the dust sample in the chimney.

3. Results and discussion

3.1. PAHs concentration in dust emitted from chimneys of SSI

From April to November 2021, PAHs were found in all of the dust samples that demonstrated the occurrence of PAHs in SSI (Table 2). This is understandable because PAHs are mostly produced by incomplete combustion [4–5]. The total average of Σ_{16}PAHs concentration in dust samples was 114.24, ranging from 97.83 to 139.48 µg/m^3.

Table 2. The PAHs concentrations (µg/m^3) in dust samples from study area.

Compound	April	June	September	November
Nap	30.87–32.68 [(a)] (31.9 ±0.67)	31.65–34.84 (33.8 ±1.18)	32.17–34.29 (33.39 ±0.78)	30.51–35.24 (33.23 ±1.75)
Acy	0.22–0.28 (0.25 ±.022)	0.24–0.28 (0.26 ±0.015)	0.18–0.23 (0.2 ±0.02)	0.23–0.30 (0.27 ±0.03)
Ace	0.36–0.51 (0.44 ±0.05)	0.47–1.33 (0.96 ±0.32)	0.35–0.43 (0.39 ±0.03)	0.46–1.0 (0.77 ±0.2)
Flu	21.59–22.68 (22.21 ±0.4)	22.15–23.50 (22.9 ±0.5)	18.77–19.61 (19.25 ±0.03)	21.36–22.68 (22.12 ±0.49)
Phe	0.38–0.45 (0.42 ±0.026)	0.46–0.53 (0.5 ±0.026)	0.32–0.37 (0.35 ±0.02)	0.45–0.62 (0.55 ±0.06)
Ant	5.88–6.84 (6.43±0.35)	6.56–7.63 (7.17 ±0.04)	5.16–5.89 (5.58 ±0.27)	6.33–8.12 (7.36 ±0.66)
Py	6.27–12.57 (9.89 ±2.33)	13.13–15.14 (14.28 ±0.74)	15.57–16.56 (16.13 ±0.37)	12.66–14.07 (13.47 ±0.5)
Flt	6.33–6.60 (6.5 ±0.12)	6.66–7.08 (6.9 ±0.15)	6.77–7.02 (6.9 ±0.09)	6.42–9.35 (8.1 ±1.1)
BaA	0.30–0.44 (0.38 ±0.05)	0.50–0.62 (0.56 ±0.004)	0.38–0.55 (0.48 ±0.06)	0.48–0.96 (0.75 ±0.18)

Compound	April	June	September	November
Chr	0.15–0.20 (0.18 ±0.02)	0.17–0.22 (0.2 ±0.02)	0.09–0.18 (0.14 ±0.03)	0.16–0.21 (0.19 ±0.02)
BbF	2.07–2.38 (2.25 ±0.11)	2.29–2.72 (2.53 ±0.16)	1.77–1.99 (1.89 ±0.08)	2.21–3.27 (2.8 ±0.4)
BkF	0.12–0.14 (0.13 ±0.007)	0.24–0.25 (33.8 ±1.18)	0.11–0.13 (0.12 ±0.007)	0.22–0.45 (0.35 ±0.08)
BaP	0.17–0.19 (0.18 ±0.007)	0.20–0.22 (0.24 ±0.004)	0.12–0.14 (0.13 ±0.007)	0.19–0.34 (0.27 ±0.06)
Ind	14.32–18.13 (16.5 ±1.4)	14.42–17.99 (16.47 ±1.32))	18.54–24.03 (21.69 ±2.0)	13.90–34.54 (25.76 ±7.6)
BghiP	4.33–4.46 (4.4 ±0.048)	4.58–4.99 (4.8 ±0.15)	5.06–5.16 (5.12 ±0.04)	4.42–6.56 (5.6 ±0.8)
DahA	1.2–1.3 (1.26 ±0.04)	1.6–1.7 (0.65 ±0.04)	1.89–2.15 (2.01 ±0.09)	1.56–1.77 (9.12 ±16.6)
L–PAHs [b]	59.33–63.44 (61.8 ±1.53)	61.53–68.11 (65.31 ±2.44)	59.65–60.82 (59.17 ±1.43)	59.34–67.96 (64.30 ±3.20)
M–PAHs [c]	13.05–19.87 (16.97 ±2.53)	20.46–23.06 (21.95 ±0.96)	22.81–24.31 (23.67 ±0.56)	19.72–24.59 (22.52 ±1.81)
H–PAHs [d]	20.01–25.3 (23.48 ±1.59)	21.73–26.17 (24.28 ±1.64)	25.6–31.45 (28.96 ±2.17)	20.94–45.16 (34.87 ±8.99)
Σ_8PAHs [e]	22.66–27.24 (25.29 ±1.69)	24.0–28.71 (26.71 ±1.74)	48.5–58.36 (52.32 ±4.40)	23.14–48.10 (37.49 ±9.25)
Σ_{16} PAHs [f]	97.83–113.0 (106.55 ±5.63)	105.32–119.04 (113.21 ±5.1)	107.25–118.73 (113.85 ±4.26)	101.56–139.48 (123.36 ±14.06)

(a) min – max (mean ± standard deviation); (b) Low molecular weight PAHs with 2 and 3 aromatic rings (Nap, Acey, Ace, Flu, Phe, Ant); (c) Middle molecular weight PAHs with 4 aromatic rings (BaA, Chr, Pyr, Fla); (d) High molecular weight PAHs with 5 and 6 aromatic rings (BbF, BkF, BaP, IcdP, BghiP); (e) sum of 8 carcinogenic PAHs compounds (BaA, Chr, BbF, BkF, BaP, Ind, BghiP, DahA); (f) sum of all 16 selected PAHs.

In Vietnam, there has been no study on PAH in incinerators before, but when compared with other studies around the world, the value of total Σ_{16}PAHsconcentration was dramatically higher than the Σ_{16}PAHs in PM10 from outside residential apartments around two MSWIs in Shenzhen, China [11] and sampling sites located 1 km from the medical waste incinerator in Taiwan, China [12]. It was found that the concentration of PAHs around these incinerators in Shenzhen and Taiwan was affected by the outside environment, including wind, temperature, and sunlight, while that of PAHs in dust samples taken from the SSI was not affected by those environmental factors. Moreover, some PAHs cause cancer to people in contact, however, the National Technical Regulation on domestic solid waste incinerators in Vietnam does not have threshold parameters for the concentration of PAHs [13].

The highest levels of Σ_{16}PAHs were found in November, ranging from 101.56 to 139.48, with a mean of 123.36 ± 14.06 µg/m^3. In contrast with November, the concentration of the Σ_{16}PAHs Vinh Phuc was lowest in April (min–max: 97.83–113.0 µg/m^3; mean: 106.55 ± 5.63 µg/m^3). The concentration of PAHs in the sampling months is not significantly different; the possible explanation could be due to the amount or pattern of biomass in the incinerator, which requires further investigation. Furthermore, PAH concentrations tend to decrease in the following order: L–PAH (min–max: 59.28–65.28 µg/m^3; mean: 62.61 ± 2.15 µg/m^3) > H–PAH (22.32–32.02; 28.9 ± 3.6)> M–PAH (19.01–22.95; 21.28 ± 1.46). This is consistent with simple incineration conditions that are more beneficial to the further degradation and conversion of PAHs with lower molecular weight (LMW) [14].

The total amount of carcinogenic PAHs compounds among the BaA, Chr, BbF, BkF, BaP, Ind, BghiP, and DahA ranged from 22.66 to 58.36. Ind (13.90–34.54) has the highest concentration in eight carcinogenic PAHs, while BkP (0.22–0.45) has lowest.

3.2. PAHs composition in dust samples

In terms of composition analyses, all 16 PAHs congeners were found in the soil samples collected. The following were the mean percentages of PAHs congeners in all dust samples: Nap (29.64), Acy (0.22%), Ace (0.55%), Flu (19.1%), Phe (0.4%), Ant (5.81%), Pyr (11.75%), Flt (6.24%), BaA (0.5%), Chr (0.16%), BbF (2.1%), BkF (0.2%), BaP (0.17%), Ind (17.3%), BghiP (4.4%), DahA (1.46%) (Figure 5). Low molecular weight PAHs like Nap, Flu, Phe, and Ant was the most abundant in the dust sample. L–PAHs were typically produced by biomass (grass, wood) and coal burning (low or moderate–temperature combustion processes), while H–PAHs were produced by vehicular emissions and industrial fuel combustion (high–temperature from combustion processes). The analysis of the PAHs profile in incinerator dust samples revealed that M–PAH and H–PAHs predominated. In 16 PAHs, four–ring PAH homologs contribute the majority, with a progression of two–ring >three–ring > six–ring > four–ring > five–ring. There is a direct correlation between PAH abundance and combustion processes. Due to this, PAHs are produced in different ways in different types of combustion. In the analyzed dust, L–PAH compounds dominated (55.72%), which indicates that combustion is the primary source of PAHs along the incinerator.

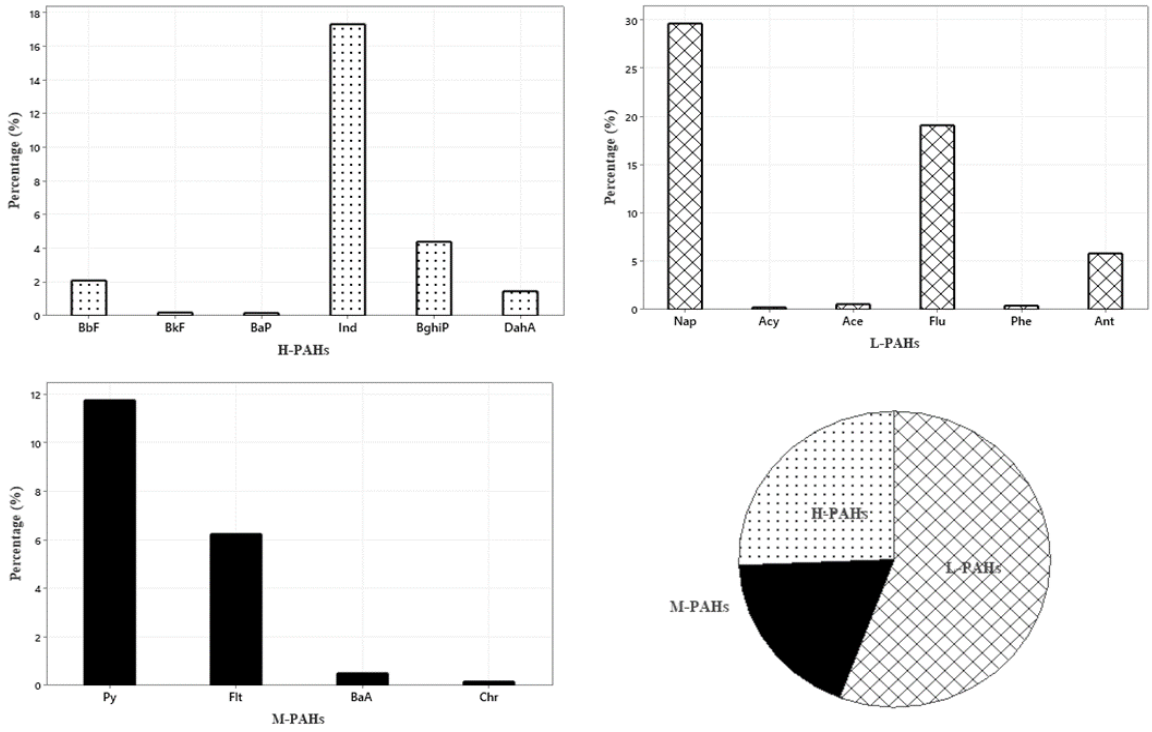

Figure 5. The percentage of PAHs concentration in dust samples from the chimneys of the SSI.

Table 3 contains isomeric ratios of selected individual PAHs compounds that can be used to discuss contaminant sources in greater detail.

Table 3. The isomeric ratio of PAHs and emission sources.

Isomeric ratio	**Ratio values**	**Emission sources** [(a)]
Ant/(Ant+Phe)	<0.1	Petroleum contamination
	>0.1	Combustion
Flt/(Flt+Pyr)	>0.5	Combustion of grass, wood, and coal
		Petroleum contamination
	<0.4	Burning of petroleum
	0.5 – 0.4	

Isomeric ratio	Ratio values	Emission sources [(a)]
BaA/(BaA+Chr)	>0.35	Combustion sources
	0.20 – 0.35	Mixed source
	<0.20	Petroleum sources
Ind/(Ind+BghiP)	<0.20	Petroleum contamination
	0.20 – 0.50	Fossil fuel combustion
	>0.50	Incomplete combustion of grass, wood, and coal

(a): [15–16]

At present, no study in Vietnam has published the ratio of PAHs in dust samples emitted from small–scale domestic waste incinerators. Therefore, the results on the ratio of PAH in dust samples from this study can be used to determine the source of PAH emissions caused by the burning of domestic waste (Figure 6).

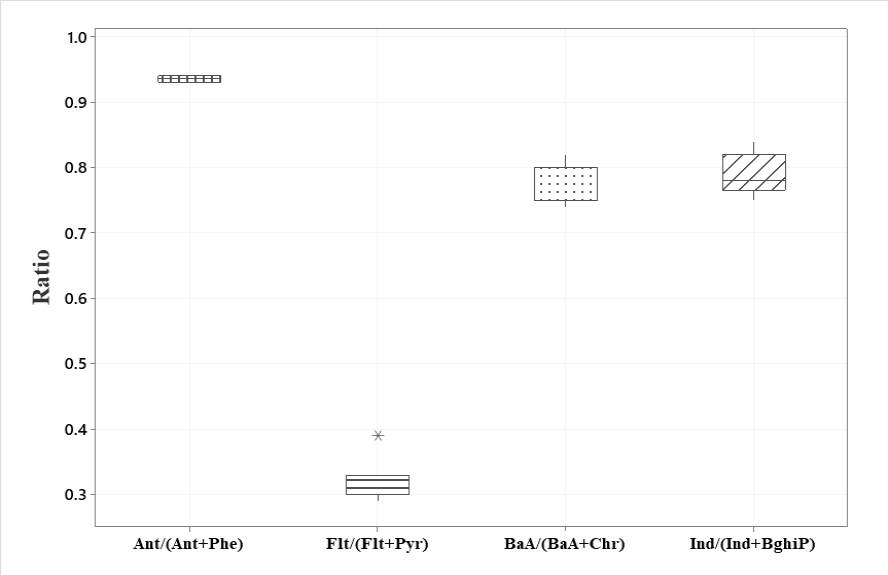

Figure 6. Range of ratio of some typical PAHs in the samples in this study.

3.3. Emission factor of PAHs

Studies on the emission factor of PAHs have been conducted from different components such as cellulose, hemicellulose, and lignin [17–18]; however, only previous studies have examined the emission factor of PAHs from rice straw in Vietnam [17, 19–20]. This is the first study in Vietnam to report on a system for detecting PAHs in the chimneys of small–scale incinerators. Table 4 displays the emission factors of individual PAHs in dust emitted from SSI chimneys. The total Σ_{16}PAHshad a mean emission factor of 10.17 ± 2.03 mg/kg. Overall, the EF of Σ_{16}PAHs levels determined during this study were similar to previous studies.

Table 4. The emission factor of PAHs (mg/kg) in this study and comparison with other studies.

Compound	The emission factor of PAHs (mg/kg–dry)					
	This study (burning biomass)	Burning rice straw, open experiment[(a)]	Burning rice straw, hood experiment[(b)]	Hood experiment[(c)]	Burning leaf litter[(d)]	Burning maize residue[(d)]
Nap	0.120	0.14	n.a.[(e)]	0.39	0.005	0.005
Acy	0.30	0.12	n.a.	n.a.	0.006	0.005
Ace	0.004	0.14	n.a.	0.002	0.000	0.000
Flu	0.0445	0.02	0.02	n.a.	0.011	0.005
Phe	0.198	0.16	n.a.	0.02	0.073	0.030
Ant	0.059	0.08	n.a.	0.01	0.037	0.034

Compound	The emission factor of PAHs (mg/kg–dry)					
	This study (burning biomass)	**Burning rice straw, open experiment[(a)]**	**Burning rice straw, hood experiment[(b)]**	**Hood experiment[(c)]**	**Burning leaf litter[(d)]**	**Burning maize residue[(d)]**
Py	0.064	1.12	0.01	0.26	0.100	0.037
Flt	0.173	6.58	n.a.	0.49	n.a.	n.a.
BaA	0.0023	0.07	0.03	0.11	0.076	0.040
Chr	0.0018	0.91	0.04	0.15	0.117	0.050
BbF	0.0016	1.26	0.08	0.12	0.115	0.055
BkF	0.0018	0.20	0.04	0.05	0.069	0.041
BaP	0.0047	0.85	0.12	0.11	0.045	0.032
Ind	0.0054	0.02	0.10	n.a.	0.055	0.041
BghiP	0.0212	0.07	0.14	0.02	n.a.	n.a.
DahA	0.0149	0.17	n.a.	0.08	0.047	0.022
Σ_{16}PAHs	10.17	12.53	15.12	1.8	0.910	0.469

(a): [17]; (b): [19]; (c): [20]; (d): [20]; (e) n.a.: not available.

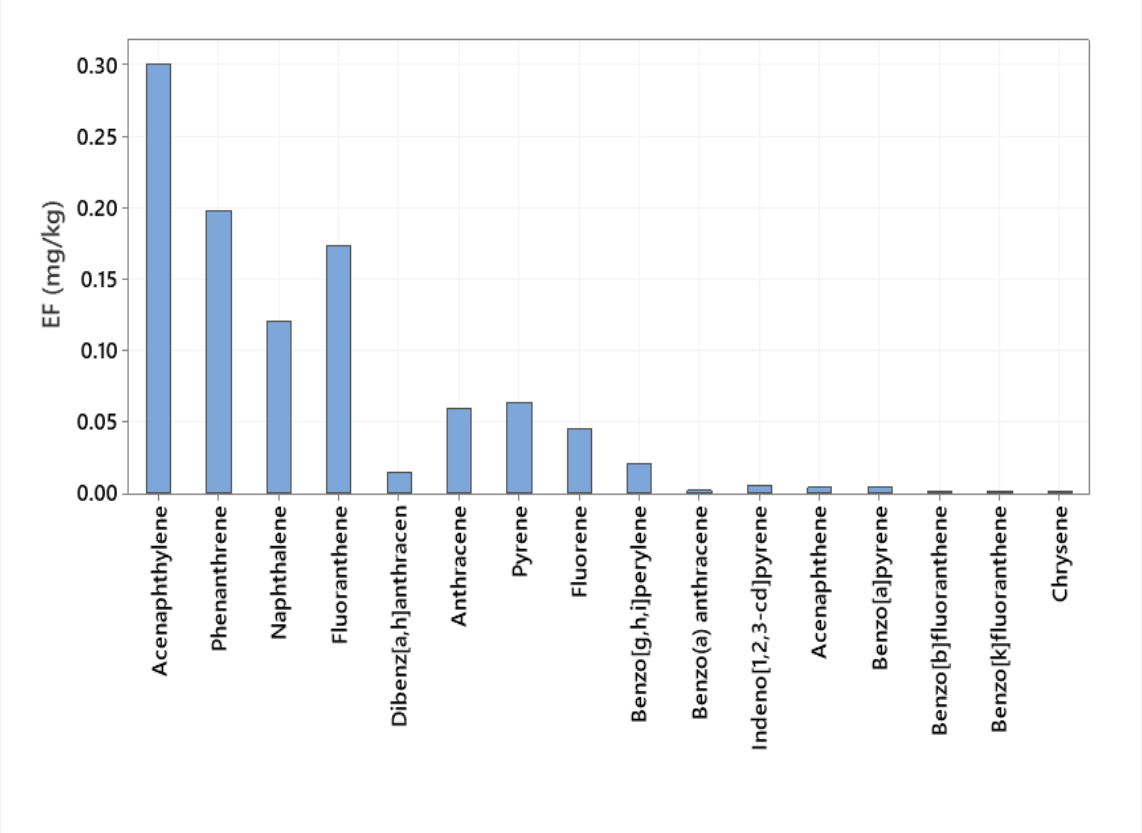

Figure 7. The mean of emission factor of PAHs of this study.

According to [21], the average Σ16PAHs emission factor from leaf litter burning and maize residue burning in Chamber was 0.910 and 0.469 mg/kg, respectively. According to [17], the total EF ofΣ_{16}PAHs of rice straw combustion in the Mekong Delta of Vietnam was 12.53 mg/kg. The EF ofΣ_{16}PAHs, on the other hand, showed a significant amount of variability due to differences in combustion conditions such as temperature, oxygen content, and biomass components. The composition of domestic waste includes organic matter, wastepaper, glass, metal, and plastic materials.

An average emission factor is shown for each PAHs (Figure 7). The EFs of each PAHs from the chimneys in descending order were Acy (0.3) > Phe (0.198) > Flt (0.173)> Nap (0.12) > Pyr (0.064) > Ant (0.059) > Flu (0.0445) > BghiP (0.0212) > DahA (0.015) > Ind (0.0054) >BaP (0.0047). PAHs such as Chr, BbP, BkP, and BaA have a relatively low emission factor average of approximately 0.002.

4. Conclusion

PAHs emission from SSI in Yen Lac district, Vinh Phuc province, Vietnam was investigated. Sixteen representative PAHs were revealed in dust samples taken from the Sankyo incinerator. PAHs levels in samples are in the medium range comparison with other incinerators in Vietnam. The PAHs composition shows that H–PAHs have a percentage higher than M–PAHs and L–PAHs. The PAHs emission factor are ranged from low to medium values which depend on each PAHs. Several substances in the group of PAHs are potentially carcinogenic and therefore require further environmental risk studies in the future. These are the initial results on the emission factor of PAH due to domestic waste incineration in rural areas. To confirm further and to be able to apply in the future inventory of PAH emissions, monitoring sessions and sample numbers must be expanded.

Authors contribution: Constructing research idea: N.T.D., V.D.T.; Select research methods: N.T.D., V.D.T.; Data processing: N.T.D., V.D.T., N.N.M.H.; Sample analysis: N.T.D.; Take samples: N.T.D.; Writing original draft preparation: N.T.D., V.D.T., N.N.M.H.; Writing review and editing: N.T.D., V.D.T.

Acknowledgments: This research is funded by Vietnam National Foundation for Science and Technology Development (NAFOSTED) under grant number "105.08–2020–05". The authors would like to thank the strong research group ROOM, Environmental and life science research Laboratory, Thuyloi University for their support during the research.

Conflicts of interest: The authors declare that this article was the work of the authors, has not been published elsewhere, has not been copied from previous research; there was no conflict of interest within the author group.

References

1. Tuyen, L.H.; Tue, N.M.; Suzuki, G.; Misaki, K.; Viet, P.H.; Takahashi, S.; Tanabe, S. Aryl hydrocarbon receptor mediated activities in road dust from a metropolitian area, Hanoi Vietnam: Contribution of polycyclic aromatic hydrocarbons (PAHs) and human risk assessment. *Sci. Total Environ*. **2014**, *491–492*, 246–254.
2. Hoang, A.Q.; Trinh, H.T.; Nguyen, H.N.M.; Nguyen, T.Q.; Nguyen, T.X.; Duc, T.V; Nguyen, T.T.; Do, T.Q.; Minh, T.B.; Tran, T.M. Assessment of cyclic votatile methylsiloxanes (cVMs) in indoor dust from different microenviroments in northern and central Vietnam. *Environ. Geochem. Health.* **2022,** https://doi.org/10.1007/s10653-022-01298-6.
3. Mosallaei, S.; Hashemi, H.; Hoseini, M.; Dehghani, M.; Naz, A. Polycyclic aromatic Hydrocarbons (PAHs) in household dust: The association between PAHs, cencer risk and sick building syndrome. *Build Environ.* **2023**, *229*, 109966.
4. Cave, M.R.; Wragg, J.; Beriro, D.J.; Vane, C.; Thomas, R.M.; Taylor, C. An overview of research and development themes in measurement and occurrences of polyaromatic hydrocarbons in dusts and particulates. *J. Hazard Mater*. **2018**, *360*, 373–390.
5. Patel, A.B.; Shaikh, S.; Jain, K.R.; Desai, C.; Madamwar, D. Polycyclic aromatic hydrocarbons: Sources, toxicity, and remediation approaches. *Front Microbiol.* **2020**, *11*, 562813.
6. Iwegbue, C.M.A.; Ehigbor, M.J.; Tesi, G.O.; Eguavoen, O.I.; Martincigh, B.S. Occurrence, sources and exposure risk of polycyclic aromatic hydrocarbons (PAHs) in street dusts from the Nigerian Megacity, Laos. *Polycycl. Aromat. Compd.* **2022**, *1*, 49–69.
7. Jesus, F.; Pereira, J.L.; Campos, I.; Santos, M.; Re, A.; Keizer, J.; Nogueira, A.; Goncalves, F.J.M.; Abrantes, N.; Serpa, D. A review on polycyclic aromatic

hydrocarbons distribution in freshwater ecosystems and their toxicity to benthic fauna. *Sci. Total Environ*. **2022**, *820*, 153282.

8. Anh, H.Q.; Tue, N.M.; Tuyen, L.H.; Minh, T.B.; Viet, P.H.; Takahashi, S. Polycyclic aromatic hydrocarbons and their methylated derivatives in settled dusts from end–of–life vehicle processing, urban, and rural areas, northern Vietnam: Occurrence, source apportionment, and risk assessment. *Sci. Total Environ*. **2019**, *672*, 468–478.
9. Dung, N.T. PhD Thesis – Research on the level of emissions and diffusion of Polycyclic aromatic hydrocarbons (PAH) in Hanoi, Hanoi University of Science and Technology, Hanoi, 2005.
10. Takahashi, S.; Tuyen, L.H.; Tue, N.M.; Suzuki, G.; Viet, P.H.; Subermania, A.; Bulbule, K.A; Parthasarathy, P.; Ramathang, A.; Tanabe, S. Methylated and unsubstituted polycyclic aromatic hydrocarbons in street dust from Vietnam and India: Occurrence, distribution and *in vitro* toxicity evaluation. *Environ. Pollut*. **2014**, *194*, 272–280.
11. Shu, W.B.; Zhao, Y.B.; Ni, H.G; Zheng, H. Size–dependent emission characteristic of airborne parent and halogenated PAHs from municipal solid waste incinerators in Shenzen, China. *Chemosphere* **2018**, *192*, 250–257.
12. Mao, I.F.; Chen, C.N.; Lin, Y.C.; Chen, M.L. Airborne particle $PM_{2.5}/PM_{10}$ mass distribution and particle–bound PAH concentrations near a medical waste incinerator. *Atmos. Environ.* **2007**, *11*, 2467–2475.
13. Ministry of Natural resources and Environment.National Technical Regulation on Domestic Solid Waste Incinerator. QCVN 61–MT: 2016/BTNMT
14. Chen, Y.; Zhao, R.; Xue, J.; Li, J. Generation and distribution of PAHs in the process of medical waste incineration. *Waste Manage.* **2013**, *33*, 1165–1173.
15. Ming, H.W.; Liping, J.; Gene, J.Z.; Minh, T.B.; Bruce, R.; Liqi, C. Persistent toxic substances in remote lake and coastal sediments from Svalbard, Norwegian Arctic: Levels, sources and fluxes. *Environ. Pollut*. **2009**, *157*, 1342–1351.
16. Hideshige, T.; Mahua, S.; Ayako, T.; Kaoruko, M.; Michio, M.; Mohamad, P.Z. Sources of sedimentary PAHs in tropical Asian waters: Differentiation between pyrogenic and petrogenic sources by alkyl homolog abundance. *Mar. Pollut. Bull.* **2009**, *58*, 189–200.
17. Phuong, P.T.H.; Nghiem, T.D.; Thao, P.T.M.; Nguyen, T.D. Emission factors of selected air pollutants from rice straw open burning in the Mekong Delta of Vietnam. *Atmos. Pollut. Res.* **2022**, *13*, 101353.
18. Wang, J.; Jiang, H.; Chen, Y.; Han, Y.; Cai, J.; Peng, Y.; Feng, Y. Emission characteristics and influencing mechanisms of PAHs and EC from the combustion of three components (cellulose, hemicellulose, lignin) of biomass. *Sci. Total Environ*. **2023**, *859*, 160359.
19. Pham, C.T.; Ly, B.T.; Nghiem, T.D.; Pham, T.H.P.; Minh, N.T.; Tang, N.; Hayakawa, K.; Toriba, A. Emission factors of selected air pollutants from rice straw in Hanoi, Vietnam. *Air Qual. Atmos. Health.* **2016**, *14*, 1757–1771.
20. Kim Oanh, N.T.; Ly, B.T.; Danutawat, T.D.; Manandhar, R.B.; Prapat, P.; Simpson, C.D.; Liu, L.S. Characterization of particulate matter emission from open burning of rice straw. *Atmos. Environ.* **2011**, *45*, 493–502.
21. Wiriya, W.; Chantara, S.; Sillapapiromsuk, S.; Lin, N.H. Emission profiles of PM10–bound polycyclic aromatic hydrocarbons from biomass burning determined in chamber for assessment of air pollutants from open burning. *Aerosol Air Qual. Res.* **2016**, *16*, 2716–2727.

VIETNAM JOURNAL OF HYDROMETEOROLOGY

Research Article

Trend and forecast the saline intrusion at estuaries in the coastal Mekong delta: A case study of the coastal sub–region between the Tien and Hau rivers

Nguyen Van Hong[1*], Nguyen Thao Hien[1], Nguyen Thi Diem[2], Le Duc Thuong[2]

[1] Sub–Institute of Hydrology Meteorology and Climate Change; nguyenvanhong79@gmail.com; nthien2710@gmail.com
[2] Mien Trung University of Civil Engineering, Phu Yen, Viet Nam; nguyenthidiem@muce.edu.vn, leducthuong1980@gmail.com

*Corresponding author: nguyenvanhong79@gmail.com; Tel.: +84−913613206

Received: 15 December 2022; Accepted: 16 February 2023; Published: 25 March 2023

Abstract: Saline intrusion is a big challenge for the Mekong Delta region, a negative factor that greatly affects water and food security. In particular, the most severely affected areas are the coastal sub–regions between the Tien and Hau rivers in the lower Mekong basin, which are directly influenced by the tidal regime. In the dry season, the salinity changes complicatedly from year to year. It is necessary to analyze and assess the trend and forecast of saltwater intrusion in 2 main tributaries. In this paper, the study are used Mann–Kendall non–parametric testing method, Sen's slope estimator test, and the MIKE 11 model (HD+AD). The results are evaluated based on statistical analysis at the significance level $\alpha < 0.1$ (probability of making type I error is 10%), ensuring the exclusion of extremely unstable values to the trend, the selecting the station that is qualified to calculate the Sen's slope tr Sen's slope trend will represent a typical regional saline intrusion regime feature. At the same time, the article also gives the results of forecasting the level of saline intrusion at a few main stations on the two tributaries of the Tien and Hau rivers in 2022.

Keywords: Saline intrusion; Tien river; Hau river; Mann–Kendall; Sen's slope; Forecast.

1. Introduction

The Tien and Hau river systems are two important international waterways from Phnom Penh (Cambodia) flowing through the center of the Mekong Delta in the East Sea, facilitating the development of regional economic trade with ASEAN countries and the world. Currently, most of the socio–economic centers of the Mekong delta are formed and developed along these two tributaries.

However, the Mekong delta is a young delta, which has been expected to be increasingly affected by climate change, especially saline intrusion, which is a negative factor that greatly affects resource security. water and food security. The problem of sea level rise, high tide, lack of upstream flow, hot weather, high and water demand, caused the Mekong delta to experience dry years, causing heavy damage to the economy, society, and the environment. In 1998, 2005, and 2010, especially in recent years, there were two historic salinity intrusions with the earlier occurrence and deeper penetration in the river and canal system [1]. Comparison of saline intrusion in 2016 and 2020 in the Mekong delta: Tien river system (Cua Dai, Cua Tieu, Ham Luong), saline intrusion from 65 to 95 km in 2020; On the Hau river tributary, in 2016 the intrusion into the field is about 55–60 km, in 2020 there is little change, from 60–65 km [2]. According to the RCP4.5 scenario by the middle of the 21st century, the sea level will rise by 23 cm (13÷31 cm); By the end of the 21st century, the sea level will rise

by 53 cm (32÷77 cm). According to the RCP8.5 scenario, by the middle of the 21st century, sea level could rise by 28 cm (19÷37 cm), and by the end of the 21st century, by 73 cm (48÷105 cm) [3]. Rising sea levels will push salinity further inland along major tributaries such as the Tien and Hau rivers, especially in the dry season when the Mekong river flows are lowest, contaminating large farming areas [4–15].

Several studies and assessments on the fields of meteorology, hydrology, and climate change relating to using the Mann–Kendall non–parametric test method and Sen's slope estimator test in Vietnam were studied in Vietnam. Such as analysis and calculation of salinity evolution: [16–19] using integrated SWAT and HEC–RAS models to simulate and analyze the trend of flooding and saline intrusion for Ho Chi Minh City according to the baseline and scenario scenarios. RCP4.5 (2016–2035) follows the Mann–Kendall method, combines the Theil–sen slope, and creates a dynamic partition map. On the field hydrology–groundwater hydraulics: [20] assesses the level of underground water level decline in Holocene and Pleistocene aquifers in the upper MD, using Mann–Kendall and Sen's slope estimator test methods in the calculation. Rainfall distribution, additional rainfall in two periods of the rainy season and dry season, period 1995–2015. For analysis and assessment of climate change: [16] calculates the trend of changes in rainfall during the period: 15', 30', 45', 60', 90', 120', and 180' at Tan Son Hoa station in the period 1971–2016 using Mann–Kendall non–parametric testing method and Sen's slope estimator test. [17] Assess the climate change trend of Binh Phuoc province in the period 1981–2018 on the factors of average temperature, and annual rainfall, combined with the assessment according to the scenarios RCP4.5 and RCP8.5 for different periods: 2025, 2030, 2050 and 2100.

The results obtained from the above studies, prove that the Mann–Kendall non–parametric test method and Sen's slope estimator test method are effective and have high reliability [16–19]. To have a basis for developing prevention and mitigation measures, strategic measures to cope with drought and salinity in the Mekong delta, and appropriate economic transformation policies for aquaculture, fishing, or energy development clean quality but still ensure and maintain a high–quality agricultural economy, it is necessary to study, analyze and evaluate the trend of saline intrusion changes from the past to the current status. From there, it is possible to make predictions about the level of development in the future. Therefore, this paper presents a study to assess the trend of saline intrusion change in the 5 coastal sub–regions between the Tien and Hau rivers in the period 1997 to 2022. To have a better overview of the fluctuations of saline intrusion the paper used the 26 years data series of the maximum salinity value from the years 1997 to the present time in 2022 in 5 coastal provinces: Tien Giang, Ben Tre, Tra Vinh, Vinh Long, Soc Trang.

2. Materials and Methods

2.1. Study area and data collection

The Mekong Delta is divided into 4 sub–regions: the East Coast, the Dong Thap Muoi, the Ban Dao Ca Mau, and the Tu Giac Long Xuyen. the East Coast includes 4 provinces: Tien Giang (the part along the Tien River accounts for 53% of the province's area, with a length of 115 km within the province), Ben Tre (including Tien river: 83 km, Ba Lai river 59 km, Ham Luong: 71 km, Co Chien: 82 km), Vinh Long (with Co Chien river being a branch of the Tien River, with a length of 90km, Hau river flowing through has a length of about 75 km), Tra Vinh (covered by Tien, Hau River with 02 gates Cung Hau and Dinh An, total length 578 km). Although Soc Trang province belongs to the Ban Dao Ca Mau, it is a coastal province located at the lower end of the Hau River, with an inadequate river system with large and small islets, more than 50 km along the Hau river and 2 large estuaries are Dinh An, Tran De empties into East Sea [21–23].

The series of data used is the maximum salinity value in the dry season (S_{max}) in 26 years from 1997 to 2022 at some stations on the main tributaries (Figure 1 and Table 1).

Figure 1. Study area and stations used to assess the trend of salt intrusion in the coastal sub–region between the Tien and Hau rivers.

Table 1. List of stations to assess the trend of salt line intrusion change in the Tien and Hau rivers.

Number	Salinity Monitoring Station	Sites
1	Vam Kenh	Cua Tieu, Tan Thanh, Go Cong Dong–Tien Giang
2	Ben Trai	Co Chien, An Thuan, Thanh Phu–Ben Tre
3	Binh Dai	Cua Dai, Binh Thang, Binh Dai–Ben Tre
4	Tra Vinh	Brand of Cung Hau, Co Chien river, Tra Vinh
5	Tra Kha	Cua Dinh An, Tra Cu–Tra Vinh
6	An Thuan	Ham Luong, An Thuy, Ba Tri–Ben Tre
7	Cau Quan	Brand of Đinh An, Hau river, Tieu Can–Tra Vinh
8	Đai Ngai	Hau, Đai Ngai, Long Phu–Soc Trang
9	Hoa Binh	Cua Tieu, Vinh Huu, Go Cong Tay–Tien Giang
10	Hung My	Co Chien, Hung My, Chau Thanh–Tra Vinh
11	Huong My	Brand of Co Chien, Huong My, Mo Cay Nam–Ben Tre
12	My Thanh	Cua Tran De, Vinh Hai, Vinh Chau–Soc Trăng

2.2. Theoretical basis of Mann–Kendall (MK–test) non–parametric testing method

The Mann–Kendall test [18] compares the relative sizes of elements in the data series, which can avoid local maxima or minima of the value series. If it is hypothesized that there is a time series data (x_1, x_2,…,x_n) with x_i representing the data at the time i, then each data value at each time point is compared with the values. across the time series. The initial values of the Mann–Kendall statistic, S are 0 (that is, there is no trend). Then the Mann–Kendall (S) statistic is calculated by:

$$S = \sum_{i=1}^{n-1} \sum_{j=i+1}^{n} sign(x_j - x_i)$$

where

$$sign(x_j - x_i) = \begin{cases} 1khi(x_j - x_i) > 0 \\ 0khi(x_j - x_i) = 0 \\ -1khi(x_j - x_i) < 0 \end{cases} \quad (1)$$

Value S > 0 indicates an uptrend, and S < 0 indicates a downtrend. However, it is necessary to calculate the probabilities associated with S and n to determine the significance level of the trend. The variance of S is calculated according to the formula:

$$VAR(S) = \frac{1}{18}\left[n(n-1)(2n+5) - \sum_{p=1}^{g} t_p(t_p-1)(2t_p+5) \right] \quad (2)$$

where g is the number of groups with the same value, t_p is the number of elements in the path group.

The normal value Z of S follows the law of the normal distribution:

$$Z = \frac{S-1}{[VAR(S)]^{1/2}}, S > 0 \quad (3)$$

where Z = 0, S = 0

$$Z = \frac{S+1}{[VAR(S)]^{1/2}}, S < 0 \quad (4)$$

2.3. Sen's slope

To determine the magnitude of the trend of the Q series (trend line slope) we use Sen's slope estimator test method [19]. Q is the median of the series n(n–1)/2 elements.

$$Q = median\left\{ \frac{x_j - x_i}{j-i} \right\} \quad (5)$$

with i = 1,2,.., n–1; j>i

Q > 0: chain tends to increase and vice versa

2.3. Establishing a model for predicting salinity in 2 tributaries of the Tien and Hau rivers

Regarding the water environment, to predict the impact of saline intrusion on the water resources of the Mekong River, it is appropriate to choose MIKE 11 as the key model. MIKE 11 (HD+AD): 1–D model for river and canal system, using input data series from MIKE NAM to simulate flow in a river basin. Combined with the AD module (1D–dimensional diffusion) to simulate the propagation of salinity on the river system.

Two important upstream factors that dominate the water resources in the Mekong Delta are the amount of water stored in Tonle Sap (TonleSap), which helps to regulate and limit the flood flow in the Mekong Delta during the flood season and increase the source of fresh water during the flood season. dry season. And the flow to Kratie station (the beginning of the Mekong Delta) is located about 300 km upstream from the Vietnam–Cambodia border, representing the starting point of the lower Mekong. The downstream point is 8 estuaries: (1) Vam Kenh, (2) Binh Dai, (3) An Thuan, (4) Ben Trai, (5) My Thanh, (6) Ganh Hao, (7) Song Doc and (8) Rach Gia (Figure 2).

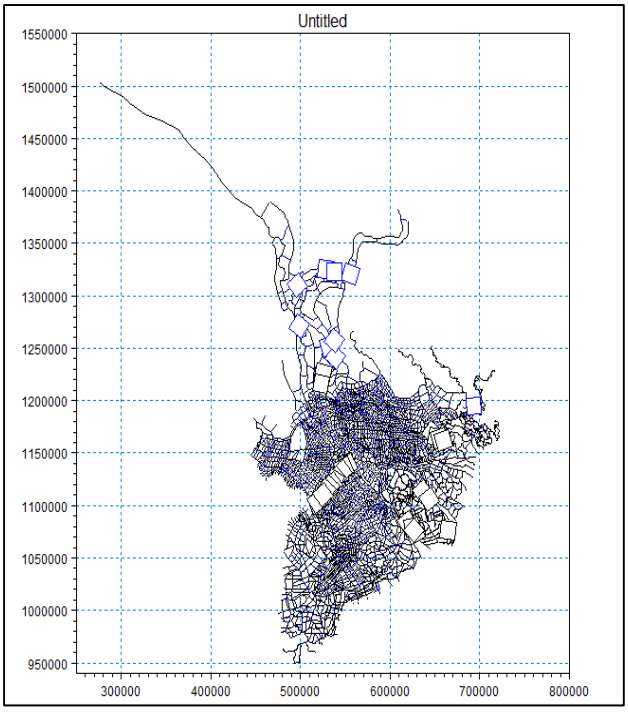

Figure 2. Network of Mekong River Delta.

The following table presents factors affecting saline intrusion in the Mekong Delta:

Table 1. Factors affecting the flow–saltwater intrusion in the Mekong Delta.

Impact factors	Featured	Methods forecast forecasts
Upstream flow to the Mekong Delta	- The development of hydropower in the upstream area; - Water regulation in upstream reservoirs; - Demand for upstream water.	- Monitor rainfall at the end of the flood season and capture information on water reserves at the beginning of the dry season in upstream reservoirs.
Water level	- There is an increasing trend over time; - Bringing salinity deep into the field.	- Tidal forecast results.
Rainfall	- dry season: low; - difficult to forecast seasonal purchases.	- Follow the current data.
Construction of sluice to prevent saltwater	- to build in coastal areas and small tributaries.	- Present.

Main river network system of the Mekong River Basin and data of irrigation works (salinity sluices):

Table 3. Construction of sluice to prevent saltwater.

Construction of sluice to prevent saltwater	Area serviced (hectare)	Featured
North Ben Tre	54,000	- Salt control; - Freshwater resources in coastal areas are still very difficult.
South Ben Tre	80,000	- Salt control; - Freshwater resources in coastal areas are still very difficult.
South Mang Thit	25,682	- Salt control; The last part of the system is worth switching to a salty–brackish ecology (shrimp farming);
Long Phu–Tiep Nhat	53,910	- Salt control; The last part of the system is worth switching to a salty–brackish ecology (shrimp farming); - Lack of fresh water in coastal areas.

3. Results and discussions

3.1. MK–test result

The results of Mann–Kendall testing at salinity measurement stations along Tien and Hau rivers in 5 provinces: Tien Giang, Ben Tre, Tra Vinh, Vinh Long, and Soc Trang are presented in Table 2.

Table 4. Mann–Kendall test results for salinity trends in the Mekong Delta.

Station	M	Min	Max	Mean	Std. deviation	MK–test (S)	Var(S)	P–value
Vam Kenh	26	20.2	30.9	25.6	2.3	–99	2051.7	0.030
Ben Trai	26	17.8	29.3	25.6	2.8	–21	2053.7	0.659
Binh Dai	26	17.5	29.4	25.8	2.8	57	2053.7	0.217
Tra Vinh	26	5.8	19.6	10.4	3.4	111	2056.3	0.015
Tra Kha	26	11.1	25.9	17.9	3.5	–16	2057.3	0.741
An Thuan	26	23.0	31.5	27.5	2.3	65	2054.3	0.158
Cau Quan	26	4.5	16.5	9.4	2.7	104	2057.3	0.023
Đai Ngai	26	3.4	14.6	9.2	2.9	2	2055.3	0.982
Hoa Binh	26	8.5	24.1	13.6	3.6	19	2053.7	0.691
Hung My	26	7.4	22.6	15.3	3.7	21	2056.3	0.659
Huong My	26	2.3	18.9	9.5	3.5	93	2053.7	0.042
My Thanh	26	18.3	35.8	24.9	4.7	–153	2058.3	0.001

Mann–Kendall test results show S>0 values at 8/12 stations, which shows that 2/3 of the stations along 2 tributaries of the Tien and Hau rivers have a trend of increased saline intrusion. The strongest growth was at Tra Vinh and Huong My stations (Co Chien river), and Cau Quan station (Hau river) with S values of 111–93–104, respectively.

However, in terms of statistical significance P–value has $\alpha < 0.1$ (probability of making type I error is 10%), removing extreme values, only 5 stations are Vam Kenh (Tieu gate), Tra Vinh and Huong My (Co Chien river), Cau Quan (Hau river), and My Thanh station (Tran De gate) met the requirements. The remaining stations all tend to increase/decrease clearly but the non–parametric level of the MK–test does not satisfy the significance $\alpha < 0.1$.

3.2. Changing trend of saline intrusion

Figure 3 shows the process of S_{max} change trend at Vam Kenh, Tra Vinh, Huong My, Cau Quan, and My Thanh stations according to the data series from 1997 to 2022. The results of increasing saline intrusion trend at 3 stations with an average speed (S–slope) are Tra Vinh station 0.2258 g/l/year; Cau Quan station 0.1731 g/l/year; Huong My station 0.1934 g/l/year. The remaining two stations, Vam Kenh in the Tien River estuary and My Thanh station at the Tran De estuary in the Hau river, tend to decrease by 0.1445 and 0.3812 g/l/year.

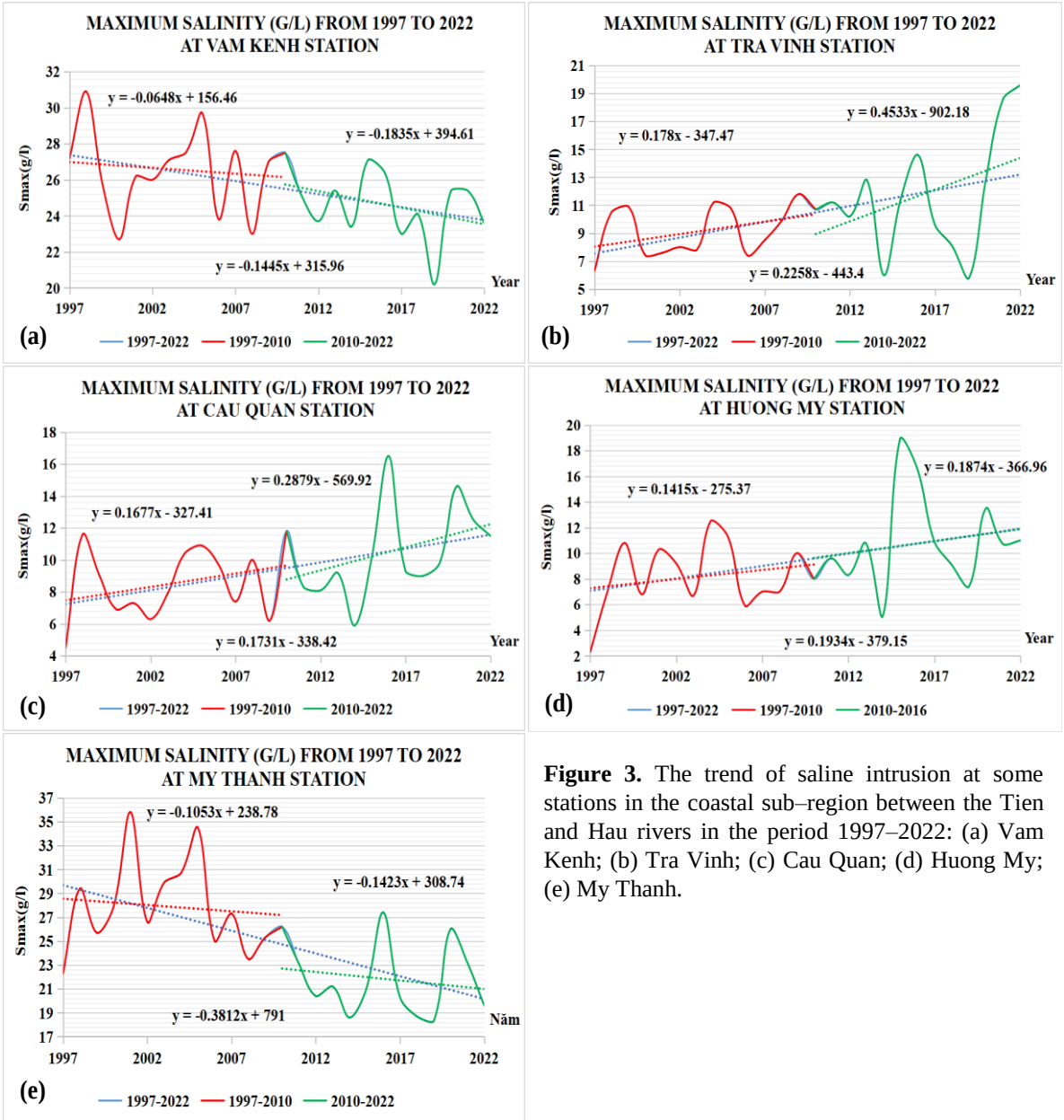

Figure 3. The trend of saline intrusion at some stations in the coastal sub–region between the Tien and Hau rivers in the period 1997–2022: (a) Vam Kenh; (b) Tra Vinh; (c) Cau Quan; (d) Huong My; (e) My Thanh.

In the calculated data series with a length of 26 years, it can be divided into two periods 1997–2010 (97–10) and 2010–2022 (10–22) to further consider the changes in salinity in the first 13 years and 12 years after. In most of the 5 calculation stations, Vam Kenh, Cau Quan, and Huong My stations, the up/down trend of each period compared to the average of many years does not change too much. The remaining two stations have trend slopes markedly different from the multi–year average value chain. At Tra Vinh station in the period 10–22, the growth trend is strong compared to the period 97–10. In contrast, the curve showing the fluctuation of salinity intrusion at My Thanh station has the S'slope period 97–10 and 10–22 decreasing relatively slightly compared to the multi–year average.

It was found that in the estuary area, salinity tends to decrease markedly, and in the inland area, on the contrary, the salinity increases rapidly, the salinity peak in recent years is much higher than in the previous period. According to the 26–year statistical data series, the highest salinity occurs in 1998, 2005, 2010, 2016, and 2020. Thus, the average salinity peak occurs once every 4–5 years.

However, the spread of salinity into the interior of the field clearly depends on the amount of water from upstream to the delta, especially the two main receiving sources at Tan Chau station (Tien river) and Chau Doc station (Hau river). The value of salinity concentration in the coastal area and tributaries here depends entirely on the tidal regime of the East and West seas, and to comprehensively assess the process of salinity fluctuations, many factors such as upstream currents must be considered. source, sea level rise, storm surge, climate change, demand for water in daily life, production, the operation process of a sluice gate to prevent saline intrusion, etc.

3.3. Forecast results of salinity intrusion in 2 tributaries of Tien and Hau rivers

The forecasts below are the highest salinity (S_x) from January to June 2022 with a forecast period of 1 time/month. At the same time, this forecast result is compared with data collected from the Southern Regional Hydrometeorological Station. From there, it is possible to accurately assess the predicted level of saline intrusion using the MIKE 11 model (HD+AD). The table below presents the evaluation results (Figure 4 and Table 5).

Table 5. The compares the forecast results with the reality.

	Station	River	Area	18–27/03/2022	
				Forecast results (S_{max})	Monitoring data
1	Vam Kenh	Cua Tieu	Tien Giang	22	21.8
2	Ben Trai	Co Chien	Ben Tre	22	19
3	Binh Đai	Cua Đai	Ben Tre	25	21
4	An Thuan	Ham Luong	Ben Tre	27	22.2
5	Tra Kha	Hau	Tra Vinh	13	14.2
6	Huong My	Co Chien	Tra Vinh	15	10.2
7	Hung My	Co Chien	Tra Vinh	20	12
8	Đai Ngai	Hau	Soc Trang	13	6

The time to choose the assessment is in the middle of the dry season (March) in 2022. Because currently, salinity usually reaches the maximum value. According to the forecast from the saline intrusion calculation model. In the Mekong Delta, salinity intrusion is greatest from March to early April and gradually decreases from mid–April onwards. From the end of May to November, the salinity intrusion in the South gradually weakens, with low intensity because this period coincides with the rainy season in the South and the water upstream of the Mekong River replenishes the Mekong Delta, so the salinity is washed away. salinity is reduced (especially in the coastal areas) and the saline boundary is restricted from entering the field.

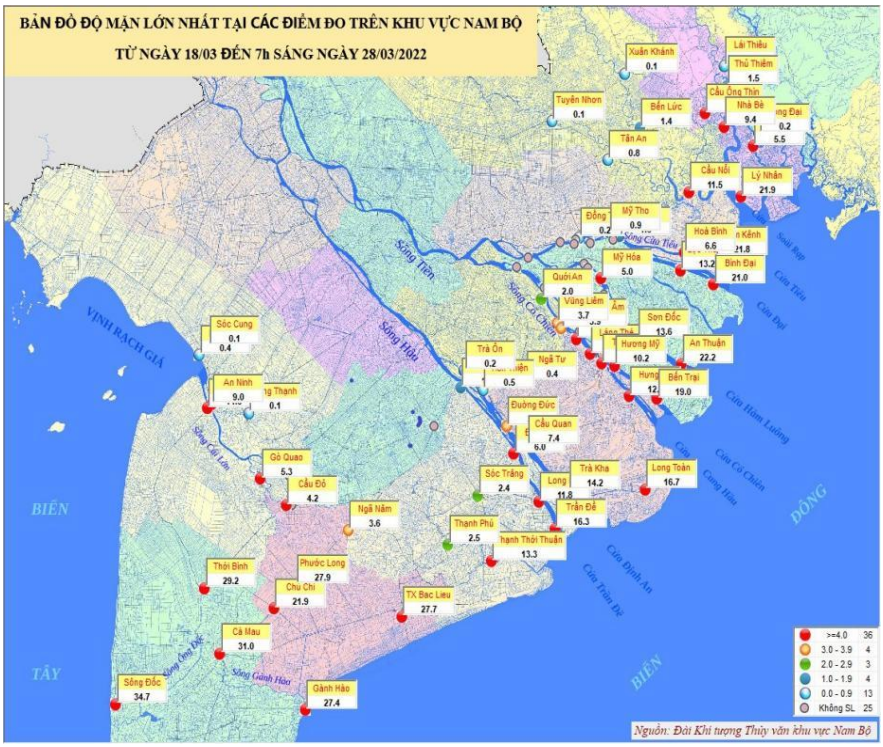

Figure 4. The map of the distribution of salinity at stations in the Southern region on March 18–27, 2022 (Resource: Southern regional hydrometeorological center).

4. Conclusion

The article has evaluated the trend of salinity change with a reliable and long enough data series of 26 years, from 1997 to the present time 2022 by the Mann–Kendall method and estimated Sen trend. It is found that, with the MK–test, there are many extreme values (local max, min) that appear to affect the general trend chain at the Mekong Delta salinity measurement stations. Out of 12 stations used for calculation, only 5 stations met the standard to estimate the Sen trend. However, in general, the trend of increasing salinity occurred in 8/12 stations and 4 stations tended to decrease according to calculated data.

The fluctuation of saltwater intrusion mainly depends on two main factors: the upstream flow of the Mekong Delta and the tidal regime in the East Sea. Part of the factor affecting the upstream flow is the amount of water at the end of the flood season. Kratie station and Kompng Luong station (Bien Ho) are considered as two points upstream of the Mekong River before pouring into the Red River Delta, which are decisive factors for the regulation of water to the Mekong Delta in the dry season. Therefore, to predict changes in saltwater intrusion in the future, it is necessary to study and evaluate the overall factors affecting the saltwater intrusion process.

Author contribution statement: Conceptualization and methodology: H.V.N., H.T.N.; validation, formal analysis: D.N.T.; investigation and project administration: H.T.N.; resources, data curation, software, draft: H.V.N., H.T.N., T.D.L; preparation and writing–original: H.V.N., H.T.N., D.N.T.; writing–review, and editing, visualization: H.V.N., H.T.N. All authors have read and agreed to the published version of the manuscript.

Acknowledgments: This research is completed in the program of regular assignment by the functions Decision No. 2339/QĐ–TNMT date 13th, Sept 2022 of MONRE of the Sub–Institute of Hydrometeorology and Climate Change in 2023, specifically Task 9: “Forecasting tides and saline intrusion in the main rivers of the Southern region”.

Competing interest statement: The authors declare no conflict of interest.

References

1. Dat, T.Q.; Likitdecharote, K.; Srisatit, T; Trung, N.H. Modeling The Influence of River Discharge and Sea Level Rise on Salinity Intrusion in Mekong Delta. In First Environment Asia International Conference on "Environmental Supporting in Food and Energy Security: Crisis and Opportunity, 2011, 685–701.
2. National Centre for Hydro–Meteorological Forecasting, 2/3/2020.
3. Ministry of Natural Resources and Environment, Climate Change Scenario. 2020.
4. Linh, V.T.; Liem, N.D.; Dung, H.M.; Loi, N.K. Research on the application of models for trending evaluation of flood and salinization in the climate change context: Pilot research in Ho Chi Minh city. *J. Hydrometeorol*. **2019**, EME2, 98–110.
5. Institute of Meteorology, Hydrology and Climate Change. The Impacts of Climate Change on Water Resources and the Mekong Delta Adaptation Measures. 2010.
6. Hong, N.V.; Dong, N.P. Simulation of saline intrusion in main rivers of Ba Ria – Vung Tau province under the context of climate change. *VN J. Hydrometeorol*. **2021**, *728*, 67–79.
7. Hong, N.V.; Dong, N.P. Studying building the flood scenarios in ho chi minh city by the impacts of climate change. *VN J. Hydrometeorol*. **2021**, *729*, 1–13.
8. Hong, N.V.; Hien, N.T.; Minh, N.T.T.; Toan, H.C. Forecasting saline intrusion under the influence of the northeast monsoon in the Mekong Delta. *VN J. Hydrometeorol.* **2021**, *9*, 23–36.
9. Hong, N.V.; Dong, N.P. Research on assessing the impact of saline intrusion on the water resources in Ho Chi Minh City in the context of climate change. *VN J. Hydrometeorol*. **2021**, *10*, 11–23.
10. Tri, D.Q. Application MIKE 11 model on simulation and calculation for saltwater intrusion in the Southern region. *VN J. Hydrometeorol*. **2016**, *671*, 39–46.
11. Nicholls, R.J.; Lowe J.A. Climate Stabilization and Impacts of Sea–Level Rise. Avoiding Dangerous Climate Change. Cambridge University Press, ISBN: 13 978-0-521-86471-8, 2006.
12. Hanh, P.T.T.; Furukawa, M. Impact of sea level rise on the coastal zone of Viet Nam. Bulletin of the College of Science, University of the Ryukyus, ISSN: 0286-9640. 2007.
13. Apel, H.; Khiem, M.; Quan, N.H.; Toan, T.Q. Brief Communication: Seasonal Prediction of Salinity Intrusion in The Mekong Delta. *Nat. Hazards Earth Syst. Sci.* **2020**, *20(6)*, 1609–1616.
14. Tien, K.D.; Adam, L.; Micheal, D.Y. Perceptions and responses to rising salinity intrusion in the Mekong River Delta: What drives a long–term community–based strategy. *Sci. Total Environ*. **2020**, *711*, 134759.
15. Khang, D.K.; Kotera, A.; Sakamoto, T.; Yokozawa, M. Sensitivity of Salinity Intrusion to Sea Level Rise and River Flow Change in Vietnamese Mekong Delta–Impacts on Availability of Irrigation Water for Rice Cropping. *J. Agric. Meteorol.* **2008**, *64*, 167–176.
16. Tin, N.V. Non–Parametric Mann–Kendall test for trend detection of the maximum of short–term rainfall in Ho Chi Minh City from 1971–2016. *J. Hydrometeorol*. **2017**, *11*, 52–55.
17. Nam, L.H. Constructing climate change scenarios for Binh Phuoc province. *J. Hydrometeorol*. **2020**, *717*, 32–43.
18. Kendall, M.G. Rank Correlation Methods. Charles Griffin, London, **1975**, pp. 272.
19. Sen, P.K. Estimates of the Regression Coefficient Based on Kendall's Tau. *J. Am. Stat. Assoc.* **1968**, 1379–1389.
20. Van, P.T.C. Assessment of groundwater level decline and the potential for

replenishment of the Holocene (qh): case studies in the upper Mekong Delta. *Vietnam J. Agric. Sci*. **2022**, *2*, 135–143.

21. World Bank. The Impact of Sea Level Rise on Developing Countries: A Comparative Analysis. World Bank Policy Research Working Paper 4136. 2007. Online available: http://go.worldbank.org/775APZH5K0 (accessed on 15 March 2017).
22. MONRE (Ministry of Natural Resources and Environment of Vietnam). Vietnam's special report on managing the risks of extreme events and disasters to advance climate change adaptation. Vietnam publishing house of Natural Resources, Environment and cartography, 2015.
23. Thuc, T.; Huong, T.T.T.; Thang, N.V.; Nhuan, M.T.; Tri, L.Q.; Thanh, L.D.; Huong, H.T.L.; Son, V.T.; Thuan, N.T.H.; Tuong, L.N. Special Report of Vietnam on Managing the Risks of Natural Disaster and Extreme Phenomena to Promote Climate Change Adaptation. Vietnam. Vietnam Publishing House of Natural Resources, Environment and Cartography. Hanoi, Vietnam, 2015.

VIETNAM JOURNAL OF HYDROMETEOROLOGY

Research Article

Assessment Model for Water Quality Progression of Gia, Re, and Da Do River for Drinking Water Purpose in Hai Phong City

An Thi Hoang[1]*, Hang Thi Dieu Tran[1], Anh Phuong Tran[1], Nam Anh Nguyen[1], Tu Van Tran[1], Chung Bao Tran[1]

[1] Water Resources Institute, Ministry of Natural Resources and Environment; Anht510@wru.vn; hangtd1001@gmail.com; phuongtran.monre@gmail.com; namanh.luna@gmail.com; trantuvfu@gmail.com; ChungTB26@wru.vn

*Corresponding author: anht510@wru.vn; Tel.: +84–963952484

Received: 15 February 2022; Accepted: 22 March 2023; Published: 25 March 2023

Abstract: Gia, Re, and Da Do Rivers are the main surface water resources providing fresh water to the habitants of Hai Phong City. They are at risk of water pollution due to the release of multiple waste streams along the rivers. The main objective of this study is to establish water quality models for Gia, Re, and Da Do Rivers using the MIKE 11 Ecolab model. The studied pollutants include BOD_5, NH_4^+, NO_3^-, DO, etc. Pollution trends can be predicted using pollutant load generation in the water quality model. The simulation results give relatively high correlation coefficients (0.8–0.88) and the relative error of 4–18% ensures the quality of the model. Concurrently, the research team calculated the water quality index (WQI) in the 2020 dry season for eleven locations on three rivers Gia, Re and Da Do based on the following parameters: T, pH, COD, BOD_5, NH_4^+, NO_3^-, DO, As, Pb, Coliform, E. coli, etc. WQI results, with the combination of field observation and simulations, show that the water quality of Gia River is very good of Re river is an average; while the water quality of Da Do River decreases gradually from upstream at a good level to downstream at an average level. These WQI results provide a high–level assessment of the river water quality, which will assist the management of surrounding wastewater treatment systems to maintain the supply of water purpose of these three rivers to Hai Phong City.

Keywords: Water Quality; MIKE 11 Model; WQI; Gia River; Re River; Da Do River.

1. Introduction

Water is a finite resource which plays an important role in life, in which water quality is always the most urgent matter of concern. Hai Phong is a city located in the coastal estuary region, downstream of the Red – Thai Binh River system of Vietnam. The city's water quality is affected simultaneously by the impact of polluting activities in the localities located in the upper reaches of the rivers as well as within the city [1]. In addition, because it is located in the estuary and coastal areas, the water source is always at risk of saltwater intrusion from the sea, and this tends to become more and more serious due to the influence of sea level rise. The city's fresh water supply is being taken mainly from the three main freshwater rivers of Hai Phong, namely the Re River, Gia River, and Da Do River. The water of Gia, Re, and Da Do Rivers is monitored and sampled by the Environmental Monitoring Center quarterly, with the analytical parameters [2]. According to the monitoring results until September 2020, most of the rivers show signs of pollution by nutrients and organic substances such as N, P, BOD_5, and Coliform.

Pollution loads exceeding national standard degrade water quality and negatively impact local economies and human health. With this issue, a good assessment and implementation

of the water quality controls will contribute greatly to the protection of water resources, ensuring the harmony between economic development and environmental protection. In water quality assessment, mathematical models play a central role. These models provide both spatial and temporal high-resolution water quality information as well as assess the ranges of water quality under different scenarios of socio-economic development and environmental protection. Mathematical models were built to simulate water quality parameters and the dispersion of pollutants in water bodies. There are a variety of models on the market that can be used to model the hydrodynamic process on river systems, allowing the simulation of water quality progression, and the evaluation of the control measures effectiveness, for instance, SWAT, Tuflow, HEC RAS, HSPF, WASP, QUAL2E, QUAL2K, RWQM, MIKE, and QUASAR. Various controls help decision–makers identify the most effective water quality control [3].

In a review by [3], the Ministry of Environment of South Korea prepared a joint plan for water environment management in 2006, which detailed six water quality forecasting models and recommended a series of numerical models including Widely used Qual2E and EFDC model. Meanwhile, MIKE model and Tuflow model have been widely applied to predict surface water quality in Australia. MIKE models have also been adapted in Denmark to address several problems in these areas such as ecology, environmental chemistry, water resources, hydraulic engineering and hydrodynamics. In China, the Delft 3D dynamic water quality model has been used to simulate water quality in Hong Kong since the 1970s and has now become the standard model of the Hong Kong Environment Agency [4]. Specifically, [5] used the QUAL2K model to simulate and forecast river water quality under different flow scenarios, serving to develop water quality management measures for each scenario in the Kaoping River basin Taiwan. [6] used the MIKE 11 and EcoLab models to evaluate the effectiveness of water quality management measures in the Lao Hewan basin, China. In the latest study in 2022, the water quality of the Sinú River, Colombia was evaluated by author Torres – Bejarano of water quality through different seasons using Environmental Fluid Dynamics Code (EFDC) software based on the construction of a hydrodynamics and water quality model [7–8] used the QUAL2E model to assess the risk of water quality pollution when untreated water is discharged directly into the water source in the Balatuin River (Philippines). [9] used MIKE 11 and EcoLab models to evaluate the effectiveness of water quality management measures in the Lao Hewan basin, China. [10] used MIKE model to simulate the level of nitrates using MIKE 11 and to establish relationship between nitrogen and phosphorus.

Meanwhile in Vietnam, there have been several studies using mathematical models for water quality estimation. In Ca Mau peninsula study by [11], a coupled 1D and 2D hydraulic and water quality model is applied for the east and west coastal estuaries; a 2D model is used to assess and test water quality in twelve coastal estuaries [11–12] used MIKE 11 Ecolab and Artificial Intelligence model to simulate water quality of Nhue–Day River in Ha Noi city. [13] used MIKE 11 Ecolab to model assessment and forecast of water quality in canals, rivers and streams in Binh Duong province. [14] used application of a one–dimensional hydrodynamic model HEC–RAS to simulate hydraulic properties (flow and water level) and water quality in the Xang Channel, the Soc Trang city.

The application of mathematical modeling tools in water resource management has been applied more and more widely in Vietnam and other countries. This is considered the most effective means because it allows decision makers to know the consequences of each pollution control measure in advance. The MIKE 11 Ecolab mathematical model is becoming a powerful tool for water quality management due to its outstanding advantages including fast calculation, flexibility in changing scenarios or both large and small river basins. Considering these different studies, the MIKE 11 Ecolab model was selected by the research

team to simulate spatial and temporal progression of water quality in Gia, Re, and Da Do Rivers for further management decisions of Hai Phong city drinking water supply.

2. Research methods and data collection

2.1. Description of the study area

Gia River is the main canal route of Thuy Nguyen irrigation system, with a length of 16.5 km, starting from Phi Liet sluice (Lai Xuan commune, Thuy Nguyen district) and ending at Minh Duc dam (Minh Duc town, Thuy Nguyen district) (Figure 1). The replenishing water source for Gia River comes from Da Bac River through Phi Liet sluice (Lai Xuan commune), Kinh Thay River through An Son sluice (An Son commune); and several other drains. The main functions of Gia River are irrigation for agricultural production; raw water supply for drinking water treatment; prevention of floods and droughts; waste sources recipients; and ecosystem protection [1].

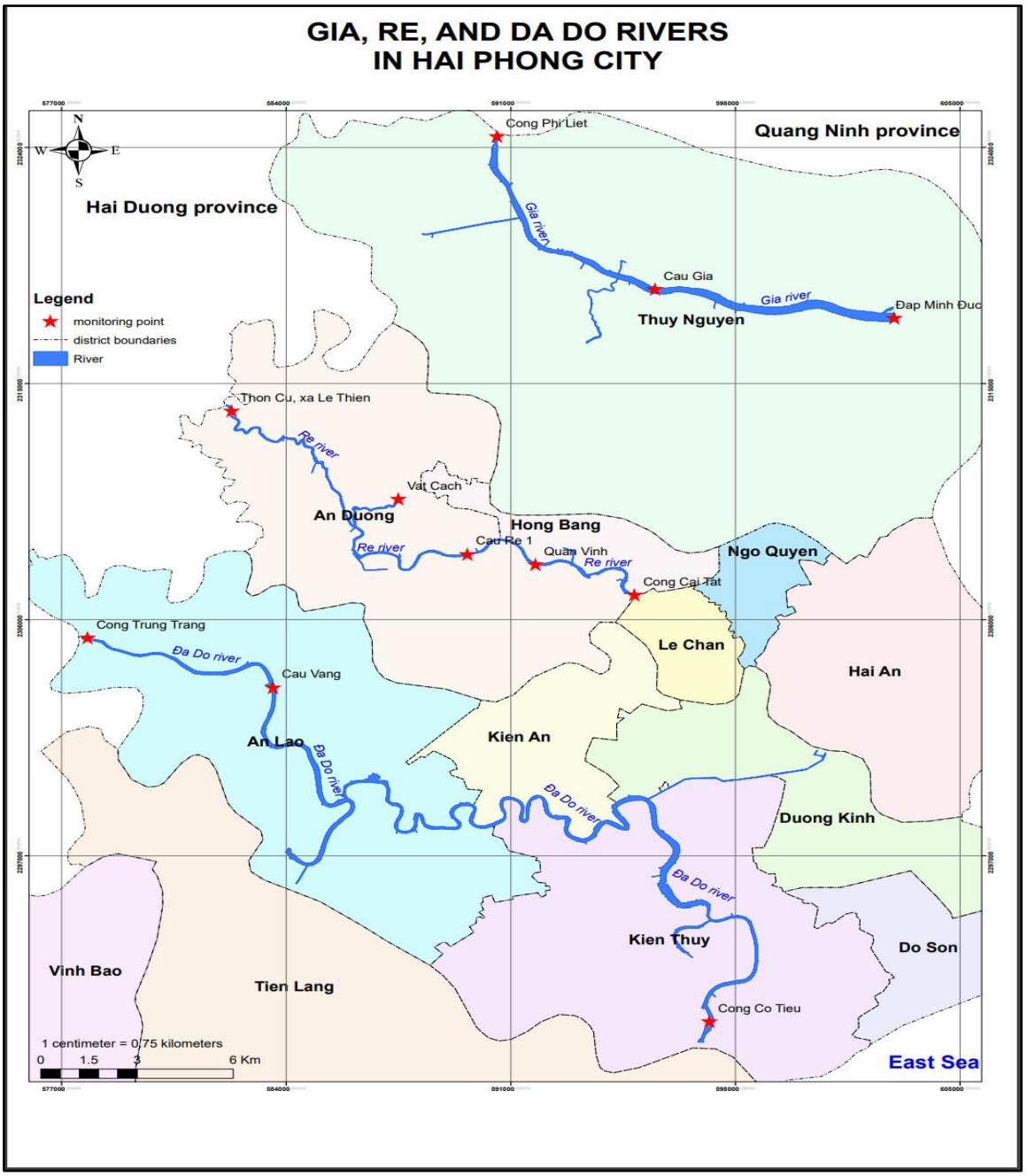

Figure 1. Map of Gia, Re and Da Do River systems in Hai Phong city.

Re River is the main canal route of An Kim Hai irrigation system, 20.6 km in length, starting from An Kim Hai canal at Bang Lai sluice (Ngu Phuc commune, Kim Thanh district, Hai Duong province) and ending at Cai Tat sluice (So Dau ward, An Duong district). The water consumption point is located at Quan Vinh Pumping Station, An Dong Commune, An Duong, Hai Phong. Functions of the Re River are irrigation for agricultural production; raw water supply for drinking water treatment; prevention of natural disasters, floods, and droughts; domestic and industrial wastewater recipient; and ecosystem protection. The Re River is currently polluted, where many indicators are exceeded, such as organic, Ammonium, Nitrite, Manganese, Total Iron, and Coliform. At the same time, the River has been affected by climate change, when sometimes there is not enough fresh water to replenish saltwater intrusion or increased pollution. All monitoring parameters exceed the allowable limit from 7% to 60%, especially Coliform and PO_4^{3-}_P [1].

Da Do River, the main canal route of the Da Do irrigation system, with a length of 48.6 km, originates from Trung Trang sluice (Quang Hung commune, An Lao district) and ends at Co Tieu sluice (Doan Xa commune, Kien Thuy district). The water collection point is located at Cau Nguyet Water Plant, Nguyet Ang village, Thai Son commune, An Lao district. The main functions of Da Do River are also raw water supply for drinking water treatment; irrigation for agricultural production; wastewater recipient; waterway transportation; and ecosystem protection. Da Do River has relatively stable water quality, but the risk of pollution is increasing, some indicators since parameters such as organic matter, Coliform tend to increase in the rainy season [1].

2.2. Methodology

2.2.1. Data collection

The topography, hydrology, hydraulics, concentration, and discharge loads (2018– 2020) were required as input for the water quality simulation model in the three rivers. Inputs for research include census report, reports on domestic activities, agriculture, industry, livestock and aquacultures, land use, and development planning up to 2030, extracted from the Hai Phong Statistical Yearbook [15].

2.2.2. Description of study modelling

Based on pollution load unit (PLU) and emission factor, pollution load was calculated to support further rapid assessment. There are two main types of pollutant discharge load for calculation: point source and area source. Using emission factors from [16–18] for various components including aquaculture area, wastewater discharge, population, number of livestock and poultry, etc., generated discharge load were computed, and environmental impacts were rapidly assessed. Four main sources of wastewater used for pollution load calculation were: domestic, industrial, livestock, and agricultural wastewater.

Waste load from domestic activities

Calculation from domestic waste source when fire-generating wastewater is connected to the water collection system and know the concentration value, wastewater flow at the wastewater treatment plant, the pollutant load from domestic wastewater can be calculated according to the actual discharge volume of the plant:

$$L = C \times Q \quad (1)$$

where L is the load (tons/year); C is the concentration of pollutants (mg/l); Q is the discharge flow (m^3/days).

For the case when there is no data on the concentration and discharge, the emission factor (source: WHO,1993) is used to calculate the discharge according to the following formula:

$$L_p = P \times PLU \quad (2)$$

where Lp is the pollution load generated (tons/year); P is the population; PLU is an emission coefficient.

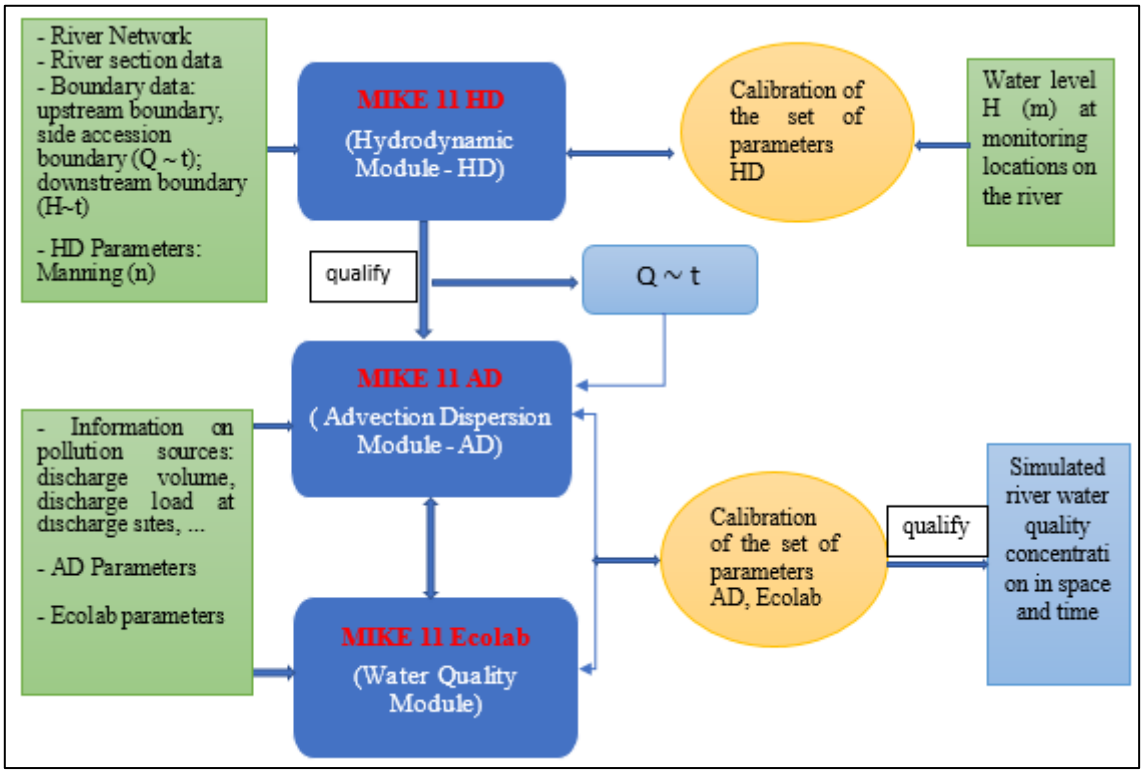

Figure 2. Research Methodology Diagram.

In the study, pollution loads from daily life were calculated in the areas of three rivers: Gia, Re and Da Do rivers. Waste load from domestic sources is based on WHO (1993) (formula 2), pollution from domestic waste generated by residents of riparian areas is calculated based on statistics on the number of inhabitants in each area. area and pollution emission coefficient per capita.

Waste load from industrial activities

The key industrial waste points are industrial parks and industrial clusters. In this study, industrial discharge load is determined based on actual measurement of wastewater concentration and flow as follows:

$$P_i = C \times Q \times 10^{-6} \quad (3)$$

where Pi is the pollution load of each industry (tons/year); Q is the discharge volume (m^3/year); Ci is the concentration of wastewater (mg/l); the concentration of pollutants in industrial wastewater needs to be treated to meet QCVN 40:2011/BTNMT standards.

Waste load from livestock activities

For livestock production, waste is calculated from livestock, livestock and poultry production activities based on the annual total herd and the emission coefficients for livestock and poultry according to the following formula:

$$L = n \times PLU \times T/12 \quad (4)$$

where n is the number of livestock/ poultry; T is an average rearing time year (month).

Waste load from cultivation activities

Based on the agricultural land area of each locality and from the pollution coefficient of rainwater runoff on the ground, based on the pollution coefficient according to WHO (1993) to calculate the amount of pollution. The formula for calculating the source of waste from soil leaching [19]:

$$Q_{rt} = S_i \times Q_i \times 10^{-3} \times n \quad (5)$$

where Q_{rt} is the contaminant load calculated for parameter i contained in stormwater runoff (ton/year); S_i is the current area of each type of land (km^2); Q_i is the pollution coefficient of rainwater runoff on the ground ($kg/km^2/day$); n is the number of rainy days in a year in the area (days).

Modeling approach

There are temporal and spatial variations in driving forces of flow in rivers, so hydrodynamic models are necessary to simulate flow regime in reality. This study applied one–dimensional hydrodynamic model (HD model) is MIKE11 with the core Saint–Venant equations which are written for each calculated node (Equation 7 and Equation 8) [20]. These equations are solved by six-point implicit scheme with initial and boundaries conditions.

Conservation of mass:
$$\frac{\partial Q}{\partial x} + b\frac{\partial h}{\partial t} = q \quad (6)$$

Conservation of momentum:
$$\frac{\partial Q}{\partial t} + \frac{\partial\left(\alpha\frac{Q^2}{A}\right)}{\partial x} + gA\frac{\partial h}{\partial x} + \frac{gQ|Q|}{C^2AR} = 0 \quad (7)$$

where Q is the flow rate, h is the water level; t is the time; x is the distance variable; g is the acceleration due to gravity; A, b are the wet cross–sectional area and width; g is the acceleration due to gravity; α is the velocity correction factor; C is the Chezy coefficient; R is the hydraulic radius.

Water quality module

Advection–Diffusion module (AD module)

The calculated discharge, water level, cross–section area and hydraulic radius in HD model are used to model advection and diffusion of pollutants. The diffusion load equation reflects two transport mechanisms: (1) The process of transporting substances by flow (advection); (2) The process of diffusion of substances by turbulent flow (turbulent diffusion). The conservation of mass of a substance in a solution in AD module is described by the equation [20]:

$$\frac{\partial AC}{\partial t} + \frac{\partial QC}{\partial x} - \frac{\partial}{\partial x}\left(AD\frac{\partial C}{\partial x}\right) = -AKC + C_2q \quad (8)$$

where C is the concentration (Kg/m^3); D is the diffusion coefficient; q is the unit flow rate (m^2/s); K is the biodegradation coefficient, K is used only when the phenomena or processes under consideration are related to biochemical reactions.

Ecolab module:

The ecological module in the MIKE 11 simulates the processes of bio–chemical development of water quality parameters (Template 4 in the MIKE 11 Ecolab module) with the following processes: heat exchange, transformation of organic matter, nitrogen change, phosphorus change, and oxygen change in rivers [20].

$$\frac{dT}{dt} = insolation - radiation \quad khi\ t \in [t_{up}; t_{down}]; \quad -radiation \quad khi\ t \notin [t_{up}; t_{down}] \quad (9)$$

$$\frac{dBOD}{dt} = -BOD_{decay} \quad (10)$$

$$\frac{dNH_4\_N}{dt} = N\_BOD_{decay} - \text{Nitrification} \quad (11)$$

$$\frac{dNO_3\_N}{dt} = \text{Nitrification} - \text{Denitrification} \quad (12)$$

$$\frac{dOP}{dt} = \text{PPdecay} - \text{PPformation} + \text{OPreleaseFromBOD} - \text{OpplantUptake} \quad (13)$$

$$\frac{dPP}{dt} = -\text{PPdecay} + \text{PPformation} - \text{PPsedimentation} + \text{PPresuspension}$$

$$\frac{dDO}{dt} = \text{Reaera} + \text{phtsyn} - \text{respT} - BOD_{decay} - SOD - Nitrification \quad (14)$$

where T is the temperature of water (°C); insolation, radiation: Incoming solar radiation and the amount of radiation emitted by river water; BOD_{decay} is the BOD of dissolved organic matter (mg/l); K_{d3} is decomposition rate of dissolved organic matter (1/day); DO is the dissolved oxygen concentration (mg/l); NH_4 _N is an ammonium in terms of Nitrogen; NO_3 _N is the nitrate as Nitrogen, PP is the phosphorus flakes; OP is the soluble phosphorus.

3. Results and discussions

3.1. Calculation Results of Discharge Loads to Gia, Re, and Da Do Rivers

Discharge loads into the Gia, Re, Da Do Rivers were calculated based on 2020 statistics for various sectors. Waste load from domestic, industrial, livestock, and agricultural activities were accordingly presented in Table 1 to Table 4.

Table 1. Domestic waste load in Da Do, Re and Gia Rivers.

River	Location	Population (people)	Pollution load (ton/year)						
			COD	BOD_5	T_P	T_N	TSS	NH^{4+}	PO_4^{3-}
Da Do	Kien An District	119,388	6,566	2,985	131.3	477.6	3,582	262.7	70.92
	Duong Kinh District	60,345	3,319	1,509	66.4	241.4	1,810	132.8	35.84
	An Lao District	148,956	8,193	3,724	163.9	595.8	4,469	327.7	88.48
	Kien Thuy District	142,788	7,853	3,570	157.1	571.2	4,284	314.1	84.82
Re	An Duong District	198,661	10,926	4,967	218.5	794.6	5,960	437.1	118.00
	Hong Bang District	96,508	5,308	2,413	106.2	386.0	2,895	212.3	57.33
Gia	Thuy Nguyen	336,960	18,533	8,424	370.7	1348.0	10,109	741.3	200.20

Table 2. Industrial discharge load in Gia River, Da Do River, and Re river.

Wastewater receiving source	Total discharge volume (m^3/year)	Load of pollutants (tons/year)				
		BOD_5	COD	TN	TP	TSS
Gia	73,000	2.19	–	3.65	0.438	15.33
Da Do	255,135	11.71	31.00	10.21	1.530	53.58
Re	23,725	0.77	0.74	0.95	0.140	4.98

Table 1. Livestock discharge load on Gia, Re and Da Do rivers in 2020 (Unit: tons/year).

River		Re		Gia	Da Do			
	District	Hong Bang	An Duong	Thuy Nguyen	An Lao	Kien Thuy	Kien An	Duong Kinh
BOD	Buffalo	–	0.08	0.03	0.08	0.11	0.00	0.01
	Cow	–	0.08	0.34	0.06	0.08	0.03	0.05
	Pig	0.003	0.12	0.25	0.12	0.25	0.02	0.06
	Poultry	0.001	0.35	0.43	0.43	0.34	0.02	0.09

River		Re		Gia	Da Do			
District		Hong Bang	An Duong	Thuy Nguyen	An Lao	Kien Thuy	Kien An	Duong Kinh
COD	Buffalo	–	0.14	0.05	0.15	0.19	0.00	0.02
	Cow	–	0.15	0.61	0.11	0.15	0.06	0.09
	Pig	0.03	1.08	2.23	1.08	2.22	0.15	0.55
	Poultry	0.25	64.36	79.01	79.29	61.90	3.45	15.61
T_N	Buffalo	–	20.41	7.53	22.56	28.34	0.18	2.23
	Cow	–	21.55	89.83	16.43	21.55	8.58	13.27
	Pig	0.69	26.83	55.12	26.68	54.86	3.61	13.72
	Poultry	3.09	785.44	964.21	967.55	755.38	42.08	190.44
T_P	Buffalo	–	5.27	1.94	5.82	7.31	0.05	0.58
	Cow	–	5.56	23.18	4.24	5.56	2.21	3.42
	Pig	0.22	8.45	17.37	8.41	17.28	1.14	4.32

The pollution sources from livestock production have the largest TSS discharge load and the smallest total phosphorus unit load of all calculated parameters. In Gia and Da Do Rivers, TSS discharge accounts for the largest pollutant load (6,978–13,929 tons/year).

Table 4. Agricultural discharge loads on Re river, Gia River and Da Do River.

River	District	Area of agricultural land (km^2)	Agricultural waste load (tons /year)				
			COD	BOD_5	T_N	T_P	TSS
Re	An Duong	49,794	206.00	133.00	265.00	59.00	18,423.78
	Hong Bang	1.159	5.00	3.00	6.00	1.37	428.83
Da Do	An Lao	53.68	222.45	143.00	286.01	63.56	19,861.60
	Kien An	7,766	32.18	20.69	41.38	9.19	2,873.42
	Duong Kinh	13.33	55.24	35.51	71.02	15.78	4,932.10
	Kien Thuy	50.32	208.5	134.05	268.10	59.58	18,618.40
Gia	Thuy Nguyen	91,448	294.46	189.29	378.6	84.13	26,291.3

The waste from agricultural activities released into the three rivers has a total volume of 94,720.48 tons/year in 2020. The Da Do River bears the largest agricultural load compared to the Re and Gia rivers, since agriculture is the most active in Da Do basin. The number of COD, TN, and TSS is almost one and a half to two times higher than that of the other two rivers. Meanwhile, Re River has the lowest load of substances.

3.2. Simulation Results of Water Quality in Gia, Re, and Da Do Rivers

The network of Gia, Re, and Da Do Rivers in the simulation model are shown in Figure 3. The results of hydraulic calibration of three rivers in the period of 2020–2021 gave relatively good results with the Nash coefficient NS = 0.72–0.88, the model verification process was simulated from January 1, 2022 to May 30, 2022 with time step results of NS = 0.7–0.82. Afterwards, the MIKE 11 Ecolab module was constructed to simulate water quality on Gia, Re, and Da Do Rivers at three locations along Gia River, five locations along Re River, and three locations along Da Do River (Figure 7). The network of Gia, Re and Da Do rivers in the simulation model as shown in Figure 3. Simulated results were verified by comparing with monitoring data of 4 water quality indicators in April 2020, shown in Figures 4 to 6.

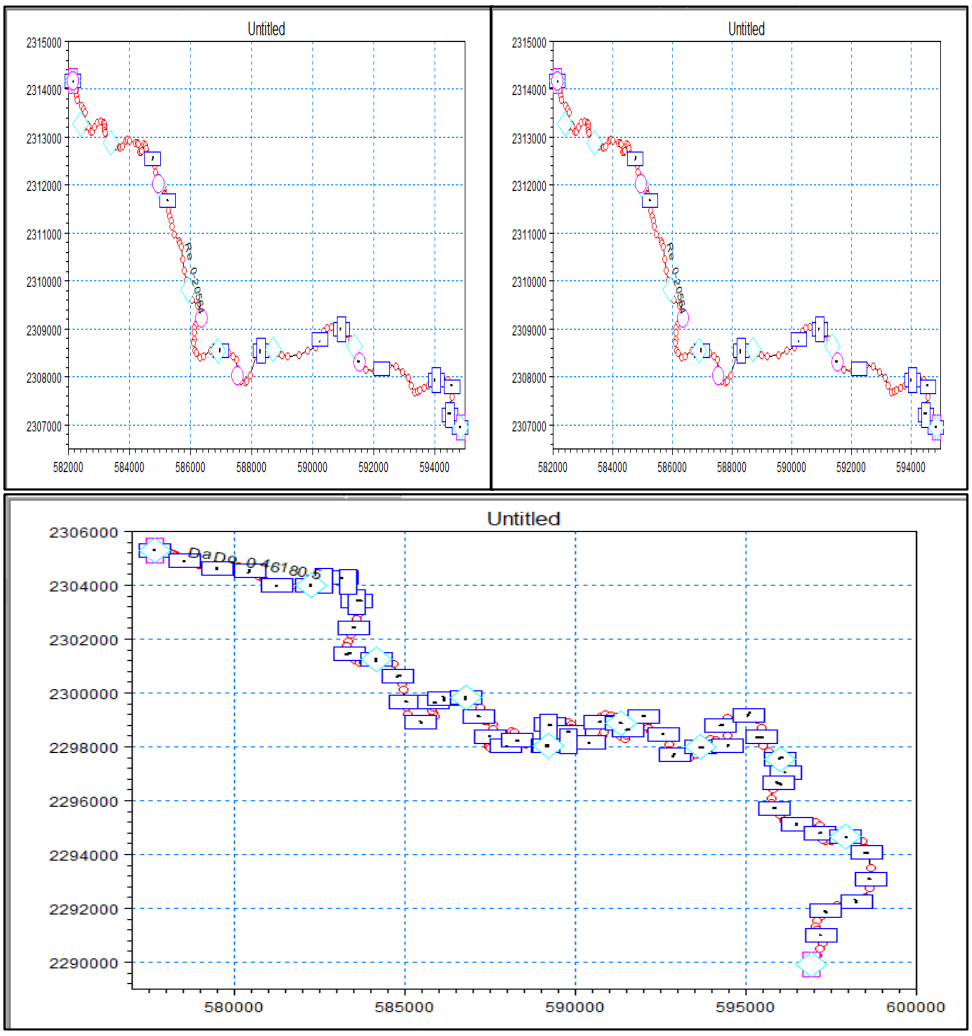

Figure 1. The Gia (Left), Re (Right), and Da Do (Bottom) river networks are used in the MIKE 11 model.

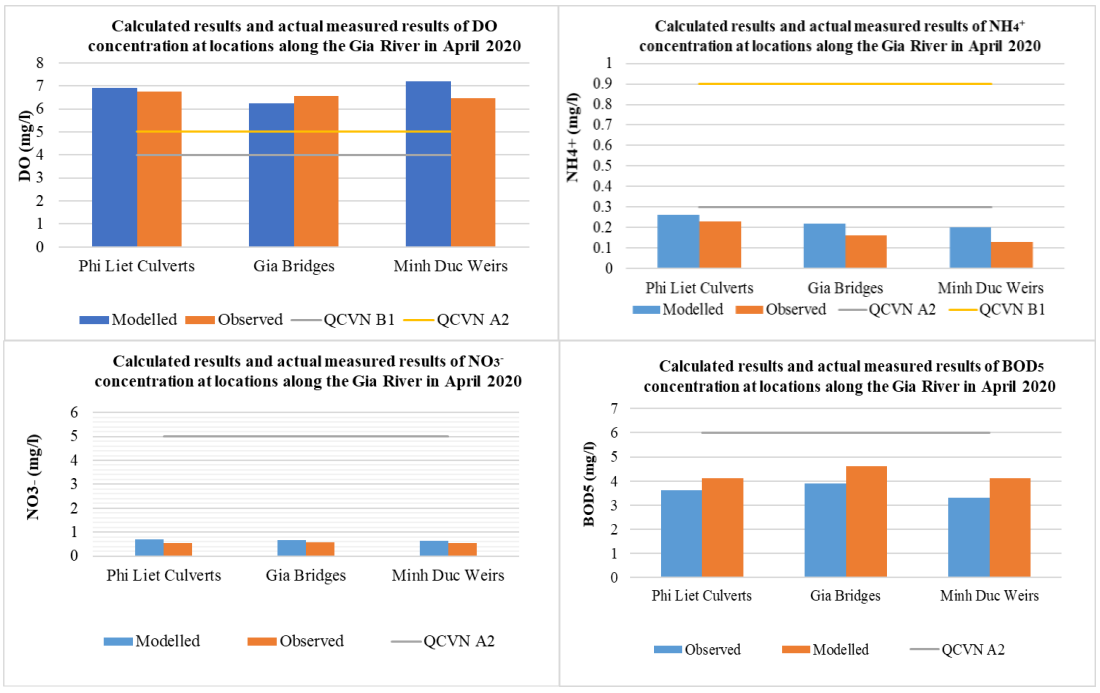

Figure 2. Calculated results and measured concentrations of DO, NH_4^+, NO_3^- and BOD_5 concentration at locations along the Gia River in April 2020.

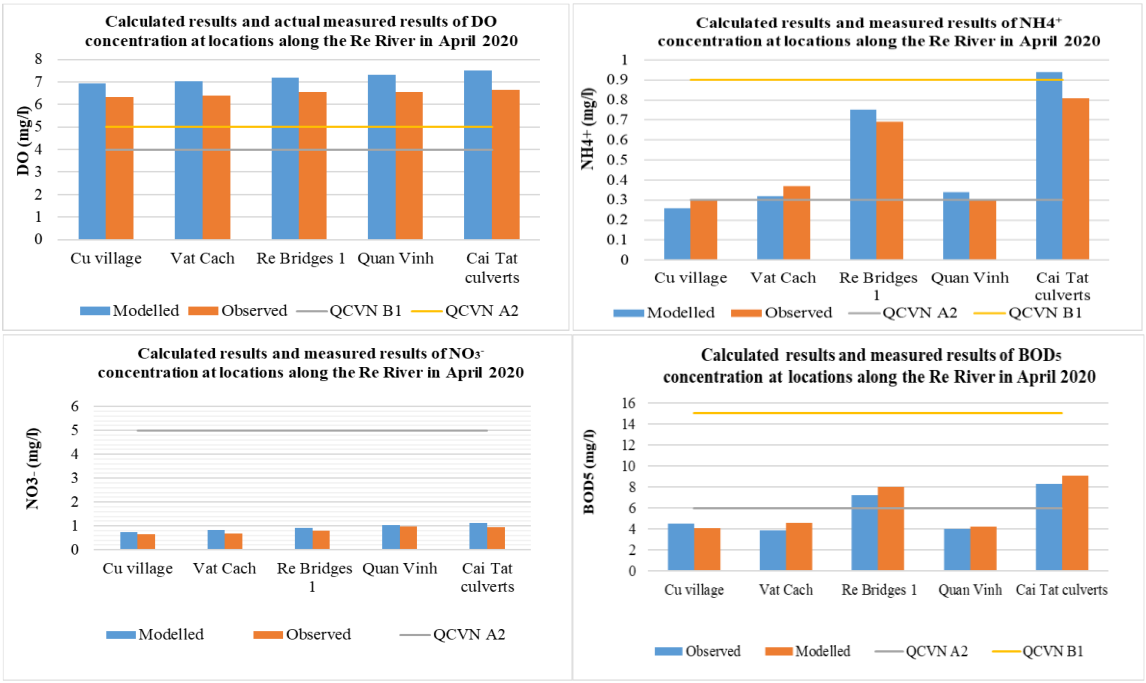

Figure 3. Calculated results and measured concentrations of DO, NH^{4+}, NO^{3-} and BOD_5 concentration at locations along the Re River in April 2020.

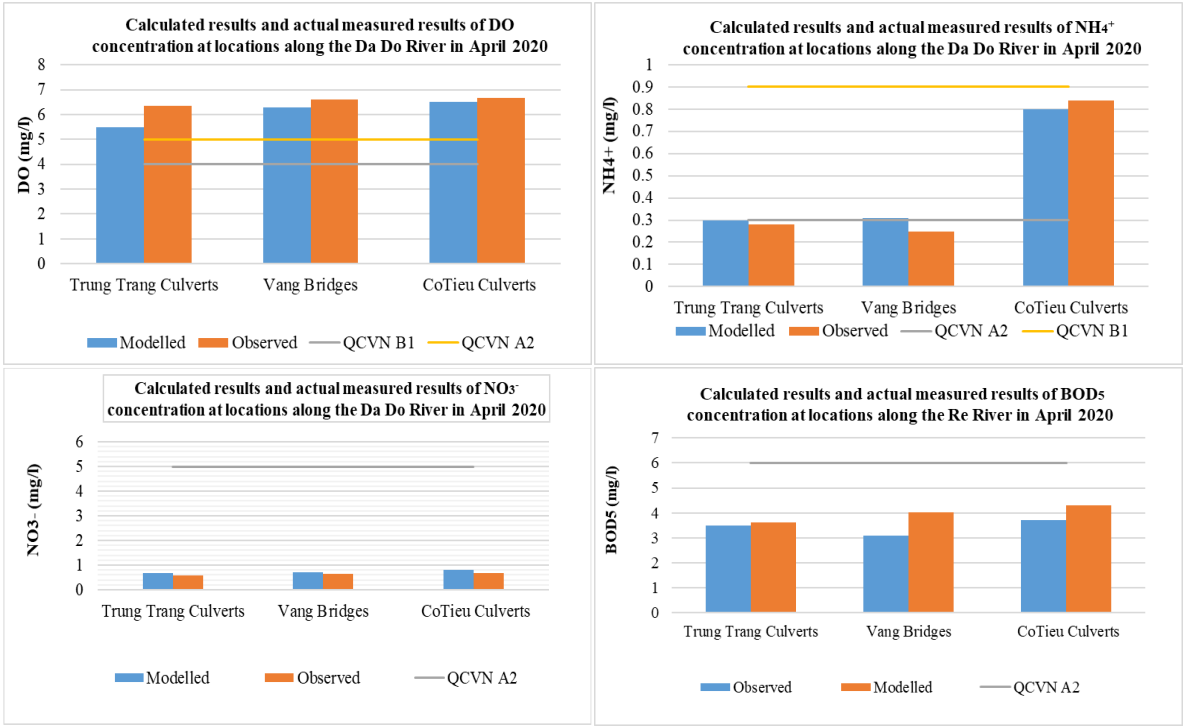

Figure 4. Calculated results and measured concentrations of DO, NH^{4+}, NO^{3-} and BOD_5 concentration at locations along the Da Do River in April 2020.

Figures 4 to 6 compares the measured and simulated concentrations with the National Technical Regulations on Surface Water Quality Category A_2 (For domestic water supply purposes accompanied with application of suitable treatment technology or uses described in Categories B_1 and B_2) and B_1 (For irrigation or other uses with similar water quality requirements or uses described in Category B_2). The calculation results compare the relative error between the measured and simulated values on three rivers, ranging from 4 to 18%, the correlation coefficient R_2 ranging from 0.8 to 0.88. This confirms that the simulation model

is relatively good and suitable for simulating water quality progression in the three rivers. More importantly, comparison between water quality concentrations and the standard shows that all 3 locations of Phi Liet culverts, Gia bridges, Minh Duc weirs in Gia river have good water quality, meeting A_2 standard. Meanwhile, on the Re River, the concentration of NH_4^+ at all locations exceeds the A_2 standard, specifically more than 2 times higher at Re bridge and Cai Tat sluice. Also, at these two locations, the BOD_5 concentration also exceeded the standard A_2. Lastly, on Da Do River, the concentration of NH_4^+ at Co Tieu culverts exceeded the standard A_2 by 2.8 times. In large, pollution occurs locally at Re bridge, Cai Tat sluice on the Re River, and Co Tieu culverts on Da Do River, with high NH_4^+ concentration. This is probably due to the wastewater discharge from nearby industrial parks, industrial clusters, and hospitals, or from agricultural activities. Therefore, to use these water sources as drinking water supply, it is necessary implement wastewater controls along the rivers to improve river water quality.

The WQI water quality index was calculated based on five groups of water quality parameters [21–24]. In this study, we focus on four groups of parameters I, III, IV, and V. The monitoring data of the above four groups combined with simulation data from the MIKE model, the research team calculates the WQI at 11 locations on three rivers, as shown in Table 5 below.

Table 2. WQI water quality index results on Gia, Re and Da Do rivers.

River	Observation location	Coordinates		Average Annual WQI				
		X	Y	2016	2017	2018	2019	2020
Gia	Phi Liet culvert	593519	2307719	96	95	92	66	99
	Gia bridge	590449	2324041	96	95	88	92	99
	Minh Duc weir	595266	2318707	89	44	96	95	95
Re	Cu village, Le Thien Commune	582303	2313965	95	95	85	38	94
	Vat Cach	587504	2310602	95	95	98	79	94
	Re bridge 1	589655	2308508	94	74	87	36	82
	Quan Vinh	591773	2308098	90	87	81	39	94
	Cai Tat culvert	589614	2280568	83	85	40	38	75
Da Do	Trung Trang culvert	577818	2305313	95	96	93	97	98
	Vang bridge	583599	2303427	45	81	96	42	98
	Co Tieu culvert	597200	2290674	98	97	87	83	80

Table 3. Range of values for assessing surface water quality.

WQI value range	Water quality	Fit for the intended use	Color
91–100	Very good	Good use for domestic water supply	Blue
76–90	Good	Used for domestic water supply but require appropriate treatment measures	Green
51–75	Medium	Used for irrigation and other equivalent purposes	Yellow
26–50	Least	Used for waterway transportation and other equivalent purposes	Orange
10–25	Heavy pollution	Water is heavily polluted, require future treatment measures	Red
< 10	Pollution is very heavy	Poisoned water, require mistake measures to treat and revert	Brown

The calculation results of the water quality index of Gia River, Re river and Da Do river show that the water quality in 2020 at most control locations was better than in 2019. Water quality in Gia River was assessed as very good quality, which can be used for domestic water supply. Re and Da Do Rivers were also polluted by several waste sources, so from the middle to the lower reaches of the river, the water source was of average to good quality, suitable

for domestic water supply purposes with appropriate treatment measures and for irrigation and other equivalent purposes.

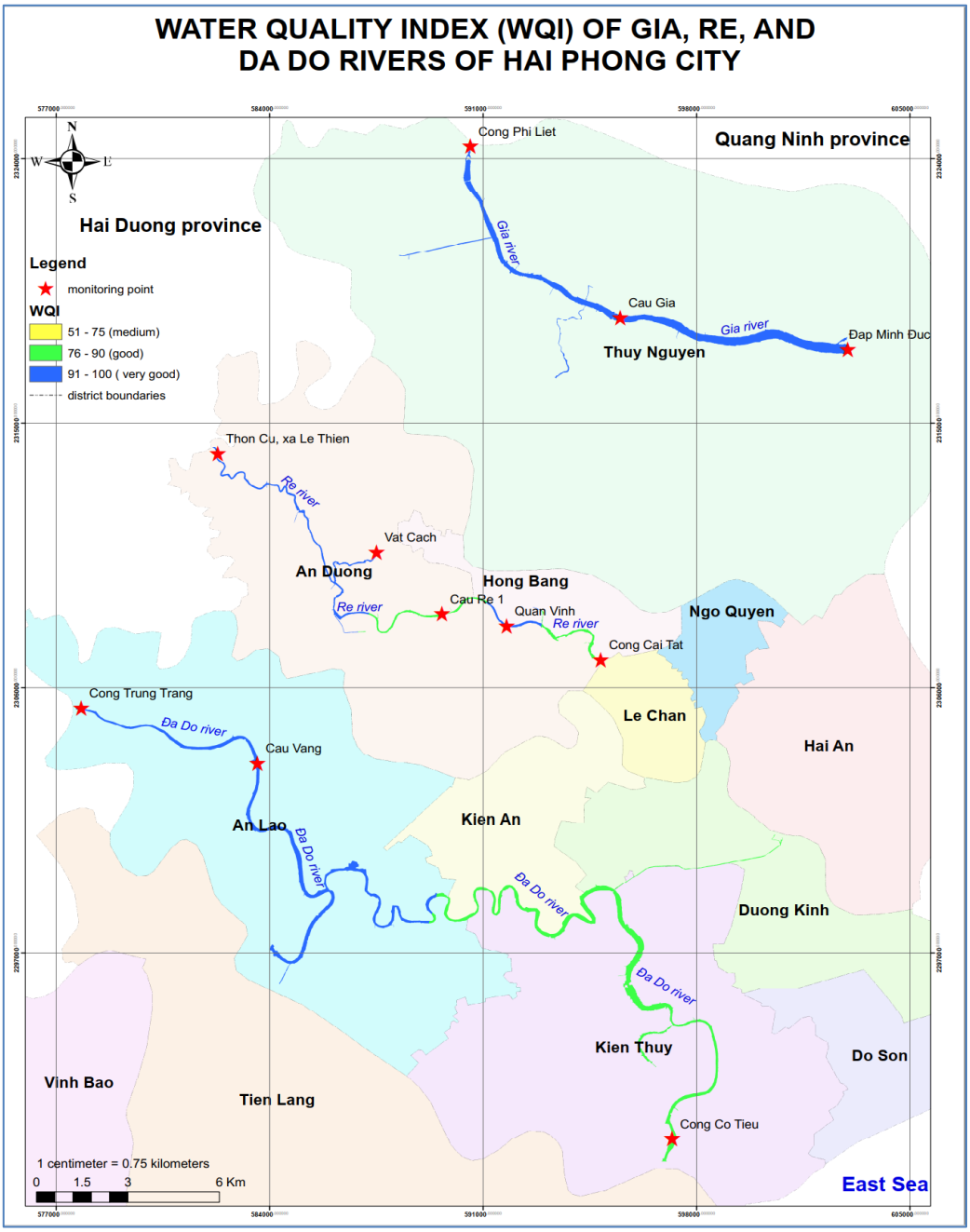

Figure 5. Map of WQI water quality index on Gia, Re and Da Do rivers in Hai Phong city.

4. Conclusion

In this paper, the research team presented the method and calculated the pollutant discharge load, water quality changes in Gia, Re, Da Do rivers using the MIKE 11 Ecolab model, showing the pollution level of each water quality index at different locations on the rivers. Concurrently, WQI index was calculated from the combination of simulation results and measured water quality to assess river water quality. Based on the results of water quality calculations at different locations on the Gia, Re and Da Do Rivers, the water quality by 2020 has improved significantly comparing to 2019, while some of the leading canals, lakes, and outlets on the Re and Da Do Rivers are still polluted by organic substances and microorganisms. Water quality in the Re River is generally of average quality, which can be used for irrigation and other equivalent purposes. More notably, the water quality at all

canals, discharge gates and river sections in receiving wastewater from landfills in these three networks show signs of pollution by organic substances, nutrients, microorganisms, etc. Therefore, to protect water sources of the Gia, Re, and Da Do Rivers systems, it is necessary to implement effective management and treatment measures for the entire system and proper planning for sustainable economic development for surrounding households and businesses.

In this study, the studied rivers are three small rivers in Hai Phong city, so the hydrological, hydraulic and water quality data is limited. The flow modeling process sometimes cannot be simulated for a long time. Therefore, future research for these rivers may take advantage of artificial intelligence models to supplement missing data. Moreover, research for the implementation of automatic water quality monitoring system in these rivers should be conducted for spatial and temporal water quality assessment.

Author contribution statement: Developing research ideas: T.A.P., T.T.D.H.; Data processing: T.A.P., H.T.A., T.B.C., T.V.T.; Building mathematical models: H.T.A.; Writing draft articles: T.A.P., H.T.A., N.N.A.

Acknowledgments: The study was carried out with the support of the National Science and Technology Project "Research on building automatic monitoring and early warning systems for water quality in Gia, Re, and Da Do Rivers serving domestic water supply for Hai Phong city" Code: ĐTL.CN–18/21.

Competing interest statement: The authors hereby declare that this article is the work of the authors' team, which has not been published elsewhere, and has not been copied from previous studies; there is no conflict of interest in the authors group.

References

1. Project Tasks and solutions to protect freshwater sources in Re, Gia, Da Do, Chanh Duong rivers, Hon Ngoc canal, Tien Lang irrigation system in Hai Phong city in the period 2013–2020.
2. The Ministry of Natural Resources and Environment. QCVN 08:MT 2015/BTNMT – National technical regulation on surface water quality, Hanoi, 2015.
3. Wang, Q.; Li, S.; Jia, P.; Qi, C.; Ding, F. A review of surface water quality models. *Sci. World. J.* **2013**, 231768. https://doi.org/10.1155/2013/231768.
4. Chapra, S.C. Surface water–quality modeling. Waveland Press, 2008.
5. Tang, P.K.; Huang, Y.C.; Huang, J.S.; Lin, Y.J. Water quality management strategies for various river flows with QUAL2K model. Trans Tech Publications Ltd. *Appl. Mech. Mater.* **2011**, *58*, 2462–2466.
6. Liang, J.; Yang, Q.; Sun, T.; Martin, JD; Sun, H.; Li, L. MIKE 11 model–based water quality model as a tool for the evaluation of water quality management plans. *J. Water Supply: Res. Techno. AQUA* **2015**, *64(6)*, 708–718.
7. Hernández–Alvarez, U.; Pinedo–Hernández, J.; Paternina–Uribe, R.; Marrugo–Negrete, J.L. Water quality assessment in Quebrada Jui, tributary of the Sinú river, Colombia. *Revista UDCA Actualidad Divulgación Científica*, **2021**, *24(1)*, 1–9.
8. McAvoy, D.C.; Masscheleyn, P.; Peng, C.; Morrall, S.W.; Casilla, A.B.; Lim, J.M. U.; Gregorio, E.G. Risk assessment approach for untreated wastewater using the QUAL2E water quality model. *Chemosphere* **2003**, *52(1)*, 55–66.
9. Liang, J.; Yang, Q.; Sun, T.; Martin, J.D.; Sun, H.; Li, L. MIKE 11 model–based water quality model as a tool for the evaluation of water quality management plans. *J. Water Supply: Res. Techno. AQUA*, **2015**, *64(6)*, 708–718.
10. Kanda, E.K.; Kipkorir, E.C.; Kosgei, J.R. Modelling of nitrates in River Nzoia using MIKE 11. *Water Prac. Technol.* **2017**, *12(1)*, 217–223.
11. Tri, D.Q.; Linh, N.T.M.; Thai, T.H.; Kandasamy, J. Application of 1D–2D coupled modeling in water quality assessment: A case study in Ca Mau Peninsula, Vietnam. *Phys. Chem. Earth, Parts A/B/C*, **2019**, *113*, 83–99.

12. An, H.T.; Nhung, T.T. Research on combining hydraulic model and artificial intelligence model to simulate water quality of Nhue – Day river in Ha Noi City. *VN. J. Hydrometeorol.* **2022**, *739*, 67–80.
13. Thien, N.D.; Dung, T.D.; Lam, N.T.T.; Quan, N.Q.; Luan, P.D.M.H. Assessment and forecast of water quality in canals, canals, rivers and streams in Binh Duong province. *VN. J. Hydrometeorol.* **2022**, *735*, 12–25.
14. Nhi, T.T.Y.; Diem, N.T.K.; Tri, V.P.D. Application of mathematics model for Hydraulic characteristics and Water Quality Characteristics on Xang channel, Soc Trang city. *J. Sci. Can Tho Uni.* **2013**, *25*, 76–84.
15. Hai Phong Provincial Statistical Yearbook, 2021.
16. United Nations Environment Program (UNEP). Pollutants from land–based resources in the Mediterranean. UNEP Regional Seas Reports and Studies No. 32, 1984.
17. San Diego–McGlone, M.L.; Smith, S.V.; Nicolas, V. Stoichiometric interpretations of C:N:P ratios in organic waste materials. *Mar. Pollut. Bull.* **2000**, *40*, 325–330.
18. Japan International Cooperation Agency (JICA). The study on Environment management for Ha Long Bay, Final report, Volume I, II, III, IV. Reserved at Institute of Environment and Resource, 1999.
19. Tran Duc Thanh, Tran Van Minh, Cao Thi Thu Trang, Vu Duy Vinh, Tran Anh Tu, Manh load lips Ha Long Bay School - Bai Tu Long, Publishing House. *Department School of Nature and Technology*, 2012.
20. DHI. MIKE 11, A modeling system for rivers and channels, user guide. 2017. Online available: http://manuals.mikepoweredbydhi.help/2017/Water_Resources/MIKE11_UserManual.pdf.
21. Decision No. 879/QD–TCMT dated July 1, 2011 by the Director General of Vietnam Environment Administration on Issuance of Guidance for Water Quality Index Calculation.
22. Le, T.N.; Tran, T.T.; Tao, Q.M. Assessing the wastewater generation in the south of Binh Duong province. *VNUHCM J. Nat. Sci.* **2018**, *2(4)*, 176–183.
23. Soares, S.S.; Vasco, J.; Scalize, P.S. Water Quality Simulation in the Bois River, Goiás, Central Brazil. *Sustainability,* **2023**, *15(4)*, 3828.
24. Jordão, C.P.; Pereira, M.G.; Bellato, C.R.; Pereira, J.L.; Matos, A.T. Assessment of Water Systems for Contaminants from Domestic and Industrial Sewages. *Environ. Monit. Assess.* **2022***, 79*, 75–100.

VIETNAM JOURNAL OF HYDROMETEOROLOGY

Research Article

Proposal of a standard experimental model to determine the contaminant removal rate constants in subsurface flow constructed wetlands

Thu Phuong Pham[1]*, Dai Quyet Truong[2], Duc Tung Le[1], Viet Quang Nguyen[1]

[1] School of Environmental Science and Technology, Hanoi University of Science and Technology; phuong.phamthu@hust.edu.vn; leductung96@gmail.com; nv.quang2027@gmail.com

[2] School of Civil and Environmental Engineering, University of Technology Sydney (UTS), City Campus, Broadway, NSW 2007, Australia; quyettruongdai@gmail.com

*Corresponding author: phuong.phamthu@hust.edu.vn; Tel.: +84–902299312

Received: 5 February 2023; Accepted: 23 March 2023; Published: 25 March 2023

Abstract: The objective of this study was to establish a standard experimental model to determine the removal rate constants of wastewater pollutants in subsurface flow–constructed wetlands. Such the rate constants of removal processes of removal processes of COD, BOD, NH_4^+, total nitrogen (TN), etc., are important parameters for calculating the size of wetlands, yet the data published in the international textbooks and research articles fluctuate in very wide ranges, that make it challenging to design constructed wetland accurately. By evaluating influencing factors and referencing available models, we proposed the experimental wetland model of cylindrical shape (Ø18cm and 30cm height), with the type of material and plant, which must be specified for each experiment determining the rate constants. The experimental procedure has been given, including setting up the system, running experiments to collect data, and processing data to calculate the rate constant. The initial experiments with small gravel and common reed plant, determining the removal rate constants of COD, NH_4^+ and TN, provided good repeatability results, and the values are within a reasonable range with the published values in the world. This result shows the applicability of the proposed experimental model and procedure to determine the contaminant removal rate constants in constructed wetlands uniformly. Eventually, a complete set of more converging rate constants data can be obtained, which improves the accuracy of the constructed wetlands setup.

Keywords: Subsurface flow constructed wetland; Rate constant; Ammonium; COD; Total nitrogen.

1. Introduction

Constructed wetlands are systems that follow the idea of natural wetlands to carry out wastewater treatment processes. In constructed wetlands, the pollutant transformation is accomplished through an integrated combination of biological, physical, and chemical interactions between the plants, the media, and the inherent microbial community [1]. Wetland treatment systems are generally classified into two categories: free-water surface wetlands (FWS), which are shallow basins with water on the surface, and subsurface flow wetlands (SSF), which are the bed with water flow under the surface. According to the flow direction, subsurface flow systems are further divided into horizontal and vertical subsurface flow. The construction of these systems can be obtained at a relatively low cost due to the simple materials and equipment used. The removal efficiencies are high, and the treated

effluent can meet the standard for secondary or tertiary biological wastewater treatment. In addition, the constructed wetland has low operation and maintenance costs owing to its natural energy's employment at work [2]. Constructed wetlands have become an increasingly popular option for wastewater treatment.

The treatment efficiency of the wetland can only be obtained when it is appropriately designed. Nowadays, many textbooks and researchers agree that the first-order rate constant (k) of the pollutant removal process is the primary tool in wetland design [1]. The pollutants of concern in wetland treatment are organic matter and nutrients; accordingly, the removal rate constants of COD, BOD, NH_4^+, NO_3^-, or TN are required. In addition, constructing a wetland requires the accurate value of those rate constants.

In some textbooks, the constant k of each parameter has a definite value, depending only on the type of wetland and the temperature rather than the type of media and plant. For example, at 20°C, the BOD removal rate constant, k_BOD, is 0.678 d^{-1} in the design of the FWS wetland; and in the design of the SSF wetland, it is 1.1 d^{-1} [3–4]. At a temperature other than 20°C, the value of k can be determined based on the Arrhenius equation with the temperature coefficient θ = 1.06 [3–4]. However, this oversimplification makes the design calculation of wetlands unreasonable and unconvincing.

On the other hand, different research papers have given a wide range of values of the removal rate constants. For example, as Magdalena Gajewska summarized from many previous publications [5], the k_BOD value ranges from 0.071 to 6.11 d^{-1}, making it difficult for the designer. That wide range of results is understandable since each author conducts experiments to determine k under very different conditions. Although a completed study on the influence of all factors on the value of removal rate constant in wetlands has yet to be published, a number of publications have evaluated the effect of several factors. Those factors can be listed as the type of wetland media, type of plant, design shape, type of wastewater, and operational mode.

The media used in wetlands are divided into three principal groups: natural materials (soil, sand, gravel, zeolite...), industrial by-products (slag, rubble, bark...), and artificial materials (activated carbon, synthetic materials, ceramite...) with a total of dozens of different materials [6]. Many studies have confirmed that the treatment efficiencies of the same type of pollutant in wetlands using different materials are not the same [7–9]. Abdelhakeem et al. [9] conducted a study to determine and compare the constant k of experimental wetland systems with the same size and type of vegetation with two different materials: gravel and vermiculite. As a result, the COD removal rate constant of gravel, k_COD, is 2.64 d^{-1}, while that of vermiculite is 2.95 d^{-1}; the NH_4 removal rate constant, k_NH_4, of gravel is 0.66 d^{-1}, and that of vermiculite is 0.96 d^{-1}.

Plant species commonly used in the wetland are *Phragmites spp. (Poaceae), Typhaspp. (Typhaceae), Scirpusspp. (Cyperaceae), Iris spp. (Iridaceae), Juncus spp. (Juncaceae)* and *Eleocharisspp. (Spikerush)*, of which the reed (*Phragmites australis*) is the world's most frequently used plant species [6]. Like the material, the pollutant removal rate in the SW using different plant species also varies. [10] conducted a study to determine the COD treatment rate constant of the wetland with four different plant species, *Phragmites australis*, *Lythrum salicaria*, *Cladium mariscus*, *Iris pseudacorus*, giving constant results k are 0.22, 0.37, 0.35 and 0.55 (d^{-1}), respectively.

Experimental models to determine the constant rate k are primarily designed with the rectangular box shape and operated in continuous mode to resemble wetlands in reality [6, 8, 11]. However, each model is designed with a very different dimension; even the length, width and depth are not the same. For example, the experimental model in the study [10] is 2.5 m long, 0.65 m wide, i.e., the ratio length: width = 3.8:1; depth is 0.6 m. [11] used the experimental model with the size of 12 m × 1.6 m × 1.1 m, i.e., the ratio of length: width = 7.5:1; 1.1 m depth. In addition, many other studies have experimental wetland models of

different sizes. Currently, there is no research to evaluate the influence of the size of the empirical model's shape on the k–constant results. However, [10] studied the constant value of k_COD at different depths and concluded that the constant k result depends on the depth of the wetland.

The wastewater used in the studies to determine the constant k has two types: natural wastewater [9, 11–13] and synthetic wastewater [10, 14–15]. The advantage of using natural wastewater is that it has a composition of pollutants (both macro– and micro–) and a realistically rich micro-organism. However, natural wastewater has a very high fluctuating component concentration, which is difficult to control. Synthetic wastewater has the advantage of being able to actively control the concentration of components, ensuring uniform characteristics of wastewater composition. The composition of microorganisms to be treated as natural wastewater can be provided by soaking the experimental wetland system with raw sewage to create the necessary microflora.

In terms of operational modes for wetlands studies, there are two categories: continuous operation [9–11, 13, 15] and batch operation [12, 14]. Most of the studies were carried out in the continuous regime to simulate a typical wetland system in nature. However, when changing different types of material and plant (due to different porosity), if operated continuously, the pumped wastewater flow rate needs to be adjusted to ensure water retention time, leading to process complexity. With batch operation, it is possible to control the exact contact time of aqueous solution in the wetland systems.

Thus, determining the constant k based on wetland systems with different designs, materials and plants and implementation procedures will always result in a wide range of k values. To uniformly determine the constant k, it is necessary to establish an experimental model with a uniform design and procedure called the standard experimental model. On this basic model, it is possible to conduct experiments to determine the constant values of k for different pollutant parameters in a uniform manner.

To determine the removal rate constant of the treatment process, the experimental wetland is considered as a simple reactor in this study. Thus, an experimental model with a compact size while ensuring that all wetland components present is entirely representative of a wetland system. Accordingly, we propose an experimental wetland model with a cylindrical shape with minimum diameter and depth, sufficient to ensure space for plant roots to develop. Experiments were then conducted to determine the treatment rate constants of TN, NH_4^+, and COD. The obtained constant k results were compared with published results to confirm the experimental model and procedure.

2. Methods and data

2.1. Experimental wetland setup

The experimental wetlands were set up in plastic containers with a diameter of 18 cm and a height of 30 cm with a drain valve at the bottom (Figure 1). In preparation, small gravels (5–10 mm diameter) were washed thoroughly with tap water several times and dried at ambient temperature before being used as wetland media. Young *Phragmites australis* reeds were taken from the Red riverbank (Hanoi, Vietnam), and the roots were washed to remove mud and dirt. After that, the reeds were planted so that the roots were close to the bottom of the gravel bed, with a density of two plants in each bed. Then, the plants were raised for two months to adapt to the system. Wastewater source collected at Kim Nguu River (Hanoi, Vietnam) and diluted 1:1 with tap water was used to feed the plants. The feed water in the wetland beds was discharged and refilled twice weekly to ensure that the plants could acclimatize well. In addition, as mentioned above, the application of raw wastewater also helped to inoculate natural microorganisms in the systems.

Figure 1. Experimental wetland systems.

2.2. Feeding, sampling and analysis

This study investigates the applicability of the proposed SSF wetland model for determining the rate constants of COD, NH_4^+ and TN removal processes. Therefore, different experiments treating wastewater with specific targets were conducted. A set of experiments with the binary synthetic solution containing COD and TN, COD and NH_4^+, and COD and NO_3^- were carried out in March, April, and December, respectively. It should be noted that owing to the lack of NO_3^- analysis, only the COD removal rate constant was studied in the third test using COD and NO_3^- artificial solution. The feed solution was prepared before each experiment using analytical chemicals purchased from Merck Co., Germany. Glucose ($C_6H_{12}O_6$) was utilized to prepare the desired COD initial concentrations. Potassium nitrate KNO_3 was used for NO_3^-, ammonium sulfate $(NH_4)_2SO_4$ for NH_4^+, and urea CH_4N_2O for the TN component. KH_2PO_4 was used as the phosphorus source. Additional compounds used in the synthetic wastewater included: 28 mg/L $CaCl_2$, 52 mg/L $MgSO_4.7H_2O$, 11 mg/L K_2SO_4, 0.03 mg/L $CuCl_2.2H_2O$, 0.08 mg/L $ZnCl_2$, and 1.7 mg/L $FeSO_4.7H_2O$ following [16]. Details about the concentrations of contaminants in each batch test are given in Table 1.

Table 1. Experimental conditions

Test	Month	Solution	COD concentration (mg/L)	NO_3^-/ NH_4^+/TN concentration (mg/L)
1	March	COD & TN	400	20
2	April	COD & NH_4^+	400	20
3	December	COD & NO_3^-	400	20

Before the batch experiments, the experimental wetland was washed with tap water once to remove the inherent water and contaminants. Specifically, the rinsing process was carried out gently by draining the water through the bottom drain valve. When the water had drained completely, the valve was closed, and clean tap water was added slowly from the top until the water filled the reservoir. Next, the wetland was kept consistently for 10 minutes to ensure that the water entered all the pores in the wetland, then it continued to drain. Repeat washing the wetland with synthetic wastewater three times to ensure that all sites in the system are filled with the wastewater homogeneously. Afterward, the experiments were conducted by feeding the synthetic wastewater into the wetland systems. The water level inside the container was maintained at the level of 5 cm under the surface of the gravel bed to create a

subsurface flow constructed wetlands configuration. After 10 minutes for stabilization, the first sample was taken from the drain valve at the bottom. Effluent samples were taken twice daily for five days or until no further removal performance could be obtained. Water temperature was immediately measured as samples were taken. COD, NH_4^+, and TN were analyzed by using HACH reagents, of which methods are compliant with US EPA methods. Effluent samples were measured by a DR6000 laboratory spectrophotometer (HACH Company, Colorado, United States).

2.3. Data analysis

2.3.1. Determination of the removal rate constant

To investigate the rate constant of the contaminant removal, first rearrange the equation $dC/dt = –kC$ to $dC/C = –kdt$, then perform integration; the linearized equation of this model can be obtained as below:

$$\ln[C] = - kt + b \quad (1)$$

where C is the concentration of pollutant (mg/L), k is the rate constant ($h^{–1}$ or $d^{–1}$), t is the time (hour or day), and b is the constant.

During experiments, the concentration C of COD, NH_4^+, and TN were determined as a function of time. By plotting ln[C] versus time t, the constant rate k can be obtained from the slope of the Y axis. The correlation coefficient (R^2) was used to evaluate the reliability of the results.

2.3.2. Determination of the Arrhenius equation

The effect of temperature on the rate constant k is demonstrated by the Arrhenius equation:

$$k_T = k_{20}.\theta^{(T–20)} \quad (2)$$

where k_T is the rate constant at temperature T, k_{20} is the rate constant at 20°C, T is the temperature (°C), and θ is the Arrhenius temperature coefficient.

Take the natural logarithm of both sides and bring the equation to the linear form:

$$\ln(k_T) = \ln(\theta).(T–20) + \ln(k_{20}) \quad (3)$$

When attaining data of k_T values at various temperatures T, plot $\ln(k_T)$ values according to (T–20) on the graph, interpolate the linear equation, then the value of θ and k_{20} can be defined.

3. Results and discussion

3.1. TN removal rate constant

To determine the TN removal rate constant, synthetic wastewater containing COD of 400 mg/L and TN of 20 mg/L was fed to the experimental wetlands for treatment. Samples were taken twice daily at 10 am and 4 pm for four consecutive days. Effluent TN concentrations of all the samples are presented in Table 2. These data were processed to obtain the natural logarithm of concentration as a function of time, which are coordinates of the graph in Figure 2. Since the time has either unit of hour or day, two graphs were plotted to obtain the two different TN removal rate constants in terms of unit.

Table 2. Results for TN analysis.

Time	10h, 26/3	16h, 26/3	10h, 27/3	16h, 27/3	10h, 28/3	16h, 28/3	10h, 29/3	16h, 29/3
TN (mg/L)	19.1	17.7	11.5	10.7	9.7	9	9	–

The rate constant is the slope of the linear equation obtained from the graph (Figure 2). It can be seen in Figure 2a that the k_TN is 0.0111 $h^{–1}$, corresponding to 0.2664 $d^{–1}$; while

the direct result in Figure 2b show k_TN is 0.2428 d^{-1}. The two results are only 10% different, with equal correlation coefficients.

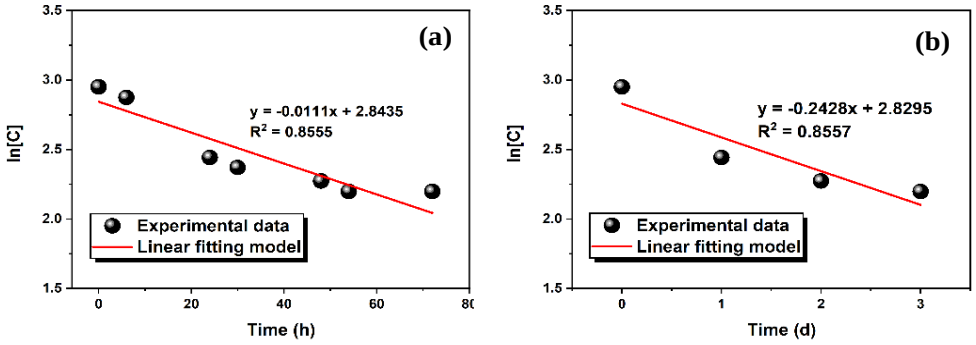

Figure 2. Plotting natural logarithms of TN concentration versus time to identify TN removal rate constant: (a) Time axis is in hour unit, k_TN (h^{-1}); b) Time axis is in day unit, k_TN (d^{-1}).

This k_TN value is equivalent to the result in the study [14] with k_TN = 0.246 d^{-1}. Although the experimental model and plant species are different, the retention time is longer than 7.5 days, and the temperature range is higher (25–30°C). [14] also conducted the study in batch mode, using synthetic wastewater.

3.2. Ammonium removal rate constant

Synthetic wastewater containing COD of 400 mg/l and NH_4^+ of 20 mg/l was fed to the experimental wetlands for treatment. Samples were taken twice daily at 10am and 4pm for four consecutive days. NH_4^+ concentrations of all the samples are presented in Table 3. These data were processed to obtain the natural logarithm of concentration as a function of time, which are coordinates of the graph ln[C] vs. time (Figure 3). Similarly, two graphs were plotted to obtain the two NH_4^+ removal rate constants in different units.

Table 3. Results for NH_4^+ analysis.

Time	10h, 8/4	16h, 8/4	10h, 9/4	16h, 9/4	10h, 10/4	16h, 10/4	10h, 11/4	16h, 11/4
NH_4^+(mg/l)	21.8	14.7	10.9	9.4	7.8	7.7	7.4	7.2

The rate constant can be determined from the slope of the line; thus, it can be seen in Figure 3a that the k_NH_4 is 0.0125 h^{-1}, corresponding to 0.3 d^{-1}, while the k_NH_4 value obtained from Figure 3b is 0.3576 d^{-1}. In this case, the graph plotting ln[C] vs. day unit gives a better correlation, which is not the same with k_TN. Thus, the number of data points does not contribute to a better correlation between the experimental data and the model. For simplicity, the data processing method with day unit is proposed to calculate the rate constant.

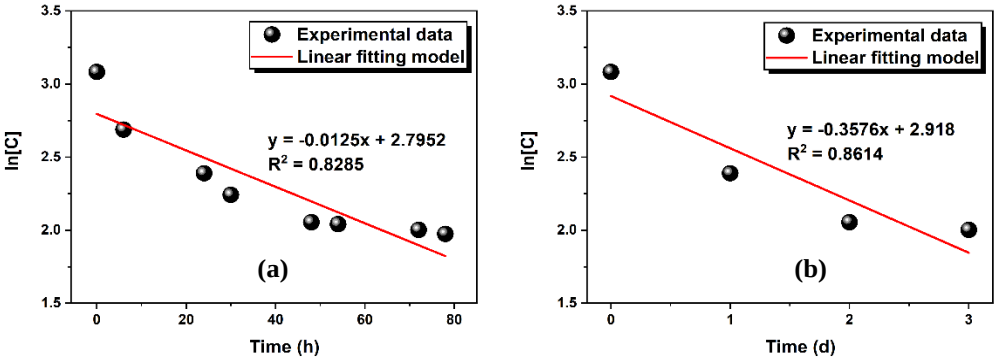

Figure 3. Plotting natural logarithms of NH_4^+ concentration vs. time to identify NH_4^+ removal rate constant: (a) Time axis is in hour unit, k_NH_4 (h^{-1}); (b) Time axis is in day unit, k_NH_4 (d^{-1}).

3.3. COD removal rate constant

Experiments to determine the COD removal constant rate were conducted at three different times of the year: March, April, and December. The initial concentrations of COD in the three experiments were kept similar, around 400 mg/l. COD concentrations of all the samples are presented in Table 4. These data were processed to obtain the COD removal rate constants in Table 4.

Table 4. Results for COD analysis.

Month	Temperature (ºC)	COD removal over time								
March	20–23	Time	10h, 26/3	16h, 26/3	10h, 27/3	16h, 27/3	10h, 28/3	16h, 28/3	10h, 29/3	16h, 29/3
		COD (mg/L)	395	255	75	72	63	65	55	55
April	28–29	Time	10h, 8/4	16h, 8/4	10h, 9/4	16h, 9/4	10h, 10/4	16h, 10/4	10h, 11/4	16h, 11/4
		COD (mg/L)	390	121	79	34	19	17	16	14
December	15–18	Time	12-Dec	13-Dec	14-Dec	15-Dec	16-Dec	17-Dec	–	–
		COD (mg/L)	387	284	140	96	44	35	–	–

For the reason that all of the experiments were conducted under natural conditions, and the recorded water temperatures during the experiment fluctuated. To explore the relationship between the constant k and the temperature, the average temperature value was chosen to correspond to the obtained constant k value. The temperature has a marked effect on the processing rate; as the temperature increases, the k_COD value increases (Table 5).

Table 5. k_COD values on the temperature.

Time	Average temperature	k_COD (d^{-1})	R^2
December	16.5ºC	0.51	0.9835
March	21.5ºC	0.61	0.7297
April	28.5ºC	1.1	0.9145

Represent the points on the graph of the relationship between the values of $\ln(k_T)$ and (T–20) (Figure 4). The obtained linear equation showed that the COD removal rate constant at 20ºC (i.e. k_COD_{20}) is 0.61 d^{-1} and the temperature coefficient $\theta = 1.07$.

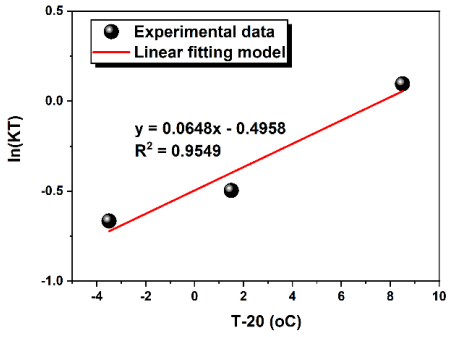

Figure 4. Plotting $\ln(k_T)$ vs. temperature difference (T–20).

This k_COD_{20} result is higher than 0.22 d^{-1}, which is the value determined [10]. Since the two studies used the same plant as reed and gravel material of similar size, the difference was due to the experimental design. The study conducted by [9] also had reeds and gravels of the same size and depth, resulting in k_COD = 2.64 d^{-1}, which is much higher than the results of this study. This result may be explained by the fact that the experiment conducted

by Abdelhakeem in Giza, Egypt, located in a hot desert climate with extremely high temperatures of 40–45ºC during the summer.

Regarding the temperature coefficient of the Arrhenius equation of COD, there are currently no published studies yet. Relative comparison with BOD removal parameters (k_{20} = 1.1 d^{-1} and θ = 1.06) [4], the temperature coefficient θ of COD in this study has the same value.

4. Conclusion

This study conducted a set of experiments in batch mode using synthetic wastewater to investigate the contaminant removal rate constant in subsurface flow constructed wetlands system. According to the obtained data, it can be concluded that:

An experimental pilot was successfully set up and operated for a long period to simulate the SSF constructed wetlands in natural conditions.

The removal rate constant (k) could be calculated and presented in different units (i.e., h^{-1} or d^{-1}) with a negligible difference and equal correlation coefficients (R^2).

The total nitrogen and ammonium removal rate constant was 0.2428 and 0.3576 d^{-1}, respectively. Furthermore, the k values for COD elimination increased along with the rise of the water temperature, which was 0.51, 0.61, and 1.1 d^{-1} at 16.5ºC, 21.5ºC, and 28.5ºC, respectively.

The Arrhenius temperature coefficient θ for COD removal in this study was 1.07.

These results demonstrate the feasibility of the proposed model to ascertain the value of the pollutant removal rate constant in the SSF CW system. From there, an accurate and complete data set of constant k can be obtained, improving the wetland design's accuracy and reliability.

Due to the lack of experimental conditions and time, this study still has some limitations, including the repeatability of the data set and the number of data points. Further studies aim to enhance the reliability by conducting the test with several reactors simultaneously, along with utilizing the actual wastewater sample as the water source instead of the synthetic one to investigate the performance of the SSF CW system in natural conditions.

Author contribution statement: Developing research ideas: T.P.P.; Data processing: D.Q.T., D.T.L., V.Q.N.; Building mathematical models: T.P.P., D.Q.T.; Writing draft articles: T.P.P., D.Q.T.

Acknowledgments: This research is funded by Hanoi University of Science and Technology (HUST) under grant number T2020–PC–029.

Competing interest statement: The authors declare no conflict of interest.

References

1. Kadlec, R.H.; Wallace, S.D. Treatment Wetlands. 2nd ed., Taylor & Francis Group, Boca Raton, 2009.
2. Vymazal, J.; Sengupta, M.; Dalwani, R. (Editors). Constructed Wetlands for Wastewater Treatment: A Review, In Proceedings of the World Lake Conference, Jaipur, Rajasthan, India, 28 October – 2 November 2007, 2008, 965–980.
3. Crites, R.; George, T. Small and Decentralized Wastewater Management systems. McGraw–Hill Higher Education, USA, 1998, pp. 1104.
4. Reed, S.C.; Crites, R..; Middlebrooks, E.J. Natural Systems for Waste Management and Treatment: 2nd edition. McGraw–Hill, New York, USA, 1995.
5. Magdalena, G.; Katarzyna, S.; Krzysztof, J.; Zbigniew, M.; Włodzimierz, W.; Agnieszka, K. P. Kinetics of pollutants removal in vertical and horizontal flow constructedwetlands in temperate climate. *Sci. Total Environ.* **2020**, *718*, 137371.
6. Haiming, W.; Jian, Z.; Huu, H.N.; Wenshan, G.; Zhen, H.; Shuang, L.; Jinlin, F.; Hai,

L. A review on the sustainability of constructed wetlands for wastewater treatment: Design and operation. *Bioresour. Technol.* **2015**, *175*, 594–601.
7. Magdi, E.K.; Gaber, Y.; El–Reash, A.; Ahmed, M.I.; Rizk, F.W. Effect of media variation on the removal efficiency of pollutants from domestic wastewater in constructed wetland systems. *Ecol. Eng.* **2020**, *143*, 105668.
8. Cao, S.; Jing, Z.; Yuan, P.; Wang, Y. Wang, Y. Performance of constructed wetlands with different substrates for the treated effluent from municipal sewage plants. *J. Water Reuse Desalin.* **2019**, *9(4)*, 452–462.
9. Abdelhakeem, S.G.; Aboulroos, S.A.; Kamel, M.M. Performance of a vertical subsurface flow constructed wetland under different operational conditions. *J. Adv. Res.* **2016**, *7*, 803–814.
10. Villasen˜, J.; Mena, J.; Ferna´ndez, F.J.; Go´mez, R.; de Lucas, A. Kinetics of domestic wastewater COD removal by subsurface flow constructed wetlands using different plant species in temperate period. *Int. J. Environ. Anal. Chem.* **2010**, *91(7)*, 693–707.
11. Trang, N.T.D.; Dennis, K.; Hans–Henrik, S.; Chiem, N.H.; Tuan, L.A.; Hans, B. Kinetics of pollutant removal from domestic wastewater in a tropical horizontal subsurface flow constructed wetland system: Effects of hydraulic loading rate. *Ecol. Eng.* **2010**, *36(4)*, 527–535.
12. Pérez, M.M.; Hernández, J.M.; Bossens, J.; Jiménez, T.; Rosa, E.; Tack, F. Vertical flow constructed wetlands: kinetics of nutrient and organic matter removal. *Water Sci. Technol.* **2014**, *70(1)*, 76–81.
13. von Sperling, M.; de Paoli, A.C. First–order COD decay coefficients associated with different hydraulic models applied to planted and unplanted horizontal subsurface–flow constructed wetlands. *Ecol. Eng.* **2013**, *57*, 205–209.
14. Sonavane, P.G.; Munavalli, G.R. Modeling nitrogen removal in a constructed wetland treatment system. *Water Sci. Technol.* **2009**, *60(2)*, 301–309.
15. Weerakoon, G.M.P.R.; Jinadasa, K.B.S.N.; Manatunge, J.; Wijesiri, B.; Goonetilleke, A. Kinetic modelling and performance evaluation of vertical subsurface flow constructed wetlands in tropics. *J. Water Process Eng.* **2020**, *38*, 101539.
16. Adelaide, A.; Fátima, C.; Maria J. Imaginário.; Ivone, C.; Ana R. Prazeres.; Carlos Ribeiro. Nitrate removal in vertical flow constructed wetland planted with Vetiveria zizanioides: Effect of hydraulic load. *Ecol. Eng.* **2017**, *99*, 535–542.

VIETNAM JOURNAL OF HYDROMETEOROLOGY

Research Article

Potential production of bioplastics PHAs (polyhydroxyalkanoates) from paper–mill wastewater

Minh Ky Quang Ho[1]*, Thai Duy Ngo[2], Thu Thi Minh Nguyen[1]

[1] Department of Environmental Science, Sai Gon University; hkqminh@sgu.edu.vn; ntmthu@sgu.edu.vn

[2] Saigon University Institute of Environment - Energy Technology; thaingo.ieet@sgu.edu.vn

*Corresponding author: hkqminh@sgu.edu.vn; Tel.: +84–947169769

Received: 15 February 2023; Accepted: 24 March 2023; Published: 25 March 2023

Abstract: The extensive use of petroleum–based synthetic plastics is leading to various environmental problems such as ecological impact, and untreated plastic waste, particularly micro–plastic pollution. Bioplastics are, therefore, considered one of the prospective solutions to replace conventional plastics. PHAs (polyhydroxyalkanoates), one of the widely studied and applied bioplastics, is synthesized by microorganisms when their living conditions are unfavorable. Many species of microorganisms capable of synthesizing PHAs are found in different environments. In the study, we focus on isolating and screening bacteria capable of synthesizing PHAs from activated sludge of paper mill wastewater treatment system. The results have shown two types of bacteria that have the highest synthesizing productivity: Bacillus Megaterium BP5 and Alcaligenes Aquatilis BP6. Their highest yield of PHAs synthesis was reached at the time 48 hours of incubation, which their dry biomass of 41.19% and 49.11%, respectively.

Keywords: PHAs; Polyhydroxyalkanoates; Polyhydroxybutyrate; Wastewater; Bioplastic.

1. Introduction

The widespread application of non–biodegradable petroleum–based synthetic plastics leads to many environmental pollution consequences [1–2] such as plastic pollution in continents and oceans, especially micro–plastic pollution. Due to their biodegradability, bioplastics are acknowledged to have the potential material to replace synthetic plastics, and thus reduce adverse environmental impacts. Bioplastics is considered a potential solution to replace conventional plastics. They are bio–based polymers synthesized from organic sources, with little impact on the environment [3]. One of the bioplastics that has attracted a lot of attention from researchers is Polyhydroxyalkanoates (PHAs). PHAs have similar physical properties to conventional plastics such as heat resistance up to 170^{o}C, high strength, and more importantly almost no toxicity [4]. PHAs are a large family of polymers that are biosynthesized by bacteria when their growing conditions are disadvantaged, such as too high a carbon–to–nitrogen ratio living environment [5–6].

PHAs are classified into two groups based on the length of the polymer units, namely short–chain PHA (poly HASCL) and medium–chain PHA (Poly HAMCL) (Figure 1). In the short–chain group, they are composed of 3 or 5 carbon atoms commonly known as 3HB (hydroxybutirate) and 3HV (hydroxyvalerate). The other group is composed of 6 or more carbon atoms [7]. PHAs has similar physical properties to conventional plastics [8] but is readily biodegradable, so PHAs is considered a potential alternative to synthetic resins [9]. PHAs are applied in many fields such as disposable plastic products, food packaging, agriculture, construction, pharmaceuticals, and medicine [10–11].

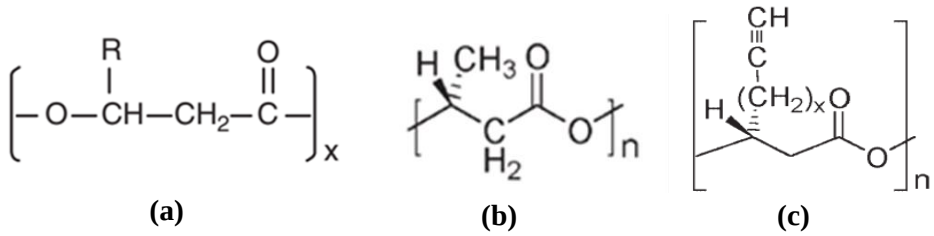

Figure 1. PHAs' chemical formulas: (a) PHAs; (b) poly HASCL (3HB); (c) Poly HAMCL.

Currently, although there have been many studies on the production of PHAs, the application of PHAs in practice is limited due to high manufacturing costs [12]. To reduce production costs, the microbial strains for synthesizing PHAs must meet the following criteria such as fast growth, high biomass of PHAs, and affordable culture materials. Other prerequisites in PHAs production include controlled living conditions, simple culture settings, uncomplicated extraction process, and reasonable cost [13–14]. To date, more than 300 species of microorganisms have been found to be able to synthesize PHAs [3]. Some common types of bacteria such as Pseudomonas, Azotobacter vinelandii Alcaligenes eutrophus, Alcaligenes latus, Bacillus megaterium, etc. are of great importance to many scientists due to their high yield of PHAs biosynthesis [15].

In the study, we isolated and screened bacterial strains capable of biosynthesis of PHAs, from activated sludge of a paper mill wastewater treatment system. The study also evaluated the capability of these bacterial species to PHAs biosynthesize under laboratory conditions. Besides, one of the main differences of this study compared to the previous ones is that we found the optimal culture time for the bacteria to synthesize PHAs.

2. Materials and Methods

2.1. Materials

Isolation materials: Nutrient agar, consist of Peptone 5 g/L; NaCl 5 g/L; Meat glue 1.5 g/L; Mushroom extract 1.5 g/L; Agar 15g/L (Figure 2).

PHAs biosynthesis environment: Improved nutrient broth, including Peptone 2.5 g/L; NaCl 2.5 g/L; Meat glue 0.75 g/L; Mushroom extract 0.75 g/L; Glucose 4 g/L.

Bateria source: the activated sludge sample taken from Minh Hung paper mill (Binh Phuoc province, Vietnam).

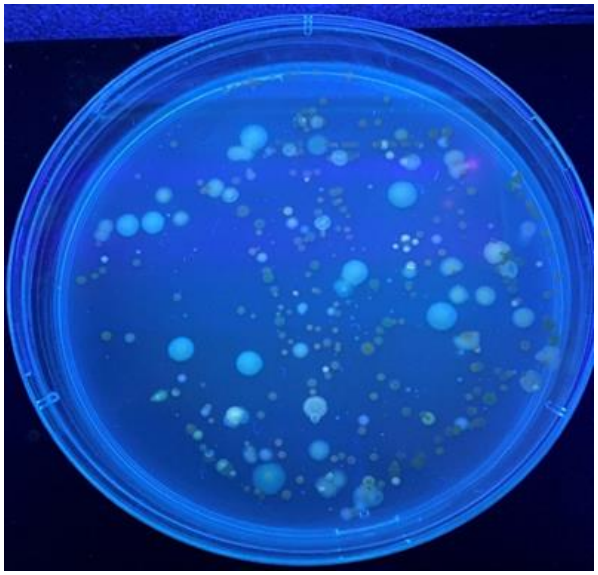

Figure 2. Isolation and screening of PHAs bacteria.

2.2. Methods

2.2.1. Isolation and screening of bacteria capable of biosynthetic PHAs

The activated sludge sample was diluted one million times before spreading on Nutrient Agar (NA) and incubated at 32^{o}C for 72 hours. Colonies of bacteria species capable of synthesizing PHAs were identified by staining with Sudan Black B (black color) [16]; then confirmed by Nile Blue A dye. Under UV light, fluorescence colonies were detected. These colonies were selected to be capable of synthesizing PHAs [17–18].

2.2.2. Evaluation of the PHAs synthesizing capability of the isolated bacterial strains

The screened bacteria were further cultured in the Nutrient broth to motivate PHAs synthesis. The culture process was carried out at 32^{o}C, pH = 7.0, shaking at 150 rpm for 72 hours. Biomass at 24, 48, and 72 hours was collected and measured to determine the highest PHAs yield duration.

The extraction method of Gulab Singh et al was applied to evaluate the PHAs' content in the biomass [19]. The process includes taking 50 ml of culture solution, centrifuging at 7800 rpm for 15 minutes, then removing the solution to collect biomass. The obtained biomass was then incubated with 10 ml of NaOCl solution (2%) at 50^{o}C for one hour. The solution was then centrifuged at 7800 rpm for 20 min. The supernatants were then removed, and washed with distilled water, alcohol, and acetone. The filtered solid substance (obtained polymer) was dissolved in hot chloroform and screened through Whatman No.1 filter paper, then dried at room temperature. Dissolve the obtained PHAs in 10 ml of concentrated H_2SO_4 and incubate at 100^{o}C to convert all the PHAs to crotonic acid. The compound was measured the optical density (OD) at 235 nm with PHAs control (sigma) to determine accumulated PHAs content in bacterial cells. The accumulation of PHAs in bacterial cells was calculated according to the following formula:

$$\text{PHAs} = \text{PHAs content/dry biomass content} \quad (1)$$

2.2.3. Bacteria identification by 16s–rRNA sequence analysis

After checking the capability of PHAs productivity, selected bacterial strains were identified by 16S–rRNA fragment analysis with primers 16sF 5'– AGA GTT TGA TCC TGG CTC AG –3' and 16sR 5'– ACG GCT ACC TTG TTA CGA CTT – 3'.

The experiment was conducted at the laboratory of the Center for Biotechnology, Ho Chi Minh City. The 16S rRNA gene sequences were compared (blast) with the US database, Genebank (NCBI) for identification.

3. Results and discussion

3.1. Isolation and screening of bacteria capable of PHAs biosynthesis

From the activated sludge sample, we isolated 32 strains of bacteria with symbols BP1 to BP32. Screening by Sudan Black B and Nile Blue A, there were two strains fluorescented under 365nm UV lamp, labeled BP5, BP6. Both of them were lighted orange on the second day of incubation. They are considered the potential bacteria of PHAs biosynthesis (Figure 3 to Figure 5).

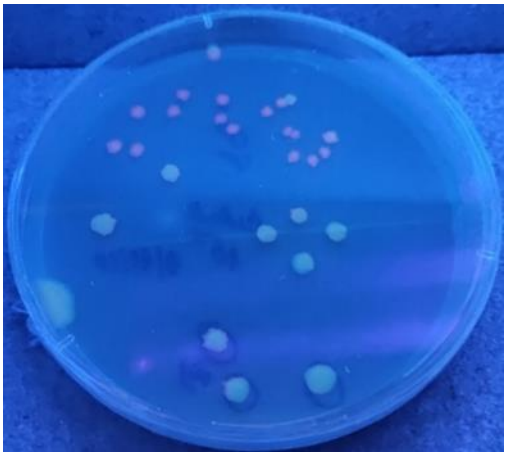

Figure 3. Fluorescent bacteria on NA medium supplemented with Nile blue A dye under 365nm UV lamp.

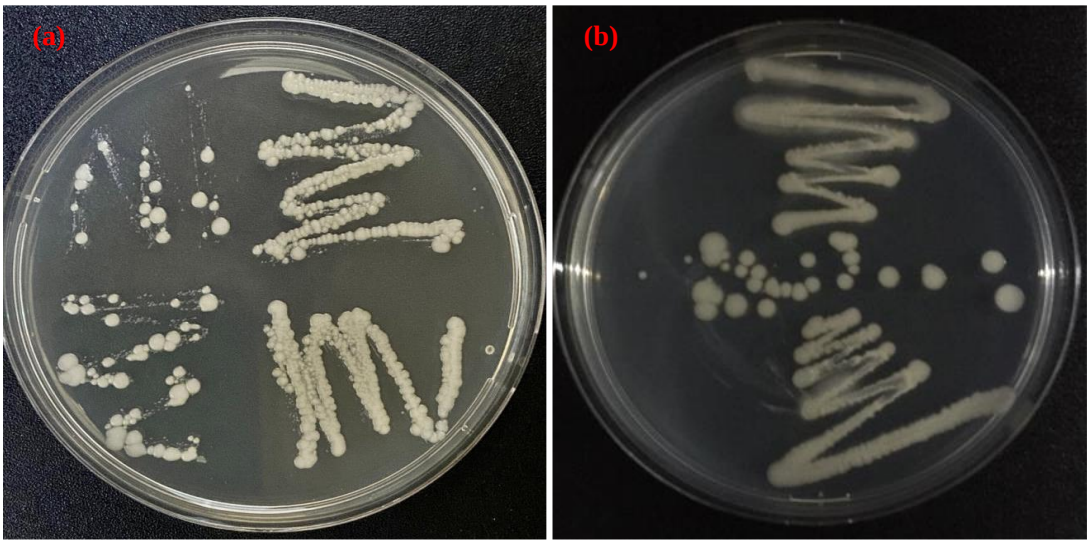

Figure 4. (a) Colony of BP5 bateria; (b) Colony of BP6 bateria.

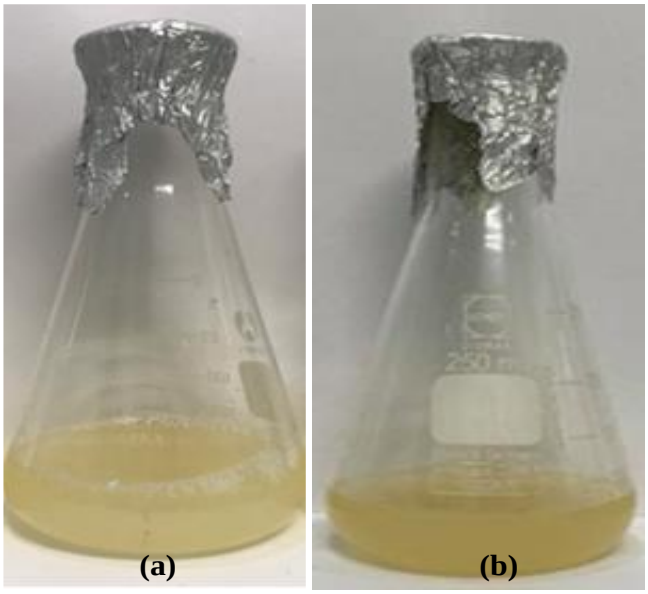

Figure 5. Nutrient broth of bacterial strain BP5 (panel a) and BP6 (panel b).

3.2. Evaluation of the PHAs synthesizing capability

The results of measuring the optical density (OD) of the 2 selected samples after culture and treatment are shown in panel (a) of Figure 6. This result shows that both selected strains have the highest PHAs synthesis yield at 48h of culture.

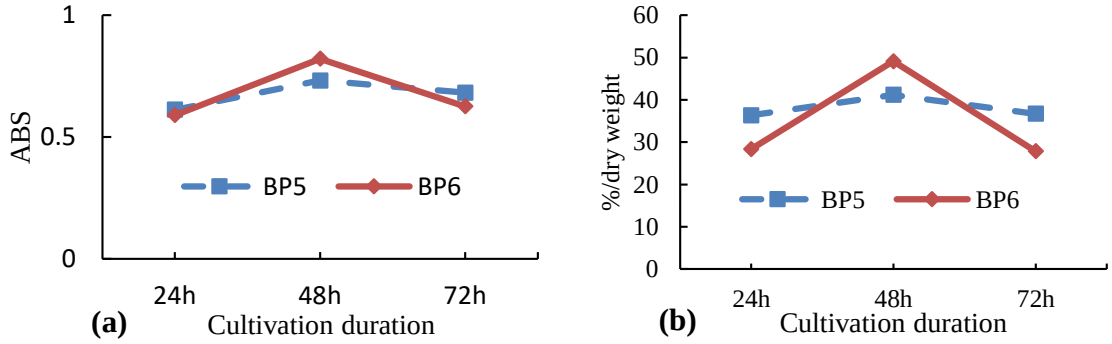

Figure 6. PHB cultivation results: (a) Optical density measurement results at the time of culture; (b) Accumulated PHAs content in bacterial cells.

Biomass from the culture solutions of the two strains at 24h, 48h, and 72h was dried and extracted PHAs according to Gulab Singh process [19]. The accumulated PHAs content on the dry biomass of bacteria is shown in Figure 5.

The assessment results on the synthesizing PHB capability of the two strains BP5 and BP6 showed that the ability to accumulate PHB of these two strains was quite high, 41.19% and 49.11% respectively, which was higher than the average level when compared with other strains (Table 1).

Table 1. PHAs biosynthesis yield in improved nutrient broth environment for 48h.

No.	Strains of bacteria	Dry biomass (g/L)	PHAs contents (g/L)	PHAs productivity (%/dry biomass)
1	BP5	0.378	0.1557	41.19%
2	BP6	0.79	0.388	49.11%

Similar ratios have been published by some other authors. One of the studies on optimizing conditions for culturing some strains of *Bacillus sp*. resulted in PHAs accumulation from 20.3% to a maximum of 70.04% of the dry biomass [6]. Rituparna Das et al (2022) studied that the *bacillus pumilus* AHSD 04, isolated from parts of an oilseed plant *(Oleaginous Plant Arachis)* can produce from 26.2% to 76.5% of the PHB dry biomass [20].

The study also showed that the optimal culture time for the two bacterial strains on PHAs biosynthesis was 48 hours (Figure 7). This result also showed that when the culture time is longer, the bacteria use PHAs as a substrate source for growth. This research results show a similarity in optimal PHAs time of synthesizing on strain *Rhizobium gallicum* R602 [23].

Figure 7. PHA extracted from BP5.

Besides, the yield of PHAs synthesis of BP6 was higher than that of BP5. From these results, it can be assessed that the potential of the two bacterial strains obtained in the study is very promising. Their capability to synthesize PHAs is quite high in sub–optimal conditions, together with their ability to adapt well to living in a wastewater environment.

3.3. Bacterial identification by 16s–rRNA sequence analysis

These bacterial strains (BP5 and BP6) were inoculated for purification on a petri–dish containing Nutrient agar. After culturing at 32^{o}C for 48 hours, the bacterial colonies were sent to the Center for Biotechnology, Ho Chi Minh City for DNA extraction and PCR amplification of the 16S rRNA fragment. Sequences were searched on BLAST NCBI (http://blast.ncbi.nlm.nih.gov/).

The results showed the match of the BP5 gene fragment with the 16S rRNA fragment of *Bacillus megaterium* mj1212 with accession number KJ451626.1. Similarly, the gene sequence of strain BP6 matches the gene fragment of strain *Alcaligenes aquatilis* RC43 with accession number MT572474.1 (Figure 8).

Figure 8. Phylogenetic tree based on NCBI data.

This result shows that the isolated bacterial strains are also the species that have been evaluated to have good PHAs synthesis ability in previously published studies.

4. Conclusion

From the activated sludge sample from the wastewater treatment system of Minh Hung paper factory (Binh Phuoc province, Vietnam), we isolated two strains of bacteria with potential for PHAs biosynthesis, particularly PHB. They are *Bacillus Megaterium* BP5 and *Alcaligenes Aquatilis* BP6. The biosynthesis research results show that the optimal time of culture for the biosynthesis of PHAs of these two strains in the modified Nutrient broth is 48h. This is one of the main findings contributing to the knowledge of PHAs biosynthesis of bacteria.

Since the research was carried out in the laboratory, further studies on the evaluation of the yield of PHAs production in practice, such as the paper mill wastewater environment, should be researched, particularly the optimal incubation time. Besides, as in this study improved nutrient broth was applied to stimulate the bacteria to synthesize PHAs, more studies on affecting living conditions of the bacteria in practice need to be implemented to improve the effectiveness. Consequently, the study's results can apply to the pilot scale.

Author contribution statement: Conceived and designed the experiments; Analyzed and interpreted the data; contributed reagents, materials, analysis tools or data; manuscript editing: M.K.Q.H.; Performed the experiments; contributed reagents, materials, analyzed and interpreted the data, wrote the draft manuscript: T.D.N., T.T.M.N.

Acknowledgements: This research was funded by the Saigon University, Ho Chi Minh City. The authors would also like to thank the members of the Center for Biotechnology, Saigon University, Ho Chi Minh City for the laboratory and discussions to improve the quality of the publication.

Competing interest statement: The authors declare no conflict of interest.

References

1. Huang, T.; Zhao, J.Q.; Shen, J.R. The progress in microbiodegradable plastics. *Plastics Industry*. **1991**, *4*, 23–27.
2. Young, R.J. Synthesis of polymers. Introduction to Polymers. Chapman and Hall, New York. 1981, pp. 9–85.
3. Mannina, G.; Presti, D.; Montiel–Jarillo, G.; Suárez–Ojeda, M.E. Bioplastic recovery from wastewater: A new protocol for polyhydroxyalkanoates (PHA) extraction from mixed microbial cultures. *Bioresour. Technol.* **2019**, *282*, 361–369.
4. Da, N.T.; Linh, N.T.; Trang, N.T.; Hai, T.M.; Huyen, L.T. Screenning and determination of polyhydroxyalkanoate production by Bacillus sp. Strains. *VN J. of Food Control* **2020**, *3*, 165–172.
5. Wang, J.; Yu, H.Q. Cultivation of polyhydroxybutyrate–rich aerobic granular sludge in a sequencing batch reactor. *Water Sci. Technol.: Water Supply* **2006**, *6*, 81–87.
6. Thirumala, M.; Reddy, S.V.; Mahmood, S.K. Production and characterization of PHB from two novel strains of Bacillus spp isolated from soil and activated sludge. *J. Ind. Microbiol. Biotechnol.* **2010**, *37*, *271–278.*
7. Kim, Y.B.; Lenz, R.W. Polyesters from microorganisms. *Biopolyesters* **2001**, 51–79.
8. Howells, E.R. Opportunities in biotechnology for the chemical industry. *Chem. Ind*. **1982**, *7*, 508–511.
9. Hieu, H.V.; Dung, T.H.; Loc, L.T.; Dung, C.A.; Hoat, P.C. Isolation and molecular identification of Polyhydroxybutyrate–producing bacterial strain in Ho Chi Minh City. *VN J. Sci. Technol. Eng*. **2016**, *5*, 54–58.
10. Ivanova, G.; Serafim, L.S.; Lemos, P.C.; Ramos, A.M.; et al. Influence of feeding strategies of mixed microbial cultures on the chemical composition and

microstructure of copolyesters P (3HB–co–3HV) analyzed by NMR and statistical analysis. *Magn. Reson. Chem*. **2009**, *47*, 497–504.

11. Reddy, C.S.K.; Ghai, R.; Kalia, V. Polyhydroxyalkanoates: an overview. *Bioresour. Technol*. **2003**, *87*, 137–146.
12. Braunegg, G.; Bona, R.; Koller, M. Sustainable Polymer Production. *Polymer–Plastics Technol. Eng*. **2004**, *43*, 1779–1793.
13. Volova, T.G. Polyhydroxyalkanoates–plastic materials of the 21st century: production, properties, applications. Nova Publishers, 2004.
14. Tian, P.; Shang, L.; Ren, H.; Mi, Y.; et al., Biosynthesis of polyhydroxyalkanoates: current research and development. *Afri. J. Biotechnol*. **2009**, *8*, 709–714.
15. Choi, J.; Lee, S.Y. Process analysis and economic evaluation for poly (3–hydroxybutyrate) production by fermentation. *Bioprocess. Eng*. **1997**, *17*, 335–342.
16. Thuoc, D.V.; Van, N.T., Bioconversion of glycerol to Polyhydroxyalkanoate by halophilic bacteria isolated from mangrove soil samples. *VN J. Sci. Technol*. **2015**, *53*, 615–624.
17. Li, R.; Gu, P.; Fan, X., Shen, J.; et al. Isolation and Characterization of PHA–Producing Bacteria from Propylene Oxide Saponification Wastewater Residual Sludge. *Appl. Biochem. Biotechnol.* **2018**, *186*, 233–244.
18. Kung, S.S.; Chuang, Y.C.; Chen, C.H.; Chien, C.C. Isolation of polyhydroxyalkanoates–producing bacteria using a combination of phenotypic and genotypic approach. *Lett. Appl. Microbiol.* **2007**, *44*, 364–371.
19. Singh, G.; Kumari, A.; Mittal, A.; Yadav, A.; et al., Poly β –Hydroxybutyrate Production by Bacillus subtilis NG220 Using Sugar Industry Waste Water. *BioMed Res. Int*. **2013**, 1–10.
20. Das, R.; Pal, A.; Paul, A.K. Optimization of Process Parameters for Production of Poly(3–hydroxybutyrate) by Bacillus pumilus AHSD 04, a Seed Borne Endophyte of Oleaginous Plant Arachis hypogaea L. *Biointerface Res. Appl. Chem*. **2021**, *12*, 5280–5295.
21. Ha, P.T.; Man, T.D.; Yutaka, T. Generating mutants to enhance Poly–β Hydroxybutyrate biosynthetic activity of Alcaligenes Latus VN1 bacteria. *J. Biotechnol*. **2008**, *6*, 489–496.
22. Lakshmi, R.S.; Hema, T.A.; Divya, T.R.; Starin, S.T. Production and optimization of polyhydroxybutyrate from Rhizobium sp. present in root nodules. *J. Pharm. Biol. Sci*. **2012**, *3*, 21–25.
23. Luan, N.T.; Thuong, N.T.L.; Mai, N.T.Q.; Chanh, N.M. Isolation and identification of poly– β –hydroxybutyratebiosynthesis from botanical resources in Binh Duong province, Vietnam. *J. Sci. Technol. Food* **2018**, *14*, 12–19.

VIETNAM JOURNAL OF HYDROMETEOROLOGY

Check for updates

Research Article

A comparative analysis of regression equations for rating curve development at a gauging station in Da river, Northern Vietnam

Minh Dang Tran Duc[1], Huy Dao Ba[1], Quynh Hoang Diem[1], Tinh Nguyen Thi[2], Hanh Nguyen Duc[1], Vinh Tran Ngoc[3], Giang Nguyen Tien[1*]

[1] Faculty of Hydrology, Meteorology and Oceanography, University of Science, Vietnam National University, Hanoi. Add: 334 Nguyen Trai Street, Thanh Xuan District, Hanoi, Viet Nam; dangtranducminh_t65@hus.edu.vn; daobahuy_t66@hus.edu.vn; diemquynhoang918@gmail.com; nguyenduchanh@hus.edu.vn; nguyentiengiang@hus.edu.vn

[2] Center for hydro–meteorological observation, Viet Nam Meteorological and Hydrological Administration. Add: 8 Phao Dai Lang, Lang Thuong, Dong Da, Ha Noi, Viet Nam; tinh.nt.198@gmail.com

[3] Department of Civil and Environmental Engineering, University of Michigan, Ann Arbor, MI, USA; vinhtn@umich.edu

*Corresponding author: nguyentiengiang@hus.edu.vn; Tel: +84–912800896

Received: 5 February 2023; Accepted: 23 March 2023; Published: 25 March 2023

Abstract: Constructing rating curves at hydrological stations is of tremendous significance for water resources management, yet in Vietnam, it has not been given the adequate attention it deserves. In this study, eight traditional regression equations representing the linear and non–linear correlation between gauging discharge and water level (stage) at PoLech station in Da river, were evaluated with the aim of determining the most suitable equations for discharge interpolation and high flow extrapolation. A straightforward segmentation technique was proposed to simplify the automatic piecewise regression. The results revealed that: i) Second–order polynomial regression equations (in which stage is independent variable and either Q or $Q^{1/2}$ is dependent variable) proved to be the most efficient for discharge interpolation, when automatic piecewise regression was applied; ii) The linear regression equation illustrating relationship between square root of discharge and stage performed the best for high flow extrapolation; iii) The amalgamated rating curve, which was formed by utilizing all–years rating data, could be used for each year interpolation with care and additional research is required in relation to its accuracy. The potential of being able to generate continual discharge estimations at a low cost and with relatively uncomplicated calibration methods is expansive. This approach has the potential to encourage researchers, aquatic ecosystem stewards, water quality monitors, or appraisers of upstream withdrawals to start gauging river discharge on a more regular basis from an operational standpoint.

Keywords: Regression; Rating curve; Da river; Interpolation; Extrapolation of discharge.

1. Introduction

The effective management of water resources necessitates the utilization of hydrologic variables such as precipitation, run–off, or discharge in streams [1–5]. The amount of water circulating in streams can significantly differ in both temporal and spatial terms, which is primarily attributed to the variations in duration, frequency, intensity, and extent of precipitation as well as the characteristics of the catchment area [5–10]. Knowledge of the

flow of rivers and their variability is an essential part of the assessment and management of surface water resources. To conduct reservoir designs, flood frequency studies, flood inundation modeling, design of flood protection and warning systems, water supply engineering, drought studies, geomorphologic studies, etc., the records of discharge measurement need to be obtained from the river [11, 12]. However, this process is often costly, laborious and can be difficult to conduct in the case of extreme floods [11, 13].

By constantly monitoring the water level, it is possible to accurately calculate river discharge through the application of a rating curve, which is a correlation between discharge and water level [14–17]. When the hydraulic properties of a river remain constant and the stage–discharge relationship is not influenced by unsteadiness, it is relatively easy to develop a reliable single–valued rating curve (a one–to–one relationship between the stage and the discharge) [17–19]. There have been many studies on building stage–discharge relationships, which followed two main approaches: the physically based approach and the data–driven approach. In a physically based approach, Manning's equation – a widely accepted and extensively utilized physical equation is typically incorporated in 1D, 2D, and 3D hydrodynamic models to quantify the interrelationship between discharge and hydraulic head [12, 20, 21]. This approach requires accurate information regarding the topography of the channel and boundary conditions of the flow. The data–driven approach is based on a relationship (linear or nonlinear) between discharge and stage and possibly other related factors such as velocity, slope, bed roughness, etc. In this paper, the data–driven approach is the focus, so the following will refer to this approach in more detail.

Following the data–driven approach, there are three groups of methods, namely: graphical [14, 22]; regression [15, 23–26]; and machine learning [27–28]. According to [5], many researchers use Machine Learning algorithms such as Artificial Neural Network (ANN), Support Vector Machine (SVM), MT, Takagi–Sugeno (TS) fuzzy inference, Genetic Algorithm (GA), Generalized Reduced Gradient (GRG) to derive discharges from other measured variables. However, these methods often require additional data (stage and/or discharge) from other stations upstream of the station under study. Therefore, in this paper, the traditional methods are used to ensure that it is possible to build rating curves that can serve to calculate the discharge at a station from only the gauged stage of that station.

The efficacy of conventional regression techniques has been established through a plethora of preceding examinations and is frequently employed. Essentially, the rating curves are calculated through a regression process with the use of measurements of stages (water surface elevation above the mean sea level) and the corresponding measured discharges, and sometimes from velocity distribution, bed roughness and friction slope [18]. [29] developed two methods for automatic computation using least–squares approximation, one based on polynomials and the other on piecewise–continuous splines. Both methods were found to work well and once the parameters for a gauging station have been determined, rating data can be processed automatically. According to [29], whereas it is sometimes a convenient approximation to the relationship Q–H over the whole range of data, in general it is an over–simplification of the real hydraulics at many gauging stations. The more general representation of Q–H relationship by a polynomial of higher degree M has been in the background for some time [1, 22, 30–32] used it successfully with just M = 3, and in general, most of all studies show that with M greater than 3, the results are not good. [14] suggested writing the polynomial for Q raised to the power (Q). [33] used the polynomial approximation methods to obtain 622 rating curves from 171 Australian Bureau of Meteorology Hydrologic Reference Stations. They found that the methods worked well except for about 0.5% of the stations, where there was difficulty approximating the low–flow data. Despite the widespread use of regression equations for flow calculation

worldwide, very few studies have been conducted to explore the suitability of such equations for Vietnamese locations that only record water level measurements. In particular, [34] suggested using the Spline regression function of third order to develop rating curves for 23 stations across 19 rivers in Vietnam. [35] proposed the use of linear and second–order nonlinear regression for rating curve development based on data from the Ha Bang hydro–station on the Ky Lo river from 2013 to 2020. A commonality among these few studies is that the authors attempted to propose a single rating curve based on a long sequence of data. However, the water level–discharge relationship often changes over time due to changes in topography/riverbed morphology, particularly in rivers affected by large reservoir systems such as the Da River. As a result, there is an urgent need to investigate the potential and effectiveness of these techniques in this context.

Specifically, in Vietnam, the discharge compilation/processing is typically conducted in accordance with the stringent provisions of the regulation of TCVN 12636–15:2021 [36]. Generally, hydrological stations in Vietnam have been relying on manual direct measurement of flow using flowmeters, floats, and acoustic doppler current profiler devices, with the subsequent manual correction achieved through a series of steps. This process involves the drawing of a cross–section of a river, investigating of the cross–relationship of factors such as discharge, water level, cross–sectional area, flow velocity and the analysis of the relationship between these factors, and selecting of the most suitable processing method. For the later task, the calculation of rating curves is usually done manually (drawn on technical papers) or using HydPro1.0 software. In this software, the following equations can be used to build a steady–flow rating curve: exponential function, polynomial of order 2 (parabola), Spline regression function of order 3; Q as a polynomial second degree of H. There have been almost no domestic studies suggesting which function is the best for rating curve construction or evaluating the possibility of rating curve extrapolation. Meanwhile extrapolation is one of the important roles of using rating curves. Therefore, this paper is focused on answering the following three research questions:

1. Which regression equation is the best for interpolating discharge given pairs of gauging Q and H for an individual year of records?

2. Is it possible to apply a regression equation using multi–year gauging data to interpolate Q for each year in a stable station?

3. Which regression equation is the best for extrapolating high discharges given pairs of gauging Q and H for an individual year of records?

Compared with the current processing approach, the utilization of regression–based approaches not only ensure the precision of flow estimation, but also boasts superior performance in terms of efficiency, capability, and transparency. Specifically, with the proposed equation, the flow correction can be accomplished expeditiously in comparison to the existing manual labor. Additionally, if the data is refreshed automatically from the automated measuring stations, the provision of real–time data can be done with considerable ease. Furthermore, with new data on both discharge and water level being updated, the equations can automatically refresh and re–optimize the coefficients rapidly through optimization algorithms. Lastly, with the proposed equations being made available to the public through this study, their application and utilization will be more widespread among numerous target groups such as administrators or researchers. In contrast, the current data processing and editing in Vietnam is only conducted internally and not made public to the relevant units. The advantage of the suggested approach is particularly prominent for stations with unique locations (e.g., PoLech station, Da river, which is the primary focus of this work) located on transnational rivers and situated at the upstream position of the largest reservoir system in Vietnam.

2. Materials and Methods

2.1. Study site

Da river originates from Yunnan province, China. The whole basin stretches from 20º40'N – 25º00'N and 100º22' – 105º24'W [37]. Its total length is approximately 1010 km with a catchment area of around 52900 km^2 (49% of area belongs to China) [38]. In Vietnam, Da river flows through Lai Chau, Dien Bien, Son La, Hoa Binh, Phu Tho provinces. The river discharge is large, which accounted for 31% of water supply for the Red river basin. Da river is in a tropical monsoon climate. The rainfall distributed unevenly in time and space. The annual rainfall in the Da River basin in the period 2016–2021 ranges from 1,300 mm to over 2,600 mm [39]. The rainy season starts from May and lasts in October, with rainfall accounting for 85 to 90% of the total annual rainfall [37]. The flow regime of the Da River is heavily influenced by rainfall, with the flood season occurring from June to October and reaching a peak in July and August. The dry season lasts from November to May of the following year.

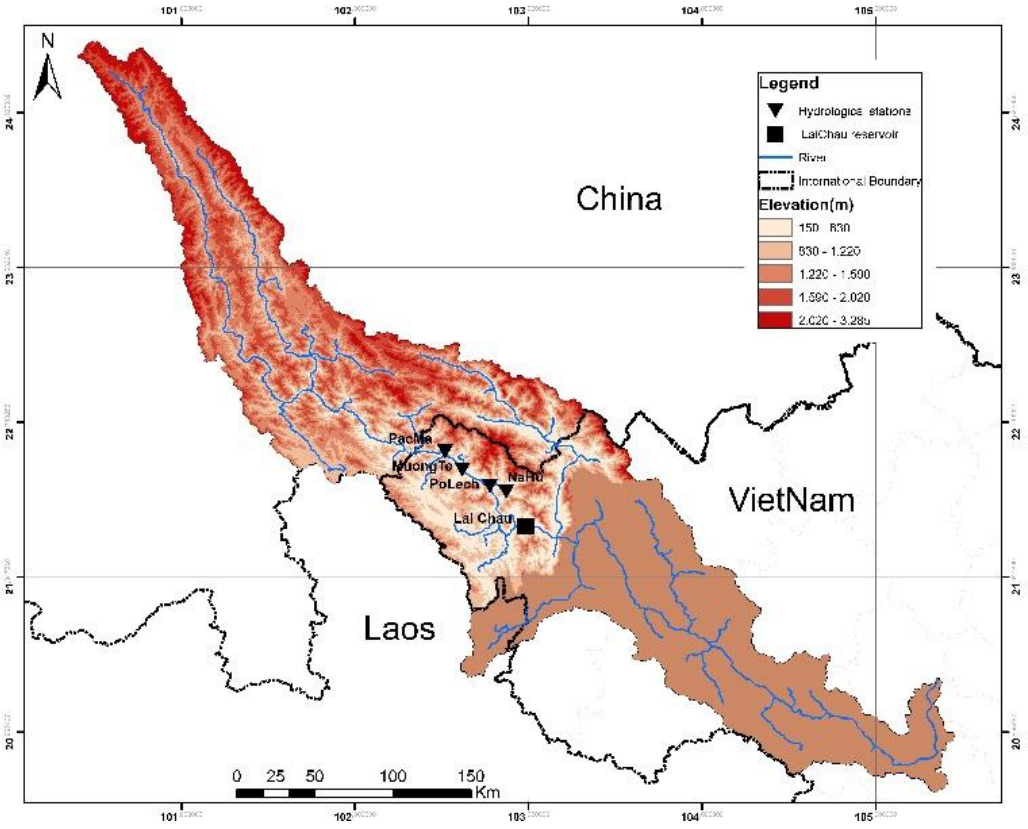

Figure 1. Da river basin and PoLech station.

The PoLech station is located on Da river in Muong Te district, Lai Chau province, Vietnam (Figure 1). Catchment area at PoLech station is 26270 km^2. PoLech is hydrological station level 1, which was established in 2003 to serve the Son La hydropower plant design and construction and continued to measure hydrological data from 2007 to 2011 for designing the Lai Chau hydropower dam. The station is located on the right bank of the Da River, 12 km downstream of the Muong Te level 3 hydrological station. The station is located on a quite straight reach of the river, with an average width of around 100 m. The gauging discharges and stages as well as recorded stages were obtained at the same cross–section. Currently, the correction of discharge at Polech station is carried out according to the standard regulation TCVN 12636–15:2021. Figure 2 illustrates the cross–section of the station in 2006 and there were no significant changes over the years. The left bank is a steep mountain slope with stable geological and topographical conditions, while

the right bank has a rocky bottom at the lower part and sand and sediment at the upper part. The highest stage measured at the station is 275.40 m. Therefore, the cross–section controls the highest water level and there is no clear floodplain delineation.

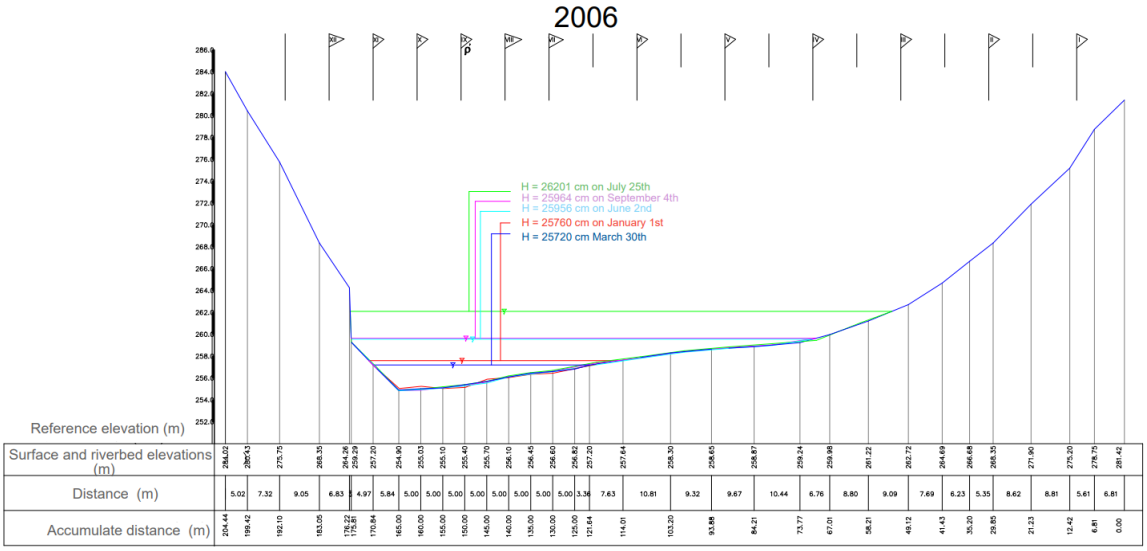

Figure 2. River cross–section at PoLech hydrometric station in 2006.

2.2. Data collection

Gauging stages and discharges in the period 2005–2011 of PoLech station are used in this study. The stage data measured at the same time as the observed discharge is called the gauging stage. The recorded stage is the stage measured frequently and without discharge measurement at the same time. Table 1 shows the number of gaugings (number of gauged Q, H pairs), the maximum and minimum values of gauging stage and discharge (H^{g}_{max}, H^{g}_{min}) and the recorded stage (H^{re}_{max}, H^{re}_{min}) of each year. Note that the gauging data or recorded data obtained from in situ measurement is different from the rating data, which is simulated from a regression equation.

Table 1. Statistics on stage and discharge data used in this study.

Year	2005	2006	2007	2008	2009	2010	2011	2005–2011
No. of gaugings	79	62	55	40	60	49	53	398
H^{re}_{max} (cm)	26790	26870	27070	26614	26700	26489	26455	27070
H^{re}_{min} (cm)	25679	25709	25671	25688	25704	25666	25689	25666
H^{g}_{max} (cm)	26784	27251	27113	26590	26637	26487	26403	27251
H^{g}_{min} (cm)	25681	25720	25678	25688	25705	25671	25700	25671
Q^{g}_{max} (m^3/s)	3810	6460	5570	2950	3050	2458	2068	6460
Q^{g}_{min} (m^3/s)	56.8	111	42.7	65.9	84.9	47.4	81.7	42.7

3. Methods

3.1. Data preprocessing

The raw hydrologic data often contains some uncertainty due to the measurement or data processing. The uncertainty in the data may lead to incorrect reflections in calculating, analyzing hydrologic data, and therefore in making decisions. Thus, outlier detection and removal in the data set are critical for improving calculation quality. There are several methods to identify the outliers, such as standard deviation, the interquartile range [40]. Because the gauging data is not continuous and does not have a normal distribution, this

research used the interquartile range theory to identify the outliers. The Interquartile range is the range of values between ¼ and ¾ positions of the ascending order data. The first and the third quartile are the 25th (Q_1) and 75th percentiles (Q_3) of the data set, respectively. The thresholds for investigating the outliers are defined as follows:

Lower threshold: $L = Q_1 - 1.5(Q_3 - Q_1)$

Upper threshold: $U = Q_3 + 1.5(Q_3 - Q_1)$

where $(Q_3 - Q_1)$ is the interquartile range (IQR).

The outliers are the points having smaller values than Lower threshold or greater values than Upper threshold.

3.2. Determining the stability of the Stage – Discharge relationship

According to the Vietnamese national standard [36], a stable Stage–Discharge relationship is represented by a smooth rating curve that has a unique discharge corresponding to each stage and passes through the center of groups of data. In addition, the stable rating curve must comply with the following requirements: (1) having a balanced number of points on either side of the curve; (2) balancing the negative and positive error; (3) the error (σ) of the rating curve calculated in section 3.4 should be smaller than five percent. In addition, to determine the stability of the stage–discharge relationship, [18] suggested: (4) plotting the gauging data points on both the up and down curve of water level to identify the loop relationship between stage and discharge or any other relationship; (5) comparing the gauging and rating data from 2 to 5 years to investigate any significant changes; and (6) plotting the gauging and recorded data during the flood and dry seasons to observe if seasonal factors such as plant growth and/or sedimentation have any influence. In this study, graphs and performance metrics representing these criteria were used to determine the stability of the stage–discharge relationship.

3.3. Seelcting regression equations

3.3.1 Traditional regression equations

A regression equation is used to estimate the relationship between the dependent variable (an unknown variable) and the independent variable (a known variable). Discharge is considered a dependent variable with a short data series that is difficult to measure continuously; water level (stage) is an independent variable with longer data and is easier to measure. Therefore, regression is a method for calculating discharge that is based on establishing the relationship between stage and discharge. Linear regression and non–linear regression are two popular methods. Linear regression equation represents the relationship between variables as a straight line. Non–linear regression equation represents the relationship between variables as a curve. Non–linear regression equations could be polynomial or power. Table 2 shows the types and the corresponding mathematical expressions of regression equations used in this study.

Table 2. Traditional regression equations.

Types of equations		**Regression Equations**	
Linear		$Q = a + H.b$	(1)
		$Q = a + (H - Ho).b$	(2)
	Logarithm	$\text{Log}\, Q = b.\log(H - Ho) + \text{loga}$	(3)
		$Q^v = a + H.b$	(4)
Non– linear	Power equation	$Q = a.(H - Ho)^b$	(5)
	Polynomial second order	$Q = a + b.H + c.H^2$	(6)
		$Q = a + b.(H - Ho) + c.(H - Ho)^2$	(7)
		$Q^v = a + b.H + c.H^2$	(8)

Depending on the order of the dependent variable, the relationship types will reflect the results differently. According to [12], using ν = ½ gives a good approximation result that is useful for calculation, and stabilizes the variance, especially for small flows. Therefore, in this study, ν = ½ was used in equations (4) and (8).

3.3.2. Piecewise regression

It is necessary to break the regression line into multiple segments (piecewise) when: (1) The river cross–section is unsteady over time (sedimentation, seasonal plant growth or other changes affecting hydraulic characteristics of river); (2) Although the river cross–section remains stable over time, variations in the Q–H relationship due to changes in both the cross–sectional shape and the riverbank. The segmentation of a stable river cross–section is oftentimes based on the shape of cross–section or the rating curve. For the cross–sections with unclear stage differentiation (i.e., no clear separation between riverbed and riverbank), breaking the regression line is difficult and inactive. In this research, a simple and automatic method was proposed to break the regression curve into 4 segments: i) low flows; ii) medium flows (2 equal segments); iii) high flows. For each segment, there will be a regression equation. Breaking points between segments were determined by finding the intercepts of a linear regression equation and a polynomial equation of second order, both of which were established from gauging data. Figure 3 illustrates our segmentation process and result.

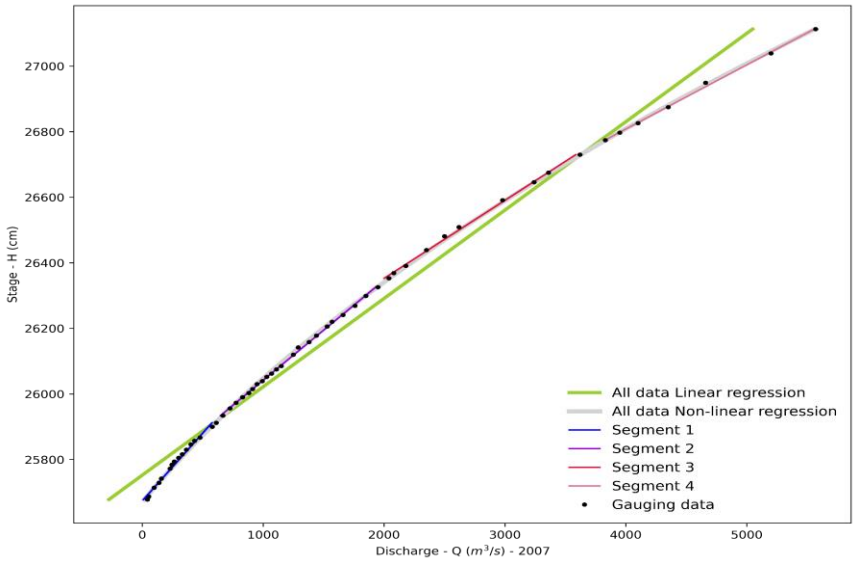

Figure 3. Result of four segments obtained by the proposed automatic segmentation method.

3.3.3. Choosing the best regression equation for discharge interpolation and extrapolation

For discharge interpolation, eight regression equations were established and evaluated by four performance metrics (mentioned in section 3.4), in both piecewise and non–piecewise fashions.

For discharge extrapolation, simple extensions and log extrapolations extend the rating curve using the rating equation for the highest limb of the existing rating curve [18]. The good regression equations of the fourth segment were used for discharge extrapolation. Five and ten percent of gaugings were left out each year. Consequently, each year has an extension ratio, which was calculated using formula (9):

$$ER = \frac{H^{g}_{max} - H^{g}_{cut}}{H^{g}_{max} - H^{re}_{min}} 100\ (\%) \quad (9)$$

where ER (%) is an extension ratio; H_{max}^{g} is the maximum gauging stage data, H_{min}^{re} is the minimum recorded stage data; H_{cut}^{g} is the maximum gauging stage data after high stage data being cut off.

The scatter plots of the ER data on the horizontal axis and the σ or MAE of piecewise ratings in the vertical axis were established and evaluated to arrive at the best model for discharge extrapolation.

3.3.4. Assessing the capability of the combined rating curve in simulating single year discharge

The combined rating curve was created from the regression equations by both Piecewise and Non–piecewise methods, which were computed from gauging data over many years (in this case, 7 years). These combined rating curves interpolate the rating discharge for each year. The discharge simulated from the combined rating curve and the year–specific rating curve were compared to each other as well as to the observed discharge based on performance metrics. These metrics reflected the capacity of the combined rating curve to simulate single–year discharges.

3.4. Performance metrics

To determine the goodness–of–fit of the regression equations this study used four performance metrics, namely KGE, MAE, Pbias and (σ), that are subsequently described as the following.

Kling Gupta efficiency (KGE) [41] can be used to assess the goodness–of–fit between model outputs such as water level, flow data, and climatic data with observed data. KGE values vary in the range from –∞ (not fit at all) to 1 (best fit). KGE is calculated by the following equations:

$$KGE = 1 - \sqrt{(CC-1)^2 + \left(\frac{P_i}{O_i} - 1\right)^2 + \left(\frac{Pm_i}{Om_i} - 1\right)^2};\ CC = \frac{\sum_{i=1}^{n}(O_i - O_m)*(P_i - P_m)}{\sqrt{\sum_{i=1}^{n}(O_i - O_m)^2} * \sqrt{\sum_{i=1}^{n}(P_i - P_m)^2}} \quad (10)$$

The MAE (Mean absolute error) is a metric often used to evaluate how much deviation of a simulated variable from an observed one. The advantage of using this metric is the ease of interpretation since it has the same unit as a variable's unit of interest. But the MAE is not sensitive to outliers. MAE value ranges between 0.0 (best goodness–of–fit) and infinitive (worst goodness–of–fit). The lower the MAE, the better the model fits gauging data [42].

$$MAE = \frac{1}{n}\sum_{i=1}^{n}|O_i - P_i| \quad (11)$$

The σ is used as the Vietnamese national standard's metric [36] to evaluate the stability of the Stage – Discharge relationship and the goodness–of–fit of regression models. The model is a good approximation of observed/gauging data when σ < 5%. This metric is formulated as the following:

$$\sigma = \sqrt{\frac{\sum_{1}^{n}\left(\frac{O_i - P_i}{P_i} * 100\%\right)^2}{n}} \quad (12)$$

The percent bias (PBias) can determine simulation bias (negative or positive change) in percentage. The Pbias cannot be applied for single event simulations or can reflect wrong results with a short data. The range value of Pbias is from –100 % to 100%, where the optimal value is 0.0% [42]. This metric can be calculated by using the following equation:

$$Pbias = \frac{\sum_{1}^{n}(O_i - P_i)}{\sum_{1}^{n} O_i} * 100\ (\%) \quad (13)$$

where O_i is observed data; P_i is simulated data; O_m, P_m are the mean of observed and simulated data; n the number of observed data points.

3.5. Building Python script

The mathematical formulations presented from sections 3.1 to 3.4 were codified as a script using Python programming language. The Gradient Descent algorithm was used to find the optimal parameters for each type of regression equation. The mean square error was used as the cost function. The following section presents the results obtained when applying this script to the case study at Polech station, on the Da River.

4. Result and discussion

4.1. Outliers detection and stability of the Q–H relation

4.1.1. Outlier detection

Outlier testing was carried out for all 7 years of gauging data (Figure 4). There is one outlier in the 2005 data set that has been detected using the interquartile range. This outlier reaches outside the upper threshold (U) of water level data and the riverbanks of PoLech station. The remaining data could be utilized for the following steps after all outliers have been removed.

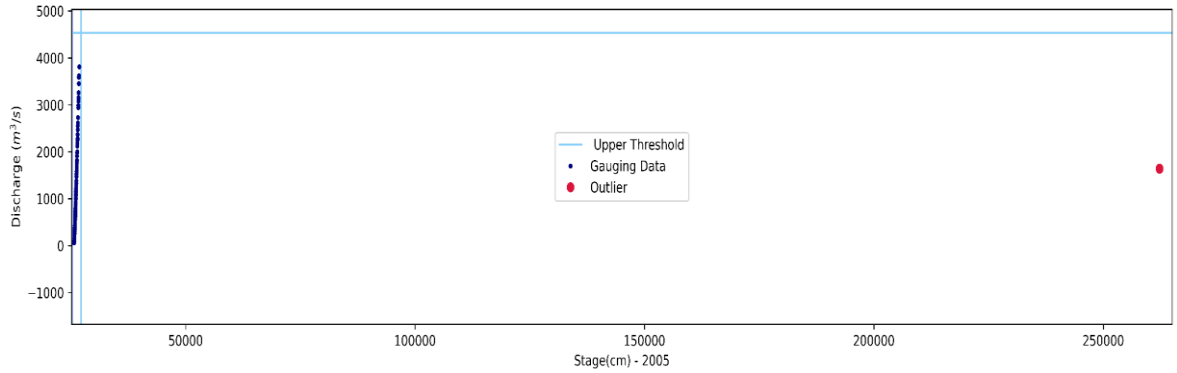

Figure 4. Detecting outlier (red point).

4.1.2. The stability of the Stage – Discharge relationship

Figure 5 depicts the seven rating curves for seven years from 2005 to 2011. There is not much of a distinction among these rating curves. The stage–discharge relationship of PoLech station is relatively steady over time.

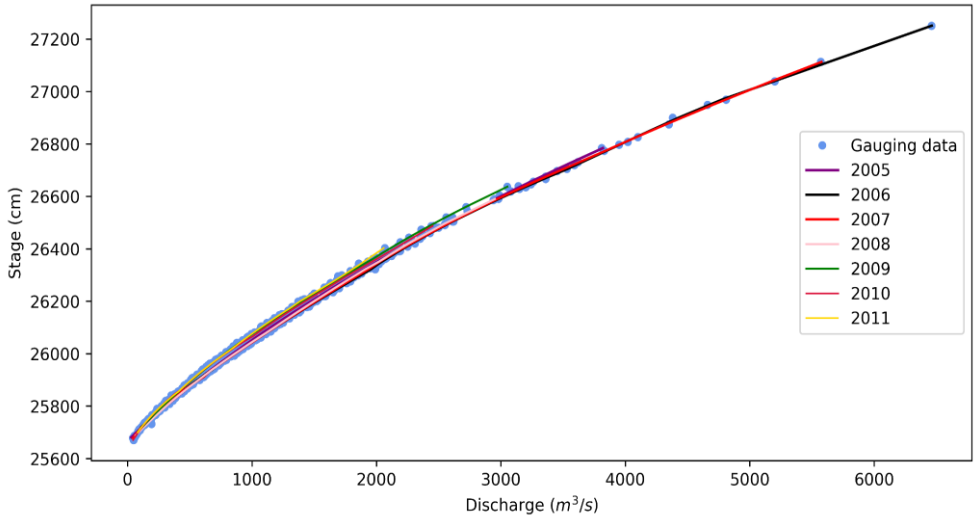

Figure 5. Gaugings (represented by dots) and each–year rating curve (represented by lines) at the PoLech station.

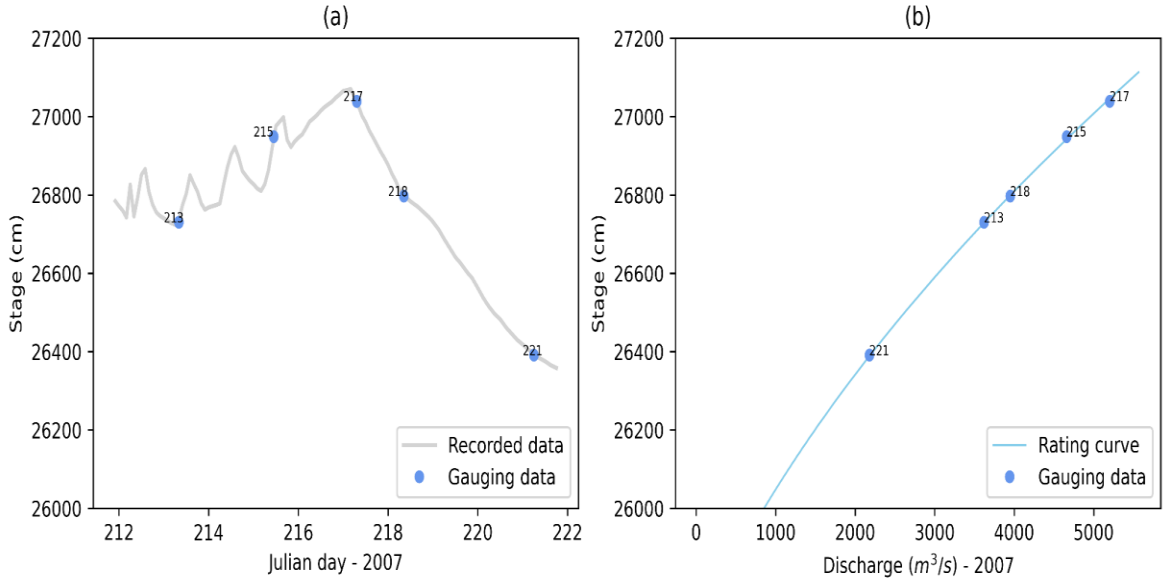

Figure 6. (a) Gauging and recorded flood data from 212 to 221 Julian day in 2007 and (b) the corresponding Stage – Discharge flood rating curve.

Figure 6a plots the gauging data on both rising and falling climbs of a flood hydrograph and all these gauging data fall in a smooth rating curve (Figure 6b). The relationship between stage and discharge is therefore steady and is not affected by flood events. In section 4.2, the performance metrics such as PBIAS, σ give more detail in quantitative analysis for the stability relationship of stage – discharge in PoLech station, which ensures the standard as described in subsection 3.2.

4.2. Discharge interpolation

4.2.1. Interpolation using non–piecewise regression

Table 4 presents four performance metrics resulting from non–piecewise regression equations for discharge interpolation. Some conclusions can be inferred from Table 4, which are: (1) the log–log equation (Eq. 3) is less effective for interpolation than other equations; (2) the non–linear regression equations give better results than linear regression equations; (3) Among the four non–linear equations (Eq. 5 to Eq. 8), it is very hard to rank which one is the best since a particular regression equation is the best in one metric but not in the others.

The rating curves using Eq. 6 and Eq. 7 in the years 2007 and 2010 have very large errors (in term of σ) as compared with those in other years (Table 4). A closer examination of the rating curve using Eq. 6 was carried out by plotting this and the rating curve using Eq. 8 (which has the smallest σ in 2010) against gauging data in Figure 7. The Eq. 6 rating curve is closer to the gauging data for medium and high stage – discharge values in comparison with one using Eq. 8. It is interesting to note that the year 2007 and 2010 have the smallest minimum recorded and gauging stages (Table 1) in which the year 2010 has the smallest recorded stage. For both years, Eq. 8 rating curves closely matched the very low observed data. This result suggested that Eq. 8 should be used for interpolating very low discharge values.

Furthermore, most of the errors of the rating curves (σ) shown in Table 4 are greater than 5%. Therefore, a piecewise regression approach was used, and the results are presented in the next subsection.

Table 4. Performance metrics resulting from non–piecewise regression equations for interpolation.

		Linear				Non – linear			
		Eq. 1	**Eq. 2**	**Eq. 3**	**Eq. 4**	**Eq. 5**	**Eq. 6**	**Eq. 7**	**Eq. 8**
2005	MAE	81.88	81.88	399.88	94.99	22.21	18.68	18.68	44.75
	KGE	0.989	0.989	–0.309	0.878	0.998	0.999	0.999	0.997
	PBias(%)	0	0	–7.440	0.226	–0.034	0	0	0.041
	σ (%)	66.86	66.86	34.04	17.57	5.9	12.45	12.45	8.1
2006	MAE	121.48	121.48	508.54	105.28	29.93	16.60	16.60	53.89
	KGE	0.9796	0.9796	–1.912	0.852	0.997	0.999	0.999	0.997
	PBias(%)	0	0	–12.400	0.246	–0.081	0	0	0.061
	σ (%)	540.13	540.09	30.36	15.56	7.87	2.19	2.19	8.42
2007	MAE	135.22	135.22	604.20	121.50	27.98	16.28	16.28	59.77
	KGE	0.984	0.984	–0.965	0.867	0.997	0.999	0.999	0.997
	PBias(%)	0	0	–12.500	0.297	–0.069	0	0	0.066
	σ (%)	91.9	91.9	39.2	20	10.37	19.23	19.23	11.47
2008	MAE	45.72	45.72	264.94	69.64	9.60	11.47	11.47	25.45
	KGE	0.993	0.993	–0.247	0.882	0.999	0.999	0.999	0.996
	PBias(%)	0	0	–6.530	0.227	–0.007	0	0	0.038
	σ (%)	85	85	29.99	15.79	5.31	8.93	8.93	8.74
2009	MAE	56.37	56.37	221.22	52.55	8.51	10.52	10.52	15.47
	KGE	0.989	0.989	–0.015	0.907	0.999	0.999	0.999	0.998
	PBias(%)	0	0	–4.540	0.108	–0.005	0	0	0.015
	σ (%)	79.36	79.36	22.66	10.79	2.71	4.39	4.39	5.13
2010	MAE	55.83	55.83	255.22	54.82	9.49	14.78	14.78	13.76
	KGE	0.986	0.986	–0.732	0.862	0.999	0.999	0.999	0.998
	PBias(%)	0	0	–8.320	0.181	0.023	0	0	0.011
	σ (%)	183.91	183.91	29.33	14.41	8.3	83.98	83.98	4.07
2011	MAE	33.54	33.54	148.22	38.54	8.20	8.98	8.98	12.98
	KGE	0.993	0.993	0.342	0.916	0.999	0.999	0.999	0.999
	PBias(%)	0	0	–2.270	0.078	0.001	0	0	0.008
	σ (%)	168.93	168.93	17.67	8.23	1.95	3.91	3.91	2.35
Average	MAE	75.72	75.72	343.18	76.76	16.56	13.90	13.90	32.29
	KGE	0.988	0.988	–0.548	0.881	0.998	0.999	0.999	0.998
	PBias(%)	0	0	–7.710	0.195	–0.025	0	0	0.034
	σ (%)	173.72	173.72	29.04	14.62	6.06	19.3	19.3	6.9

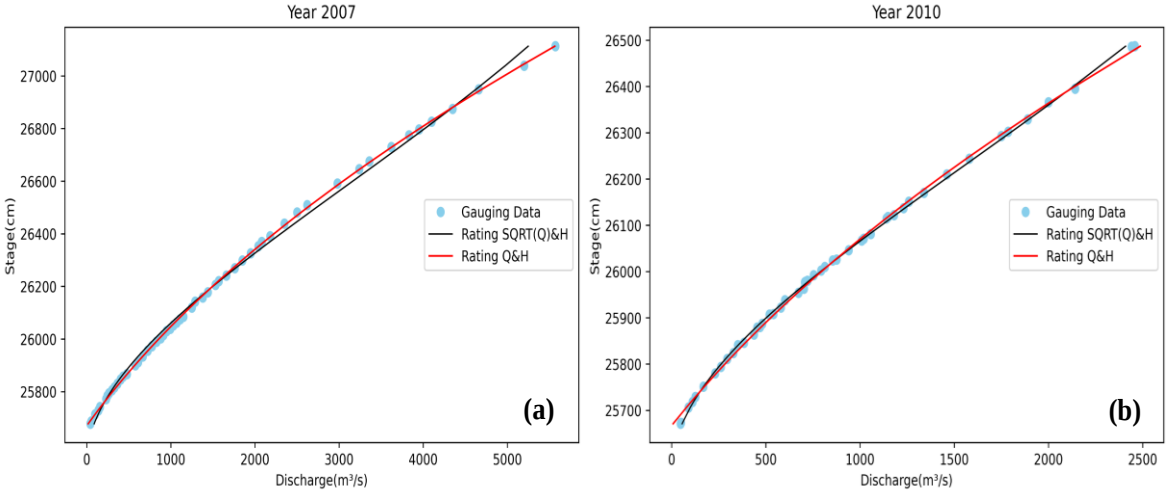

Figure 7. Eq.6 and Eq.8 non–piecewise rating curves in 2007 (a) and 2010 (b).

4.2.2. Interpolation using piecewise regression

The performance metrics shown in Table 5 indicate that piecewise non–linear regression equations give excellent results (lower MAE, KGE close to 1, PBias mostly equal 0, σ less than 5%). Comparing performance metrics in Table 4 and Table 5, it can be concluded that the piecewise method is better than the non–piecewise method, and the non–linear equation is more suitable than linear equation for discharge interpolation.

Table 5. Performance metrics resulting from piecewise regression equations for interpolation.

		Linear				Non – linear		
		Eq. 1	**Eq. 2**	**Eq. 3**	**Eq. 4**	**Eq. 6**	**Eq. 7**	**Eq. 8**
2005	MAE	14.59	14.59	25.21	15.22	12.60	12.60	12.37
	KGE	0.99960	0.99960	0.99823	0.99959	0.99968	0.99968	0.99966
	PBias(%)	0	0	–0.081	0.005	0	0	0.003
	σ(%)	10.97	10.97	7.04	2.48	2.63	2.63	1.69
2006	MAE	15.69	15.69	31.68	14.82	7.98	7.98	8.43
	KGE	0.99962	0.99962	0.99595	0.99947	0.99989	0.99989	0.99989
	PBias(%)	0	0	–0.095	0.006	0	0	0.002
	σ(%)	3.49	3.49	6.38	2.74	1.13	1.13	1.16
2007	MAE	14.64	14.64	33.24	13.29	7.59	7.59	8.29
	KGE	0.99979	0.99979	0.99713	0.99929	0.99994	0.99994	0.99995
	PBias(%)	0	0	–0.166	0.005	0	0	0.002
	σ(%)	42.41	42.41	10.32	4.20	1.51	1.51	1.99
2008	MAE	10.18	10.18	17.29	9.85	7.68	7.68	7.90
	KGE	0.99969	0.99969	0.99708	0.99921	0.99979	0.99979	0.99985
	PBias(%)	0	0	–0.046	0.013	0	0	0.009
	σ(%)	4.97	4.97	8.87	6.17	4.89	4.89	4.96
2009	MAE	10.10	10.10	14.14	8.01	7.23	7.23	7.19
	KGE	0.99967	0.99967	0.99837	0.99976	0.99979	0.99979	0.99983
	PBias(%)	0	0	–0.031	0.004	0	0	0.003
	σ(%)	2.48	2.48	4.97	2.83	1.98	1.98	2.04
2010	MAE	9.83	9.83	12.57	7.61	7.09	7.09	6.87
	KGE	0.99960	0.99960	0.99863	0.99982	0.99977	0.99977	0.99979
	PBias(%)	0	0	–0.073	0.004	0	0	0.003
	σ(%)	10.90	10.90	6.12	1.88	2.00	1.99	1.50
2011	MAE	9.21	9.21	10.05	7.60	7.19	7.19	7.26
	KGE	0.99931	0.99931	0.99805	0.99969	0.99950	0.99950	0.99950
	PBias(%)	0	0	–0.022	0.005	0	0	0.004
	σ(%)	3.59	3.59	3.29	1.68	1.55	1.55	1.54
Average	MAE	12.03	12.03	20.60	10.91	8.19	8.19	8.33
	KGE	0.99961	0.99961	0.99763	0.99955	0.99977	0.99977	0.99978
	PBias(%)	0	0	–0.074	0.006	0	0	0.004
	σ(%)	11.26	11.26	6.71	3.14	2.24	2.24	2.13

To further illustrate the effectiveness of the piecewise regression, both piecewise rating curves using Eq. 6 and Eq. 8 in 2007 and 2010 are shown in Figure 8. As compared with the corresponding rating curves using non–piecewise regression (Figure 7), the automatic segmentation method for piecewise regression proposed in this study substantially improved the goodness–of–fits of the two regression equations.

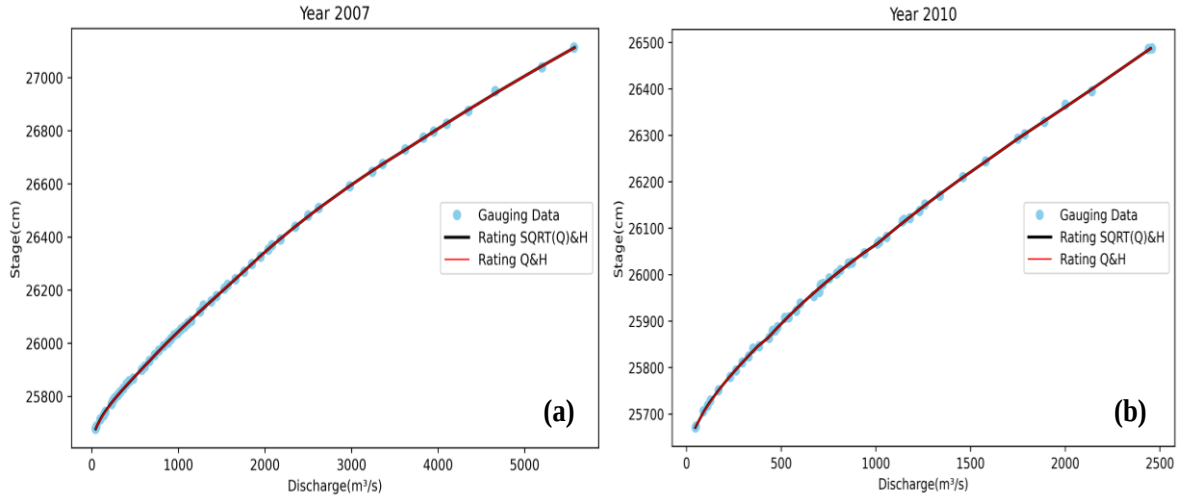

Figure 8. Eq. 6 and Eq. 8 piecewise rating curves in 2007 and 2010.

Regarding selection of the best equation for interpolation, all the three non–linear equations give very similar and satisfactory results. Therefore, either of them can be selected for the purpose of interpolation, given that automatic piecewise regression has been applied.

4.3. Applying the combined rating curve to interpolate discharge for each year

For discharge interpolation, the non–linear regression gives better results in both piecewise and non–piecewise methods. Therefore, to assess the ability of the combined rating curve (being built using all gauging data from 2005 to 2011) for individual year discharge interpolation, the non–linear regression equations (Eqs. 6, 7, 8) were used. Four performance metrics resulting from regressing these equations are presented in Table 6. Inferring from Table 6 is that piecewise regression improved the σ (approaching 5 %), but not for other metrics. Applying the combined rating curve to interpolate each year's discharge requires more research.

Table 6. Seven–year averaged performance metrics computed by the Combined rating curve (Non – linear regression).

		MAE	KGE	PBias(%)	σ (%)
Non piecewise	Eq. 6	33.26	0.95589	–0.583	17.48
	Eq. 7	33.26	0.95589	–0.583	17.48
	Eq. 8	47.31	0.90867	–0.364	9.75
Piecewise	Eq. 6	37.04	0.95656	–0.825	5.95
	Eq. 7	37.04	0.95656	–0.825	5.95
	Eq. 8	37.45	0.95140	–1.014	5.28

4.4. Extrapolation of flow at high water level

Table 7 presents the analysis results using both linear and non–linear regressions for flow extrapolation. In overall, the linear regression using Eq. 4 outperformed the other equations, and the Eq. 3 performed the worst. Except for the log–log relation (Eq. 3), the linear regression did a better job than the non–linear regression.

Table 7. Performance metrics and the extension ratios in 7 years.

Cut–off percentage	Year	ER (%)	Linear						Non–linear			
			Eq. 1		Eq. 3		Eq. 4		Eq. 6		Eq. 8	
			MAE	σ (%)	MAE	σ (%)	MAE	σ (%)	MAE	σ (%)	MAE	σ (%)
5%	2010	11.27	7.19	0.38	130.86	5.08	61.62	2.47	46.29	1.88	41.94	1.71
	2005	11.6	45.19	1.42	67.58	2.36	28.58	1.02	29.33	0.97	29.61	0.95
	2007	16.59	60.06	1.19	226.53	4.32	81.83	1.63	122.53	2.37	131.51	2.54
	2009	17.6	52.01	2.06	77.26	2.9	5.67	0.22	147.49	6.16	176.80	7.6
	2011	18.21	32.74	1.74	159.95	8.1	87.08	4.53	125.95	6.45	131.37	6.73
	2008	18.85	62.85	2.52	76.74	2.83	3.48	0.13	96.34	3.9	114.47	4.72
	2006	28.94	160.82	3.69	558.11	9.73	150.74	2.84	64.35	1.56	83.91	1.76
10%	2005	16.41	76.52	2.5	49.98	1.96	32.46	1.03	29.46	1.28	37.14	1.57
	2007	22.02	70.67	1.75	200.28	4.56	51.66	1.28	26.02	0.69	22.00	0.57
	2010	22.67	30.57	1.57	137.24	6.55	41.63	2.23	31.42	1.66	29.03	1.51
	2008	24.94	31.43	1.5	116.37	4.74	46.90	1.88	130.46	5.25	151.39	6.13
	2009	27.15	27.82	1.39	155.02	6.08	55.10	2.16	41.54	1.63	44.32	1.74
	2011	29.02	47.81	2.99	100.48	6.45	33.31	2.04	33.81	2.25	43.08	2.71
	2006	40.24	242.92	6.48	471.23	10.19	51.89	1.26	191.05	4.5	238.44	5.59
Average			**67.76**	**2.23**	**180.55**	**5.42**	**52.28**	**1.77**	**79.72**	**2.9**	**91.07**	**3.27**

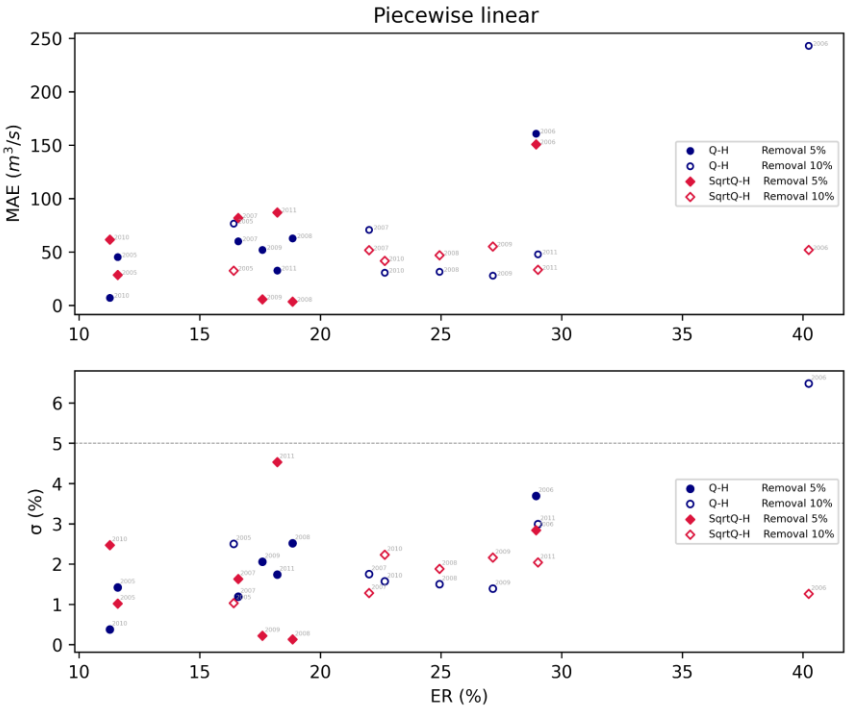

Figure 9. Scatterplots of σ against MAE (the upper) and ER (the lower) computed by two linear regression equations (Eq. 1 and Eq. 4).

In Fig. 9, the scatterplots of σ against MAE (the upper) and ER (the lower) computed by two linear regression equations for seven years (each year has two paired values corresponding to 5% and 10 % cut–off rate). In 2006, although the highest gauging discharge was 6460 m^3/s, the Eq. 4 still gives excellent results when the extension ratio is of more than 40%. For all the other pairs, both linear equations give very satisfactory results (considering both σ and MAE) even when ER goes up to 30%. The smallest discharge value needed to be extrapolated in all of seven years is 1420 m^3/s (in 2011), and all values of MAE of pairs are smaller than 100 m^3/s. Only one exception is 2006 where discharge of 6460 m^3/s needed to be found. According to [18], the error of minus/plus 10 % for high discharge extrapolation is exceptionally ideal, and this is the case in this study.

5. Concluding remarks and Outlooks

In this research, eight regression equations (Equations in Table 2) were evaluated and compared to determine the most suitable rating curve equation for interpolating discharge and extrapolating high–flow rates with the use of water level (stage) measured at the PoLech station in the Da river. To aid in the process, a straightforward segmentation approach was employed. The outcome of the comprehensive investigations revealed that: (1) For a single–year dataset, the second–order polynomial regression equations (in which stage is the independent variable and either Q or $Q^{1/2}$ is the dependent variable) demonstrated superior performance in capturing the non–linearity of the data as compared to other approaches for interpolating the discharge. (2) For extrapolation, the linear regression equation was suggested as the most appropriate. (3) For all–year data (i.e., 7 years), the combined rating curve produced discharge estimations that were less accurate than those from a single–year rating curve. The potential of being able to produce ongoing discharge estimations at minimal expense and with relatively straightforward calibration techniques is far-reaching. From an operational standpoint, this approach may stimulate researchers, aquatic eco–system stewards, water quality monitors, or assessors of upstream withdrawals to begin gauging river discharge on a more frequent basis.

The work is not without limitations. First, further efforts should be invested in the evaluation of utilizing a combined rating curve for each year's discharge interpolation. Observations acquired from the current case study demonstrate that the shifting of rating curves over time (years) should be considered even though for a specific year, the hydraulic regime is regarded as constant and stable. Second, although many regression experiments were conducted in this study, other equations, such as spline and Chebyshev polynomial, should be tested using this case study data in a piecewise manner to determine if improved outcomes can be attained. Third, in this study, our goal was to find the most suitable equation based on the best–fitted rating curve, so the uncertainty was not considered. It is important to note that numerous factors influence rating curve uncertainty estimation regardless of the modeling approach, such as the non–linearity relationship between the water stage and discharge or the alteration of the riverbed. Investigating the uncertainty of these factors would be our next step. Lastly, although seven year–station datasets were utilized in this study, more datasets obtained from other stations will help to increase the generality of our approach.

Author contribution statement: Designed the study conception: G.N.T.; collected data: G.N.T., T.N.T.; developed the theoretical research: G.N.T., H.N.D.; processed the data and performed the calculations: M.D.T.D., H.D.B., Q.H.D.; analyzed the data: G.N.T., H.N.D., M.D.T.D., H.D.B., Q.H.D.; contributed largely to revising the final manuscript: G.N.T., V.T.N.

Acknowledgements: This study is supported by project No. ĐTĐL.CN–06/23 of the 562–programme funded by Vietnam Ministry of Science and Technology.

Conflicts of interest: All authors have no conflicts of interest to declare in this research.

References

1. ISO 7066-2:1988. Assessment of uncertainty in the calibration and use of flow measurement devices – Part 2: Non–linear calibration relationships. In: International Standard 7066–2, International Organization for Standardization, Geneva, 1988.
2. Karimi, P.; Bastiaanssen, W.G.M. Spatial evapotranspiration, rainfall and land use data in water accounting–Part 1: Review of the accuracy of the remote sensing data. *Hydrol. Earth Syst. Sci*. **2015**, *19(1)*, 507–532.
3. Stewart, B. Measuring what we manage–the importance of hydrological data to water resources management. Proceedings of the International Association of Hydrological Sciences **2015**, *366*, 80–85.
4. Xu, C.y. Issues influencing accuracy of hydrological modeling in a changing environment. *Water Sci. Eng*. **2021**, *14(2)*, 167–170.
5. Zakwan, M.; Muzzammil, M.; Alam, J. Application of data driven techniques in discharge rating curve–an overview. *Aquademia* **2017**, *1(1)*, 02.
6. Leopold, L.B. River channel change with time: an example: address as retiring president of the Geological Society of America, Minneapolis, Minnesota, November 1972. *Geol. Soc. Am. Bull*. **1973**, *84(6)*, 1845–1860.
7. Booth DB. Stream-channel incision following drainage-basin urbanization 1. *JAWRA J. Am. Water Resour. Assoc.* **1990**, *26(3)*, 407–417.
8. Jennings, D.B.; Taylor Jarnagin, S. Changes in anthropogenic impervious surfaces, precipitation and daily streamflow discharge: a historical perspective in a mid–Atlantic subwatershed. *Landsc Ecol*. **2002**, *17*, 471–489.
9. Ajami, N.K.; Hornberger, G.M.; Sunding, D.L. Sustainable water resource management under hydrological uncertainty. *Water Resour Res*. **2008**, *44(11)*, W11406.

10. Leopold, L.B. Hydrology for Urban Land Planning: A Guidebook on the Hydrologic Effects of Urban Land Use. US Geolgoical Survey, 1968, 554, pp. 18.
11. Wharton, G.; Tomlinson, J.J. Flood discharge estimation from river channel dimensions: results of applications in Java, Burundi, Ghana and Tanzania. *Hydrol. Sci. J.* **1999**, *44(1)*, 97–111.
12. Wara, C.; Thomas, M.; Mwakurya, S.; Katuva, J. Development of River Rating Curves for Simple to Complex Hydraulic Structure Based on Calibrated HEC–RAS Hydraulic Model, in Kwale, Coastal Kenya. *J. Water Resour. Prot.* **2019**, *11(04)*, 468.
13. Sivapragasam, C.; Muttil, N. Discharge rating curve extension–a new approach. *Water Resour. Manage.* **2005**, *19*, 505–520.
14. Fenton, J.D.; Keller, R.J. The calculation of streamflow from measurements of stage. Technical Report 01/6, 2001, pp. 77.
15. Venetis, C. A note on the estimation of the parameters in logarithmic stage–discharge relationships with estimates of their error. *Hydrol. Sci. J.* **1970**, *15(2)*, 105–111.
16. McMillan, H.; Krueger, T.; Freer, J. Benchmarking observational uncertainties for hydrology: rainfall, river discharge and water quality. *Hydrol. Process.* **2012**, *26(26)*, 4078–4111.
17. Petersen–Øverleir, A. Modelling stage—discharge relationships affected by hysteresis using the Jones formula and nonlinear regression. *Hydrol. Sci. J.* **2006**, *51(3)*, 365–388.
18. Ramsbottom, D.M.; Whitlow, C.D. Extension of Rating Curves at Gauging Stations Best Practice Guidance Manual. Environment Agency, Rio House, Waterside Drive, Aztec West, Almondsbury, Bristol, BS32 4UD, 2003, pp. 247.
19. Holmes Jr, R.R. River rating complexity. Constantinescu, editor, River Flow. Proceeding of the International Conference on Fluvial Hydraulic (River Flow 2016), St. Louis, Missouri, July 11-14, 2016: CRC Press, 2016, 679–686.
20. Léonard, J.; Mietton, M.; Najib, H.; Gourbesville, P. Rating curve modelling with Manning's equation to manage instability and improve extrapolation. *Hydrol. Sci. J.* **2000**, *45(5)*, 739–750.
21. Domeneghetti, A.; Castellarin, A.; Brath, A. Assessing rating–curve uncertainty and its effects on hydraulic model calibration. *Hydrol. Earth Syst. Sci.* **2012**, *16(4)*, 1191–1202.
22. Herschy, R.W. Streamflow Measurement. *CRC Press*. 1995, pp. 536. https://doi.org/10.1201/9781482265880.
23. Petersen–Øverleir, A.; Reitan, T. Objective segmentation in compound rating curves. *J. Hydrol. (Amst).* **2005**, *311(1–4)*, 188–201.
24. Zarzer, E.A. Some considerations concerning the optimal calculation of stage–discharge functions. *Zeitschrift für Oper. Res.* **1987**, *31(6)*, B193–B212.
25. Petersen–Øverleir, A. Accounting for heteroscedasticity in rating curve estimates. *J Hydrol. (Amst).* **2004**, *292(1–4)*, 173–181.
26. Moyeed, R.A.; Clarke, R.T. The use of Bayesian methods for fitting rating curves, with case studies. *Adv. Water Resour.* **2005**, *28(8)*, 807–818.
27. Aggarwal, S.K.; Goel, A.; Singh, V.P. Stage and discharge forecasting by SVM and ANN techniques. *Water Resour. Manage.* **2012**, *26*, 3705–3724.
28. Londhe, S.; Panse–Aglave, G. Modelling stage–discharge relationship using data–driven techniques. *ISH J. Hydraul. Eng.* **2015**, *21(2)*, 207–215.
29. Fenton, J.D. On the generation of stream rating curves. *J. Hydrol. (Amst).* **2018**, *564*, 748–757.
30. Herschy, R.W. Streamflow Measurement. *CRC Press* 2008, pp. 536.

31. Morgenschweis, G. Hydrometrie: Theorie Und Praxis Der Durchflussmessung in Offenen Gerinnen. Springer Vieweg Berlin, Heidelberg, 2010, XVI, pp. 637.
32. Mirza, M.M.Q. The choice of stage–discharge relationship for the Ganges and Brahmaputra rivers in Bangladesh. *Hydrol. Res*. **2003**, *34(4)*, 321–342.
33. McMahon, T.A.; Peel, M.C. Uncertainty in stage–discharge rating curves: application to Australian Hydrologic Reference Stations data. *Hydrol. Sci. J*. **2019**, *64(3)*, 255–275.
34. Khai, N.H.; Cau, L.V. Results of research on the stable rating curve in the tidal unaffected area using the function Spline 3. *VN J. Hydrometeorol*. Published online 1996.
35. Dao, N.V.; Hai, Hai, L.Q.; Ky, N.D.; Phong, P.H.; Dat, D.V.; Phung, N.V.; Chien, L.Q. Study on building correlation of water level and discharge at Ha Bang hydrological station in the period 2013–2020. *VN J. Hydrometeorol*. **2021**, *723*, 38–47.
36. Vietnamese national standard TCVN 12636–15:2021. Hydro–Meteorological Observations – Part 15: Editing of water flow documents discharge in river on non – tidal affected zones. 2021.
37. Anh, T.V.; Hien, N.T.; Khanh, D.Q. Estimating the foreign flow from China to Vietnam supporting water resources planning and management in Da river basin. *VN J. Hydrometeorol*. **2017**, *678*, 54–62.
38. Linh, B.H.; Phuong, T.A. Assessment of the impact of reservoirs on flow variations on the Da River. *VN J. Hydrometeorol*. **2021**, *731*, 97–107.
39. Ministry of natural resources and environment of the Socialist Republic of Vietnam. National Water Resources Report Period 2016–2021, 2022.
40. Barbato, G.; Barini, E.M.; Genta, G.; Levi, R. Features and performance of some outlier detection methods. *J. Appl. Stat*. **2011**, *38(10)*, 2133–2149. doi:10.1080/02664763.2010.545119.
41. Gupta, H.V.; Kling, H.; Yilmaz, K.K.; Martinez, G.F. Decomposition of the mean squared error and NSE performance criteria: Implications for improving hydrological modelling. *J. Hydrol. (Amst)*. **2009**, *377(1–2)*, 80–91.
42. Moriasi, D.N.; Gitau, M.W.; Pai, N.; Daggupati, P. Hydrologic and water quality models: Performance measures and evaluation criteria. *Trans ASABE*. **2015**, *58(6)*, 1763–1785.

VIETNAM JOURNAL OF HYDROMETEOROLOGY

Research Article

Assessment of the pollution concentration of phthalate este (PAEs) affecting the water quality of Ho Tay Lake

Vu Thu Huyen[1]*, Vu Duc Toan[2]

[1] Customs Inspection Department, General Department of Vietnam Customs; thuhuyenvu98@gmail.com
[2] ROOM strong research, Environmental and life science research laboratory, Thuyloi University; vuductoan@tlu.edu.vn

*Corresponding author: thuhuyenvu98@gmail.com; Tel.: +84–837086095

Received: 13 February 2023; Accepted: 24 March 2023; Published: 25 March 2023

Abstract: The study presents the evaluation results of typical PAEs (6 PAE indicators) of the PAE family in water samples from Ho Tay Lake, Hanoi. The quality of lake water in general and in Hanoi in particular is influenced by many factors. The sources of treatment in lake water such as restaurant businesses and residential areas nearby, can degrade lake water quality. In order to assess water quality, three methods are still implemented: survey method, data collection, sampling and sample analysis method, and risk assessment method. DEP with the largest value in May 2022 and November 2022 is 0.048 and 0.0846 respectively, in the very low to low-risk range.

Keywords: PAEs; Risk assessment; Composition; Pollution.

1. Introduction

In Vietnam, assessment of the residues of hazardous chemicals in the environment is of great concern, including phthalate esters (PAEs). PAE is commonly used as a plasticizer and additive in a wide variety of products such as PVC resins, some flooring materials and wall coverings. PAE is also used in plastic toys, adhesives, and in plastic films for food packaging [1]. Around the world, PAE pollution in rivers has been studied extensively. For example, there are some published reports on the concentration of PAEs in the Seine River, showed the spread of this group of substances in the environment [2]. PAE is a carcinogenic and teratogenic toxic chemical that is bioaccumulated widely in the environment, which includes: Pseudarthrobacter defluvii E5 and soil agricultural products showing degradability. and mineral PAE for DBP, DEHP. Further research shows that P. defluvii E5 has a promising broad application in microplastic contaminated environments [3]. PAEs have been identified as endocrine disrupting chemicals (EDCs) due to their estrogen and endocrine disrupting properties causing adverse health effects including reproductive system malformations, atherosclerosis [4]. In addition, PAE is teratogenic and carcinogenic, which is metabolized by organisms in the sediment [5], used as a moisture repellent, in filter papers and paper towels, as a substrate in bioactive paper [6], as a popular product of the e–waste recycling area, PAE is released into the environment more aggressively and exposure is higher [7]. PAE is widely used in industrial and household plastic products. The global annual consumption of PAEs was around 6–8 million tons in 2015, while more than a third was in China. In China, about 2.46 million tons of plastic films were used in agriculture in 2018 [8].

PAE was also studied in the accumulation and transport model of 6 PAEs in dicotyledonous vegetables under hydroponic conditions. The PAEs tested included DBP, DEP, DAP, DiBP, DMP, BBP, which resulted in 6 PAEs being absorbed by vegetables from solution, although their accumulation and distribution varied among PAEs [9].

In the world, the occurrence of partitions and six components and partitions of six phthalate esters (PAEs) include: DMP, DEP, DiBP, DBP, BBP, DEHP [10].

The different relationships between flow and low– and high–carbon PAEs may suggest their different sources. DnBPs present a much greater ecological risk than other studied PAE congeners as indicated by its likelihood factor (PAF) and margin of safety (MOS10). The studied PAE congeners pose little health risk to neighboring species [11].

This 5–month study consisted of two parts: (1) monitoring the levels of 11 phthalate ester metabolites (PAEMs) and two beta agonists in human urine samples collected from a small group of people agreed to be tested. Each type of human urine and drinking water contained 183 individual samples. The results of the analysis showed that nine PAEMs were detected in human urine and eight PAEs were detected in drinking water samples [12].

Baseline microplastic pollution and the occurrence, spatial distribution, and ecological risks of phthalate ester (PAE) absorbent microplastics in coastal sandbar sediments of the Gulf of Guinea were investigated. Land–based anthropogenic activities are the major source of MP, while the area's oceanographic characteristics form the main distribution driver [13].

In addition, PAEs with their interactions and with the environment and aquatic animals are still controversial. In this study, PAE is present in many parts of the developing world, and total PAE concentrations even exceed 200 µ/l, exposure to PAE also induces oxidative stress, disorders, and immunosuppression [14].

PAE accounted for 65% of global plasticizer consumption in 2017. DEHP was the most used in 2016 with plasticizers consuming up to 3.1 million tons. PAE is found in plastic and PCP products at concentrations up to several percent by volume [15].

In fact, PAE is a group of flexible, malleable, and elastic compounds of plastics that simplify plastic production [16].

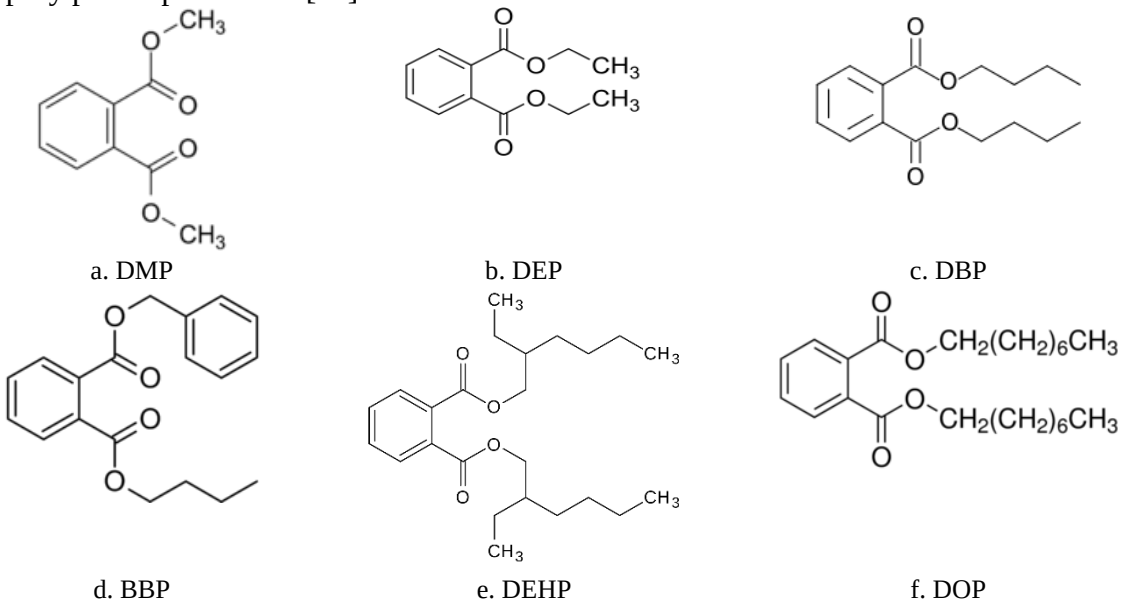

Figure 1. Structure of 6 PAE.

The above studies have contributed to confirm the penetration of PAE into environmental components in some cities in Vietnam and need to be inherited for further assessment of PAE pollution.

Table 1. Some physicochemical properties of PAE.

Symbol	Molecular Formula	S (mg/l)	lg K_{ow}
DMP	$C_{10}H_{10}O_4$	4000	1.6
DEP	$C_{12}H_{14}O_4$	1000	2.5

Symbol	Molecular Formula	S (mg/l)	lg K_{ow}
DBP	$C_{16}H_{22}O_4$	13	4.5
BBP	$C_{19}H_{20}O_4$	0,7	4.9
DEHP	$C_{24}H_{38}O_4$	0,3	7.5
DOP	$C_{24}H_{38}O_4$	0,27	8.1

2. Materials and Methods

2.1. Description of study site

Ho Tay is the largest lake in Hanoi city with an area of 500 ha, circumference of 14.8 km, located in the northwest of Hanoi center, with an area of 500 ha. Ho Tay Lake is a place to drain water when flooded, a place for aquaculture, sightseeing and entertainment. Ho Tay Lake is an area with many beautiful natural landscapes with famous historical and cultural relics such as Tran Quoc Pagoda, Quan Thanh Temple, Tay Ho Palace,... socio-economic development, cultural tourism, as well as an important part of ecological balance and environmental protection of Hanoi Capital. Adjacent to the lake, there are many residential households and agencies, tourist facilities, and services for exploiting the lake's surface. Around the lake, there are 12 main sluices and a drainage system for wastewater entering the lake from surrounding households.

The main culverts are Tau Bay sluice, Cay Si sluice (connecting with Truc Bach), Nhat Tan sluice That is the basic and main cause of environmental pollution in Ho Tay Lake, sampling locations are shown in Figure 2.

Table 2. Location of sampling sites in the Ho Tay Lake.

Numerical order	Location Description	Longitude	Latitude
1.	NM1: Opposite house number 117 Trich Sai street.	105°48’52E	21°02’53N
2.	NM2: Opposite Ly Tu Trong flower garden. No. 5 Nguyen Dinh Thi Street	105°50’05E	21°02’37N
3.	NM3: Tran Quoc Pagoda	105°50’14E	21°02’53N
4.	NM4: Gate of Thang Loi Hotel	105°50’02E	21°03’22N
5.	NM5: Opposite Sheraton Hanoi Hotel, corner of road intersects with Xuan Dieu Street	105°49’53E	21°03’39N
6.	NM6: Opposite house number 35 Quang An street, near Tay Ho district	105°49’11E	21°03’16N
7.	NM7: Opposite Quang Ba guesthouse	105°49’07E	21°58’01N
8.	NM8: Cong Cai – Next to Ho Tay Lake water park	105°49’06E	21°04’22N
9.	NM9: Ve Ho Street, where 2 stone dragons are located, the intersection with Xuan La and Xuan Dinh streets	105°48’45E	21°04’08N
10.	NM10: At the end of Ve Ho Street, it intersects with Lac Long Quan Street. Opposite house number 447 Lac Long Quan	105°48’32E	21°03’34N

Figure 2. Map of sampling locations in Ho Tay.

2.2. Data collection

Using the method to investigate information on the main waste sources of Ho Tay Lake. At the same time, collect information of existing researches in the country and in the world on research subjects.

Sampling locations were selected to represent the space and waste sources of the study area. Based on field survey, nine sampling locations were selected (symbols from M1 to M10), from locations near the beginning of To Ngoc Van Street to the end of Lac Long Quan Street. At each location, a surface water sample was taken in May 2022 (sample symbols from NM1 to NM10). November 2022, repeat 10 samples at 10 locations above (symbols from NM1' to NM10').

2.3. Sampling method and sample analysis

Treat the sample by liquid extraction according to EPA method 3510C and clean the sample according to EPA method 3630C. Samples after extraction and cleaning were injected into a gas chromatograph mass spectrometer (GC–MS).

Take 500 ml of water sample with a measuring cup, pour into a separating funnel, add 60 ml of dichloromethane solvent, cover the separating funnel, unlock the separating funnel to allow the excess vapor in the separating funnel to escape. Lock the separating funnel, shake for 3–5 minutes, stop shaking and let stand for 3–5 minutes for layering, collect the lower separating solvent. Repeat the above process 2 more times. The solvent obtained after shaking 3 times was filtered through anhydrous Na_2SO_4 to remove water. Add 30 ml of Dichloromethane solvent to rinse the separating funnel flask and pass through anhydrous Na_2SO_4. The solution obtained after passing through anhydrous Na_2SO_4 was evaporated at 60^oC until almost dry, changed the n–hexane solvent by adding 30 ml of n–hexane solvent to the flask, shook well and returned to 1–2 ml. The solution after changing the n–hexane solvent and evaporating is aspirated into the cleaning column prepared as follows: Using a locking glass cleaning column, lining the bottom is a layer of glass wool, followed by a layer of Florisin. activated (about 5–7 cm thick), and topped with a thin layer of anhydrous

Na_2SO_4, rinse the column with 50 ml of n–hexane. Aspirate the solution obtained after evaporating in the above step into the cleaning column, rinse the flask with 20 ml of n–hexane solvent and pass it through the cleaning column, using an additional 30 ml of n–hexane solvent to rinse the cleaning column. The cleaning solution was collected into a flask, returned to about 1 ml, aspirated into a graduated cylinder, rinsed the flask with about 2 ml of n–hexane solvent, and collected it completely. Using nitrogen gas to blow gently, concentrate the solution to exactly 1ml, put it into a 1.5 ml bottle with a tight lid, and analyze it by GCMS.

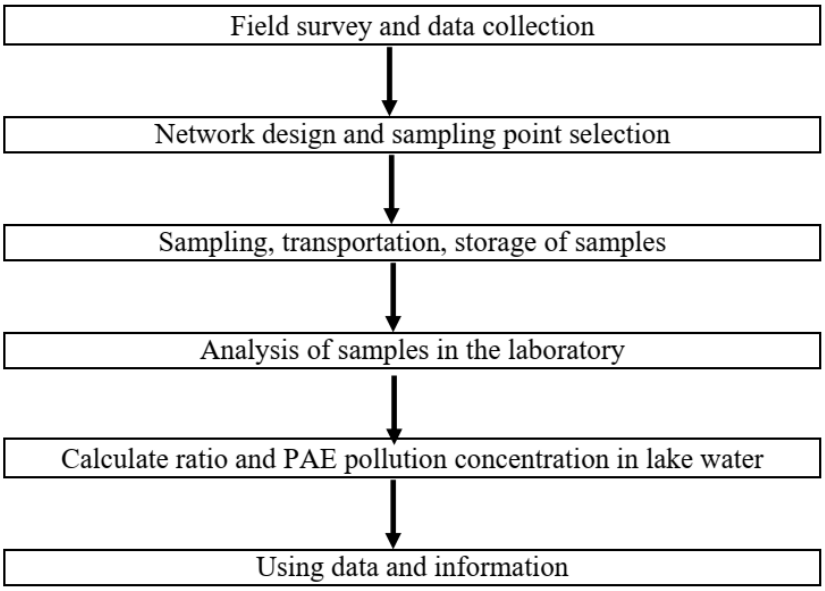

Figure 1. Research structure diagram.

2.4. Methods of risk assessment

Environmental risks due to PAE in Ho Tay Lake surface water were assessed using the risk quotient (Risk quotient, RQ). RQ is calculated according to the formula:

$$RQ = C/ MAC \quad (1)$$

where C is the concentration of PAEs in water samples; MAC is the maximum allowable concentration for PAEs in surface water of river. The following qualitative ranking of cancer risk estimates was used to rank the risk as: very low ($RQ \leq 0.01$), low ($0.01 < RQ \leq 0.1$), moderate ($0.1 < RQ < 1$), high ($RQ \geq 1$) [17].

3. Results and discussion

3.1. Assessment of PAE pollution in Ho Tay Lake water

The analysis results showed that all 6 selected PAEs were detected in the lake water samples (Table 3).

Table 3. PAE concentration (µg/l) in Ho Tay Lake water.

Compound	May 2022	November 2022
DMP	0.15–0.87 (0.49±0.22)	0.12–0.78 (0.42±0.26)
DEP	5.68–11.26 (7.65±1.81)	5.69–15.69 (10.38±3.03)
DBP	2.84–2689.00 (272.92±848.92)	3.98–5.99 (4.91±0.66)
BBP	0.02–0.09 (0.06±0.02)	0.01–0.06 (0.02±0.02)
DEHP	13.98–21.63 (20.13±5.19)	15.69–32.10 (21.77±5.01)
DOP	1.36–2.85 (1.90±0.54)	1.21–1.86 (1.49±0.20)
Σ_6PAE	24.03–2725.7 (303.15±856.7)	26.7–56.48 (38.99±9.16)

Analysis results in May 2022 obtained a concentration of Σ6PAE in Ho Tay Lake water.

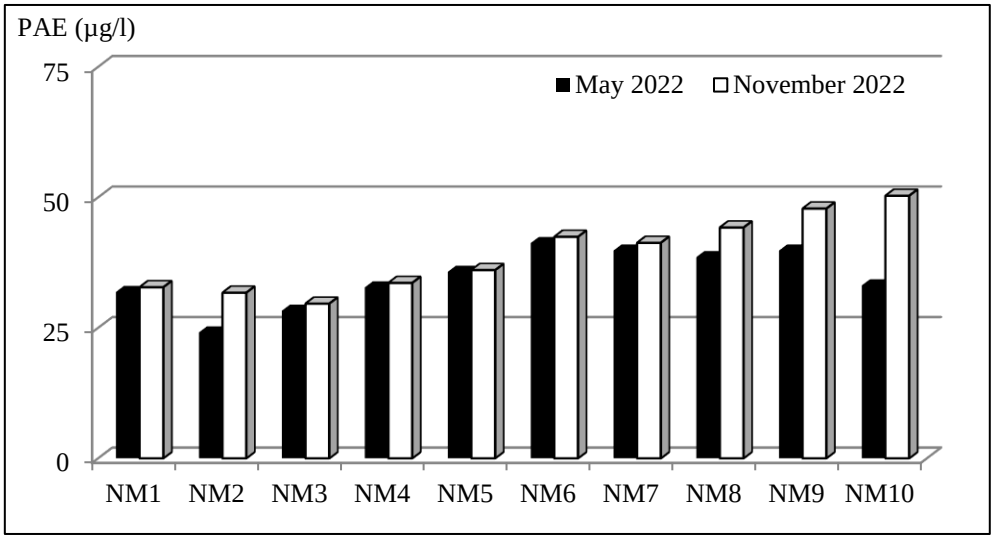

Figure 4. Month–to–month variation of concentrations in Ho Tay Lake water, Hanoi.

Analytical results in May 2022 obtained concentrations of Σ6PAE in Ho Tay Lake water ranging from 31.86 to 51.23 µg/l. Overall value from Table 3 shows that the concentration of Σ6PAE and its components tended to decrease gradually according to the positions from NM6 > NM7 > NM9 > NM5 > NM8 > NM4 > NM10 > NM1 > NM3 > NM2. The concentration of Σ6PAE did not decrease gradually along the length of the studied lake, but reached the highest value at NM6 location, which is near Trich Sai road. This may be due to this location, the source of PAE emissions arising from the neighboring houses and residential areas. From these sources, PAE enters wastewater, affecting river water quality at point NM6.

When compared with world studies, the concentration of Σ6PAE in lake water is also higher than that of Selangor River, Malaysia (0.069–0.688 µg/l), Yellow River, China (0.358–59,474 µg/l) and river Tama, Japan (< 0.001–4.542 µg/l)) [18].

Comparing the analysis results in May 2022 and November 2022, it shows that the concentration of Σ6PAE at each location fluctuates with a slight downward trend. Sampling time in November was selected on a day without rain. The water level in Ho Tay Lake at the two sampling times did not have large fluctuations. In addition, the possibility of PAE entering the lake is mainly from dispersed waste sources around the lake and there is no data to assess the PAE load into the lake. at two sampling times. Therefore, the pollution level and evolution trend of 6 PAE in lake water as well as potential sources of PAE discharge around the lake need to be further studied and evaluated in the coming time, thereby serving as a premise for the assessment. more detail.

3.2. Evaluation of PAE composition in Ho Tay Lake water

PAE composition in lake water is related to the variation and physicochemical properties of each PAE. The mean percentages of PAEs in the lake water samples are presented in Figures 5 and 6.

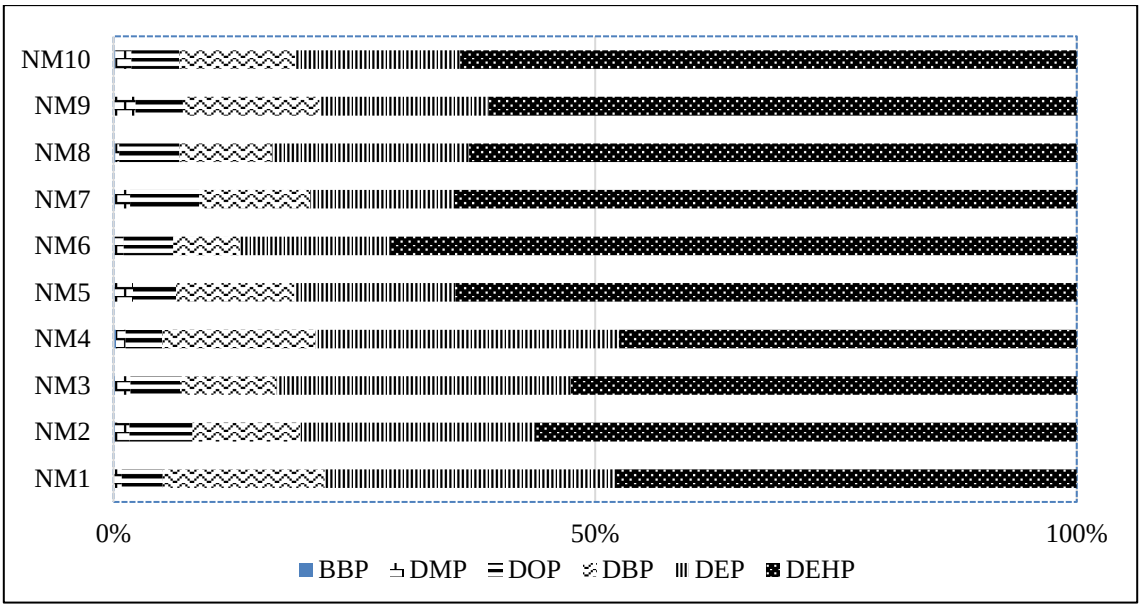

Figure 5. Mean percentage of 6 PAEs in water samples May 2022.

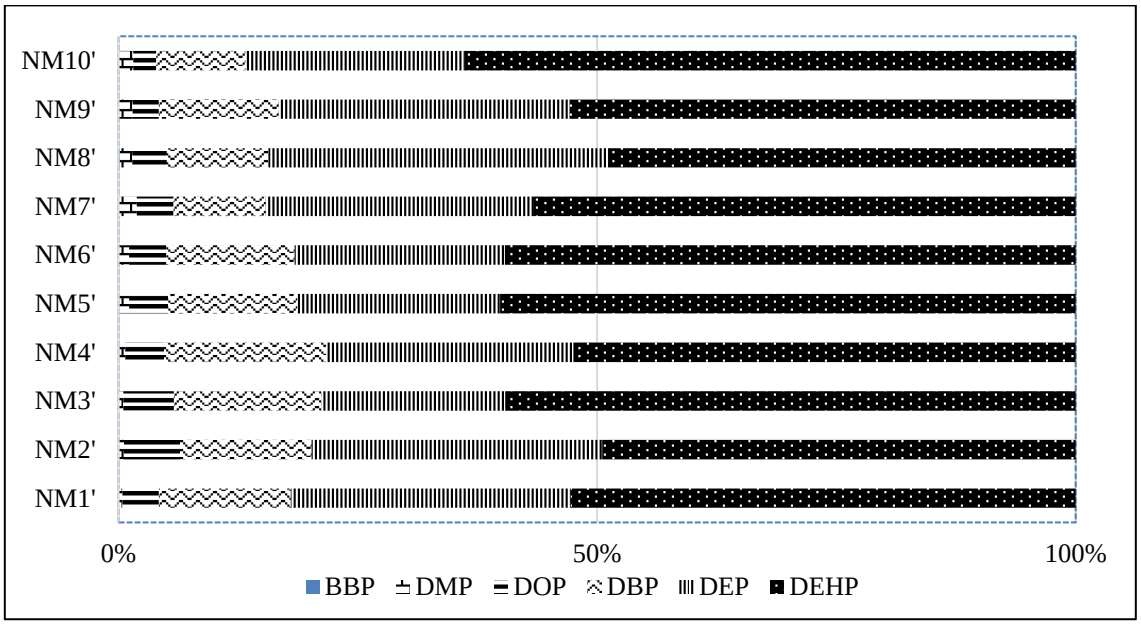

Figure 2. Mean percentage of 6 PAEs in water samples November 2022.

The results showed that the average percentage of 6 PAEs did not change much according to the sampling time of the year. At positions M1 to M5, DEHP, DEP and DBP have a larger mean percentage than the rest of the PAEs. DEHP has the largest percentage of samples. Of the 6 PAEs, DEHP is produced in larger volumes and has more applications than the other PAEs. As a result, the waste source is likely to contain more DEHP, contributing to a larger concentration and percentage of DEHP in the sample. DEP and DBP belong to PAE group with small molecular weight (Low molecular weight PAE, L–PAE), higher water solubility than PAE group with large molecular weight (High molecular weight PAE, H–PAE), so it is easy Soluble in water. H–PAE tends to accumulate in sediments due to its high bioaccumulation capacity. The results of the analysis of the percentage of PAEs in the river water sample showed that there was a match for the physicochemical properties of PAE and the ability to change PAE in the environment. Particularly at position NM6, the percentage of DEHP is smaller than DEP and DBP.

3.3. Risk assessment due to PAH pollution in Ho Tay Lake, Ha Noi

PAE has penetrated the Ho Tay Lake and from there could spread in a wide range. A risk assessment due to domestic PAE is required to consider the potential impact on the Ho Tay Lake environmental quality. The selected MAC values for some PAE compounds in lake water are presented in Table 3 [19]. RQ values at the sampling points are calculated and presented in Table 4.

The results showed the match of the BP5 gene fragment with the 16S rRNA fragment of *Bacillus megaterium* mj1212 with accession number KJ451626.1. Similarly, the gene sequence of strain BP6 matches the gene fragment of strain *Alcaligenes aquatilis* RC43 with accession number MT572474.1 (Figure 8).

Table 3. MPC value of PAEs.

PAE	MPC (mg/l)
DMP	– (*)
DEP	3.7
DBP	10
BBP	–
DEHP	0.19
DOP	–

(*) : no data

Table 4. RQ value of PAEs in water samples.

PAE	RQ May 2022		RQ November 2022	
	Min	Max	Min	Max
DEP	0.0004	0.048	0.0004	0.0846
DBP	0.0002	0.008	0.0002	0.0058
DEHP	0.0002	0.853	0.0005	0.7815

The results of calculating RQ from the results in Table 5 show that the DBP at all sampling points in the river water environment is in a very low level of risk ($RQ \leq 0.01$). DEP at sampling points ranges from very low risk to low risk ($0.01 < RQ \leq 0.1$). Particularly, DEHP at most positions is in the medium risk level ($0.1 < RQ < 1$).

4. Conclusion

Ho Tay Lake, Hanoi contains PAE contamination in a rather wide range. Six representative PAEs were found in lake water samples taken in May 2022 and November 2012. The level of PAE pollution in Ho Tay Lake water is higher than in some rivers in Vietnam and in the world. Evaluation of PAE pollution composition showed that DEHP, DEP and DBP had a higher percentage than the remaining PAEs. The level of environmental risk from PAE contamination varies from very low to moderate, depending on the individual PAE and the sampling point. The above study presents the results of water quality pollution in 2022 to assess the overall status of the water environment of Ho Tay Lake. This is a scientific basis to help managers make plans to conserve and develop organisms.

Currently, several zooplankton species living in Ho Tay Lake are not intrinsic to the lake but an alien species. The snail group is very few. The natural fish composition of Ho Tay Lake is increasingly shrinking, while the composition of fish farming is increasing day by day. Currently, there is only a very small amount of large aquatic plants left in the lake bed, the number of often difficult to quantify. The composition of birds that have been and are present in Ho Tay Lake has identified 43 species belonging to 26 them and 10 sets, decreasing compared to before. The composition of the group of reptiles – frogs in the

study area in Ho Tay Lake has many species are not many and there is no change in species composition over time [20].

Although the water pollution of Ho Tay Lake is not too serious, it has also had a significant impact on the Ho Tay Lake ecosystem. To assess the overall status of the water environment of Ho Tay Lake and come up with effective management solutions to improve water quality, it is necessary to have a plan to monitor and monitor water quality in Ho Tay Lake at many points and regularly.

Author contribution statement: Constructing research idea: V.T.H., V.D.T.; Select research methods: V.T.H., V.D.T.; Data processing: V.T.H., V.D.T; Sample analysis: V.T.H.; Take samples: V.T.H.; Writing original draft preparation: V.T.H., V.D.T.; Writing review and editing: V.T.H., V.D.T.

Acknowledgements: The authors would like to thank the strong research group ROOM, Environmental and life science research Laboratory, Thuyloi University for their support during the research.

Competing interest statement: The authors declare that this article was the work of the authors, has not been published elsewhere, has not been copied from previous research; there was no conflict of interest within the author group.

References

1. De Wit, C.A. An overview of brominated flame retardants in the environment. Chemosphere 2002, 46(5), 583–624. Doi:10.1016/S0045-6535(01)00225-9.
2. Eremina, N.; Paschke, A.; Mazlova, E.A.; Schüürmann, G. Distribution of polychlorinated biphenyls, phthalic acid esters, polycyclic aromatic hydrocacbons and organochlorine substances in the Moscow river, Russia. *Environ. Pollut.* **2016**, *210*, 409–418.
3. Chen, F.; Chen, Y.; Chen, C.; Feng, L.; Dong, Y.; Chen, J.; Lan, J.; Hoi, H. High–efficiency degradation of phthalic acid esters (PAEs) by Pseudarthrobacter defluvii E5: Performance, degradative pathway, and key genes. *Sci. Total Environ.* **2021**, *794*, 148719. Doi:10.1016/j.scitotenv.2021.148719.
4. Wang, J.; Shi, J.; Zhao, Y.; Xue, L.; Li, G.; Wang, B.; Huang, J.; Wu, S.; Guo, X. Cardiorespiratory responses in healthy young adults with exposure to indoor airborne PAEs: A randomized, crossover trial of air purification. *Environ. Int.* **2021**, *156*, 106761. Doi:10.1016/j.envint.2021.106761.
5. Chen, F.; Li, X.; Dong, Y.; Li, J.; Li, H.; Chen, L.; Zhou, M.; Hou, H. Biodegradation of phthalic acid esters (PAEs) by Cupriavidus oxalaticus strain E3 isolated from sediment and characterization of monoester hydrolases. *Chemosphere* **2021**, *266*, 129061. Doi: 10.1016/j.chemosphere.2020.129061.
6. Huang, Z.; Gengenbach, T.; Tian, J.; Shen, W.; Garnier, G. The role of polyaminoamide–epichlorohydrin (PAE) on antibody longevity in bioactive paper. *Colloids Surf. B* **2017**, *158*, 197–202. Doi: 10.1016/j.colsurfb.2017.07.005.
7. Li, X.; Duan, Y.; Sun, H.; Zhang, P.; Xu, J.; Hua, X.; Jin, L.; Li, M. Human exposure levels of PAEs in an e–waste recycling area: Get insight into impacts of spatial variation and manipulation mode. *Environ. Int.* **2019**, *133*, 105143. Doi: 10.1016/j.envint.2019.105143.
8. Du, P.P.; Huang, Y.H.; Lü, H.; Xiang, L.; Li, Y.W.; Li, H.; Mo, C.H.; Cai, Q.Y.; Li, Q.X. Rice root exudates enhance desorption and bioavailability of phthalic acid esters (PAEs) in soil associating with cultivar variation in PAE accumulation. *Environ. Res.* **2020**, *186*, 109611. Doi:10.1016/j.envres.2020.109611.
9. Li, Y.; Yan, H.; Liu, Q.; Li, X.; Ge, J.; Yu, X. Accumulation and transport patterns of six phthalic acid esters (PAEs) in two leafy vegetables under hydroponic conditions. *Chemosphere* **2020**, *249*, 126457.

10. He, Y.; Wang, Q.; He, W.; Xu, F. The occurrence, composition and partitioning of phthalate esters (PAEs) in the water–suspended particulate matter (SPM) system of Lake Chaohu, China. Sci. *Total. Environ.* **2019**, *661*, 285–293. Doi: 10.1016/j.scitotenv.2019.01.161.
11. He, W. Qin, N.; Kong, X.; Liu, W.; He, Q.; Ouyang, H.; Yang, C.; Jiang, Y.; Wang, Q.; Yang, B.; Xu, F. Spatio–temporal distributions and the ecological and health risks of phthalate esters (PAEs) in the surface water of a large, shallow Chinese lake. *Sci. Total. Environ.* **2013**, *461–462*, 672–680. Doi: 10.1016/j.scitotenv.2013.05.049.
12. Liou, S.H.; Yang, G.C.C.; Wang, C.L.; Chiu, Y.H. Monitoring of PAEMs and beta–agonists in urine for a small group of experimental subjects and PAEs and beta–agonists in drinking water consumed by the same subjects. *J. Hazar. Mater*. **2014**, *277*, 169–179. Doi:10.1016/j.jhazmat.2014.02.024.
13. Benson, N.U.; Fred–Ahmadu, O.H. Occurrence and distribution of microplastics–sorbed phthalic acid esters (PAEs) in coastal psammitic sediments of tropical Atlantic Ocean, Gulf of Guinea. *Sci. Total. Environ.* **2020**, *730*, 139013. Doi: 10.1016/j.scitotenv.2020.139013.
14. Zhang, Y.; Jiao, Y.; Li, Z.; Tao, Y.; Yang, Y. Hazards of phthalates (PAEs) exposure: A review of aquatic animal toxicology studies. *Sci. Total. Environ*. **2021**, *771*, 145418. Doi: 10.1016/j.scitotenv.2021.145418.
15. Le, T.M.; Nguyen, H.M.N.; Nguyen, V.K.; Nguyen, A.V.; Vu, N.D.; Yen, N.T.H.; Hoang, A.Q.; Minh, T.B.; Kannan, K.; Tran, T.M. Profiles of phthalic acid esters (PAEs) in bottled water, tap water, lake water, and wastewater samples collected from Hanoi, Vietnam. *Sci. Total. Environ.* **2021**, *788*, 147831. Doi: 10.1016/j.scitotenv.2021.147831.
16. He, Y.; Wang, Q.; He, W.; Xu, F. The occurrence, composition and partitioning of phthalate esters (PAEs) in the water–suspended particulate matter (SPM) system of Lake Chaohu, China. *Sci. Total. Environ.* **2019**, *661*, 285–293. Doi: 10.1016/j.scitotenv.2019.01.161.
17. Tran, L.T.H. Environmental risk assessment. Science and Engineering Publishing House, 2018.
18. Eremina, N.; Paschke, A.; Mazlova, E.A.; Schüürmann, G. Distribution of polychlorinated biphenyls, phthalic acid esters, polycyclic aromatic hydrocacbons and organochlorine substances in the Moscow river, Russia. *Environ. Pollut.* **2016**, *210*, 409–418.
19. Verbruggen, E.M.J.; Postthumus, R.; Wezel, A.P.V. RIVM report 711701 020: Ecotoxicological Serious Risk Concentration for soil, sediment and ground water: updated proposals for first series of compounds. National Institute for Public Health and the Environment, Netherlands, 2001.
20. Thuy, N.T.T. Evolution of diversity into biological parts of the West Lake ecological system. University of Natural Sciences, 2012.

VIETNAM JOURNAL OF HYDROMETEOROLOGY

Rerearch Article

Ecological risk assessment attributed to rice and maize yield reduction due to long-term ground-level O_3 impacts: A case study in Tay Ninh, Vietnam

Loan Tuyet Thi Le[1,2], Phong Hoang Nguyen[1,2], Long Ta Bui[1,2*]

[1] Ho Chi Minh City University of Technology; loan.le2402@hcmut.edu.vn; nhphong@dcselab.edu.vn; longbt62@hcmut.edu.vn

[2] Vietnam National University Ho Chi Minh City; loan.le2402@hcmut.edu.vn; nhphong@dcselab.edu.vn; longbt62@hcmut.edu.vn

*Corresponding author: longbt62@hcmut.edu.vn; Tel.: +84–918017376

Received: 8 February 2023; Accepted: 23 March 2023; Published: 25 March 2023

Abstract: The agricultural sector of Tay Ninh province accounts for about 28% of the province's economic structure with agricultural land areas of 269,250 ha, contributing to 66.7%; particularly, cultivation accounts for 80% of the agricultural economic structure value. Sustainable agricultural development is an urgent mission as the local agricultural sector plays a quite important role in the local economy. Currently, tropospheric O_3 has been evaluated as an air pollutant, causing crop yield reduction and significant economic damage. This study had built a methodological framework based on the application of the coupled Weather Research and Forecasting (WRF)/ Community Multiscale Air Quality Modeling System (CMAQ) model to assess the status of ground-level O_3 concentration allocation in Tay Ninh province, Vietnam with typical cases of crop seasons (spring paddy and maize) in 2018, combined with existing exposure-response functions to quantify agro-economic losses. With the simulated 8-hour mean surface O_3 concentration (daytime) ranging from 10.9 to 113.5 μg/m^3, the economic impacts on rice (the spring season) and maize production were determined to reach more than 184 billion VND, contributing to roughly 0.18% in the total Gross Regional Domestic Product (GRDP) of Tay Ninh province in 2018. Moreover, this is also considered a baseline study to serve as a basis for extensive assessments and propose O_3 precursor emissions control measures shortly.

Keywords: Ground-level O_3; Spatio-temporal distributions; Exposure; Crop production losses; Economic impacts.

1. Introduction

Tropospheric ozone or ground-level ozone (O_3) is one of the major global pollutants, proven to have harmful effects on natural vegetation and harvest in previously available studies [1–3]. High concentrations of O_3 disrupt plant metabolism, promote leaf senescence, and reduce chlorophyll content and photosynthesis rate, leading to reduced crop yields, especially for O_3 sensitive crops such as rice from Asia [4]. Ground-level O_3 is a secondary air pollutant formed from the oxidation of the hydroxyl radical of CO or hydrocarbons in the presence of nitrogen oxides (NO_x) and sunlight [5]. Ozone is not only one of the greenhouse gases that directly contributes to global warming, but also indirectly reduces the carbon sink of the terrestrial ecosystems [6]. Notably, O_3 concentration in Asia is still trending up as rapid industrialization and urbanization continue in these areas, but emissions of precursors of O_3 such as NO_x and VOCs have increased significantly [7]. Particularly in China, O_3 concentration levels have

increased at a much higher rate than in other countries in the region, whose quite high O_3 concentration is threatening security of national food staples and could be exacerbated in the future if this trend continues [8]. Several study results reported that China and India might experience heavier crop yield losses (CYLs) soon due to the expected increase in O_3 concentrations [9]. These outcomes presented that the high O_3 concentration predicted in 2020 had resulted in a China-wide corn loss of 7.2%. The study of [10] estimated that O_3 pollution caused a relative yield loss (RYL) for winter wheat in China of 6.4% in 2000 and by 2020 it was about 4.8%. Meanwhile, the RYL for rice ranged from 2.5% to 6.6% between 1990 and 1999 and rose to 9.2% in 2020 in the Yangtze River Delta (YRD). Furthermore, estimates have shown that global crop losses caused by surface O_3 could continue to increase towards 2030, from 4.0% to 26.0% for wheat in specific, from 2.5–26.0% for wheat, 8.7% for corn, and from 9.5–19.0% for soybeans [11].

To assess the effects of O_3 pollution on crop yields, several metrics were developed based on results from both field and open-chamber experiments (OTC). One of the first studies in the world to quantitatively evaluate the effects of surface O_3 concentrations on crops was carried out by the National Crop Loss Assessment Network (NCLAN) based on OTC by establishing seasonal average daytime O_3 concentrations under review including M7 and M12 [12]. Meanwhile, researchers in Europe have found similar adverse effects caused mainly by the cumulative effects of O_3 pollution, hence the concept of critical level (CL). The new metric has been proposed and acknowledged as AOT40 to reflect the cumulative threshold of the dose of surface O_3 concentration (40 ppb) for plants and vegetation [13]. Many studies have been developed to construct correlation functions of productivity-interactions in Asian countries such as China and India. Typically, the study of [14] applied OTC to establish AOT40–interaction function for wheat and rice in YRD, China or similar studies by [15] and [16] based on experiments that increase free emissions (FACE-Free atmospheric concentration enrichment). In India, the study of [17] constructed new yield – O_3 interaction functions based on AOT40 and M7 indices for wheat, rice, and maize through a literature review of OTC studies on these cultivars in South Asia.

Nowadays, air quality simulations play an important role as technical tools applied to air quality management [18]. Air quality simulations provide information about the causal relationship between meteorology, emissions, and pollutant concentrations by simulating transport, conversion, and deposition mechanisms. stagnation [19]. In which for O_3, because of lack issues of data to monitor ground-level O_3 concentrations on a regional scale, chemical transport models have been used more commonly to determine the distribution of O_3 concentrations, as well as assess the risk of CYL for the area under consideration [10, 20–21].

This study has built calculations using data sources at the provincial and local administrative levels of Tay Ninh province to better reflect spatial differences in the effects of ground-level O_3 over the entire province. At the same time, the study also carried out an ecological risk assessment of surface O_3 using the long-term cumulative surface O_3 exposure metric (AOT40) through concentration-response functions (C-R) to estimate yield and yield losses of two common crops, including rice and maize based on multiple O_3-crop models and the corresponding general economic losses for Tay Ninh province in 2018.

2. Methods and data

2.1. Study area

Tay Ninh province is located in the Southeast region of Vietnam, having the coordinate system from 10°57’08” to 11°46’36” North and from 105°48’43” to 106°22’48” East [22] shown in Figure 1. Tay Ninh province is known as a spiritual land with potential and advantages for socio-economic development, especially tourism potential with many ideal attractions. The province is one of the crucial international exchange gateways between

Vietnam and neighboring Cambodia and Asian countries. Tay Ninh is also a province with an important position in the exchange of goods between the provinces of the Mekong Delta and the Southern key economic regions. Therefore, in recent years, the province's economy has developed relatively comprehensively and continuously. Industry and handicrafts are developing steadily. Currently, Tay Ninh province has 2 economic zones (Moc Bai and Xa Mat); 6 industrial zones/export processing zones (Trang Bang Industrial Park, Phuoc Dong - Boi Loi Industrial Park, Thanh Thanh Cong Industrial Park, Cha La Industrial Park, TMTC Industrial Park and Linh Trung Industrial Park & Export Processing Zone) and 5 industrial clusters (Tan Hoi 1 Industrial Park, Thanh Xuan Industrial Park) 1, Hoa Hoi Industrial Park, Ninh Dien Industrial Park and Ben Keo Industrial Park) are operating and are implementing infrastructure construction; In addition, the province has over 150 factories processing agricultural products such as processing sugar, processing tapioca, processing rubber latex and cashew nuts [23].

Facing economic development, specifically industrial development, the problem of pollution and environmental degradation tends to go up. The main source of pollution to the environment in Tay Ninh province is industrial waste from industrial production activities. In addition, activities such as transportation, animal husbandry, farming, etc. also affect the quality of the environment. Under the pressure of population growth, the increasing consumer demand has led to the development of many industries such as textiles, paper production, mechanical engineering, machine manufacturing, shoes, sandals, and tires vehicle... which increases a series of air pollutants, precursors of ground-level O_3 such as NO_x, SO_2, CH_4, CO... from fuel burning, open biomass burning and VOCs from activities textile industry, chemical factories.

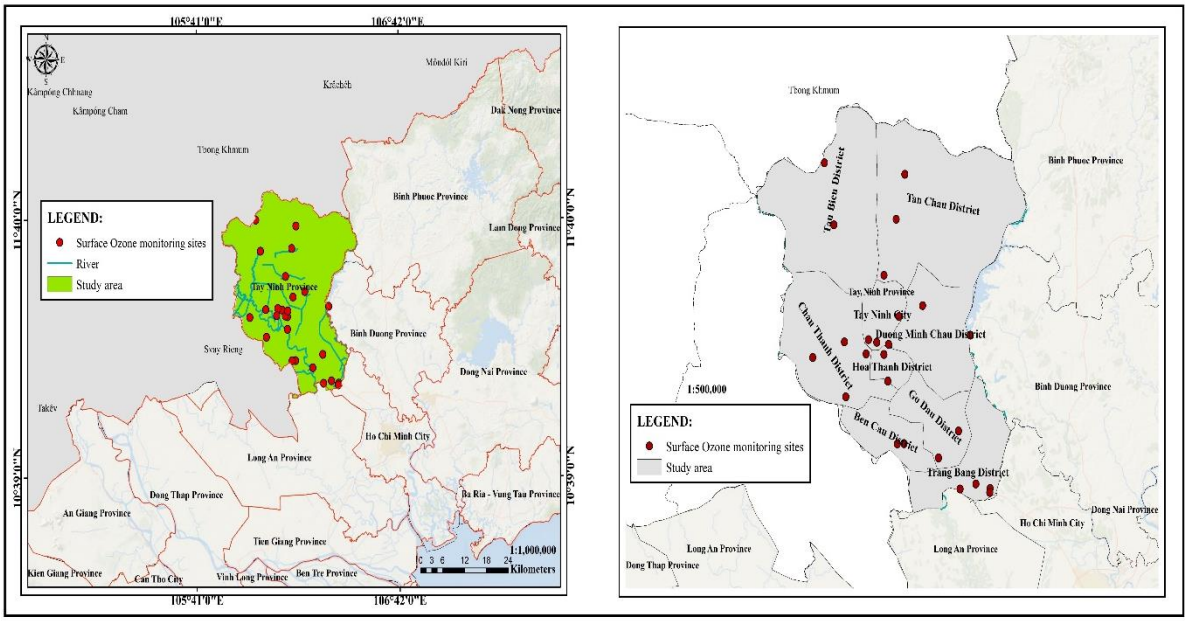

Figure 1. Description of the study area in Tay Ninh province.

2.2. Ground-level O_3 concentration-based exposure metrics

In this study, we considerd a type of long-term cumulative O_3 exposure metrics that have been widely used in quantifying O_3 exposure and its effects on crops. It is the norm in the form of cumulative exposure AOT40. The AOT40 metric for the hourly cumulative daytime O_3 concentration above the 40 ppbV threshold [24]. At the same time, the cumulative index (AOT40) reflects a greater degree of influence from O_3 concentrations with greater accuracy when estimating CYLs than using averages (M7 and M12 metrics) [25]. The cumulative metric AOT40 as well as the relationship between the indexes in the C-R functions (Table 1) estimated according to equation (1) [24, 26] as follows:

$$\text{AOT40 (ppm h)} = \sum_{i=1}^{n}([C_{O_3}]_i - 0.04), \text{ with } C_{O_3} \geq 0.04 \text{ ppm h} \quad (1)$$

where C_{O_3} is the hourly average O_3 concentration according to daylight hours in the study area from 08:00 to 19:59 hours, the ground-level O_3 concentration used in the study is the simulation result by the coupled WRF/CMAQ models for Tay Ninh province from January 2018 to March 2018 and n is the number of hours in the growing seasons of the crop under consideration, including Spring rice (paddy) and maize in 2018.

2.3. Estimation of crop yield and economic cost losses

The relative yield value (RY) calculated for maize and rice was used to further determine the relative yield loss (RYL) and crop-production loss values (CPL) according to below equations [27–28]. RYL is defined as the decline in crop yield, specifically in the study for Spring rice (paddy) and maize, which is based on the basic theoretical yield that is not due to O_3-induced damage [29]. RYL for crops is determined according to equation (2) as follows:

$$\text{RYL} = 1.0 - \text{RY} \quad (2)$$

The rice and maize production losses (CPLs) are calculated based on the rice production and maize production (CP) respectively combined with RYL according to equation (3) [30–31], where CP of rice and maize can be obtained from a source of national statistical database and annual Statistical Yearbook Reports of Tay Ninh province.

$$\text{CPL} = \text{CP} \times \frac{\text{RYL}}{1 - \text{RYL}} \quad (3)$$

As evidenced by the many previous studies available, the total economic loss (TEL) from the levels of economic cost loss (ECL) has been defined as the financial losses caused by the effects of ground-level O_3 exposure on crops and these are determined based on the minimum agricultural purchase price (MPP) for each considered crop. Therefore, the total economic cost damage caused by ground-level O_3 pollution can be determined by the equation (4) as follows:

$$\text{TEL} = \sum_{i=1} \text{ECL}_i = \sum_{i=1} \text{CPL}_i \cdot \text{MPP}_i \quad (4)$$

where ECL is the total economic cost loss with ECL_i being the component economic cost loss for each crop; CPL_i is the yield losses for each crop in turn; and MPP_i is the minimum annual Government purchasing price for rice and maize in 2018, respectively.

2.4. Data sources

2.4.1. Simulated surface O_3 concentration allocation over Tay Ninh province

The WRF model with version 3.8 combined with CMAQ air quality model with version 5.2.1 were used to simulate the distribution of ground-level O_3 concentration in tis study area. The CMAQ simulation is a modern scientific method widely used in much current research and policy-making to analyze and evaluate physical and chemical processes that determine the transport, reaction, and formation of tropospheric O_3 [32–33]. The entire research framework applies to the simulation of surface O_3 pollution in Tay Ninh province, specifically the process of setting up computational spatial domains for the combined WRF/CMAQ models, inventory of precursor emissions. The applied chemical mechanisms, initial conditions, boundary conditions, and efficiency verification of WRF models as well as CMAQ models have been detailed in many our previously published studies as a detailed description can be found in studies such as [34–35].

2.4.2. Ground-level O_3-crop models to assess RYL

The C-R function represents the relationship between surface O_3 exposure and RY of crops, including rice (as equations from (5) to (10)) and crops maize (as equation (11)) and based on available empirical studies, presented in Table 1.

Table 1. Overview of the exposure–response functions (ERFs) for evaluating relative yield loss (RYL) of rice and maize in this study.

Crop types	Sign of O_3-crop models	ERFs used for RYL estimation	References
Rice	Model (1)	RY = 1 – 0.0095×AOT40 (5)	[14]
	Model (2)	RY = 1 – 0.0160×AOT40 (6)	[36]
	Model (3)	RY = 1 – 0.0053×AOT40 (7)	[37]
	Model (4)	RY = 1 – 0.0390×AOT40 (8)	[38]
	Model (5)	RY = 1 – 0.0041×AOT40 (9)	[4]
	Model (6)	RY = 0.95 – 0.00001×AOT40 (10)	[17]
Maize	Model	RY = 1 – 0.00577×AOT40 (11)	[39]

2.4.3. Data of purchase prices of crops (MPP)

The MPP value is defined as the fixed price at which farmers sell their crops to the government [28] or purchase prices of crops (CPP) [40]. CPP values are referenced based on the World Food Organization's (FAOSTAT) aggregated statistical database, where the CPP in 2018 for rice was $287.8/ton and for maize was 267.8 USD/ton (http://www.fao.org/faostat/). In addition, the currency value conversion rate between USD and VND of Vietnam for 2018 is 1 USD = 22,602.05 VND according to the data of the World Bank (https://data.worldbank.org/indicator/PA.NUS.ATLS?locations=VN).

2.4.4. Crop area, yield, and production statistics

Statistical data related to the area of crop production (rice and maize production) in the study area in 2018 are collected from the website of the General Statistics Office of the Government and Detailed Statistical Yearbook Reports of Tay Ninh Province in 2018, 2019 and 2020 [22, 41], including area, yield, and yield of Dong Xuan rice and maize by each administrative unit in Tay Ninh province were used in this study. The related information collected from the Department of Agriculture and Rural Development of the province showed that the winter-spring rice production of the province is usually sown concentratedly and simultaneously in 3 batches depending on each locality as follows: (1) the first phase of early winter-spring from November 6 to November 14, 2017, (2) Phase 2 of the main winter-spring season from December 5 to December 13, 2017, and (3) Phase of the late Winter-Spring season from January 3 to January 11, 2018 (up to January 20, 2018) [23]. In the research area, rice variety OM 5451 is grown mainly by many advantages, especially good pest resistance, high yield; along with other key rice varieties from the Mekong Delta such as OM 6976, OM 4900, OM 576, IR 50404,... and production models of new rice varieties such as ST20, ST21, ST24, Hong Ngoc (red rice),…[23].

Rice, along with maize, is one of the traditional crops of Tay Ninh province, occupying a significantly larger area than other local crops (Figure 2) [42–43]. Specifically, in the period from 2010–2018, the province's rice and maize area, respectively, ranged from 142,224 to 155,909 hectares (up to 96.8% of the total cultivated area) and 4,359 to 5,865 hectares (up to 3.7% of the total area), respectively. cultivated area). In which, from 2010 to 2018 the area of winter-spring rice crops was from 42,568 to 47,603 hectares (accounting for 29.9 to 30.5% of the total cultivated area) with the yield and yield of winter-spring rice reaching 51.07 to 59.11, respectively. quintals/ha and 234,408–273,647 tons. On the other hand, from the statistics in Table 2. It could be seen that Tan Chau district and Hoa Thanh town, respectively, have the lowest planting areas of Dong Xuan rice and maize in the province; The highest yield and yield of winter-spring rice were obtained in Chau Thanh district and Trang Bang town, while maize area, yield and yield of Go Dau district was the highest in the whole of Tay Ninh province [22]. Thus, in this study, the total loss of rice and maize production due to ground-level O_3 pollution in Tay Ninh province was estimated by summing up all rice and maize production losses in each administrative unit of the province.

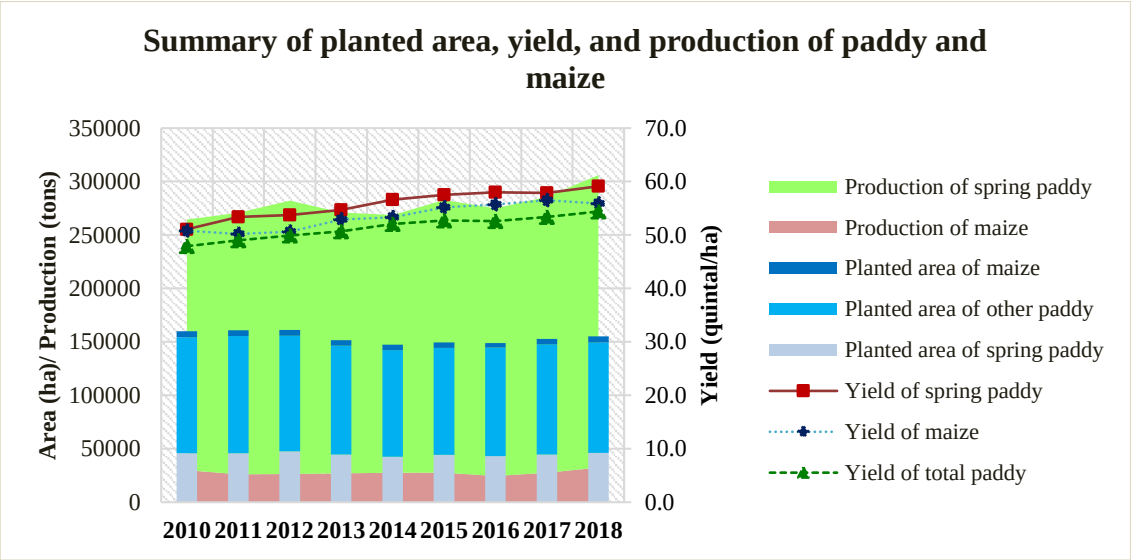

Figure 2. Statistical summary of spring paddy and maize in terms of planted areas, yield, and production in Tay Ninh Province from 2010 to 2018.

Table 2. Statistical planted area (ha), yield (quintal/ha), and production (tons) of spring paddy (rice) and maize by each county in Tay Ninh Province in 2018.

District/ Town/ City	Spring rice (paddy)			Maize		
	Planted area	Yield	Production	Planted area	Yield	Production
Tay Ninh City	463.75	45.10	2,091.66	188.55	44.13	832.06
Tan Bien District	1,531.00	52.01	7,962.90	648.30	46.63	3,022.88
Tan Chau District	144.10	45.63	657.53	200.39	49.02	982.26
Duong Minh Chau District	920.50	50.95	4,690.00	818.60	50.32	4,118.88
Chau Thanh District	14,061.80	57.26	80,516.60	389.00	49.46	1,924.10
Hoa Thanh Town	1,128.20	56.49	6,373.65	104.00	45.05	468.47
Go Dau District	7,311.69	59.94	43,826.27	1,261.30	68.21	8,603.56
Ben Cau District	10,027.65	57.96	58,116.21	599.00	64.11	3,840.11
Trang Bang Town	10,703.50	64.85	69,412.20	743.15	51.27	3,810.16
Total	**46,292.19**	**59.11**	**273,647.02**	**4,952.29**	**55.74**	**27,602.48**

The flow chart of the entire structure of this study is shown in Figure 3.

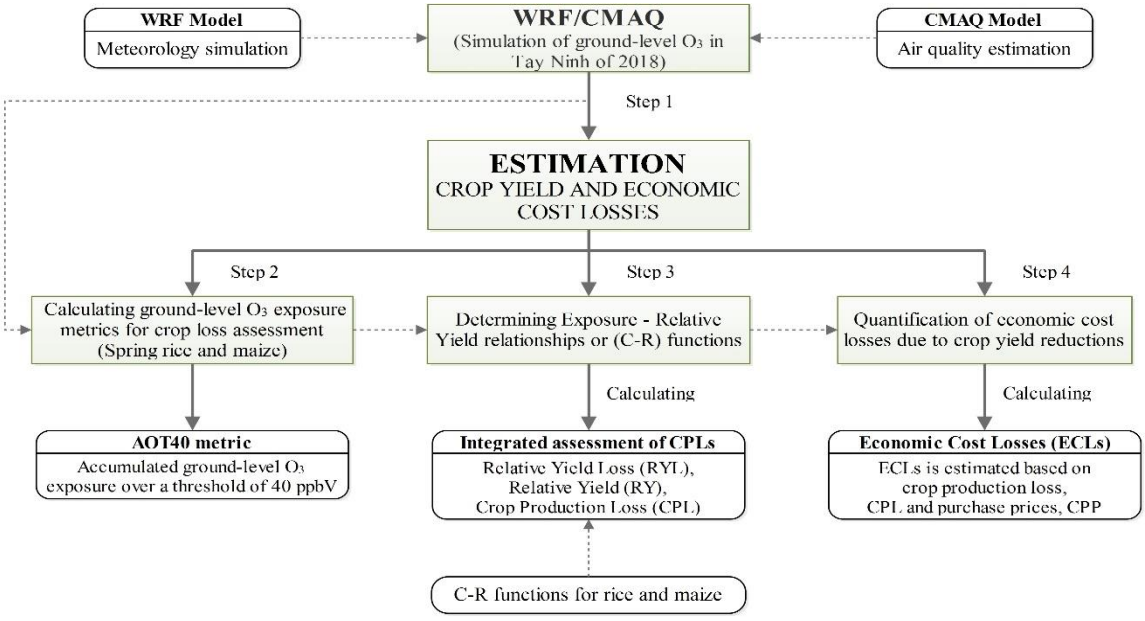

Figure 3. The flow chart of this study structure.

3. Results and discussion

3.1. Assessment of ground-level O_3 concentration levels in Tay Ninh province

In the period from January 2018 to March 2018, the average O_3 concentration level on the ground is the 8-hour day (daytime) from 8:00 a.m. until 7:59 p.m. and tends to fluctuate between 10.987 and 113.496 µg/m^3. Figure 4 represents the spatial-temporal distribution of the 8-hour average ground-level O_3 concentration of the days of the highest concentration in Tay Ninh province in the period January to March 2018. In general, the localities with high average ground-level O_3 concentration in the 8-hour day are mainly concentrated in the northern and eastern districts of Tay Ninh province, including: Tan Chau, Tan Bien, and Duong Minh districts. Chau, Trang Bang, and Go Dau. At the same time, over time, the average ground O_3 concentration level of 8-hour also tends to go up gradually from January 2018 < February 2018 < March 2018 with levels ranging from 10.987 to 75.022 µg/m^3 < from 30.662 to 106.855 µg/m^3 < from 22.831 to 113.496 µg/m^3 as in Figure 5.

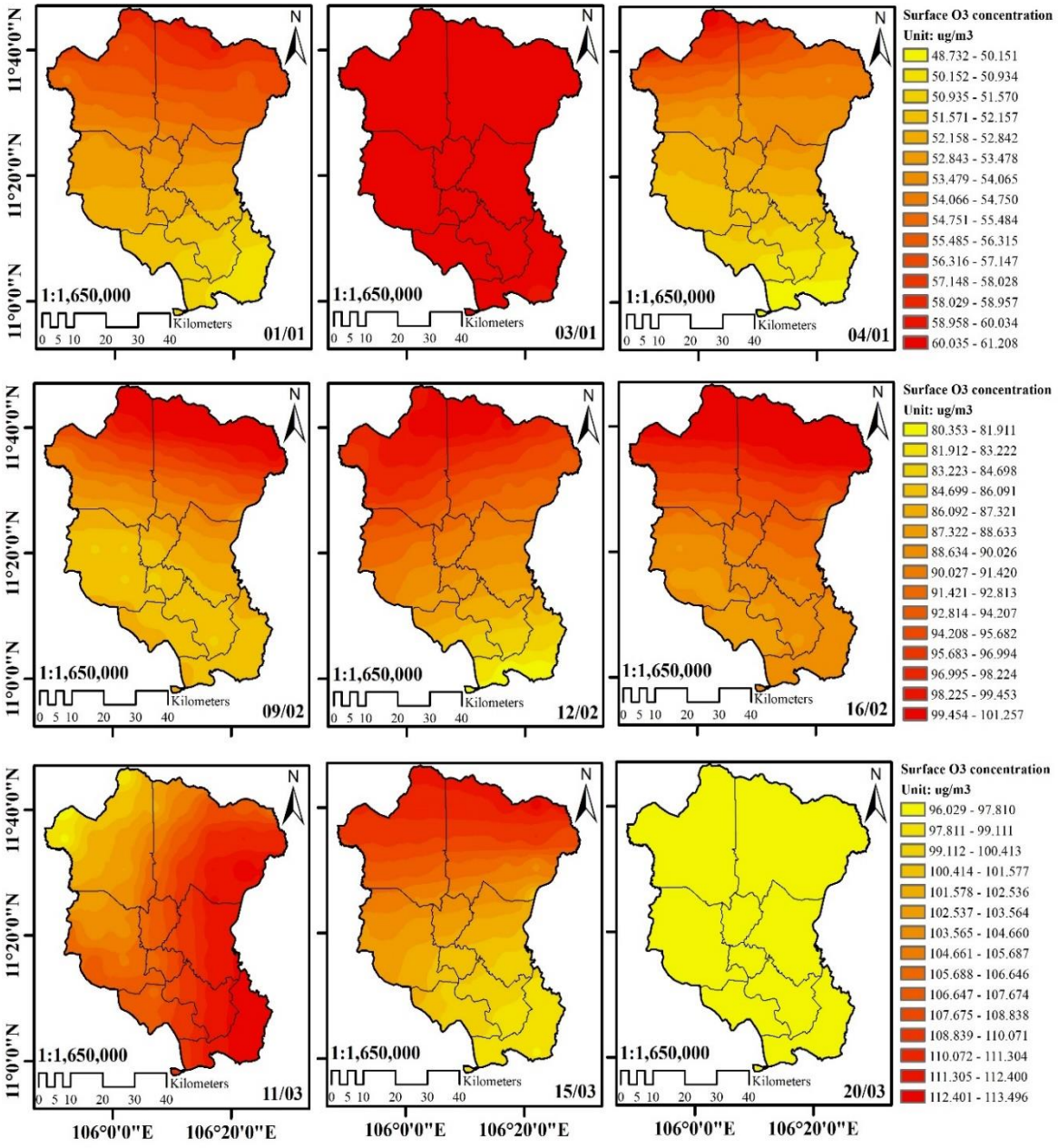

Figure 4. Spatio-temporal ground-level O_3 concentration distributions of the days of the highest concentration in Tay Ninh province between January 2018 and March 2018.

Specifically, in January 2018, ground-level O_3 concentration averaged 8-hour daytime from 8:00 a.m. until 7:59 p.m. average range from 28,236 ± 2,005 µg/m^3 to 33,840 ± 2,573 µg/m^3, still ensuring the allowable limit of NAAQS (particularly QCVN 05:2013/BTNMT, average 8-hour is 120 µg/m^3). The average high 8-hour ground O_3 concentration level usually concentrates on the first days of the month from January 1 to 6, 2018. The ground-level O_3 concentration level tended to decrease from January 1 to 10, 2018 and from January 11 to January 31, 2018, the ground-level O_3 concentration remained relatively stable at 19.955–38.930 µg/m^3. The largest 8-hour average O_3 concentration occurred on January 3, 2018, in the range of 59.724–75.022 µg/m^3. Next in February 2018, the average ground-level O_3 concentration level in 8-hour daytime averaged from 64.406 ± 2.932 µg/m^3 to 75.146 ± 3.499 µg/m^3 and continued to ensure the allowable limit of NAAQS. However, compared to January 2018, the average ground-level O_3 concentration on the 8-hour day was 2.20–2.28 times higher than in January 2018. During the period from February 1, 2018 to February 16, 2018 and peaking on February 16, 2018, the concentration of ground-level O_3 tended to increase sharply from 53.917–63.309 µg/m^3 to 87.966–106.855 µg/ m^3, and from February 17, 2018 to February 28, 2018 the ground-level O_3 concentration level remained stable, with slight fluctuation at a lower level from 60.879 to 87.902 g/m^3. And in March 2018, the average ground-level O_3 concentration in the 8-hour day during day fluctuated from 60.664 ± 4.476 µg/m^3 to 69.739 ± 5.052 µg/m^3 and continued to ensure the allowable limit of NAAQS. Nevertheless, there was a slight decrease compared to February 2018 between 1.06 and 1.08 times. During the period from March 1, 2018 to March 9, 2018 the concentration of O_3 on the ground was relatively low, only from 22.831 to 40.405 µg/m^3; then, from March 10, 2018 to March 20, 2018, the ground-level O_3 concentration tended to go up strongly, ranging from 40.092 to 113.496 µg/m^3 and peaking on March 11, 2018 with concentrations from 96.029 to 113.496 µg/m^3. From March 21, 2018 to the end of March 2018, ground-level O_3 concentration tended to decrease and remained stable at 58.586–92.807 µg/m^3.

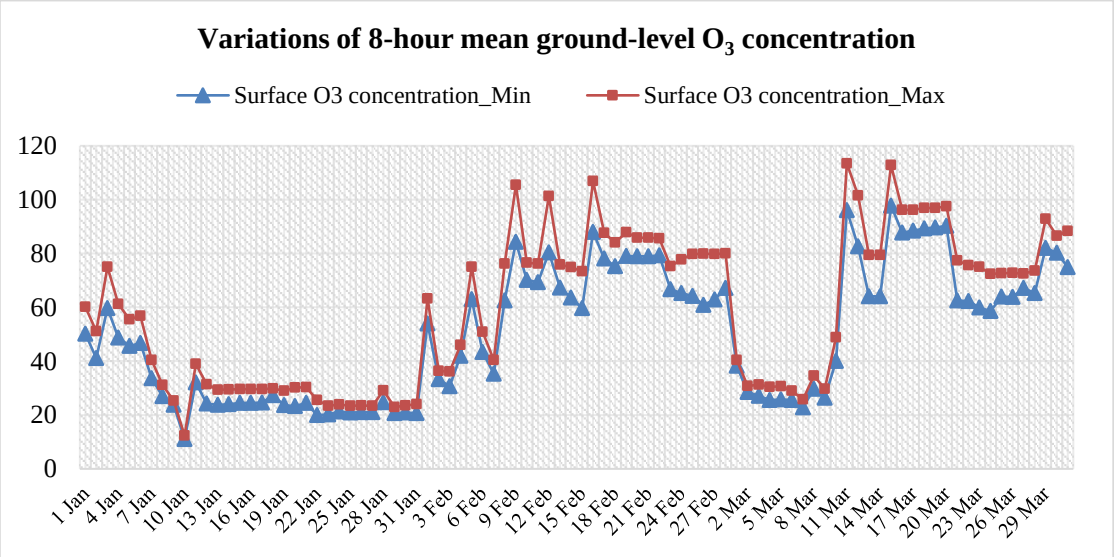

Figure 5. The fluctuation of daytime 8-hour average ground-level O_3 concentration (maximum and minimum) of days in the period January to March 2018 in Tay Ninh province.

3.2. Assessment of AOT40 spatio-temporal distribution

During the period from January 2018 to March 2018, the average AOT40 across the entire Tay Ninh province was 2.561 ppm h, ranging from 2,014 to 3.766 ppm h (Figure 6). The AOT40 level in Tan Chau and Tan Bien districts was higher than in other localities in the study area, ranging from 2.316–3.615 ppm h (average at 3.018 ppm h) and 2.184–3.513 ppm h (average at 2.673 ppm h), respectively. Meanwhile, Chau Thanh, Hoa Thanh, Go Dau, and Ben Cau districts are the localities with the lowest AOT40 levels in the study area during this period. In specific,

the AOT40 range occurs from 2.014 to 2.272 ppm h (average at 2.105 ppm h) in Chau Thanh district, 2.027 to 2.236 ppm h (average at 2.119 ppm h) in Hoa Thanh district, respectively. 2.075–2.414 ppm h (average at 2.213 ppm h) in Go Dau district, and 2.038–2.194 ppm h (average at 2.138 ppm h).

Generally, the spatial variation of AOT40 levels tended to increase gradually from localities in the direction from West to East and from Southwest to Northeast during the evaluation period. At the same time, the accumulation of ground-level O_3 exposure according to AOT40 also tended to increase gradually from January 2018 to March 2018 (Figure 6). Specifically, in January 2018 the average AOT40 level across Tay Ninh province was 0.003 ppm h (ranging from 0.0000 to 0.0048 ppm h) mainly on January 3, 2018; for February 2018 the average AOT40 level was 0.9805 ppm h (ranging from 0.6522–1.8167 ppm h) mainly occurred in the period from February 5, 2018 to February 28, 2018; and for March 2018 the average AOT40 level reached 1.5800 ppm h (ranging from 1.3374–2.0492 ppm h) mainly occurred in the period from 11 March 2018 to 31 March 2018. The highest AOT40 levels occurred in Tan Bien district in January 2018 and Tan Chau district in February 2018 and March 2018.

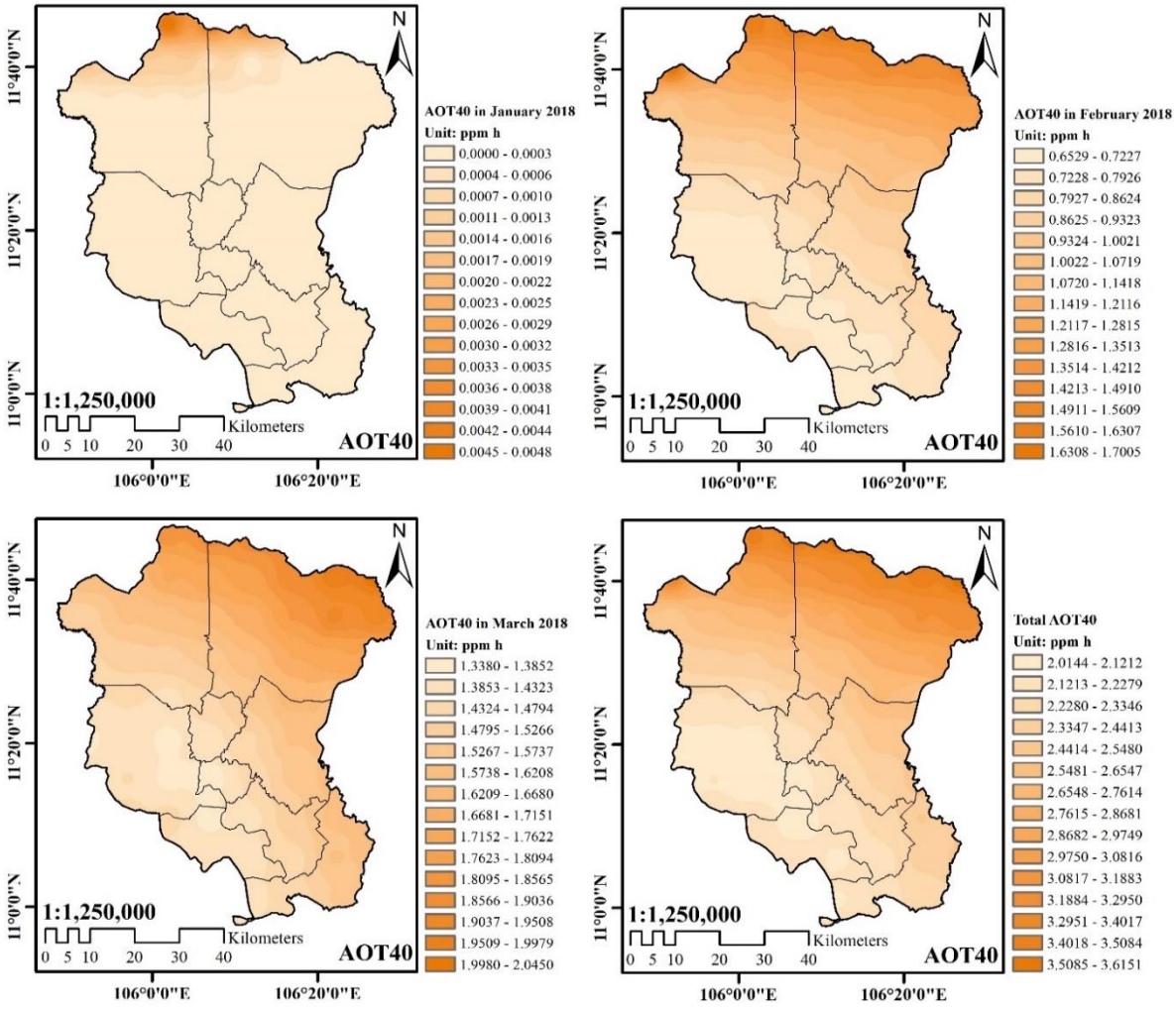

Figure 6. Spatio-temporal AOT40 metric distributions in Tay Ninh province between January 2018 and March 2018 based on ground-level O_3 concentration.

Thus, from the above analysis and evaluation results, the space-time distribution of the cumulative surface O_3 exposure metric (AOT40) in the first 3 months of 2018 shows a consistent trend for surface O_3 concentrations across Tay Ninh province. The surface O_3 concentration and cumulative AOT40 exposure have continuously increased from January 2018 to March 2018 and peaked in March 2018 due to the relatively high temperature increase occurring at the peak

period of the dry season in 2018 in the Southeast provinces of Vietnam, of which Tay Ninh is one of the typical areas, with the average temperature of January, February and March 2018 being 27.0°C < 27.4°C < 28.7°C, respectively [22, 41]. It is the difference in ground-level O_3 concentration in different localities and the time-varying changes of AOT40 levels in the growth stages of different crops in the study area that have had a significant impact in terms of yield and yield of crops [38].

3.3. The mean rice and maize RYL estimated using O_3-crop multiple models

In this study, we calculated the RYL for the winter-spring rice and maize crops in different localities of Tay Ninh province from various O_3-crop models (Table 1) and the results have been shown. shown in Table 3 and Figure 7. The mean RYL for Winter-Spring rice in 2018 from the O_3-crop models was 3.988% (ranging from 3.315% to 5.472%) and the average RYL for maize was 1.478% (ranging from 1.162% to 2.173%). On the other hand, for rice, the O_3-crop (4) model had the highest RYL level with an average RYL of 9.987% (ranging from 7.856% to 14.687%) and the O_3-crop (5) model had a low RYL level with an average RYL of 1.050% (ranging from 0.826% to 1.544%).

Table 3. The RYL of Spring rice and maize by each county in Tay Ninh province between January and March 2018 estimated using the corresponding O_3-crop models.

District/ Town/ City	Spring paddy (rice)						Maize
	RYL_1 [(a)]	RYL_2 [(b)]	RYL_3 [(c)]	RYL_4 [(d)]	RYL_5 [(e)]	RYL_6 [(f)]	RYL [(g)]
	min	min	min	min	min	min	min
Tay Ninh City	2.067	3.481	1.153	8.485	0.892	5.0022	1.255
Tan Bien District	2.042	3.439	1.139	8.382	0.881	5.002	1.240
Tan Chau District	2.198	3.701	1.226	9.021	0.948	5.002	1.335
Duong Minh Chau District	1.926	3.244	1.075	7.907	0.831	5.0020	1.170
Chau Thanh District	1.914	3.223	1.068	7.856	0.826	5.0020	1.162
Hoa Thanh Town	1.926	3.244	1.075	7.907	0.831	5.0020	1.170
Go Dau District	1.936	3.261	1.080	7.948	0.836	5.0020	1.176
Ben Cau District	1.936	3.261	1.080	7.948	0.836	5.0020	1.176
Trang Bang Town	2.007	3.381	1.120	8.241	0.866	5.0021	1.219
District/ Town/ City	**Spring paddy (rice)**						**Maize**
	RYL_1 [(a)]	RYL_2 [(b)]	RYL_3 [(c)]	RYL_4 [(d)]	RYL_5 [(e)]	RYL_6 [(f)]	RYL [(g)]
	max	max	max	max	max	max	max
Tay Ninh City	2.314	3.897	1.291	9.499	0.999	5.0024	1.405
Tan Bien District	3.382	5.697	1.887	13.885	1.460	5.004	2.054
Tan Chau District	3.578	6.026	1.996	14.687	1.544	5.004	2.173
Duong Minh Chau District	2.542	4.282	1.418	10.437	1.097	5.0027	1.544
Chau Thanh District	2.106	3.546	1.175	8.644	0.909	5.0022	1.279
Hoa Thanh Town	2.100	3.536	1.171	8.619	0.906	5.0022	1.275
Go Dau District	2.326	3.918	1.298	9.550	1.004	5.0024	1.413
Ben Cau District	2.088	3.517	1.165	8.573	0.901	5.0022	1.268
Trang Bang Town	2.397	4.037	1.337	9.840	1.034	5.0025	1.456
District/ Town/ City	**Spring paddy (rice)**						**Maize**
	RYL_1 [(a)]	RYL_2 [(b)]	RYL_3 [(c)]	RYL_4 [(d)]	RYL_5 [(e)]	RYL_6 [(f)]	RYL [(g)]
	average	average	average	average	average	average	average
Tay Ninh City	2.176	3.664	1.214	8.932	0.939	5.0023	1.321
Tan Bien District	2.540	4.277	1.417	10.426	1.096	5.003	1.543
Tan Chau District	2.867	4.829	1.600	11.772	1.238	5.003	1.742
Duong Minh Chau District	2.256	3.800	1.259	9.262	0.974	5.0024	1.370
Chau Thanh District	2.000	3.369	1.116	8.211	0.863	5.0021	1.215
Hoa Thanh Town	2.013	3.390	1.123	8.263	0.869	5.0021	1.223
Go Dau District	2.103	3.541	1.173	8.632	0.907	5.0022	1.277

Ben Cau District	2.031	3.420	1.133	8.336	0.876	5.0021	1.233
Trang Bang Town	2.210	3.721	1.233	9.071	0.954	5.0023	1.342

Note: (a) Wang et al. 2012; (b) Pang, Kobayashi, and Zhu 2009; (c) Feng et al. 2003; (d) Xu et al. 2021; (e) Mills et al. 2007; (f) Sinha et al. 2015; (g) Peng et al. 2019
Min: Minimum; max: Maximum

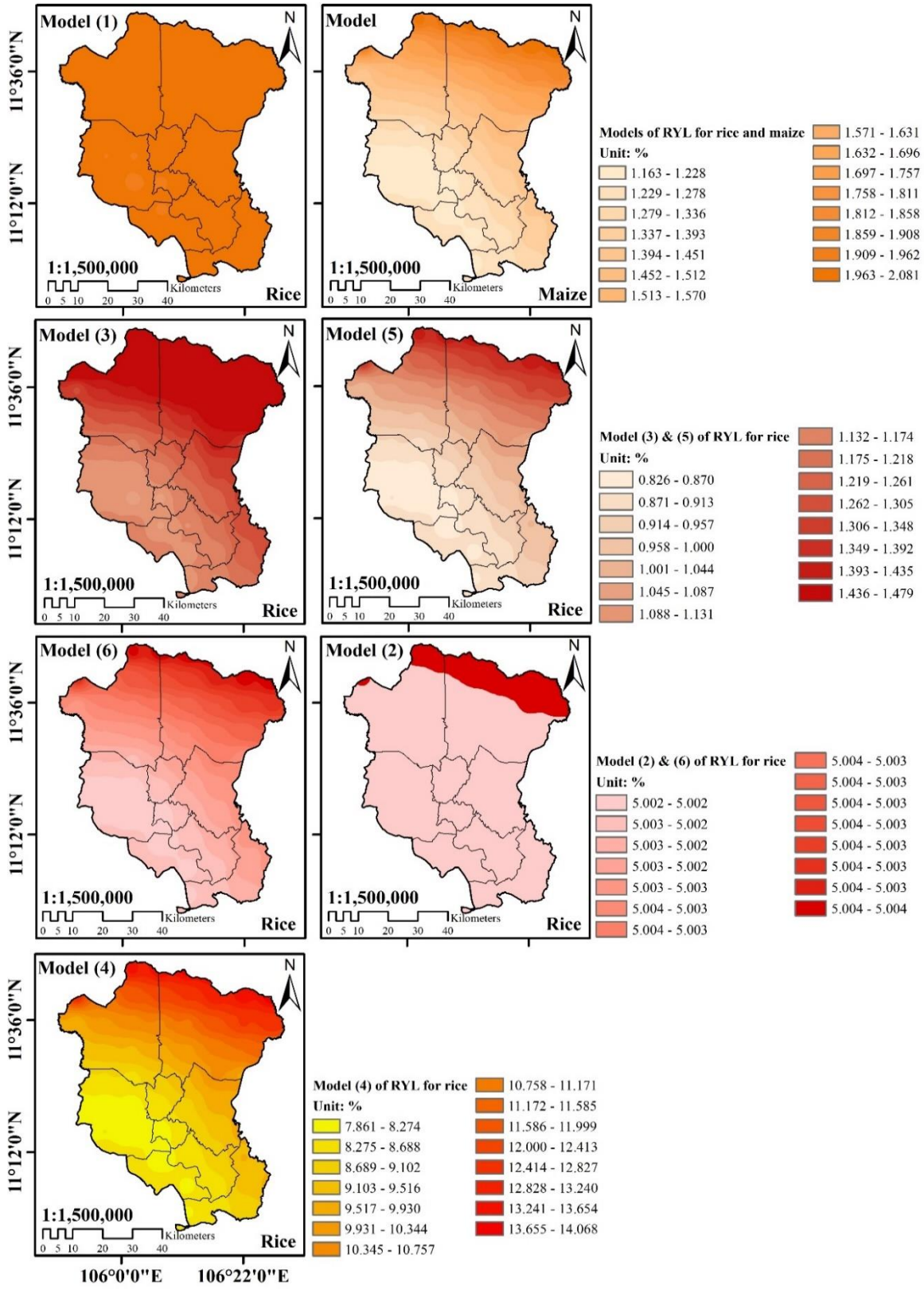

Figure 7. The RYL spatial distributions are estimated according to corresponding O_3-crop models in Tay Ninh province for Spring rice and maize.

Because RYL values are determined based on AOT40 the cumulative level of ground-level O_3 exposure; therefore, they tend to have a similar spatial distribution to the AOT40. Specifically, Tan Chau and Tan Bien districts had the highest RYL of winter-spring rice 2018 in the whole of Tay Ninh province, ranging from 9.047–14.068% and 8.520–13.672% for the the O_3-crop model (4), and in turn from 0.951–1.479% and 0.896–1.437% for the O_3-crop model (5). Chau Thanh, Hoa Thanh, Go Dau, and Ben Cau districts are respectively the localities with the lowest RYL of winter-spring rice in 2018 in the whole of Tay Ninh province, with levels ranging from 7.861–8.841%, 7.911–8.708%, 8.112–9.406% and 7.950–8.554%, respectively for the O_3-crop (4) model, and from 0.826–0.929%, 0.832–0.915%, 0.853–0.989% and 0.836–0.899%, respectively for the O_3-crop model (5). Similarly, Tan Chau and Tan Bien districts have the highest maize RYL levels in the entire study area at 1.338–2.081% and 1.260–2.023%, respectively; meanwhile, the lowest maize RYL levels occurred in Chau Thanh, Hoa Thanh, Go Dau, and Ben Cau districts of Tay Ninh province with values of 1.163–1.308%, 1.170–1.288%, 1.200–1.392%, and 1.176–1.266%, respectively.

3.3. CPL and TEL in Tay Ninh province attributed to surface O_3 pollution

Detailed statistics of CPL (tons) and ECL (thousand USD) results by administrative unit under Tay Ninh province are presented in Table 4. Because of the relatively large difference in crop production (including rice and maize) between localities in Tay Ninh province, the distribution of CPLs is not completely in the same trend as the distribution of RYL and RYL. The localities with large CPLs are mainly concentrated in the central and southern areas of Tay Ninh province. For rice, the total CPL of Spring rice in 2018 in Tay Ninh province ranges from 2.34 to 27.98 thousand tons and the equivalent total economic loss (ECL) can be up to from 15.20 to 181.98 billion VND (about 672.35–8,051.28 thousand USD). It could be found that Chau Thanh and Trang Bang districts have the highest CPL of Spring rice in the province with 670.91–7,808.80 tons and 606.65–7,442.30 tons, respectively with an EPL equivalent of about 4.36–50.80 billion VND (about 193.0–2,247.37 thousand USD) and 3.95–48.41 billion VND (roughly 174.59–2,141.89 thousand USD). The lowest CPL level of Winter-Spring rice occurs in Tan Chau district of Tay Ninh province at merely from 6.31 to 107.64 tons and the total equivalent ECL is estimated about from 41.07 to 700.22 million VND (between 1.82 and 30.98 thousand USD).

Table 4. Summary of CPL (tons) and ECL (thousand USD) outcome details of major crops by each county in this study area.

District/ Town/ City	Spring rice (paddy)				Maize			
	CPL min	CPL max	ECL min	ECL max	CPL min	CPL max	ECL min	ECL max
Tay Ninh City	18.2	218.4	5.2	62.9	10.2	11.8	2.7	3.2
Tan Bien District	72.0	1,261.1	20.7	363.0	38.6	62.4	10.3	16.7
Tan Chau District	6.3	107.6	1.8	31.0	13.3	20.9	3.6	5.6
Duong Minh Chau District	41.9	542.4	12.1	156.1	52.0	64.2	13.9	17.2
Chau Thanh District	670.9	7,808.8	193.1	2,247.4	22.6	25.5	6.1	6.8
Hoa Thanh Town	53.5	608.0	15.4	175.0	5.5	6.1	1.5	1.6
Go Dau District	377.0	4,550.1	108.5	1,309.5	104.5	121.4	28.0	32.5
Ben Cau District	489.8	5,436.5	141.0	1,564.6	45.7	49.2	12.2	13.2
Trang Bang Town	606.7	7,442.3	174.6	2,141.9	47.0	55.4	12.6	14.8
Total	**2,336.2**	**27,975.3**	**672.4**	**8,051.3**	**339.6**	**416.9**	**90.9**	**111.6**

Similarly, for maize, the total CPL level of maize in Tay Ninh province ranges from 339.55 to 416.88 tons and the equivalent total economic loss cost can be up to 2.06–2.52 billion VND (about 90.93–111.64 thousand USD). Specifically, Go Dau district has the highest corn CPL level, up to 104.51–121.41 tons with an EPL equivalent of about 632.60–734.89 million VND

(roughly 27.99–32.51 thousand USD), followed by Duong Minh Chau and Trang Bang, Ben Cau, and Tan Bien districts; whilst the lowest maize CPL occurs in Hoa Thanh district with a CPL of between 5.55 and 6.11 tons and an equivalent EPL at 33.58–37.01 million VND (about 1.486–1.637 thousand USD). Thus, from the estimated results, the total CPL level for 2 main crops in Tay Ninh province in the period from January 2018 to March 2018 can be up to 2.68–28.39 thousand tons and total economic losses (TEL) are estimated at 17.25–184.50 billion VND (equivalent to roughly 763.28–8,162.92 thousand USD). At the same time, it is also easy to see that the total CPL and TEL levels for Spring rice in 2018 are significantly higher than CPL and TEL for maize in Tay Ninh province, specifically from 6.88 to 67.11 times for CPL and from 7.39 to 72.12 times for TEL.

4. Conclusion

The ground-level O_3 pollution simulation results based on WRF/CMAQ model are used to estimate damage in agricultural production due to ground ozone (O_3) exposure for 2 major crops in the province. Tay Ninh, including rice and maize. The values of the cumulative exposure metric of AOT40 were determined for the crop seasons (Spring rice and maize) to calculate the damage caused by ground-level O_3 to crop yield and yield. Relative yield loss, RYL and crop yield loss, CPL for each administrative unit of Tay Ninh province for each crop due to ground-level O_3 exposure were estimated using multi-model O_3-crop to determine economic losses in the study area during the 2018 crop seasons. Total yield loss, CPL and total economic loss, TEL for Winter-Spring rice, respectively, are possible. up to 28 thousand tons and 182 billion VND (equivalent to about 8 million USD). In the case of maize, the total yield loss, CPL, and total economic loss, ECL could amount to 417 tons and 2.5 billion VND (roughly 112 thousand USD), respectively. The results of estimating damage because of ground-level O_3 exposure in Tay Ninh province in January, February, and March 2018 are the basis for initial judgments in the implementation of evaluation studies for the following stages as well as the implementation of policies to control ground-level O_3 pollution in Tay Ninh province and the whole Southeast region of Vietnam in general.

Nevertheless, the outcomes of this study also have certain limitations, and the research will continue to be developed to comprehensively demonstrate the impact of the ground-level O_3 problem on the activity of agricultural production in Tay Ninh province shortly. Specifically, the study will need to be extended to the remaining months (April to December) in 2018; furthermore, the effects on rice will be further calculated for the summer-autumn and winter rice crops, as well as extending the calculation to other crops such as sweet potatoes, cassava, and legumes.

Author contribution statement: Conceived and designed the experiments; Analyzed and interpreted the data; contributed reagents, materials, analysis tools or data: L.T.T.L.; Performed the experiments; contributed reagents, materials, analyzed and interpreted the data, wrote the draft manuscript: N.H.P.; and Manuscript editing: B.T.L.

Acknowledgements: We acknowledge the support of time and facilities from Ho Chi Minh City University of Technology (HCMUT), VNU-HCM for this study.

Competing interest statement: The authors declare no conflict of interest.

References

1. Betzelberger, A.M.; Yendrek, C.R.; Sun, J.; Leisner, C.P.; Nelson, R.L.; Ort, D.R. Ainsworth, E.A. Ozone exposure response for U.S. soybean cultivars: Linear reductions in photosynthetic potential, biomass, and yield. *Plant Physiol.* **2012**, *160(4)*, 1827–1839.
2. Feng, Z.; Hu, E.; Wang, X.; Jiang, L.; Liu, X. Ground-level O_3 pollution and its impacts on food crops in China: A review. *Environ. Pollut.* **2015**, *199*, 42–48.

3. Mills, G.; Sharps, K.; Simpson, D.; Pleijel, H.; Broberg, M.; Uddling, J.; Jaramillo, F.; Davies, W.J.; Dentener, F.; den Berg, M.V.; Agrawal, M.; Agrawal, S.B.; Ainsworth, E.A.; Büker, P.; Emberson, L.; Feng, Z.; Harmens, H.; Hayes, F.; Kobayashi, K.; Paoletti, E.; Dingenen, R.V. Ozone pollution will compromise efforts to increase global wheat production. *Glob. Chang. Biol.* **2018**, *24(8)*, 3560–3574.
4. Mills, G.; Buse, A.; Gimeno, B.; Bermejo, V.; Holland, M.; Emberson, L.; Pleijel, H. A synthesis of AOT40-based response functions and critical levels of ozone for agricultural and horticultural crops. *Atmos. Environ.* **2007**, *41(12)*, 2630–2643.
5. Monks, P.S.; Archibald, A.T.; Colette, A.; Cooper, O.; Coyle, M.; Derwent, R.; Fowler, D.; Granier, C.; Law, K.S.; Mills, G.E.; Stevenson, D.S.; Tarasova, O.; Thouret, V.; von Schneidemesser, E.; Sommariva, R.; Wild, O.; Williams, M.L. Tropospheric ozone and its precursors from the urban to the global scale from air quality to short-lived climate forcer. *Atmos. Chem. Phys.* **2015**, *15(15)*, 8889–8973.
6. Sitch, S.; Cox, P.M.; Collins, W.J.; Huntingford, C. Indirect radiative forcing of climate change through ozone effects on the land-carbon sink. *Nature* **2007**, *448(7155)*, 791–794.
7. Verstraeten, W.W.; Neu, J.L.; Williams, J.E.; Bowman, K.W.; Worden, J.R.; Boersma, K.F. Rapid increases in tropospheric ozone production and export from China. *Nat. Geosci.* **2015**, *8(9)*, 690–695.
8. Lin, Y. et al. Impacts of O_3 on premature mortality and crop yield loss across China. *Atmos. Environ.* **2018**, *194*, 41–47.
9. Amin, N.; Ken, Y.; Toshimasa, O.; Junichi, K.; Kazuyo, Y. Evaluation of the effect of surface ozone on main crops in East Asia: 2000, 2005, and 2020. *Water. Air. Soil Pollut.* **2013**, *224(5)*.
10. Tang, H.; Takigawa, M.; Liu, G.; Zhu, J.; Kobayashi, K. A projection of ozone-induced wheat production loss in China and India for the years 2000 and 2020 with exposure-based and flux-based approaches. *Glob. Chang. Biol.* **2013**, *19(9)*, 2739–2752.
11. Cao, J.; Wang, X.; Zhao, H.; Ma, M.; Chang, M. Evaluating the effects of ground-level O_3 on rice yield and economic losses in Southern China. *Environ. Pollut.* **2020**, *267*, 115694.
12. Lesser, V.M.; Rawlings, J.O.; Spruill, S.E.; Somerville, M.C. Ozone Effects on Agricultural Crops: Statistical Methodologies and Estimated Dose-Response Relationships. *Crop Sci.* **1990**, *30(1)*, 148–155.
13. Fuhrer, J.; Skärby, L.; Ashmore, M.R. Critical levels for ozone effects on vegetation in Europe. *Environ. Pollut.* **1997**, *97(1)*, 91–106.
14. Wang, X.; Zhang, Q.; Zheng, F.; Zhen, Q.; Yao, F.; Chen, Z.; Zhang, W.; Hou, P.; Feng, Z.; Song, W.; Feng, Z.; Lu, F. Effects of elevated O_3 concentration on winter wheat and rice yields in the Yangtze River Delta, China. *Environ. Pollut.* **2012**, *171*, 118–125.
15. Shi, G.; Yang, L.; Wang, Y.; Kobayashi, K.; Zhu, J.; Tang, H.; Pan, S.; Chen, T.; Liu, G.; Wang, Y. Impact of elevated ozone concentration on yield of four Chinese rice cultivars under fully open-air field conditions. *Agric. Ecosyst. Environ.* **2009**, *131(3)*, 178–184.
16. Zhu, X.; Feng, Z.; Sun, T.; Liu, X.; Tang, H.; Zhu, J.; Guo, W.; Kobayashi, K. Effects of elevated ozone concentration on yield of four Chinese cultivars of winter wheat under fully open-air field conditions. *Glob. Chang. Biol.* **2011**, *17(8)*, 2697–2706.
17. Sinha, B.; Singh Sangwan, K.; Maurya, Y.; Kumar, V.; Sarkar, C.; Chandra, B.P.; Sinha, V. Assessment of crop yield losses in Punjab and Haryana using 2 years of continuous in situ ozone measurements. *Atmos. Chem. Phys.* **2015**, *15(16)*, 9555–9576.
18. Nguyen, G.T.H.; Shimadera, H.; Uranishi, K.; Matsuo, T.; Kondo, A.; Thepanondh,

S. Numerical assessment of $PM_{2.5}$ and O_3 air quality in continental Southeast Asia: Baseline simulation and aerosol direct effects investigation. *Atmos. Environ.* **2019**, *219*, 117054.

19. Daly, A.; Zannetti, P. Air Pollution Modeling - An Overview. 2007.
20. Stevenson, D.S.; Dentener, F.J.; Schultz, M.G.; Ellingsen, K.; van Noije, T.P.C.; Wild, O.; Zeng, G.; Amann, M.; Atherton, C.S.; Bell, N.; Bergmann, D.J.; Bey, I.; Butler, T.; Cofala, J.; Collins, W.J.; Derwent, R.G.; Doherty, R.M.; Drevet, J.; Eskes, H.J.; Fiore, A.M.; Gauss, M.; Hauglustaine, D.A.; Horowitz, L.W.; Isaksen, I.S.A.; Krol, M.C.; Lamarque, J.F.; Lawrence, M.G.; Montanaro, V.; Müller, J.F.; Pitari, G.; Prather, M.J.; Pyle, J.A.; Rast, S.; Rodriguez, J.M.; Sanderson, M.G.; Savage, N.H.; Shindell, D.T.; Strahan, S.E.; Sudo, K.; Szopa, S. Multimodel ensemble simulations of present-day and near-future tropospheric ozone. *J. Geophys. Res. Atmos.* **2006**, *111(D8)*.
21. Sicard, P.; Serra, R.; Rossello, P. Spatiotemporal trends in ground-level ozone concentrations and metrics in France over the time period 1999-2012. *Environ. Res.* **2016**, *149*, 122–144.
22. Statistical Office of Tay Ninh Province. Statistical Yearbook of Tay Ninh Province in 2020, Tay Ninh City, 2021.
23. DARD of Tay Ninh Province. Report on the assessment of the implementation of the first 9 months of 2018 and the key tasks of the last 3 months of 2018 of the Agriculture and Rural Development sector. Tay Ninh City, 2018.
24. Van Dingenen, R.; Dentener, F.J.; Raes, F.; Krol, M.C.; Emberson, L.; Cofala, J. The global impact of ozone on agricultural crop yields under current and future air quality legislation. *Atmos. Environ.* **2009**, *43(3)*, 604–618.
25. Lefohn, A.S.; Laurence, J.A.; Kohut, R.J. A comparison of indices that describe the relationship between exposure to ozone and reduction in the yield of agricultural crops. *Atmos. Environ.* **1988**, *22(6)*, 1229–1240.
26. Emberson, L.D.; Büker, P.; Ashmore, M.R.; Mills, G.; Jackson, L.S.; Atikuzzaman, A.M.; M.D.; Cinderby, S.; Engardt, M.; Jamir, C.; Kobayashi, K.; Oanh, N.T.K.; Quadir, Q.F.; Wahid, A. A comparison of North American and Asian exposure-response data for ozone effects on crop yields. *Atmos. Environ.* **2009**, *43(12)*, 1945–1953.
27. Hu, T.; Liu, S.; Xu, Y.; Feng, Z.; Calatayud V. Assessment of O_3-induced yield and economic losses for wheat in the North China Plain from 2014 to 2017, China. *Environ. Pollut.* **2020**, *258*, 113828.
28. Kumari, S.; Lakhani, A.; Kumari, K.M. First observation-based study on surface O_3 trend in Indo-Gangetic Plain: Assessment of its impact on crop yield. *Chemosphere* **2020**, *255*, 126972
29. Avnery, S.; Mauzerall, D.L.; Liu, J.; Horowitz, L.W. Global crop yield reductions due to surface ozone exposure: 1. Year 2000 crop production losses and economic damage. *Atmos. Environ.* **2011**, *45(13)*, 2284–2296.
30. Dong, C.; Gao, R.; Zhang, X.; Li, H.; Wang, W.; Xue, L. Assessment of O_3-induced crop yield losses in northern China during 2013–2018 using high-resolution air quality reanalysis data. *Atmos. Environ.* **2021**, *259*, 118527.
31. Feng, Z.; Hu, T.; Tai, A.P.K.; Calatayud, V. Yield and economic losses in maize caused by ambient ozone in the North China Plain (2014–2017). *Sci. Total Environ.* **2020**, *722*, 137958.
32. Luecken, D.J.; Yarwood, G.; Hutzell, W.T. Multipollutant modeling of ozone, reactive nitrogen and HAPs across the continental US with CMAQ-CB6. *Atmos. Environ.* **2019**, *201*, 62–72.
33. Ring, A.M.; Canty, T.P.; Anderson, D.C.; Vinciguera, T.P.; He, H.; Goldberg, D.L.;

Ehrman, S.H.; Dickerson, R.R.; Salawitch, R.J. Evaluating commercial marine emissions and their role in air quality policy using observations and the CMAQ model. *Atmos. Environ.* **2018**, *173*, 96–107.

34. Phong, N.H.; Ha, D.T.T.; Duyen, N.C.M.; Long, B.T. Assessment Ground Ozone (O_3) Impacts on Agricultural Crop Yields in Mekong Delta, Vietnam. Proceeding of the International Forum on Green Technology and Management 2021 - Green Pathways Towards a Sustainable Future, 2021, pp. 37.
35. Bui, L.T.; Nguyen, P.H. Ground - level ozone in the Mekong Delta region : precursors , meteorological factors , and regional transport. *Environ. Sci. Pollut. Res.* **2022**, *30*, 23691–23713.
36. Pang, J.; Kobayashi, K.; Zhu, J. Yield and photosynthetic characteristics of flag leaves in Chinese rice (Oryza sativa L.) varieties subjected to free-air release of ozone. *Agric. Ecosyst. Environ.* **2009**, *132(3)*, 203–211.
37. Feng, Z.W.; Jin, M.H.; Zhang, F.Z.; Huang, Y.Z. Effects of ground-level ozone (O_3) pollution on the yields of rice and winter wheat in the Yangtze River Delta. *J. Environ. Sci. (China).* **2003**, *15(3)*, 360–362.
38. Xu, M.; Yao, Q.; Chen, D.; Li, M.; Li, R.; Gao, B.; Zhao, B.; Chen, Z. Estimating the impact of ground ozone concentrations on crop yields across China from 2014 to 2018: A multi-model comparison. *Environ. Pollut.* **2021**, *283*, 117099.
39. Peng, J.; Shang, B.; Xu, Y.; Feng, Z.; Pleijel, H.; Calatayud, V. Ozone exposure- and flux-yield response relationships for maize. *Environ. Pollut.* **2019**, *252*, 1–7.
40. Zhao, H.; Zheng, Y.; Wu, X. Assessment of yield and economic losses for wheat and rice due to ground-level O_3 exposure in the Yangtze River Delta, China. *Atmos. Environ.* **2018**, *191*, 241–248.
41. Statistical Office of Tay Ninh Province. Statistical Yearbook of Tay Ninh Province in 2019. Tay Ninh City, 2020.
42. GSO. National Statistical Yearbook 2019. Statistical Publishing House, Vietnam, Ha Noi Capital, 2019.
43. GSO. National Statistical Yearbook 2020. Statistical Publishing House, Vietnam, Ha Noi Capital, 2020.

VIETNAM JOURNAL OF HYDROMETEOROLOGY

Research Article

Modified methods of oil cleanup with cellulose–based adsorbents: a review

Trinh Trong Nguyen[1,2], Nguyen Dinh Loc[1], Thai Van Nam[1]*

[1] HUTECH Institute of Applied Sciences, HUTECH University, 475A Dien Bien Phu Street, Ward 25, Binh Thanh District, Ho Chi Minh City 700000, Vietnam; tt.nguyen@hutech.edu.vn; 6009220001@hufi.edu.vn; lochenni@gmail.com; tv.nam@hutech.edu.vn

[2] Ho Chi Minh City University of Food Industry, 140 Le Trong Tan Street, Tay Thanh Ward, Tan Phu District, Ho Chi Minh City 700000, Vietnam; tt.nguyen@hutech.edu.vn; 6009220001@hufi.edu.vn

*Corresponding author: tv.nam@hutech.edu.vn; Tel: +84–945007990

Received: 18 February 2023; Accepted: 24 March 2023; Published: 25 March 2023

Abstract: Oil spills and contaminated water sources are responsible for polluting marine environments, which in turn has adverse effects on marine ecosystems and public health. Among various oil removal methods, adsorption is the preferred technique due to its speed, simplicity, low cost, and eco–friendliness. In this paper, we will review methods for modifying the oil adsorption properties of cellulose to enhance its adsorption capacity. We have reviewed 287 relevant worldwide documents in recent years and selected 142 documents for use in this study. The review results of the number of documents show that there are three main methods for transforming cellulose–based adsorbents, including (1) Physical transformation methods such as mechanical crushing, or pressing, heat treatment, and the plasma technique; (2) Chemical modification methods such as mercerization, acetylation, grafting, acidification, aerogel modification, cationic surfactant; and (3) Bioremediation (immobilization of microorganisms). Among these modification methods, cellulose–based aerogels have shown remarkable oil absorption capabilities of up to 170.0 g/g, superhydrophobicity (with a water contact angle of 156.7^o), and the ability to be reused up to 80 times. Cellulase denaturation and microbial immobilization are eco–friendly techniques that have potential to replace non–biodegradable oil adsorbents. Furthermore, utilizing agricultural by–products to produce high–capacity absorbent materials is a promising solution that benefits both the economy and the environment.

Keywords: Adsorption; Cellulose; Modified methods; Natural adsorbents; Oil cleanup.

1. Introduction

The worldwide deterioration of water quality and negative impact on the underwater ecosystem is caused by oil pollution resulting from oil spills and leaks during various activities such as transportation, shipping, exploration and production, oil refining, and disposal [1]. This has led to severe health consequences [2]. The majority of oil spill volumes in water originate from oil refinery ports (25%), ships (25%), oil tankers (20%), barge tankers (15%), and oil rigs (15%). The oil spills consist of various types of oil, with crude oil being the most common (35%), followed by diesel oil (20%), marine oil (10%), gasoline (8%), and the lowest is bunker oil (3%) [3].

There are various methods available for removing oil from water, including in–situ burning, chemical techniques such as solidification and dispersion, biological methods, and

physical methods such as skimming and oil sorbents [4]. Nevertheless, oil absorbent materials are the most favored method due to their quickness [5], convenience, affordability [6], and eco–friendliness [7]. There are about 200 different sorbent materials available in the market, and the choice of sorbent material depends on factors such as availability, cost, and safe usage [8]. The three main categories of oil sorbent materials are inorganic mineral products, synthetic organic products, and natural organic products [9]. Inorganic products like perlite, vermiculite, and diatomite are mostly buoyant and have low oil absorption capacity [10], while organic polymer products such as polypropylene, polyethylene, and polyurethane have a major drawback of being difficult to biodegrade [11]. However, lignocellulose sorbent materials have significant advantages over other materials, especially in terms of their environmental friendliness and lightweight nature, making them easily recoverable and reusable [12].

Natural adsorbents from agricultural waste and byproducts, including rice straw [13], sawdust [12], onion skin [14], garlic skin [14], walnut shell [15], bagasse [16], barley straw [17], banana stem fibers [18], banana stem [18], peanut shell [19], rice husk [20], corn stalk [21], corn cob [22], pomelo peel [23], wheat straw [24], mango seed coat [25], banana peel [4], rice bran [26], Cha La seeds [27], flax fiber [28], durian peel [29], and coconut coir [30], have gained significant attention from researchers in recent years for their effectiveness in removing oil from water.

Natural absorbent materials are an appealing choice for cleaning up oil spills owing to their cost–effectiveness, widespread availability, biodegradability, and non–toxic nature. Nevertheless, they exhibit limitations such as low adsorption capacity, limited floatability, and hydrophilicity [31]. Researchers have reported different conversion methods in literature to enhance the properties of natural absorbent materials, such as their adsorption capacity and buoyancy, while maintaining their original properties. Ideally, these modifications should be minimal and should not affect the biocompatibility of the material [32].

To improve these properties, adsorbent materials can be modified by physical methods: mechanical [33], thermal [34–35]; chemical methods: alkaline treatment [36], acetylation [37], benzoylation and grafting [38–40], and biological methods [41], which can significantly enhance the adsorption properties of the natural base material.

This study will delve into investigating and evaluating methods to improve the oil adsorption capability of natural organic sorbents derived from environmentally friendly plant sources.

2. Cellulose–based adsorbents

Lignocellulosic, which refers to wood and plant materials, is a type of composite material that consists of three different polymers, namely cellulose, hemicelluloses, and lignin [42]. Cellulose is made up of straight crystalline chains of glucose units that are joined together by 1,4–β–glycosidic bonds, and the length of the polymer chain can be as long as 15,000 units [43]. One of the remarkable characteristics of cellulose is its ability to biodegrade and regenerate. Additionally, cellulose exhibits high strength and stiffness, low density, and excellent biocompatibility [44].

Natural organic sorbents are composed of cellulose, hemicellulose, and lignocellulose, which mainly composed of carbon (C), hydrogen (H), oxygen (O), and nitrogen (N), as noted by [45]. As pointed out by [46], high levels of carbon or oxygen content are important for improving the oil recovery capacity of sorbent materials in water. Although cellulose can serve as an efficient oil sorbent, its hydrophilic characteristics due to the hydroxyl (–OH) groups on the material's surface can impede oil clean–up efforts in water. One solution is to substitute the hydroxyl groups to modify the sorbent's surface and increase its hydrophobicity [47]. This is also the rationale behind numerous modification methods used to substitute the hydroxyl groups.

The structure of the sorbent is a significant factor, including its hydrophobicity, porosity, suitable pore size, and surface area [46]. An oil absorbent that is considered ideal should exhibit high porosity and surface area while also being able to selectively absorb oil. To be useful for oil spill treatment purposes, the sorbent must also be stable chemically and mechanically, environmentally friendly, buoyant, and possess low density, in addition to being recyclable [48].

The next section will analyze methods of modifying sorbents to improve their hydrophobicity and oil sorption capacity of natural adsorbents.

3. Adsorbent modification method

Natural sorbents are typically only effective for oil absorption in non–aqueous environments [49]. To improve their performance, pretreatment methods are used to enhance functional groups, such as hydrophobic and ankylic groups, and increase pore numbers. Sorbent modification methods include physical modification, chemical modification (such as hydrolysis, acetylation, benzylation, grafting, and other methods), and biological modification [33].

3.1. Physical modification methods

3.1.1. Mechanical crushing or pressing

According to [33], mechanical crushing or pressing does not affect the hydrophobicity of natural adsorbents, but it can affect their effectiveness in removing oil. Crushing or pressing the absorbent can increase its oil absorption capacity by increasing the contact surface area between the absorbent and oil. However, if the absorbent is highly compressed, its oil absorption capacity may decrease because the oil has difficulty infiltrating the material [17, 50].

3.1.2. Heat treatment

Natural adsorbent modification by high–temperature treatment methods includes drying [35], hydrothermal treatment [33], and pyrolysis [34].

By drying, the material's porosity can be augmented, leading to an increase in the surface area of the adsorbent and an improvement in oil absorption capacity. However, conventional drying methods can cause a substantial reduction in the porous structure of the natural adsorbent, thereby decreasing its ability to adsorb and be reused [51]. Additionally, the drying process does not enhance the oil absorption capacity and water repellency of the organic natural adsorbent in comparison to raw fibers [35].

According to [52], hydrothermal treatment is an economical and eco–friendly technique that can eliminate cellulose components that are hydrophilic. When adsorbent materials are subjected to hot water treatment, it can help eliminate impurities, wax coatings, and volatile compounds from cellulose fibers, increasing their contact with the adsorbing environment [53]. Dried moss fibers were soaked in deionized water at temperatures of 80°C and 100°C for an hour, and the results showed that the adsorbent material treated with hot water at 80°C had a 12.4% increase in diesel oil adsorption capability, while treatment at 100°C showed a 6.7% increase when compared to untreated materials [33]. In another study, [54] utilized superheated steam treatment to remove hemicellulose from coir fibers. The findings of [33] indicated that hot water modification of the fiber surface resulted in a greater contact surface area, which improved the oil adhesion of the modified fiber surface and removed the wax coating and some volatile components. In addition, the heat treatment will increase the oil absorption capacity, enhancing the hydrophobicity and oil affinity of the fibers [55].

Pyrolysis is an alternative heat treatment method that can increase the hydrophobicity and oil absorption capacity of materials through carbonization. However, this process is

expensive and time–consuming [56]. Carbonized rice husk has been found to be a superior natural adsorbent due to its high content of oil–affinity SiO_2 group, which enhances its oil absorption capacity and hydrophobicity. However, the efficiency of pyrolysis depends on the number of natural fibers in the plant material being used [34]. Rice husk waste is rich in silica, and pyrolyzing the husk leads to the decomposition of organic matter and the breakdown of bonds between silica and organic matter. This increases the hydrophobicity of the husk, allowing it to selectively absorb crude oil [20]. Table 1 presents a summary of the synthesis of natural adsorbents using various heat treatment methods such as drying, hydrothermal treatment, and pyrolysis.

Table 1. Synthesis of natural adsorbents treated by heat methods.

Material	Method	Oils	Sorption capacity/ Removal	Ref.
Barley straw	Drying	Gas oil	7 – 8.5 g/g	[57]
	Carbonization, 400°C in 0.5 to 3 hours	Gas oil	8.5 – 9 g/g	[57]
Calotropis procera fiber	Thermally treated, 150°C	Crude oil	76.32 g/g	[58]
	Thermally treated, 200°C	Crude oil	94.31 g/g	[58]
	Hot water treatment at 80°C in 1 hour	Crude oil	99.2 g/g	[36]
	Oven drying, 60°C, 24 hours	Engine oil	1.107 g/g	[59]
Coconut husk	Oven drying, 60°C, 24 hours	Engine oil	0.058 g/g	[59]
Kapok fiber	Oven drying, 60°C, 24 hours	Engine oil	0.827 g/g	[59]
	Sun–drying	Diesel oil	19.35 g/g	[60]
	Sun–drying	Engine oil	60.51 g/g	[60]
	Sun–drying	Used engine oil	49.94 g/g	[60]
Luffa (an agricultural waste)	Cutting, Sieving, washing, and drying (105°C)	Diesel oil	> 85 %	[60]
Moss	Hot water treatment, 100°C	Diesel oil	7.85 ± 0.09 g/g	[33]
	Hot water treatment, 80°C	Diesel oil	8.27 ± 0.06 g/g	[33]
Potato peel	Drying, 70°C and crushing	Waste lubricating oil	2.15 g/g	[23]
Rice husks	Oven drying, 60°C, 24 hours	Engine oil	0.298 g/g	[59]
	Sun–drying	Diesel oil	2.60 g/g	[60]
	Sun–drying	Engine oil	9.26 g/g	[60]
	Pyrolysis	Diesel oil	5.02 g/g	[20]
	Pyrolysis (N_2 or inert atmosphere)	Diesel oil	2.78 g/g	[20]
	Pyrolysis (Carbonized), 480°C	Diesel oil	5.5 kg/kg	[34]
	Pyrolysis (Carbonized), 480°C	Motor oil	7.5 kg/kg	[34]
Salvinia cucullata Roxb	Oven drying, 60°C, 24 hours	Engine oil	0.944 g/g	[59]
Silkworm cocoon waste	Oven drying, 110°C reduced to 60 °C, cutting and milling	Motor oil	42 – 52 g/g	[62]
Sugarcane bagasse	Oven drying, 60°C, 24 hours	Engine oil	0.019 g/g	[59]
	Sun–drying	Diesel oil	10.51 g/g	[60]
	Sun–drying	Engine oil	19.95 g/g	[60]
	Sun–drying	Used engine oil	18.01 g/g	[60]
	Oven drying	Engine oil	3.2 – 5.3 g/g	[61]
Wood chips	Oven drying, 60°C, 24 hours	Engine oil	0.343 g/g	[59]

Table 1 provides information on the oil adsorption capacities of naturally derived organic adsorbents that have undergone thermal treatment. Calotropis procera fiber and Kapok fiber are examples of natural fiber adsorbents with excellent oil adsorption capabilities. Heat treatment of Calotropis procera fiber at 150ºC and 200ºC for 1 hour resulted in the reduction of functional groups, such as C–H (2920 cm^{-1}), C=O (1734, 1368, and 1244 cm^{-1}), and C–O (1032 cm^{-1}), and the disappearance of lignin (1505 and 1597 cm^{-1}) and hemicellulose (1737 and 1248 cm^{-1}) peaks. Furthermore, the heat treatment helped eliminate the water–repellent waxes from the fiber surface, thereby increasing its oil adsorption capacity. The *Calotropis procera* fiber with a large lumen, has a high oil adsorption capacity of up to 74.04 g/g. Raising the temperature from 150ºC to 200ºC results in an increase in the maximum adsorption capacity from 94.31 g/g to 124.60 g/g [58]. Similarly, Kapok fiber has oil adsorption capacities of 19.35 g/g, 49.94 g/g, and 60.51 g/g for diesel oil, used engine oil, and engine oil, respectively, after being sun–dried [60].

3.1.3. The plasma technique

The plasma method is a physical process that transforms the surface of fibers by forming strong bonds between the fiber matrix and the new functional groups, leading to improved mechanical properties of natural fibers [63–64]. Low–pressure flo plasma treatment has been used to enhance the surface hydrophilicity of cellulose fibers towards hydrocarbons that are dispersed in water, which improves their ultra–hydrophobic adsorption properties. The cellulose fibers were obtained from various vegetables, treated by NaOH (0.5% w/w) at 353 K for 20 minutes, and then treated with low–pressure plasma in the laboratory. The results of the kinetic analysis demonstrated that the fibers treated with plasma achieved a removal efficiency ranging from 80% to 90% after only one minute of exposure, which depended on the initial weight ratio of hydrocarbon to fiber (ranging from 20 mg/g to 240 mg/g). Moreover, the maximum adsorption capacity of the treated fibers exceeded 270 mg/g, and the adsorption process adhered to the Langmuir adsorption isotherm, as noted by [65].

3.2. Chemical modification method

The chemical treatment of adsorbents is a technique that can be used to cleanse the surface of fibers, alter the surface chemically, and increase the roughness of the surface [66]. This modification can lead to a reduction in water adsorption and an improvement in oil adsorption as compared to unmodified adsorbents [33]. Many techniques have been studied to improve the ability of adsorbents to repel water (hydrophobic) and attract oil (lipophilic), including alkalization, acetylation, benzoylation, crosslinking agents (with or without heat), grafting, and other techniques [67]. In order to attach different chemical groups to the hydroxyl (–OH) group on the cellulose chain, a variety of reactions are used. These reactions typically involve chemicals such as alkali, acetic anhydride, coupling agents, peroxide, stearic acid, fatty acid derivatives (oleoyl chloride), and others [68–69].

3.2.1. Mercerization

Alkali treatment is defined by the ASTM D1965 as a method in which strong bases are used to treat plant fibers, causing significant swelling and changing the fibers' fine structure, size, shape, and mechanical properties [70]. Mercerization, a process that breaks down fiber bundles into smaller ones by treating them with alkali, is widely used for modifying organic adsorbents because it is simple and effective [47, 71]. The initial alkali treatment is used to remove non–cellulose components like lignin and pectin, which exposes the inner surface and creates a rougher surface structure for natural fibers [56]. This increases surface roughness and promotes mechanical interlocking and better contact of cellulose on the fiber surface, which increases the number of reactive sites [72]. Hasim has shown that the change

in natural crystalline structure depends on the type and concentration of alkali used [73]. Increasing the NaOH concentration in the alkali treatment increases water repellency, leading to a reduced water adsorption capacity of single abaca fiber [74]. Table 2 summarizes the literature on the parameters of the alkali treatment process, focusing on NaOH concentration, treatment temperature, and soaking time.

Table 2. Mercerization conditions of natural cellulose fibers.

Material	NaOH treatment parameters	Oils	Effect/Comments	Sorption capacity	Ref.
Calotropis procera fiber	Agitate NaOH 0.1 M for 1 hour	Crude oil	The functional groups' intensity was reduced, and the surface became slick with a waxy hydrophobic coating on the inner surface of the hollow structure. The fiber diameter increased from an average of 23.84 ± 4.44 µm to 37.47 ± 3.80 µm, and the specific surface area improved from 146.6 to 390.8 m²/kg. Furthermore, 93% of the structure is made up of voids.	103.9 g/g	[36]
Hybrid peel waste (banana skins + orange peel)	Hybridization of peels with NaOH 1 M, stirred at 350 rpm for 24 hours and drying at 70°C for 24 hours	Lubricant oil	The process of hydrolyzing the adsorption band of $–COOCH_3$ on the surface of fruit peels results in an augmentation of carboxylic acid amount due to the formation of –COO– groups.	38.12%	[75]
Moss	NaOH solvent (5%) at 25°C for 48 hours	Diesel oil	The treatment of moss fibers with mercerization resulted in an enhancement of surface roughness and area, leading to swelling and an increase in diesel sorption capacity by 22%.	8.99 ± 0.08 g/g	[33]
Plant fibers (soybean)	The fibers were subjected to alkali treatment by immersing and shaking them in a 5% NaOH solution for two different periods: 48 hours at 25°C and 1 hour at 300°C. Following the treatment, the fibers were drained and dried at 105°C for 24 hours	Crude oil		5 g/g	[76]
Rice Husks	NaOH 4 M at 90°C	Marine diesel	The use of low NaOH concentrations (0.1 M) can effectively eliminate surface fat, wax, and hemicellulose, whereas comparable oil uptake outcomes are seen for samples treated with NaOH concentrations ranging from 2–6 M.	20 g/g	[77]

Table 2 shows that *Calotropis procera* fibers treated with 0.1 M NaOH for 1 hour resulted in a reduction in functional groups' intensity, such as CH (2920 cm^{-1}), C=O (1734, 1368, and 1244 cm^{-1}), and CO (1032 cm^{-1}). This is because the treatment removed impurities, wax and pectin from the surface of the fibers. The contact angle θ of the hydrophobic surface was measured at 119° and 0° for diesel. Mercerisation considerably increased the inner diameter and surface area of *Calotropis procera* lumens, leading to an increased absorption

capacity of up to 103.9 g/g [36]. The mercerization process using NaOH concentrations ranging from 0.1 M to 6 M on rice husks resulted in broken cellulose hydrogens and increased surface roughness. Wax and oil coatings on the outer layer of fiber cells were eliminated, leading to an improved absorption capacity of up to 20 g/g for marine fuel RMG380 [77]. Anuzyte discovered that the alkaline hydrolysis process using 5% NaOH induced swelling and increased surface area and roughness of moss fibers, resulting in an additional 22% increase in diesel absorption capacity [33]. Additionally, alkali treatment serves as a pretreatment method for other adsorbent transformation techniques. In the study by [24], wheat straw underwent a pretreatment process by extraction with a toluene–ethanol solvent system (2:1, v/v) to remove the wax layer, followed by treatment with 1.3% $NaClO_2$ solution and 10% NaOH solution at 20°C for 10 hours to eliminate hemicellulose and expand the cellulose before acetylation reactions.

3.2.2. Acetylation

The process of acetylation is commonly used to modify cellulose under appropriate reaction conditions, either in industrial production of cellulose acetate or in laboratory synthesis. During acetylation, the –OH bonds in cellulose are replaced by ester [–COO] or acetyl (CO) bonds, resulting in increased hydrophobicity compared to the original hydroxyl groups, which can be hydrolyzed with water [52]. The acetylation process replaces the hydroxyl groups with hydrophobic acetyl groups, which enhances the oil adsorption capacity of cellulose adsorbents, making them easier to recover [78]. Table 3 summarizes the oil adsorption capacity and agents used for some natural adsorbents that have been modified through the acetylation reaction.

According to Table 3, the oil adsorption capacity of the adsorbent significantly increased after acetylation, showing an increase from 67.51% to 195.60% compared to before the acetylation process. Notably, a study by [79] found that the acetylation of corn cobs with acetic anhydride in a solvent–free system in the presence of iodine under mild reaction conditions resulted in excellent oil adsorption capacity both before and after modification, with values of 28.2 g/g and 68.8 g/g, respectively. Similarly, [24] reported that the acetylation process modified the surface properties of wheat straw of wheat straw, creating new sites for oil adsorption and storage. This resulted in an increase in oil adsorption capacity by 177.46% to 195.60% compared to the original values. Corn silk was also acetylated by [49] to improve its oil adsorption capacity using acetic anhydride and N–bromosuccinimide as a catalyst, resulting in a maximum weight percentage gain of 11.45% and an increase in oil adsorption capacity from 72.02% to 77.45%. Acetylated flax fibers were synthesized by [28] using a mixture of liquid acetylation agents and observed an increase in oil adsorption capacity from 13.25 g/g to 17.42 g/g and 24.54 g/g after microwave treatment and acetylation modification, respectively. Finally, [37] found that acetylated sugarcane bagasse had a higher affinity for oil than raw sugarcane bagasse and that acetylation could increase the oil adsorption capacity in salty water by approximately 88.33%.

The disadvantage of acetylation method by acetic anhydride that it produces acetic acid as a byproduct. Acetic acid causes residual odor, loss of material durability due to acid hydrolysis of hemicellulose, and metal corrosion [13].

Table 3. The agents used and oil adsorption capacity of some natural adsorbents modified by acetylation reaction.

Adsorbent	Agent	Oils	Adsorption capacity before modification	Adsorption capacity after modification	The adsorption efficiency increased	Ref.
Bagasse	The process of acetylation with acetic anhydride as a	Crude oil	6 g/g	11.3 g/g	88.33 %	[37]

Adsorbent	Agent	Oils	Adsorption capacity before modification	Adsorption capacity after modification	The adsorption efficiency increased	Ref.
	reactant and NBS as a catalyst is carried out under mild conditions					
		Crude oil	5.4 g/g	9.1 g/g	68.52 %	[37]
Cocoa pods (natural fiber)	Acetylation with acetic anhydride and (1 % of the solvent) N–bromosuccinimide (NBS) as a catalyst	Crude oil	3.97 g/g	6.65 g/g	67.51 %	[80]
Corn Cobs	Acetylation with iodine and acetic anhydride	Oil spill	28.2 g/g	68.8 g/g	143.97 %	[79]
Corn silk fiber	The catalyst used for the acetylation reaction was NBS, which was added at a concentration of 1–3% by weight of the sorbent. Acetic anhydride was used in a solid–to–liquid ratio of 1 g/30 mL.	Tapis crude oil	8.15 g/g	14.02 g/g	72.02 %	[81]
		Arabian crude oil	9.4 g/g	16.68 g/g	77.45 %	[49]
Flax fiber	A blend of 200 mL methylbenzene, 100 mL ethanoic anhydride, and 3 mL perchloric acid as a catalyst for acetylation	Motor oil	13.25 g/g	24.54 g/g	85.21 %	[28]
Oil palm empty fruit bunch (natural fiber)	Acetylation with acetic anhydride and (1 % of the solvent) N–bromosuccinimide (NBS) as a catalyst	Crude oil	3.04 g/g	6.48 g/g	113.16 %	[80]
Peat moss	Acetylation with acetic acid	Oil spill	–	7.6 – 8 g/g	–	[82]
Rice Husks	Acetylation in a solvent free system using NBS	Crude oil	–	10.31 g/g	–	[83]
Sugarcane bagasse	Under mild conditions and without the use of a solvent, an acetylation reaction be carried out with acetic anhydride as the reactant and N–bromosuccinimide as the catalyst	Machine oil	–	18.8 g/g	–	[84]
Wheat straw	Acetic anhydride as an acetylation reagent and NBS as a catalyst	Diesel oil	8.19 ± 0.47 g/g	24.21± 0.76 g/g	195.60 %	[24]
		Diesel oil slick	7.83 ± 1.14 g/g	22.39 ± 0.77 g/g	185.95 %	[24]
		Corn oil	9.23 ± 1.34 g/g	25.61 ± 2.13 g/g	177.46 %	[24]
		Corn oil slick	8.68 ± 1.23 g/g	24.73 ± 1.19 g/g	184.91 %	[24]

3.2.3. Grafting

The process of grafting is a straightforward and efficient approach to modify natural fibers for better oil adsorption by introducing oil–friendly groups onto the fibers, which

increases their hydrophobicity [52]. Various reactions, including silylation, etherification, and esterification, can be used for grafting [38]. Esterification grafting, which involves attaching fatty acids onto the adsorbent material's surface, is commonly employed to modify natural oil adsorbents. This section aims to provide a comprehensive description of the esterification grafting method.

a) Esterification

Cellulose esterification is a process of acylation that involves using carboxylic acids as acylating agents, catalyzed by strong acids or activated derivatives like anhydrides or acid chlorides with a base or Lewis acid [85]. The two types of cellulose esterification are chemical esterification [86] and mechanochemical esterification [39]. Chemical esterification of cellulose is often performed using pyridine–acyl chloride or anhydride reactions, which generate hydrochloric acid as a by–product, leading to cellulose degradation and environmental harm [87–88].

According to [89], ionic liquids like EmimOAc could serve as catalysts and reaction media for cellulose hydroxy group esterification. The researchers performed cellulose modification using oleic acid in the TsCl/BmimOAc system through mechanochemical esterification, and a new absorption peak was observed at 1731 cm^{-1} in the Fourier transform infrared spectra, indicating the formation of C=O groups [39]. In another mechanochemical esterification method conducted by [90], cellulose fibers were ground to create microcrystals, and these microcrystalline cellulose particles were then reacted with asymmetric mixed anhydrides (formed from acetic anhydride and oleic acid) in a ball mill. The study found that the ball–milling method was an effective way to modify cellulose powder surfaces with acetic–oleic acid mixtures, and the modified cellulose esters demonstrated improved hydrophobicity and thermal stability when compared to untreated cellulose powder.

Typical fatty acids, including oleic acid, stearic acid, lauric acid, decanoic acid, fatty acid chlorides (oleoyl chloride and octanoate chloride), and N–bromosuccinimide (NBS), can be used as agents for cellulose esterification reactions to enhance oil absorption and hydrophobicity of natural adsorbents [12, 29, 86, 91–94]. Table 4 presents the agents used for cellulose esterification reactions and the oil absorption capacity of the modified adsorbents by esterification reactions.

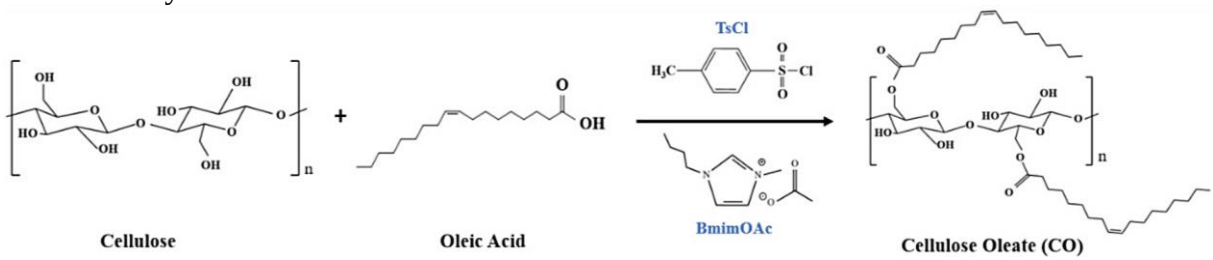

Figure 1. Diagrammatic illustration of the esterification process of cellulose in BmimOAc with oleic acid and TsCl as an activating agent [39].

Table 4. The agents and oil adsorption capacity of the modified adsorbents through esterification reaction.

Adsorbent	Esterifiers	Solvent	Catalyst	Oils	Sorption capacity/ Removal	Ref.
Coconut coir	Fatty acid chloride (oleoyl chloride)	DMaC/LiCl	N–bromosuccinimide (NBS) 1% (v/v)	Engine oil	15.31 g/g	[94]
	Fatty acid chloride (octanoate chloride)	DMaC/LiCl	N–bromosuccinimide (NBS) 1% (v/v)	Engine oil	11.96 g/g	[94]
Coconut husk	Stearic acid	n–hexane	H_2SO_4			[86]

Adsorbent	Esterifiers	Solvent	Catalyst	Oils	Sorption capacity/ Removal	Ref.
Cotton fiber	Stearic acid (C18 fatty acid)	Solvent free system	5.0 g of p–TsCl/ 100 mL of pyridine	Crude oil	35.58 g/g (49 % raw cotton fiber)	[95]
Durial Peel	Stearic acid	n–hexane	H_2SO_4	Diesel oil	0.3780	[29]
Microcrystalline cellulose [MCC] powder	Oleic acid	Solvent free system	TsCl/BmimOAc	–	–	[39]
Pineapple Leaf	Stearic acid	Methanol	Pyridine/p–toluenesulfonyl clorua	Crude oil (100 ppm)	0.108 ± 0.004 g/g	[93]
	Lauric acid	Methanol	Pyridine/p–toluenesulfonyl clorua	Crude oil (100 ppm)	0.138 ± 0.002 g/g	[93]
Sago bark	Stearic acid	Ethyl acetate	CaO	Used engine oil	2.14–2.30 g/g	[96]
Sawdust	Oleic acid	n–hexane	H_2SO_4	Crude oil	6.40	[12]
	Stearic acid	n–hexane	H_2SO_4	Crude oil	5.23	[12]
	Decanoic acid	n–hexane	H_2SO_4	Crude oil	4.23	[12]
Sugarcane bagasse	N–bromosuccinimide used as a catalyst in the acetylation reaction with acetic anhydride	Solvent free system	N–bromosuccinimide (NBS) 1% (v/v)	Machine oil	20.2 g/g	[91]
	Esterification with stearic acid			Engine oil	1.3 – 3.2 g/g	[61]
Grapefruit peel	Stearic acid	n–hexane	H_2SO_4	Diesel oil Lubricating oil	10.93 g/g 10.53 g/g	[92]
	Oleic acid	n–hexane	H_2SO_4	Diesel oil Lubricating oil	11.39 g/g 13.35 g/g	[92]

According to studies by [65, 90], oleic acid, which has a long carbon chain and is hydrophobic, is considered the most suitable agent for cellulose esterification. It has advantages such as flexibility, a wide thermal range, low melting point, easy processing, renewability, and does not produce harmful by–products. Fatty acids with longer carbon chains have better oil absorption capacity. Table 4 shows that [12] found that sawdust modified with oleic acid (6.40 g/g) had higher crude oil absorption capacity than that treated with stearic acid (5.23 g/g) or decanoic acid (4.23 g/g). Similarly, grapefruit peel modified with oleic acid had better absorption capacity for diesel and lubricating oils than that treated with stearic acid [92]. The higher solubility of oleic acid in n–hexane than stearic acid can be a possible explanation for these results. Pineapple leaves modified with stearic acid showed higher oil absorption capacity than lauric acid, which has a shorter carbon chain [93]. In summary, the oil absorption capacity of cellulose modified with fatty acids can be ranked as follows: oleic acid > stearic acid > lauric acid > decanoic acid.

In esterification reactions, powerful acids are typically used as catalysts, with concentrated sulfuric acid being the most used [86, 92]. Other catalysts used include TsCl [96], CaO [96], and N–bromosuccinimide (NBS) 1% (v/v) [94]. The solvent plays a crucial role in dissolving and transforming fatty acids into absorbent materials during esterification reactions. Some of the catalyst/solvent systems used include sulfuric acid/n–hexane [29, 86, 92], TsCl/ethanol [95], CaO/ethyl acetate [96], and N–bromosuccinimide (NBS) 1% (v/v)/DMaC/LiCl [94].

Once the dry adsorbent has undergone pre–treatment, the esterification process can take place. For example, esterifying the –OH group of sawdust with a fatty acid, such as oleic acid, stearic acid, or decanoic acid, or with vegetable oil, such as castor oil or mustard oil. To carry out this process, 1 gram of dry sawdust is mixed with 0.2 grams of the fatty acid or 0.5 grams of vegetable oil in 100 mL of n–hexane, which contains a drop of concentrated H_2SO_4 as a catalyst. The mixture is then refluxed in a Dean–Stark system at a temperature of 65 ± 2°C for 6 hours. After the reaction has occurred, the product is washed with n–hexane multiple times, dried in an oven at 80°C for 24 hours, and then stored for later use. According to equation [1,12], this process will result in the desired reaction.

$$\text{SD-OH} + C_{17}H_{33}\text{-COOH} \xrightarrow[H_2O]{H^+} \text{Cell-OCO}C_{17}H_{33} \quad (1)$$

The process of esterification can be integrated with the carbonization process. Example carbonizing ogbono shell at 600°C for 4 hours [97], coconut husk at 800°C for 6 hours [86], and rice husk and sawdust at 600°C for 8 hours, followed by esterification with stearic acid [98].

Moreover, the esterification process can be accomplished by initially modifying the material with oleic acid, followed by a second modification using leaving group chemistry with a different fatty acid. This process entails replacing the surface hydroxyl group with a p–toluenesulfonyl group, and then covalently bonding a fatty acid on the sawdust surface through high–temperature (55°C) esterification process (Figure 2).

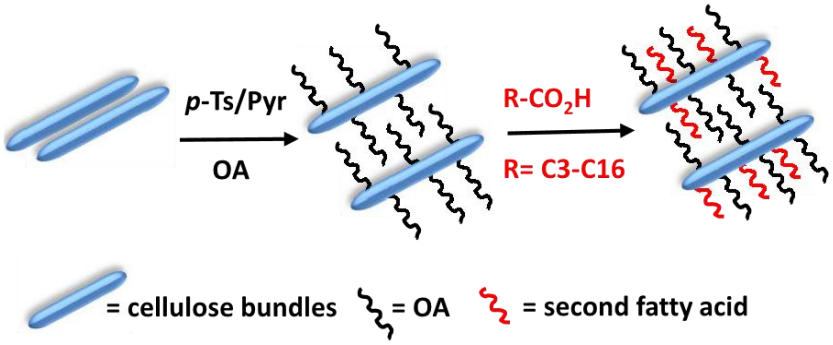

Figure 2. An illustration depicting the hydrophobic modification of cellulose networks in sawdust [99].

Shin prepared a reaction mixture containing p–TsCl and sawdust in pyridine, and added oleic acid while stirring for 6–10 hours at 55–58°C. The resulting material was purified by Soxhlet extraction and vacuum–dried, then modified with different fatty acids at 55°C for 8 hours. Two basic materials (pine/OA–106 and pine/OA–124) were used in the study [99].

b) Other grafting reactions

In the study of [38], they altered cotton fibers by attaching alkyl groups to them. Specifically, the cotton fibers were grafted with silyl ether substituents through solvent–free silylation reactions, replacing dialkyl groups. This conversion transformed the hydroxyl groups on the surface of the cotton into hydrophobic alkylsilyl ether chains. The resulting oil sorption capacity was about 18 g g/g, which was 5 times greater than that of unmodified cotton fibers [38]. In a similar vein, [100], the hydrophobicity of cellulose fibers was increased by grafting them with epoxidized soybean oil through an open–ring polymerization reaction. The modified cellulose film that contained nano ESO polymer particles demonstrated increased smoothness and improved water repellency properties [100]. Meanwhile, [40] utilized corn stalk pith to create a biosorbent with excellent oil sorption and water–repelling properties. They modified the biosorbent by attaching octadecylamine to its structure through a laccase/TEMPO–mediated Schiff–Base reaction (Figure 3). This method

resulted in an increase in oil adsorption capacity from 13.24 g/g to 44.25 g/g, accompanied by a decrease in water adsorption capacity from 15.52 g/g to 2.76 g/g.

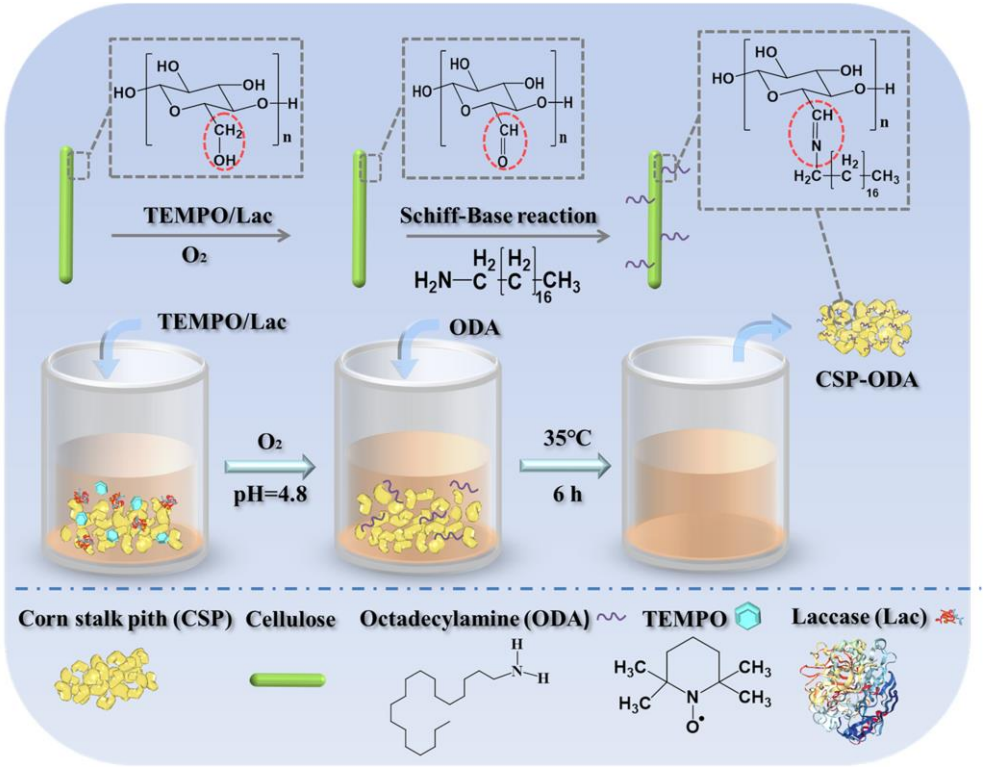

Figure 3. The diagrammatic representation of the steps involved in the surface modification of corn stalk pith [40].

3.2.4. Other chemical modification methods

a) Acidification

Acid treatment is a common form of wet oxidation process used for chemical modification [101]. Typically, acid treatment is used as a preliminary reaction to adjust the processed adsorbent [102], and it involves the use of inorganic acids and other oxidizing agents. The primary goal of acid treatment is to eliminate wax content, increase cellulose hydroxyl groups, and prevent exposure on the surface of the adsorbent [56]. Several chemicals can be used for acid treatment, including dodecylbenzene sulfonic acid [14], and H_2SO_4 [103], which is popularly used to remove wax content and increase the corresponding cellulose hydroxyl groups. Acid treatment has been shown to affect the surface area, surface charge, oil and water affinity, oxygen functional group content, and pore volume, which make it useful for adsorption in wastewater treatment [101].

In study of [4], sawdust was treated with a solution of 0.5 wt.% NaOH and 30% H_2O_2 for 13 hours at room temperature. The pH was then adjusted to 6.5–7.5 by adding drops of 6 mol/L HCl. Acid hydrolysis was employed to decrease the total amount of hydroxyl (–OH) groups in the sawdust, indicating a successful reduction of the alcohol content. On the other hand, [103] performed acid hydrolysis on wheat straw using a 0.045 N H_2SO_4 catalyst with a liquid: solid ratio of 20:l at temperatures ranging from 160–220^oC for 0–50 minutes. The process was conducted in a heated reactor with continuous stirring.

b) Aerogel modification

Aerogel is a highly porous solid material with a porosity of up to 99% and a large surface area of over 100 m^2/g that is well–suited for absorbing oil spills. It can be produced from either inorganic or bio–based materials [104]. Using cellulose as a raw material for aerogel

production has several advantages over chemically sourced aerogels, including biodegradability and lower cost. Recently, [105] developed cellulose–based aerogels with high porosity and low density by using *Eichhornia crassipes* as the cellulose source and polyvinyl alcohol as the crosslinking agent. These aerogels had oil/solvent uptake capacity ranging from 60.33 to 152.21 g/g, superhydrophobicity (water contact angle of 156.7°), and reusability up to 16 times. Sugarcane bagasse aerogels were also produced by using polyvinyl alcohol as the binder and freeze–drying at –70°C. These aerogels had a very low density (0.016–0.112 g/cm^3), high porosity (91.9–98.9%), and low thermal conductivity. They were superhydrophobic and had a high oil absorption capacity after being coated with methyltrimethoxysilane [106]. Pyrolyzed twisted carbon fiber aerogels developed by [107] showed exceptional oil uptake capacity up to 192 times their own weight and could be reused multiple times without a reduction in absorption capacity.

Nanocellulose–based aerogels are highly porous, lightweight materials that have excellent absorption capacity [108]. Nanocellulose is composed of cellulose nanofibers, nanocrystals, and nanoparticles, which can be isolated using various techniques [109]. The properties of nanocellulose depend on the isolation technique, precursor material, and surface modifications [110]. Researchers often modify the surface of nanocellulose to enhance its properties [111]. In one study, researchers developed aerogels using modified nano–crystalline cellulose (CNC) with 3–triethoxysilyl propyl isocyanate (TEPIC) for oil absorption. The aerogels had a porous structure, low density, small pore diameter, and high specific surface area. All TEPIC–modified CNC aerogels exhibited hydrophobicity, with a water contact angle greater than 130°. The sample modified with 3% TEPIC had the highest absorption capacity for motor oil at 130 ± 7.22 g/g [112]. Another study created a hydrophobic/hydrophilic nanostructured aerogel absorbent by functionalizing cellulose fibers with low surface energy moieties, dissolving and cross–linking the product in an organic solvent, and freeze–drying it. The resulting aerogel had a high oil absorption capacity, comparable to most synthetic oil sorbents [113]. The aerogels had ultralow density, high porosity, and extremely good absorption capabilities for numerous oils and solvents, with selectivity in absorbing marine diesel oil. They were much more effective than commercial absorbent materials and maintained a high absorption capacity for at least 30 cycles, indicating their potential for remediation of oil and chemical spills [114]. A recent study on modification of cellulose and nanocellulose–based aerogels for oil treatment is presented in Table 5.

Table 5. The synthesis of the oil adsorption results of some nanocellulose–based aerogel modifications.

Aerogel composites	Preparation Method	Density	Porosity	Cycle	Water Contact Angle	Absorption Capacity	Ref.
Cellulose–based aerogels from waste biomass (*Eichhornia crassipes*)	Freeze–drying and crosslinking	6.5 mg/cm^3	99.56 %	16	156.7°	60.33 – 152.21 g/g	[105]
Sugarcane bagasse aerogels	Freeze–drying at –70 °C	16 – 112 mg/cm^3	91.9–98.9 %	–	142.2 – 150.05°	25 g/g (Crude oil)	[106]
Cellulose nanofiber (CNF)	Freeze drying and modified via chemical vapor deposition (CVD) of hexadecyltrimethoxylan (HDTMS)	11 – 17.5 mg/cm^3	98.8 – 99.3 %	–	> 90°	78.8 g/g (Motor oil)	[115]
Macroporous cellulose aerogel via dissolving–	Sol–gel and freeze–drying techniques	–	–	80 cycles	154°	~ 25 g/g (Diesel oil)	[116]

Aerogel composites	Preparation Method	Density	Porosity	Cycle	Water Contact Angle	Absorption Capacity	Ref.
regenerating raw cotton fiber							
Hybrid coffee–cellulose aerogels from spent coffee grounds	Freeze drying and surface modification	45.8 – 79.7 mg/cm^3	92.1 – 95.5 %	–	124.7 – 139.1°	16 g/g (Motor oil)	[117]
Nano–crystalline cellulose (CNC)		–	–	–	> 130°	130 ± 7.22 g/g (Motor oil)	[112]
Cotton cellulose–based aerogel	Dissolution, cross–linking and freeze–drying	–	–	–	134.7 – 138.7°	40.7 g/g (Crude oil – Balal field oil) 57.0 g/g (Crude oil – Soroush field oil) 47.3 g/g (Crude oil – Azadegan field oil)	[113]
Waste cellulose fibers (Recycled box board and recycled milk–container board)	Freeze–drying	2.9 mg/cm^3	99.81 %	Adsorpticapacity about 71.4 – 81.0 % after 30 cycles	159.0°	42.9 g/g (Marine diesel oil)	[114]
Wool waste fiber aerogel	Direct freeze–drying	4 – 23 mg/cm^3	97.73 – 99.63 %		138.0°	136.2 g/g	[118]
Kapok/microfibrillated cellulose (MFC) aerogels	Simple vacuum freeze–drying and surface modification	5.1 mg/cm^3	99.58 %	–	140.1°	104 – 190.1 g/g	[119]
Kapok/microfibrillated cellulose (MFC) aerogels	Hydrophobic modification and freeze–drying	4.9 mg/cm^3	–	–	147.6°	141.9 g/g [Crude oil]	[120]
Natural cellulose aerogel from rice straw	Freeze–drying	2.2 – 24 mg/cm^3	98.4 – 99.8 %	–	151 ± 7°	170.0 g/g [Crude oil]	[121]

Table 5 displays various cellulose or nanocellulose–based aerogel absorbents derived from natural materials like sugarcane bagasse, cotton fiber, coffee grounds, kapok fiber, and rice straw. Aerogels are modified using techniques like freeze–drying, cross–linking, sol–gel, surface modification, and hydrophobic modification. The aerogels typically have low densities, ranging from 2.2 to 79.7 mg/cm^3, with some examples including natural cellulose aerogel from rice straw (2.2 mg/m^3) [121], waste cellulose fibers from recycled box board and recycled milk–container board (2.9 mg/cm^3) [114], cellulose–based aerogels from waste biomass (*Eichhornia crassipes*) (6.5 mg/cm^3) [105], and kapok/microfibrillated cellulose (MFC) aerogels (4.9–5.1 mg/cm^3) [119–120]. The porosity of modified aerogels ranges from 91.9–99.81 %, with some of the highest porosity aerogels listed as cellulose–based aerogels from waste biomass (*Eichhornia crassipes*) (99.56%) [105], cellulose nanofiber (CNF) (99.3 %) [115], wool waste fiber aerogel (99.63%) [118] and natural cellulose aerogel from rice straw (99.8 %) [121]. Additionally, modified aerogels have high water repellency, with water contact angles ranging from 130° to 159°, and excellent oil absorption capabilities, with the

highest oil absorption capacity up to 170.0 g/g [121] and the average absorption capacity of aerogels listed in Table 5 being about 76.8–80.5 g/g.

c) Cationic surfactant

The natural materials are treated with surfactants to remove oil from water, such as wheat straw [123] and barley straw [122]. The addition of cationic surfactants results in an attraction between the surfactant and the positively charged adsorption sites on the adsorbent's surface [124]. One such surfactant, hexadecylpyridinium chloride monohydrate (CPC), has a 16–carbon chain tail attached to a pyridine head group with a permanent +1 charge. Barley straw was treated with sodium hydroxide solution to enhance the formation of carboxyl groups responsible for binding activities before being modified with CPC to enhance its oil adsorption capacity [125]. The Langmuir isotherm showed that the maximum adsorption capacity for standard mineral oil at 25°C was 584.2 mg/g. Desorption experiments in aqueous solution demonstrated that the adsorbent had a strong oil binding affinity, with only 1–2% desorption in 24 hours [122].

3.3. Bioremediation

The immobilization of microorganisms is a commonly used and effective method for biological treatment [126–127] due to its many advantages, including its low cost, simplicity, and minimal effect on microbial activity [128–129]. Compared to free–floating bacteria, immobilized bacteria can avoid unfavorable conditions in the environment, such as predators, native microorganisms, and toxic compounds [130]. Moreover, in an open water system, immobilization also helps to prevent the loss of bacteria due to being washed away [131].

In study of [41], they immobilized bacterial cells from the Vibrio and Acinetobacter genera on cotton fiber surfaces. Both immobilized and planktonic bacteria exhibited a degradation ability of over 60% for saturated hydrocarbons in crude oil, over a pH range of 5.6 to 8.6 and a NaCl concentration of up to 70 g/L. The degradation efficiency of immobilized bacterial cells was found to be approximately 30% higher than that of the planktonic cells. The effectiveness of the MPD–M bacterial group immobilized on polypropylene fibers in treating crude oil at different salinity levels was also demonstrated by [132]. In an experiment of [133], corn stalk pads were supplemented with different amounts of bacteria (1, 3, and 5 mL) and exposed to crude oil for 4 hours at 25 ± 1°C, resulting in higher oil adsorption efficiency compared to a control sample without bacteria. The chemical properties of the hydrocarbon compounds, environmental conditions, and bacterial species influence the biodegradation of oil components, while oxygen molecules are essential for the process. In addition, [134] suggests that providing fertilization with nitrogen and organic phosphorus can significantly boost the growth of hydrocarbon–degrading bacteria. Fertilization with nitrogen and organic phosphorus can significantly enhance the growth of hydrocarbon–degrading bacteria. *Pseudomonas*, *Achromobacter*, *Arthrobacter*, *Micrococcus*, *Nocardia*, *Vibrio*, *Acinetobacter*, *Brevibacterium*, *Corynebacterium*, *Flavobacterium*, *Candida*, *Rhodotorula*, and *Sporobolomyces* are among the important bacterial communities involved in crude oil biodegradation in marine environments [135].

Additionally, it is possible to modify an oil sorbent material by treating it with cellulase solution. To create an oil sorbent material from corn stalk, the raw material is treated in cellulase solution at various temperatures (40 – 60°C) and enzyme loadings (50–200 U/g) for 6 hours. This treatment method reduces the amount of hydrophilic cellulose in the corn stalk and increases its specific surface area. Compared to chemical methods, using cellulase to modify corn stalk is more effective, uses fewer hazardous chemicals, and has the potential to replace non–biodegradable oil sorbents. In systems with only oil, the cellulase–treated corn stalk has sorption capacities of 18.47 g/g for vegetable oil, 16.15 g/g for diesel oil, and 27.23 g/g for crude oil. In systems with crude oil and water, the sorption capacity is 24.98 g/g [21].

The advantages, disadvantages, and limitations of 03 methods in the article are summarized in Table 6.

Table 6. The advantages, disadvantages, and limitations of 03 methods in the article: Chemical modification method, Physical modification methods and Bioremediation.

Method	Advantages	Disadvantages and limitations
Chemical modification method	– High modification efficiency	– May require toxic or hazardous reagents that can cause environmental problems
	– Chemical modification can alter surface properties	– Limited stability in harsh environments, making it difficult to use for long–term remediation
	– Can modify a wide range of materials	– Expensive and time–consuming
Physical modification methods	– Simple and cost–effective	– Limited effectiveness for removing complex pollutants
	– Can use natural or recycled materials	– Modification process may be slow and require long–term maintenance
	– Can modify the physical and chemical properties of adsorbents	– Limited modification capacity for some materials
Bioremediation	– Can use natural, eco–friendly methods	– May require specialized expertise and equipment
	– Can be used for in situ remediation	– Limited effectiveness for removing persistent pollutants
	– Can potentially degrade pollutants into harmless byproducts	– May take a long time to achieve desired results

4. Conclusions

4.1. Conclusions

Lignocellulosic biomass is attracting the attention of researchers because it is a renewable and environmentally friendly natural source. However, the natural material has limitations such as buoyancy and hydrophilic properties due to the existence of hydroxyl groups on the material surface, which can affect its effectiveness and oil absorption in water environment. Substituting hydroxyl groups through chemical reactions can make the water affinity surface of cellulose more hydrophobic. This study presented different methods to enhance the hydrophobic and buoyancy properties of materials, including (1) Physical transformation methods such as mechanical crushing or pressing, heat treatment, and the plasma technique; (2) Chemical modification methods such as mercerization, acetylation, grafting, acidification, aerogel modification, cationic surfactant; and (3) Bioremediation (immobilization of microorganisms). Each method has its own advantages and disadvantages, and selecting the appropriate modifying agent requires considering the characteristics of pollutants and the modification process conditions. Physical and chemical methods are often considered as pre–treatment methods to enhance the potential of functional groups and increase the cellulose content. However, direct chemical modification methods using acetylation or esterification have some drawbacks, including residual odor, material durability loss, cellulose degradation, and environmental harm. Meanwhile, cellulose–based aerogels have high oil absorption capacity that can be up to 170.0 g/g, superhydrophobicity, and potential for reuse more than 80 times. Using cellulase or immobilized microorganisms can also reduce the use of harmful chemicals and replace non–biodegradable oil absorbents.

Some naturally derived adsorbent materials also have high adsorption capacity, but they are not readily available in Vietnam, such as *Calotropis procera* fiber, Kapok fiber, and Silkworm cocoon waste.

4.2. Recommendation for future work

Experimental research in the laboratory will focus on modifying materials from agricultural waste that have not undergone high–level transformation using aerogel and bioremediation methods. The final adsorbent product will be in the form of compressed pellets or freeze–dried aerogel to be suitable for practical conditions.

Author contribution statement: Defining and developing the research idea and research framework: T.V.N.; Collecting data and literature, data analysis and synthesis: T.T.N., N.D.L.; Drafting the manuscript: T.T.N.; Manuscript editing and revision: T.V.N.

Acknowledgements: We would like to express our sincere gratitude to HUTECH University for their support in our scientific research project, as well as to Ho Chi Minh City University of Food Industry for providing us with an excellent education and training as a research student here. Finally, we would like to thank the AKIHIKO IKAI Family Scholarship Fund for providing us with financial support to carry out this project.

Competing interest statement: The authors declare that this article was the work of the authors, has not been published elsewhere, has not been copied from previous research; there was no conflict of interest within the author group.

References

1. Kolokoussis, P.; Karathanassi, V. Oil spill detection and mapping using sentinel 2 imagery. *J. Mar. Sci. Eng.* **2018**, *6(1)*, 1–12. doi: 10.3390/jmse6010004.
2. Wardley–Smith, J. The control of oil pollution. Graham and Trotman Publication, London, UK. 1983.
3. Zamparas, M.; Tzivras, D.; Dracopoulos, V.; Ioannides, T. Application of sorbents for oil spill cleanup focusing on natural–based modified materials: A review. *Molecules.* **2020**, *25*, 4522. doi: 10.3390/molecules25194522.
4. Alaa El–Din, G.; Amer, A.A.; Malsh, G.; Hussein, M. Study on the use of banana peels for oil spill removal. *Alexandria Eng. J.* **2018**, *57(3)*, 2061–2068. doi: 10.1016/j.aej.2017.05.020.
5. Gheorghiu, A.D.; Torok, Z.; Ozunu, A.; Antonioni, G.; Cozzani, V. Natech risk analysis in the context of land use planning. Case study: Petroleum products storage tank farm next to a residential area. *Chem. Eng. Trans*. **2014**, *36*, 439–444. doi: 10.3303/CET1436074.
6. Nurul, I.H.; Nor, A.A.W.; Norain, I.; Rozan, B. Sorption equilibrium and kinetics of oil from aqueous solution using banana pseudostem fibers. International Conference on Environment and Industrial Innovation. **2011**, *12*, 177–181. doi: 10.1016/j.jhazmat.2008.01.098.
7. El–Nafaty, U.A.; Muhammad, I.M.; Abdulsalam, S. Biosorption and kinetics studies on oil removal from produced water using banana peel. *Civ. Environ. Res.* **2013**, *3(7)*, 125–136.
8. Idris, J.; Eyu, G.D.; Mansor, A.M.; Ahmad, Z.; Chukwuekezie, C.S. A preliminary study of biodegradable waste as sorbent material for oil–spill cleanup. *Sci. World J.* **2014**, 5, 638–687. doi: 10.1155/2014/638687.
9. Lim, T.; Huang, X. Evaluation of kapok (*Ceiba pentandra (L.) Gaertn.*) as a natural hollow hydrophobic–oleophilic fibrous sorbent for oil spill cleanup. *Chemosphere*. **2007**, *66(5)*, 955–963. doi: 10.1016/j.chemosphere.2006.05.062.
10. Warr, L.N.; Perdrial, J.N.; Lett, M.C.; Heinrich–Salmeron, A.; Khodja, M. Clay

mineral–enhanced bioremediation of marine oil pollution. *Appl. Clay Sci*. **2009**, *46(4)*, 337–345. doi: 10.1016/j.clay.2009.09.012.

11. Gerald, D.; Herve, C.; Marie–Elisabeth, B.; Christophe, B.; Christian, V. Oil removal from water by selective sorption on hydrophobic cotton fibers. 1. study of sorption properties and comparison with other cotton fiber–based sorbents. *Environ. Sci. Technol.* **2003**, *37*, 1013–1015. doi: 10.1021/es020061s.
12. Banerjee, S., Joshi, M.V., Jayaram, R.V. Treatment of oil spill by sorption technique using fatty acid grafted sawdust. *Chemosphere* **2006**, *64*, 1026–1031. doi: 10.1016/j.chemosphere.2006.01.065.
13. Sun, X.F.; Sun, S.; Sun, J.X. Acetylation of rice straw with or without catalysts and its characterization as a natural sorbent in oil spill cleanup. *J. Agric. Food Chem*. **2002**, *50(22)*, 6428–6433. doi: 10.1021/jf020392o.
14. Sayed, S.A.; Zayed, A.M. Investigation of the effectiveness of some adsorbent materials in oil spill clean–ups. *Desalination* **2006**, *194(1–3)*, 90–100. doi: 10.1016/S0011-9164(01)00375-7.
15. Srinivasan, A.; Viraraghavan, T. Removal of oil by walnut shell media. *Bioresour. Technol.* **2008**, *99*, 8214–8220. doi: 10.1016/j.biortech.2008.03.072.
16. Hussein, M.; Amer, A.A.; Sawsan, I.I. Oil spill sorption using carbonized pith bagasse. Application of carbonized pith bagasse as loose fiber. *Global NEST J*. **2009**, *11(4)*, 440–448.
17. Ibrahim, S.; Wang, S.; Ang, H. Removal of emulsified oil from oily wastewater using agricultural waste barley straw. *Biochem. Eng. J*. **2010**, *49*, 78–83. doi: 10.1016/j.bej.2009.11.013.
18. Sathasivam, K.; Haris, M.R.H.M. Adsorption kinetics and capacity of fatty acid–modified banana trunk fibers for oil in water. *Water Air Soil Pollut*. **2010**, *213*, 413–423. doi: 10.1007/s11270-010-0395-z.
19. Uzoije, A.P.; Onunkwo, A.A.; Egwuonwu, C.C. Crude oil sorption onto groundnut shell activated carbon: kinetic and isotherm studies research. *Res. J. Environ. Earth Sci*. **2011**, *3(5)*, 555–563. doi: 10.13140/RG.2.2.23418.95680.
20. Vlaev, L.; Petkov, P.; Dimitrov, A.; Genieva, S. Cleanup of water polluted with crude oil or diesel fuel using rice husks ash. *J. Taiwan Inst. Chem. Eng*. **2011**, *42(6)*, 957–964. doi: 10.1016/j.jtice.2011.04.004.
21. Peng, D.; Lan, Z.; Guo, C.; Yang, C.; Dang, Z. Application of cellulase for the modification of corn stalk: Leading to oil sorption. *Bioresour. Technol*. **2013**, *137*, 414–418. doi: 10.1016/j.biortech.2013.03.178.
22. Nwadiogbu, J.O.; Ajiwe, V.I.E.; Okoye, P.A.C. Removal of crude oil from aqueous medium by sorption on hydrophobic corncobs: Equilibrium and kinetic studies. *J. Taibah Univ. Sci.* **2016**, *10*, 56–63. doi: 10.1016/j.jtusci.2015.03.014.
23. Tontiwachwuthikul, P.; Zubaidi, I.A.; Rennie, E.; Schubert, S.; Seitz, Cassandra, M.; Selinger, S. Remediation of water from waste lubrication oil spill using potato peels. Proceedings of the 3rd International Conference on Fluid Flow, Heat and Mass Transfer (Ottawa, Canada). **2016**, pp. 163. doi: 10.11159/ffhmt16.163.
24. Lv, E.; Xia, W.; Tang, M.; Pu, Y. Preparation of an efficient oil–spill adsorbent based on wheat straw. *BioRes*. **2017**, *12(1)*, 296–315. doi: 10.15376/biores.12.1.296-315.
25. Olufemi, B.A.; Otolorin, F. Comparative adsorption of crude oil using mango (mangnifera indica) shell and mango shell activated carbon. *Environ. Eng. Res*. **2017**, 1–26. doi: 10.4491/eer.2017.011.
26. Odoh, R.; Yebpella, G.G.; Archibong, C.S. Analysis of crude oil removal from the environment using activated carbon produced from rice husks. *Int. Arch. App. Sci. Technol*. **2018**, *9(2)*, 27–35. doi: 10.15515/iaast.0976-4828.9.2.2735.
27. Alsulaili, A.D.; Fahim, A.M. Oil removal from produced water by agriculture waste

adsorbents. *Int. J. Environ. Waste Manage*. **2019**, *25(1),* 12–31. doi: 10.1504/IJEWM.2020.104345.
28. Mahmoud, M.A. Oil spill cleanup by raw flax fiber: Modification effect, sorption isotherm, kinetics and thermodynamics. *Arabian J. Chem*. **2020**, *13(6)*, 5553–5563. doi: 10.1016/j.arabjc.2020.02.014.
29. Nam, T.V.; Nguyen, T.T.; Dung, D.N.; Phuong, P.T.H. Esterified durian peel adsorbents with stearic acid for spill removal. *Chem. Eng. Trans*. **2020**, *78*, 271–276. doi: 10.3303/CET2078046.
30. Ukpong, A. Mathematical and kinetic modelling of the adsorption of crude oil spill using coconut coir activated carbon. *J. Energy Environ. Chem. Eng*. **2021**, *6(1)*, 1–9. doi: 10.11648/j.jeece.20210601.11.
31. Maleki, H. Recent advances in aerogels for environmental remediation applications: a review. *Chem. Eng. J.* **2016**, *300*, 98–118. doi: 10.1016/j.cej.2016.04.098.
32. Kizil, S.; Sonmez, H.B. Oil loving hydrophobic gels made from glycerol propoxylate: Efficient and reusable sorbents for oil spill clean–up. *J. Environ. Manag*. **2017**, *196*, 330–339. doi: 10.1016/j.jenvman.2017.02.016.
33. Anuzyte, E.; Vaisis, V. Natural oil sorbents modification methods for hydrophobicity improvement. *Energy Procedia* **2018**, *147*, 295–300. doi: 10.1016/j.egypro.2018.07.095.
34. Angelova, D.; Uzunov, I.; Uzunova, S.; Gigova, A.; Minchev, L. Kinetics of oil and oil products adsorption by carbonized rice husks. *Chem. Eng. J.* **2011**, *172*, 306–311. doi: 10.1016/j.cej.2011.05.114.
35. Rengasamy, R.S.; Das, D.; Karan, C.P. Study of oil sorption behavior of filled and structured fiber assemblies made from polypropylene, kapok and milkweed fibers. *J. Hazard. Mater.* **2011**, *186*, 526–532. doi: 10.1016/j.jhazmat.2010.11.031.
36. Anjos, R.B.; Hilário, L.S.; Juviniano, H.B.M.; Silva, D.R. Crude oil removal using *Calotropis procera*. *BioRes*. **2020**, *15(3),* 5246–5263. doi: 10.15376/biores.15.3.5246-5263.
37. Behnood, R.; Anvaripour, B.; Fard, N.J.H.; Farasati, M. Crude oil layer sorption from saline water surface by raw and acetylated sugarcane bagasse. *Sci. Int. (Lahore)*. **2014**, *26(3)*, 1157–1161.
38. Jarrah, K.; Hisaindee, S.; Al–Sayah, M.H. Preparation of oil sorbents by solvent–free grafting of cellulose cotton fibers. *Cellulose* **2018**, *25*, 4093–4106. doi: 10.1007/s10570-018-1846-8.
39. Lease, J.; Kawano, T.; Andou, Y. Esterification of cellulose with long fatty acid chain through mechanochemical method. *Polymers* **2021**, *13*, 4397. doi: 10.3390/polym13244397.
40. Peng, D.; Li, H.; JieLia, W.; Zheng, L. Biosorbent with superhydrophobicity and superoleophilicity for spilled oil removal. *Ecotoxicol. Environ. Saf.* **2021**, *209*, 111803. doi: 10.1016/j.ecoenv.2020.111803.
41. Lin, M.; Liu, Y.; Chen, W.; Wang, H., Hu, X. Use of bacteria–immobilized cotton fibers to absorb and degrade crude oil. *Int. Biodeterior. Biodegrad.* **2014**, *88*, 8–12. https://doi.org/10.1016/j.ibiod.2013.11.015.
42. Stamm, A.J. Wood and cellulose. Science Ronald Press Co, New York, NY, USA. 1964.
43. Joseph, B.; Sagarika, V.K.; Sabu, C.; Kalarikkal, N.; Thomas, S. Cellulose nanocomposites: Fabrication and biomedical applications. *J. Bioresour. Bioprod*. **2020**, *5*, 223–237. doi: 10.1016/j.jobab.2020.10.001.
44. Wu, Q.; Henriksson, M.; Liu, X.; Berglund, L.A. *Biomacromolecules* **2007**, *8*, 3687.
45. Aqsha, A.; Tijani, M.M.; Mahinpey, N. Catalytic pyrolysis of straw biomasses (wheat, flax, oat and barley straw) and the comparison of their product yields. *WIT*

Trans. Ecol. Environ. **2014**, *190*, 1007–1015. doi: 10.2495/EQ140942.
46. Al–Jammal, N.; Juzsakova, T. Review on the effectiveness of adsorbent materials in oil spills clean up. Proceeding of the 7th International Conference of ICEEE (Budapest, Hungary). 2016.
47. Wang, Y.; Zheng, A. Effect of kapok fiber treated with various solvents on oil absorbency. *Ind. Crops Prod.* **2012**, *40*, 178–184. doi: 10.1016/j.indcrop.2012.03.002.
48. Gupta, S.; Tai, N.H. Carbon materials as oil sorbents: a review on the synthesis and performance. *J. Mater. Chem*. **2016**, *4*, 1550–1565. doi: 10.1039/C5TA08321D.
49. Asadpour, R.; Sapari, N.B.; Tuan, Z.Z.; Jusoh, H.; Riahi, A.; Orji. K.U. Application of sorbent materials in oil spill management: A review. *Caspian J. Appl. Sci. Res*. **2013**, *2(2)*, 46–58.
50. Huang, X.; Lim, T.T. Performance and mechanism of a hydrophobic–oleophilic kapok filter for oil/water separation. *Desalination* **2006**, *190*, 295–307. doi: 10.1016/j.desal.2005.09.009.
51. Minh, Q.C.; Truong, T.T.; Anh, T.H.; Hieu, T.L. Oil spill cleanup by raw cellulose–based absorbents: a green and sus–tainable approach. *Energ. Source Part A.* **2021**, 1–14. doi: 10.1080/15567036.2021.1928798.
52. Tan, J.Y.; Low, S.Y.; Ban, Z.H.; Siwayanan, P. A review on oil spill clean–up using bio–sorbent materials with special emphasis on utilization of kenaf core fibers. *BioResources*. **2021**, *16(4)*, 8394–8416. doi: 10.15376/biores.16.4.Tan.
53. Bajwa, D.S.; Sitz, E.D.; Bajwa, S.G.; Barnick, A.R. Evaluation of cattail (*Typha spp.*) for manufacturing composite panel. *Ind. Crops. Prod*. **2015**, *75*, 195–199. doi: 10.1016/j.indcrop.2015.06.029.
54. Nordin, N.I.; Ariffin, H.; Andou, Y.; Hassan, M.A.; Shirai, Y.; Nishida, H.; Ibrahim, N.A. Modification of oil palm mesocarp fiber characteristics using superheated steam treatment. *Molecules* **2013**, *18(8)*, 9132–9146. doi: 10.3390/molecules18089132.
55. Tu, L.; Duan, W.; Xiao, W.; Fu, C.; Wang, A.; Zheng, Y. Calotropis gigantean fiber derived carbon fiber enables fast and efficient absorption of oils and organic solvents. *Sep. Purif. Technol.* **2018**, 192, 30–35. doi: 10.1016/j.seppur.2017.10.005.
56. Wahi, R.; Chuah, L.A.; Choong, T.S.Y.; Ngaini, Z.; Nourouzi, M.M. Oil removal from aqueous state by natural fibrous sorbent: An overview. *Sep. Purif. Technol.* **2013**, *113*, 51–63. doi: 10.1016/j.seppur.2013.04.015.
57. Husseien, M.; Amer, A.A.; El–maghraby, A. Experimental investigation of thermal modification influence on sorption qualities of barley straw. *J. Appl. Sci. Res.* **2008**, *4(6)*, 652–657.
58. Hilário, L.S.; Anjos, R.P.D.; Juviniano, H.B.D.M.; Silva, D.R.D.S. Evaluation of thermally treated calotropis procera fiber for the removal of crude oil on the water surface. *Materials*. **2019**, *12*, 3894. doi: 10.3390/ma12233894.
59. Khan, E.; Virojnagud, W.; Ratpukdi, T. Use of biomass sorbents for oil removal from gas station runoff. *Chemosphere* **2014**, *57(7)*, 681–689. doi: 10.1016/j.chemosphere.2004.06.028.
60. Ali, N.; El–harbawi, M.; Jabal, A.A.; Yin, C. Characteristics and oil sorption effectiveness of kapok fibre, sugarcane bagasse and rice husks: oil removal suitability matrix. *Environ. Technol*. **2012**, *33(4)*, 481–486. doi: 10.1080/09593330.2011.579185.
61. Said, A.E.A.S.; Ludwick, A.G.; Aglan, H.A. Usefulness of raw bagasse for oil absorption: a comparison of raw and acylated bagasse and their components. *Bioresour. Technol*. **2009**, *100(7)*, 2219–2222. doi: 10.1016/j.biortech.2008.09.060.
62. Moriwaki, H.; Kitajima, S.; Kurashima, M.; Hagiwara, A.; Haraguchi, K.; Shirai, K.;

Kanekatsu, R.; Kiguchi, K. Utilization of silkworm cocoon waste as a sorbent for the removal of oil from water. *J. Hazard Mater.* **2009**, *165*, 266–270. doi: 10.1016/j.jhazmat.2008.09.116.

63. Santos, A.L.; Botelho, E.C.; Kostov, K.G.; Ueda, M.; G. da Silva, L.L. Carbon fiber surface modification by plasma treatment for interface adhesion improvements of aerospace composites. *Adv. Mater. Res.* **2016**, *1135*, 75–87. doi: 10.4028/www.scientific.net/AMR.1135.75.
64. Alekseeva, A.A.; Stepanova, S.V. Effect of plasma surface modification of mixed leaf litter on the mechanism of oil film removal from water bodies. *Russ. J. Gen. Chem.* **2019**, *89*, 2763–2768. doi: 10.1134/S107036321913005X.
65. Tursi, A.; Vietro, N.D.; Beneduci, A.; Milella, A.; Chidichimo, F.; Fracassi, F.; Chidichimo, G. Low pressure plasma functionalized cellulose fiber for the remediation of petroleum hydrocarbons polluted water. *J. Hazard. Mater.* **2019**, *373(5)*, 773–782. doi: 10.1016/j.jhazmat.2019.04.022.
66. Mohd Edeerozey, A.M.; Akil, H.M.; Azhar, A.B.; Zainal, A.M.I. Chemical modification of kenaf fibers. *Materials Letters*. **2007**, *61(10)*, 2023–2025. https://doi.org/10.1016/j.matlet.2006.08.006.
67. Kalia, S.; Thakur, K.; Celli, A.; Kiechel, M.A.; Schauer, C.L. Surface modification of plant fibers using environment friendly methods for their application in polymer composites, textile industry and antimicrobial activities: A review. *J. Environ. Chem. Eng.* **2013**, *1*, 97–112. doi: 10.1016/j.jece.2013.04.009.
68. Hokkanen, S.; Bhatnagar, A.; Sillanpaa, M. A review on modification methods to cellulose–based adsorbents to improve adsorption capacity. *Water Res.* **2016**, *91*, 156–173. doi: 10.1016/j.watres.2016.01.008.
69. Kabir, M.M.; Wang, H.; Lau, K.T.; Cardona, F. Chemical treatments on plant–based natural fibre reinforced polymer composites: An overview. *Composites* **2012**, *43*, 2883–2892. doi: 10.1016/j.compositesb.2012.04.053.
70. Bledzki, A.K.; Gassan, J. Composites reinforced with cellulose based fibres. *Prog. Polym. Sci.* **1999**, *24*, 221–274.
71. Kamel, S., El–Sakhawy, M. Using of agriculture residue in removing of oil spill. *Trade Science Inc.* **2011**, *5(2)*, 64–70.
72. Li, X.; Tabil, L.G.; Panigrahi, S. Chemical treatments of natural fiber for use in natural fiber–reinforced composites: a review. *J. Polym. Environ*. **2007**, *15*, 25–33. doi: 10.1007/s10924-006-0042-3.
73. Hasim, M.Y.; Roslan, M.N.; Amin, A.M.; Ahmad, Z.A.M.; Ariffin, S. Mercerization treatment parameter effect on natural fiber reinforced polymer matrix composite: A brief review. *WASET*. **2012**, *6(8)*, 784–790.
74. Ramadevi, P.; Sampathkumar, D.; Srinivasa, C.V.; Bennehalli, B. Effect of alkali treatment on water absorption of single cellulosic abaca fiber. *BioResources* **2012**, *7(3)*, 3515–3524.
75. Abdullah, M.; Muhamad, S.H.A.; Sanusi, S.N.; Jamaludin, S.I.S.J.; Mohamad, N.F.; Rusli, M.A.H.R. Preliminary study of oil removal using hybrid peel waste: musa balbisiana and citrus sinensis. *Appl. Environ. Biol. Sci*. **2016**, *6(8S)*, 59–63.
76. Wong, C.; McGowan, T.; Bajwa, S.G.; Bajwa, D.S. Impact of fiber treatment on the oil absorption characteristics of plant fibers. *BioResources* **2016**, *11(3)*, 6452–6463. doi: 10.15376/biores.11.3.6452–6463.
77. Bazargan, A.; Tan, J.; Hui, C.W.; McKay, G. Utilization of rice husks for the production of oil sorbent materials. *Cellulose* **2014**, *21*, 1679–1688. doi: 10.1007/s10570-014-0203-9.
78. Chen, J.; Xu, J.; Wang, K.; Cao, X.; Sun, R. Cellulose acetate fibers prepared from different raw materials with rapid synthesis method. *Carbohydr. Polym.* **2016**, *137*,

685–692. doi: 10.1016/j.carbpol.2015.11.034.
79. Nwabueze, H.O.; Chiaha, P.N.; Ezekannagha, B.C.; Okoani, O.E. Acetylation of corn cobs using iodine catalyst, for oil spills remediation. *IJES* **2016**, *5(9)*, 53–59.
80. Onwuka, J.C.; Agbaji, E.B.; Ajibola, V.O.; Okibe, F.G. Treatment of crude oil contaminated water with chemically modified natural fiber. *Appl. Water Sci.* **2018**, *8(3)*, 86. doi: 10.1007/s13201-018-0727-5.
81. Asadpour, R.; Sapari, N.B.; Isa, M.H.; Kakooei, S.; Orji, K.U. Acetylation of corn silk and its application for oil sorption. *Fibers Polym.* **2015**, *16(9)*, 1830–1835. doi: 10.1007/s12221-015-4745-8.
82. Rotar, O.V.; Iskrizhitskaya, D.V.; Iskrizhitsky, A.A.; Oreshina, A.A. Cleanup of water surface from oil spills using natural sorbent materials. *Procedia Chem.* **2014**, *10*, 145–150. doi: 10.1016/j.proche.2014.10.025.
83. Thompson, N.E.; Emmanuel, G.C.; Adagadzu, K.J.; Yusuf, N.B. Sorption studies of crude oil on acetylated rice husks. *Arch. Appl. Sci. Res.* **2010**, *2(5)*,142–151.
84. Sun, X.F.; Sun, R.C.; Sun, J.X. A convenient acetylation of sugarcane bagasse using NBS as a catalyst for the preparation of oil sorption–active materials. *J. Mater. Sci.* **2003**, *38*, 3915–3923. doi: 10.1023/A:1026189911651.
85. Heinze, T.; Liebert, T.; Koschella, A. Esterification of polysaccharides. *J. Am. Chem. Soc*. **2006**, *129(7)*, 2195–2196. doi: 10.1021/ja069801d.
86. Asadu, C.O.; Anthony, E.C.; Elijah, O.C.; Ike, I.S.; Onoghwarite, O.E.; Okwudili, U.E. Development of an adsorbent for the remediation of crude oil polluted water using stearic acid grafted coconut husk (*Cocos nucifera*) composite. *Appl. Surf. Sci. Adv.* **2021**, *6*, 100179. doi: 10.1016/j.apsadv.2021.100179.
87. Andou, Y.; Lee, H.S.; Kim, D.; Nagasawa, N.; Nishida, H.; Shirai, Y. Enhancement of compatibility based on vapor–phase–assisted surface polymerization (VASP) method for polymer composites with agricultural wastes. *Compos. Interfaces*. **2014**, *9*, 773–785. doi: 10.1080/15685543.2014.960318.
88. Jebrane, M.; Terziev, N.; Heinmaa, I. Biobased and sustainable alternative route to long–chain cellulose esters. *Biomacromolecules* **2017**, *18*, 498–504. doi: 10.1021/acs.biomac.6b01584.
89. Kakuchi, R.; Ito, R.; Nomura, S.; Abroshan, H.; Ninomiya, K.; Ikai, T.; Maeda, K.; Kim, H.J.; Takahashi, K. A mechanistic insight into the organocatalytic properties of imidazolium–based ionic liquids and a positive co–solvent effect on cellulose modification reactions in an ionic liquid. *RCS Adv.* **2017**, *7*, 9423–9430. doi: 10.1039/C6RA28659C.
90. Huang, L.; Wu, Q.; Wang, Q.; Wolcott, M. One–step activation and surface fatty acylation of cellulose fibers in a solvent–free condition. *ACS Sustainable Chem. Eng.* **2019**, *7(19)*, 15920–15927. doi: 10.1021/acssuschemeng.9b01974.
91. Sun, X.F.; Sun, R.C.; Sun, J.X. Acetylation of sugarcane bagasse using NBS as a catalyst under mild reaction conditions for the production of oil sorption–active materials. *Bioresour. Technol.* **2004**, *95(3)*, 343–350. doi: 10.1016/j.biortech.2004.02.025.
92. Zou, J.; Liu, X.; Chai, W.; Zhang, X.; Li, B.; Wang, Y. Sorption of oil from simulated seawater by fatty acid–modified pomelo peel. *Desalin. Water Treat.* **2015**, *56(4)*, 939–944. doi: 10.1080/19443994.2014.941302.
93. Cheu, S.C.; Kong, H.; Song, S.T., Saman, N., Johari, K., Mat, H. High removal performance of dissolved oil from aqueous solution by sorption process using fatty acid esterified pineapple leaf as novel sorbents. *RSC Adv.* **2016**, *6*, 13710–13722. doi: 10.1039/C5RA22929D.
94. Yusof, N.A.; Mukhair, H.; Malek, E.A.; Mohammad, F. Esterified coconut coir by fatty acid chloride as biosorbent in oil spill removal. *BioResources* **2015**, *10(4)*,

8025–8038. doi: 10.15376/biores.10.4.8025-8038.
95. Shin, Y.; Han, K.S.; Arey, B.W.; Bonheyo, G.T. Cotton fiber–based sorbents for treating crude oil spills. *ACS Omega*. **2020**, *5*, 13894–13901. doi: 10.1021/acsomega.0c01290.
96. Ngaini, Z.; Noh, F.; Wahi, R. Esterified sago waste for engine oil removal in aqueous environment. *Environ. Technol.* **2014**, *35(21–24)*, 2761–2766. doi: 10.1080/09593330.2014.920051.
97. Onwu, D.O.; Ogbodo, O.N.; Ogbodo, N.C.; Chime, T.O.; Udeh, B.C.; Egbuna, S.O.; Onoh, M.I.; Asadu, C.O. Application of esterified ogbono shell activated biomass as an effective adsorbent in the removal of crude oil layer from polluting water surface. *J. Appl. Sci. Environ. Manage.* **2019**, *23(9)*, 1739–1746. doi: 10.4314/jasem.v23i9.20.
98. Maxwell, O.I.; Ngozi, A.E.; Onyebuchukwu, M.G. Kinetic, isotherm and thermodynamics studies of the adsorption of crude oil from surface water using esterified rice husk and saw dust American. *J. Eng. Res.* **2019**, *8(5)*, 324–336.
99. Shin, Y.; Winder, E.M.; Han, K.S.; Lee, H.; Bonheyo, G.T. Enhanced capacities of mixed fatty acid–modified sawdust aggregators for remediation of crude oil spill. *ACS Omega*. **2019**, *4*, 412–420. doi: 10.1021/acsomega.8b02293.
100. Huang, X.; Wang, A.; Xu, X.; Liu, H.; Shang, S. Enhancement of hydrophobic properties of cellulose fibers via grafting with polymeric epoxidized soybean oil. *ACS Sustainable Chem. Eng.* **2016**, *5(2)*, 1619–1627. doi: 10.1021/acssuschemeng.6b02359.
101. Abegunde, S.M.; Idowu, K.S.; Adejuwon, O.M.; Adejolu, T.A. A review on the influence of chemical modification on the performance of adsorbents. *Resour. Environ. Sustainability.* **2020**, *1*, 100001. doi: 10.1016/j.resenv.2020.100001.
102. Kamaruzaman, A.M.M.F.M.; Zulkifli, A.A.; Kamis, N.H.M.; Shahar, N.A.M. Oil removal using durian peel wastes: effect of adsorbent condition. *Malays. J. Ind. Technol*. **2016**, *1(1)*, 56–61.
103. Sidiras, D.; Konstantinou, I. A new oil spill adsorbent from sulfuric acid modified wheat straw. *Latest Trends Environ. Manuf. Eng.* **2012**, *132(6)*, 132–137.
104. Doshi, B.; Sillanpaa, M.; Kalliola, S. A review of bio–based materials for oil spill treatment. *Water Res.* **2018**, *135*, 262–277. doi: 10.1016/j.watres.2018.02.034.
105. Yin, T.; Zhang, X.; Liu, X.; Wang, C. Resource recovery of *Eichhornia crassipes* as oil superabsorbent. *Mar. Pollut. Bull*. **2017**, *118(1–2)*, 267–274. doi: 10.1016/j.marpolbul.2017.01.064.
106. Thai, Q.B.; Nguyen, S.T.; Ho, D.K.; Tran, T.D.; Huynh, D.M.; Do, N.H.N.; Duong, H.M. Cellulose–based aerogels from sugarcane bagasse for oil spill–cleaning and heat insulation applications. *Carbohydr. Polym*. **2020**, *228*, 115365. doi: 10.1016/j.carbpol.2019.115365.
107. Bi, H.; Yin, Z.; Cao, X.; Xie, X.; Tan, C.; Huang, X.; Zhang, H. Carbon fiber aerogel made from raw cotton: A novel, efficient and recyclable sorbent for oils and organic solvents. *Adv. Mater*. **2013**, *25(41)*, 5916–5921. doi: 10.1002/adma.201302435.
108. Zhao, X.Q.; Wahid, F.; Cui, J.X.; Wang, Y.Y.; Zhong, C. Cellulose–based special wetting materials for oil/water separation: A review. *Int. J. Biol. Macromol*. **2021**, *185*, 890–906. doi: 10.1016/j.ijbiomac.2021.06.167.
109. Qiao, A.; Cui, M.; Huang, R.; Ding, G.; Qi, W.; He, Z.; Klemeš, J.J.; Su, R. Advances in nanocellulose–based materials as adsorbents of heavy metals and dyes. *Carbohydr. Polym*. **2021**, *272*, 118471. doi: 10.1016/j.carbpol.2021.118471.
110. Thomas, B.; Raj, M.C.; Joy, J.; Moores, A.; Drisko, G.L.; Sanchez, C. Nanocellulose, a versatile green platform: From biosources to materials and their applications. *Chem. Rev*. **2018**, *118*, 11575–11625. doi:

10.1021/acs.chemrev.7b00627.

111. Chen, Y.; Zhang, L.; Yang, Y.; Pang, B.; Xu, W.; Duan, G.; Jiang, S.; Zhang, K. Recent progress on nanocellulose aerogels: Preparation, modification, composite fabrication, applications. *Adv. Mater*. **2021**, *33*, 2005569. doi: 10.1002/adma.202005569.
112. Jonoobi, M.; Mekonnen, T.H. Adsorption of oil by 3–(triethoxysilyl) propyl isocyanate–modified cellulose nanocrystals. *Processes*. **2022**, *10(10)*, 2154. doi: 10.3390/pr10102154.
113. Bidgolia, H.; Mortazavia, Y.; Khodadadi, A.A. A functionalized nano–structured cellulosic sorbent aerogel for oil spill cleanup: synthesis and characterization. *J. Hazard. Mater.* **2019**, *366*, 229–239. doi: 10.1016/j.jhazmat.2018.11.084.
114. Laitinen, O.; Suopajärvi, T.; Österberg, M.; Liimatainen, H. Hydrophobic, superabsorbing aerogels from choline chloride–based deep eutectic solvent pretreated and silylated cellulose nanofibrils for selective oil removal. *ACS Appl. Mater. Interfaces*. **2017**, *9(29)*, 25029–25037. doi: 10.1021/acsami.7b06304.
115. Fatemeh, R., Maleksadat, H., Mehdi, J., Qingliang, Y. Development of hydrophobic nanocellulose–based aerogel via chemical vapor deposition for oil separation for water treatment. *Cellulose*. **2018**, 25(8), 4695–4710. doi: 10.1007/s10570-018-1867-3.
116. Wang, J.; Liu, S. Remodeling of raw cotton fiber into flexible, squeezing–resistant macroporous cellulose aerogel with high oil retention capability for oil/water separation. *Sep. Purif. Technol.* **2019**, *211*, 303–310. doi: 10.1016/j.seppur.2019.03.097.
117. Zhang, X.; Kwek, L.P.; Duyen, K.L.; Tan, M.S.; Duong, H.M. Fabrication and properties of hybrid coffee–cellulose aerogels from spent coffee grounds. *Polymers* **2019**, *11*, 1942. doi: 10.3390/polym11121942.
118. Loh, J.W.; Goh, X.Y.; Phuc, T.T.N.; Quoc, B.T.; Ong, Z.Y.; Hai, M.D. Advanced aerogels from wool waste fibers for oil spill cleaning applications. *J. Polym. Environ.* **2021**, *30*, 681–694. doi: 10.1007/s10924-021-02234-y.
119. Zhang, H.; Wang, J.; Xu, G.; Xu, Y.; Wang, F.; Shen, H. Ultralight, hydrophobic, sustainable, cost–effective and floating kapok/microfibrillated cellulose aerogels as speedy and recyclable oil superabsorbents. *J. Hazard. Mater.* **2021**, *406*, 124758. doi: 10.1016/j.jhazmat.2020.124758.
120. Zhang, H.; Zhang, G.; Zhu, H.; Wang, F.; Xu, G.; Shen, H.; Wang, J. Multiscale kapok/cellulose aerogels for oil absorption: The study on structure and oil absorption properties. *Ind. Crops Prod*. **2021**, *171*, 113902. doi: 10.1016/j.indcrop.2021.113902.
121. Dilamian, M.; Noroozi, B. Rice straw agri–waste for water pollutant adsorption: Relevant mesoporous super hydrophobic cellulose aerogel. *Carbohydr. Polym.* **2021**, *251*, 117016. doi: 10.1016/j.carbpol.2020.117016.
122. Ibrahim, S.; Ang, H.M.; Wang, S. Removal of emulsified food and mineral oils from wastewater using surfactant modified barley straw. *Bioresour. Technol*. **2009**, *100*, 5744–5749. doi: 10.1016/j.biortech.2009.06.070.
123. Fanta, G.F.; Abbott, T.P.; Burr, R.C.; Doane, W.M. Ion exchange reactions of quaternary ammonium halides with wheat straw. Preparation of oilabsorbents. *Carbohydr. Polym.* **1987**, *7*, 97–109. doi: 10.1016/0144-8617(87)90052-X.
124. Namasivayam, C.; Sureshkumar, M.V. Removal of chromium (VI) from water and wastewater using surfactant modified coconut coir pith as a biosorbent. *Bioresour. Technol*. **2008**, *99*, 2218–2225. doi: 10.1016/j.biortech.2007.05.023.
125. Tan, G.; Xiao, D. Adsorption of cadmium ion from aqueous solution by ground wheat stems. *J. Hazard. Mater.* **2009**, *164*, 1359–1363. doi:

10.1016/j.jhazmat.2008.09.082.

126. Wang, Y.; Tian, Y.; Han, B.; Zhao, H.; Bi, J.; Cai, B. Biodegradation of phenol by free and immobilized *Acinetobacter* sp. strain PD12. *J. Environ. Sci.* **2007**, *19*, 222–225. doi: 10.1016/s1001-0742(07)60036-9.
127. Mollaei, M.; Abdollahpoura, S.; Atashgahi, S.; Abbasi, H.; Masoomi, F.; Rad, I.; Lotfi, A.S.; Zahiri, H.S.; Vali, H.; Noghabi, K.A. Enhanced phenol degradation by *Pseudomonas* sp. SA01: gaining insight into the novel single and hybrid immobilizations. *J. Hazard. Mater.* **2010**, *175*, 284–292. doi: 10.1016/j.jhazmat.2009.10.002.
128. Oh, Y.S.; Maeng, J.; Kim, S.J. Use of microorganisme–immobilized polyurethane foams to absorb and degrade oil on water surface. *Appl. Microbiol. Biotechnol*. **2000**, *54*, 418–423. doi: 10.1007/s002530000384.
129. Lee, Y.C.; Shin, H.J.; Ahn, Y.; Shin, M.C.; Leed, M.; Yang, J.W. Biodegradation of diesel by mixed bacteria immobilized onto a hybrid support of peat moss and additives: a batch experiment. *J. Hazard. Mater*. **2010**, *183*, 940–944. doi: 10.1016/j.jhazmat.2010.07.028.
130. Wang, Z.Y.; Xu, Y.; Wang, H.Y.; Zhao, J.; Gao, D.M.; Li, F.M.; Xing, B. Biodegradation of crude oil in contaminated soils by free and immobilized microorganisms. *Pedosphere* **2012**, *22*, 717–725. doi: 10.1016/S1002-0160(12)60057-5.
131. Rahman, R.N.Z.A.; Ghazali, F.M.; Salleh, A.B.; Basri, M. Biodegradation of hydrocarbon contamination by immobilized bacterial cells. *J. Microbiol*. **2006**, *44*, 354–359.
132. Díaz, M.P.; Boyd, K.G.; Grigson, S.J.; Burgess, J.G. Biodegradation of crude oil across a wide range of salinities by an extremely halotolerant bacterial consortium MPD–M, immobilized onto polypropylene fibers. *Biotechnol Bioeng.* **2002**, *79(2)*, 145–153. doi: 10.1002/bit.10318.
133. Hussein, M.; Amer, A.A.; Zahran, H.F.; Ali, S.M.; Elgohary, M.; Nasr, M. Agricultural waste as a biosorbent for oil spills. *Int. J. Dev.* **2013**, *2(1)*, 127–135.
134. Atlas, R.M. Petroleum biodegradation and oil spill bioremediation. *Mar. Pollut. Bull*. **1995**, *31(4–12)*, 178–182. doi: 10.1016/0025-326X(95)00113-2.
135. Atlas, R.M.; Bartha R. Hydrocarbon biodegradation and oil spill bioremediation. *Adv Microb Ecol.* **1992**, 287–338. doi: 10.1007/978-1-4684-7609-5_6.

Table of content